AN ABSTRACT OF THE THESIS OF

Sebastián Naranjo Álvarez for the degree of Doctor of Philosophy in Mathematics presented on February 25, 2021.

Title: Virtual Element Methods for Magneto-hydrodynamics on General Polygonal and Polyhedral Meshes

Abstract approved: _____

Vrushali A. Bokil

The aim of this dissertation is to construct a virtual element method (VEM) for models in magneto-hydrodynamics (MHD), an area that studies the behavior and properties of electrically conducting fluids such as a plasma. MHD models are a coupling of the Maxwell's equations for electromagnetics and models for fluid flow. First we consider a simplified resistive MHD sub-model where we assume that the fluid flow is prescribed, along with a resistive term in Ohm's law. This approach is called Kinematics of MHD, and we use it to predict the evolution of the electric and magnetic fields. Then we consider the full coupled MHD system in two spatial dimensions (2D) where the flow is not prescribed and design another novel VEM for the discretization of Maxwell's and Stokes' equations. We present variational formulations for each of these models. These formulations reveal two chains of spaces where the exact solutions lie. Our study focuses on developing discrete versions of these chains in both two (2D) and three (3D) spatial dimensions for MHD Kinematics and in 2D for the full MHD system. By defining a series of computable projectors, each of the terms in the continuous problem are approximated. In all our studies we present analysis of the stability of the VEM method by exploiting well-known techniques from the theory of saddle-point problems. The VEMs developed can be implemented on a very general class of polygonal/polyhedral meshes. Moreover, these methods are guaranteed to preserve the divergence of the magnetic field at the discrete level.

In the last chapter, we present a study of opinion dynamics applied specifically to debates between legislators, which forms the topic for an interdisciplinary chapter requirement for the NRT program in ”Risk and Uncertainty Quantification in the Marine Sciences”. The context of the study is the preservation of cultural keystone species (CKS) that are part of the core of indigeneous peoples culture. In this chapter, we explore how we can use mathematical modeling to design strategies to influence legislation that supports the protection of CKS.

Virtual Element Methods for Magneto-hydrodynamics on General Polygonal and Polyhedral Meshes

by

Sebastián Naranjo Álvarez

A THESIS

submitted to

Oregon State University

in partial fulfillment of
the requirements for the
degree of

Doctor of Philosophy

Presented February 25, 2021
Commencement June 2021

Doctor of Philosophy thesis of Sebastián Naranjo Álvarez presented on February 25, 2021

APPROVED:

Major Professor, representing Mathematics

Head of the Department of Mathematics

Dean of the Graduate School

I understand that my thesis will become part of the permanent collection of Oregon State University libraries. My signature below authorizes release of my thesis to any reader upon request.

Sebastián Naranjo Álvarez, Author

ACKNOWLEDGEMENTS

Academic

S. Naranjo Alvarez's work was supported by the National Science Foundation (NSF) grant #1545188, "*NRT-DESE: Risk and uncertainty quantification in marine science and policy*", which provided a one year fellowship and internship support at Los Alamos National Laboratory. S. Naranjo Alvarez also received graduate research funding from V. A. Bokil's DMS grant #1720116 and # 2012882, an INTERN supplemental award to Professor Bokil's DMS grant # 1720116 for a second internship at Los Alamos National Laboratory, and teaching support from the Department of Mathematics at Oregon State University. In addition, S. Naranjo Alvarez was also supported by the DOE-ASCR AM (Applied Math) base program grant for a summer internship.

Parts of the contents of this dissertation will be available in peer-reviewed manuscripts. We list them below:

- S. NARANJO ALVAREZ, V. A. BOKIL, V. GYRYA, G. MANZINI , *A virtual element method for magnetohydrodynamics*. ArXiv preprint arXiv:2004.11467, 2020. (Submitted in April 2020 to Elsevier Journal on Computer Methods in Applied Mechanics and Engineering).

- S. NARANJO ALVAREZ, V. A. BOKIL, V. GYRYA, G. MANZINI , *A Mimetic Finite Difference Method for Resistive Magnetohydrodynamics*. (In preparation)

- S. NARANJO ALVAREZ, V. A. BOKIL, V. GYRYA, G. MANZINI, *A virtual element method for the full system of magnetohydrodynamics.*. (In preparation)

- S. NARANJO ALVAREZ, V. A. BOKIL, V. GYRYA, G. MANZINI , *The virtual element method for the coupled system of magneto-hydrodynamics*, book chapter in "The Virtual Element Method and its Applications", Springer, 2021 (Accepted).

Personal

Throughout my stay at OSU I met many people that guided me. Their advice and support have been invaluable to me. Firstly, I would like to thank my advisor Dr. Vrushali A. Bokil who has been great support from day one. I am greatly indebted to Dr. Vitaliy Gyrya and Dr. Gianmarco Manzini who welcomed me to the theoretical division of Los Alamos National Laboratory. Special thanks are also due to Dr. Fernando Moralez, Dr. Konstantin Lipnikov, Dr. Adam Stanier, Dr. Luis Chacón and Dr. Nathan Gibson as well as the Ph.D. candidates Daniel Restrepo, Alexander Zhiliakov, Branwen Schaub and Daniel Erickson.

I would also like to thank Dr. Enrique Thomann as well as the members of my committee Dr. Vitaliy Gyrya, Dr. Edward Waymire, Dr. Adel Faridani, Dr. Vrushali A. Bokil, Dr. Lorenzo Ciannelli and Dr. Henri Jansen for their input on my thesis.

TABLE OF CONTENTS

TABLE OF CONTENTS (Continued)

TABLE OF CONTENTS (Continued)

LIST OF FIGURES

LIST OF FIGURES (Continued)

LIST OF TABLES

VIRTUAL ELEMENT METHODS FOR MAGNETO-HYDRODYNAMICS ON GENERAL POLYGONAL AND POLYHEDRAL MESHES

1. INTRODUCTION

The number of applications involving plasmas has skyrocketed in the modern age with applications ranging from fusion-based nuclear power to low power thrusters for contemporary spacecraft. Great efforts have been devoted to the development of predictive models. One such approach that has withstood the test of time is Magneto-hydrodynamics (MHD) [51]. The theory of MHD considers plasmas as magnetized fluids. Thus, models in MHD come about from a coupling between fluid flow and electromagnetics.

The evolution of the electric and magnetic fields are described by Maxwell's system plus a set of assumptions about the material properties of the fluid. Faraday's law reveals that the evolution in time of the flux of the magnetic field across an open surface results from a non-zero circulation of the electric field along the boundary of the surface. Ampére's law indicates that the electric current that passes through an open surface depends on the circulation of the magnetic field along this surface. Electric currents will generate electric fields. The relationship between these two quantities is described by Ohm's law and is entirely dependent upon the medium. In summary, electric fields generate magnetic fields which, at the same time, generate electric currents and fields. The final set of equations are Gauss's law which states that the divergence of the magnetic field is necessarily zero implying the non-existence of magnetic monopoles (magnets with only one magnetic pole). The electric and magnetic fields generate a force named the Lorentz force. This force acts upon each charged particle in the fluid and generates momentum. The velocity and pressure of the flow can be described in terms of a statement of conservation of momentum over

each fluid parcel (arbitrarily small or large volumes of fluid). Thus, the coupling between the electromagnetic and mechanical models can be summarized as follows: magnetized fluids in the presence of magnetic fields experience the Lorentz force which influences the momentum of the fluid and alters its velocity. Likewise, charged particles in motion generate electric and magnetic fields which generate the Lorentz force.

The final equation that we consider in order to attain our differential equation model requires a statement of the conservation of mass of every fluid parcel. Some models further assume that the fluid is incompressible meaning that fluid parcels are disallowed from gaining or losing its volume. This implies that the mass density remains constant and the statement of conservation of mass implies that the velocity field must be divergence-free. The models we present are of incompressible fluids. Details about the derivation of the model are separated into two sections, the first is Section 3.2 and involves the electromagnetics and the second is Section 5.2 in which derive the mechanical model. The details of the MHD model, its derivation and properties are nowadays well-understood and explained in many textbooks and review papers, e.g., [51, 73].

The development of numerical methods capable of capturing important features of MHD is an active area of research. For example, in [58, 59], two finite element methods are developed and analyzed. In [87], the convergence of finite volume methods for MHD is studied and in [38, 78] the classic upwind and Godunov methods are adapted to ideal MHD. In [37], the author presents a variant of the finite difference method named the summation by parts and simultaneous approximation terms (SBP/SAT) method. Finally, in [67], the authors develop a maker and cell (MAC) scheme for the fluid flow sub-system of the incompressible MHD equations, coupling it to the Yee-scheme, introduced in [93], for the electromagnetic sub-system.

The main goal of this dissertation is to extend the framework of the virtual element method (VEM) to models in MHD. The VEM was born as a re-framing of the older Mimetic Finite Difference (MFD) method, see [43]. In the MFD method, the modeling spaces contain arrays of degrees of freedom, whereas in the VEM each of these arrays is associated with a shape function yielding

a theory that closely resembles the finite element method (FEM), see [14]. Thus, many authors consider the VEM to be a generalization of the FEM. However, there are significant differences. The first is that the VEM is specifically designed to be implemented on meshes with a very general definition for its polygonal or polyhedral cells. Another difference lies in the definition of the space of shape functions. The FEM is based on polynomials approximations. This means that each of the shape functions is known pointwise to any precision of accuracy. In the VEM the shape functions can be proven to exist but no explicit formula is attained for their evaluations. This creates a large number of complications that do not appear in the FEM. Perhaps, the most prominent regards integration. The shape functions form an inner-product space, and this inner product is usually given in the form of an integral. Hence, if the functions are not known pointwise then the integrals required in the inner products become very difficult to estimate efficiently. The solution is that the approximations to these integrals can be computed to the degree of accuracy required using *only the degrees of freedom of the shape function*. This philosophy was inherited from the MFD method. We discuss this technique for the approximation of inner-products in Section 2.3.

The VEM was originally proposed for solving diffusion problems in [14] as a conforming FEM, and later extended to the nonconforming formulation in [7] and the mixed Brezzi Douglas Marini (BDM)-like and Raviart Thomas (RT)-like formulations in [28] and [17], respectively. Generalizations to convection-reaction-diffusion problems with variable coefficients can be found in [2, 19, 30, 47]. In a series of papers [16, 40–42], $H(div)$- and $H(curl)$-conforming virtual element spaces on general polygonal and polyhedral elements have been proposed to generalize the well known RT and Nédélec finite elements to unstructured meshes, see [72, 76]. These methods, combined with the Serendipity strategy, that reduces the total number of degrees of freedom, see [11, 12], have successfully been applied to the numerical resolution of the magnetostatic Kikuchi's model, see [62]. In these papers, exact virtual De-Rham sequences (explored in Sections 3.7 and 4.4) with commuting-diagram interpolation operators are built which guarantees that the discrete magnetic flux field remains solenoidal. Finally, VEMs have also been designed for

hyperbolic problems, see [1, 89].

The VEM provides several advantages over more classical methods. The first is that it can be implemented on a very general class of meshes. This makes the method exceptionally versatile and capable of handling complex problems like those involving material interfaces or free boundaries. For example, many practical applications of MHD involve the fluid passing several media. When extracted, for commercial purposes, metals are often dissolved and pumped through different layers of sand and rock. When modeling this situation it would be ideal if the mesh were to be fitted to the material layers in such a way that the boundaries of these layers fall along the edges of the cells. The result, in real-life scenarios, is often times a highly unstructured mesh, making VEM-based modeling software particularly well-suited for this application. In some other applications the computational domain is deformed. This is the case in fusion-based nuclear power generators. In this application, a gas is heated to the point of fusion, at temperatures that any container built to hold the gas would melt. Thus, modern techniques that are explored involve suspending the gas using external magnetic fields bypassing the need for a container at all. This method is called *magnetic confinement*. By using computational models we can predict the motion of the fluid and immediately apply an appropriate magnetic field to guarantee that the gas remains suspended. Since the boundaries of the gas are not fixed by a physical container they are free to deform into odd shapes, which need to be captured by the mesh. This implies that the mesh has to constantly be updated for real time simulation. Thus, high order VEM technology can provide an efficient solution.

A second major advantage of VEM is related to accurately capturing the divergence of the magnetic field. According to electromagnetic theory the magnetic field should remain solenoidal, i.e, its divergence should remain zero (Gauss's Law). This is not an additional equation, rather it is a consequence of Faraday's law and the fact that the divergence of any curl is zero as we will note in Section 3.2. Often times discretization methods will fail to capture this property yielding a remainder that compounds in time. The result is that, at the discrete level, the magnetic field

may not be divergence free. The consequences are well-documented, see [21, 22]. Simulations that do not conserve this property present significant errors, see [21, 22, 48, 88]. The conclusion in [48] is that these simulations experience fictitious forces that render the simulation unfaithful to the physics involved. A great deal of research has gone into the development of "divergence cleaning" techniques; we mention three approaches. In [52], they add $\nabla \cdot \boldsymbol{B} = 0$ as an additional equation and add a Lagrange multiplier to the set of unknowns to enforce this constraint. A different approach involves the development of specialized flux limiters, see [64]. Finally, least squares finite element methods involve solving differential equations by minimizing energy functionals one of which can involve the condition on the divergence of the magnetic field, see [60]. However, in the VEM that we develop divergence cleaning is unnecessary. As we will prove, our VEM discretization will yield divergence-free approximations to the magnetic field provided that the initial conditions satisfy this condition. The main result required for this property to hold is the commutativity of a De-Rham complex introduced in 2D and 3D in Sections 3.7 and 4.4 respectively. However, there is a conflict that needs to be resolved regarding one of the spaces involved since an important L^2-orthogonal projector used to build the inner-product is not computable. The literature resolves this by enhancing the space and redefining it in such a way that this projector is computable, see [3, 15]. However, this implies that the De-Rham complex may no longer hold. In order to find a solution to this complication we construct an oblique projector to build the inner product in this space. Not every oblique projector will suffice, thus we present criteria that can be used to discern which projectors are useful and which are not. This approach is unique to this work and one of our major contributions to the theory of the VEM.

Funding for the research we present in this dissertation came partly from the Oregon State University, National Research Traineeship (NRT) in Risk and Uncertainty Quantification in Marine Science funded by the NSF. As part of the requirements of the NRT, the last chapter of this dissertation presents an application of mathematical modeling to the social sciences involving cultural keystone species (CKS). The CKS are species that are central to a people's culture. In

this dissertation, we will explore how mathematical modeling can provide strategies to influence legislators to approve policy aimed at protecting CKS. Votes on these types of policies come after deliberation between these legislators. Thus, our main contribution will be in developing and studying two models for these debates, one in which we consider the influence of the electorate and one in which we do not. These models will be based on a system of ordinary differential equations. We will use Runge-Kutta methods to approximate the solutions and study these models and conduct a simulation based analysis of the models.

This dissertation is structured as follows: Chapter 2., will be dedicated to the preliminary results required to understand the subsequent chapters. In Chapter 3., we consider a prescribed flow and develop a VEM capable of predicting the electric and magnetic fields as described by Maxwell's equations, this is done in two spatial dimensions. Chapter 4., is dedicated to extending the VEM introduced in Chapter 3. to three dimensions. Then, in Chapter 5., we omit the assumption that the flow is prescribed and develop a VEM for the full MHD system. In Chapter 6., the reader will find a series of numerical experiments. The code developed is hosted at https://github.com/sebnaran. Chapter 7., is dedicated to discussing two mathematical models and their simulations to address the conservation of CKS. We finish with Chapter 8., where we present some concluding remarks and open questions.

2. MATHEMATICAL PRELIMINARIES

2.1 Notation and Definitions

In this section we will formally define the concepts and notation that we will be referring to throughout this dissertation.

Firstly, we will use bold letter to denote vector-valued functions. The dimension of the co-domain of these functions will be either 2 or 3, this detail will be clear from context. For a pair of sufficiently regular real-valued functions $f, g : U \to \mathbb{R}$ or vector valued-functions $\boldsymbol{f}, \boldsymbol{g} : U \to \mathbb{R}$ we define

$$\big(f, g\big) = \int_U fg dx, \quad \big(\boldsymbol{f}, \boldsymbol{g}\big) = \int_U \boldsymbol{f} \cdot \boldsymbol{g} dx. \tag{2.1}$$

Here we are assuming that $U \subset \mathbb{R}^N$ is measurable. Moreover, we will denote the L^2-norm by

$$\forall f \in L^2(U): \quad \|f\|_{0,U} = \left(\int_U |f|^2 dx\right)^{1/2}, \quad \|f\|_{1,U} = \left(\|f\|_{0,U}^2 + \|\nabla f\|_{0,U}^2\right)^{1/2}, \tag{2.2a}$$

$$\forall \boldsymbol{f} \in [L^2(U)]^N: \quad \|\boldsymbol{f}\|_{0,U} = \left(\int_U |\boldsymbol{f}|^2 dx\right)^{1/2}, \quad \|\boldsymbol{f}\|_{1,U} = \left(\|\boldsymbol{f}\|_{0,U}^2 + \|\nabla \boldsymbol{f}\|_{0,U}^2\right)^{1/2}. \tag{2.2b}$$

In the case that $f : U \to \mathbb{R}$ and $\boldsymbol{g}, \boldsymbol{f} : U \to \mathbb{R}^2$ we will, abusing the notation, use the symbol for cross product to denote:

$$f \times \boldsymbol{g} = f \begin{pmatrix} -B_y \\ B_x \end{pmatrix}, \quad \boldsymbol{f} \times \boldsymbol{g} = f_x g_y - f_y g_x. \tag{2.3}$$

2.2 Results from Functional Analysis

The analysis of the VEM that we will develop will rely on results from functional analysis. The first result is the generalized form of the Brezzi-Babuska-Lax Milgram Theorem:

Theorem 2.20.1 *Let U and V be Hilbert spaces and $a : U \times V \to \mathbb{R}$ be a bilinear form satisfying*

$$\exists M > 0 \forall (u, v) \in U \times V : \quad a(u, v) \leq M \|u\|_U \|v\|_V, \tag{2.4a}$$

$$\forall v \in V \setminus \{0\} : \quad \sup_{u \in U} a(u, v) > 0, \tag{2.4b}$$

$$\inf_{v \in V} \sup_{u \in U} \frac{a(u, v)}{\|u\|_U \|v\|_V} > 0. \tag{2.4c}$$

Then, for any $\ell \in V'$ there exists a unique $u \in V$ such that

$$\forall v \in V : \quad a(u, v) = \ell(v). \tag{2.5}$$

Moreover,

$$\exists C > 0 : \|u\|_U \leq C \|\ell\|_{V'}. \tag{2.6}$$

A proof of this Theorem can be found in [5].

The second result that we will need is one of the main conclusions of the Ladyzhenskaya-Babuska-Brezzi Theory.

Theorem 2.20.2 *Let U and P be Hilbert spaces and $a : U \times U \to \mathbb{R}$, $b : U \times P \to \mathbb{R}$ be bounded bilinear forms satisfying:*

$$\inf_{u \in U_0} \sup_{v \in U_0} \frac{a(u, v)}{\|u\| \|v\|} > 0, \quad \inf_{p \in V} \sup_{u \in U} \frac{b(u, p)}{\|u\| \|p\|} > 0. \tag{2.7}$$

Where

$$U_0 = \{u \in U : \forall v \in V \quad b(u, v) = 0\}. \tag{2.8}$$

The for every pair of bounded linear functionals $f \in U'$ and $g \in V'$ there exists unique $u \in U$

and $v \in V$ such that for any $v \in U$ and $q \in V$ it is the case that

$$a(u,v) - b(v,p) = f(v), \tag{2.9a}$$

$$b(u,q) = g(q). \tag{2.9b}$$

More over there exists a constant $C > 0$ independent of f and g such that

$$\|u\| + \|p\| \leq C\left(\|f\| + \|g\|\right). \tag{2.10}$$

Here we consider

$$\|f\| = \sup_{u \in U \setminus \{0\}} \frac{|f(u)|}{\|u\|}, \quad \|g\| = \sup_{p \in P \setminus \{0\}} \frac{|g(p)|}{\|p\|}. \tag{2.11}$$

A proof of this Theorem can be found in [20, 27].

2.3 Approximating Bilinear Forms in the VEM framework

In this section we will describe how inner product matrices are constructed in the framework of the VEM. The procedure is relatively standard. Consider a symmetric and positive definite bilinear form $a : U(\mathsf{P}) \times U(\mathsf{P}) \to \mathbb{R}$ where P is a cell in a mesh Ω_h and $U(\mathsf{P})$ a Hilbert space defined over the cell P. We approximate $U(\mathsf{P})$ using a finite dimensional space of shape functions that we denote as $\mathcal{X}_h(\mathsf{P})$. Our goal is to define $a_h : \mathcal{X}_h(\mathsf{P}) \times \mathcal{X}_h(\mathsf{P}) \to \mathbb{R}$ to estimate a. We require that a_h satisfies two important properties. The first regards its **accuracy**, it should be the case that

$$\forall p, q \in [\mathbb{P}_k(\mathsf{P})]^N \quad a_h(p,q) = a(p,q). \tag{2.12}$$

Here, k is the degree of the largest polynomial space that is contained in $\mathcal{X}_h(\mathsf{P})$ and $N = 1$ if functions in $\mathcal{X}_h(\mathsf{P})$ are scalar valued or $N = 2, 3$ in the case that that they are vector valued. We

also require that a_h satisfy the **stability** property, meaning that

$$\exists c_*, c^* > 0, \forall x_h \in \mathcal{X}_h(\mathsf{P}): \quad c_* a(x_h, x_h) \leq a_h(x_h, x_h) \leq c^* a(x_h, x_h). \tag{2.13}$$

The procedure we present is partially laid out in [15]. For now we will assume that we have a means, using only the degrees of freedom in the space $\mathcal{X}_h(\mathsf{P})$ to compute a projector $\Pi : \mathcal{X}_h(\mathsf{P}) \to [\mathbb{P}_k(\mathsf{P})]^N$. Generally this is done by selecting a basis for $[\mathbb{P}_k(\mathsf{P})]^N$ say $\{p_1, \ldots, p_n\}$ and another basis for $\mathcal{X}_h(\mathsf{P})$, consistent with the degrees of freedom. We denote this basis as $\{x_h^1, \ldots, x_h^m\}$. Then, for any $x_h \in \mathcal{X}_h(\mathsf{P})$ we expand

$$\Pi x_h = \Pi \left(\sum_{i=1}^{N} d_i x_h^i \right) = \sum_{i=1}^{n} c_i p_i. \tag{2.14}$$

Where d_i is the $i-$th degree of freedom of x_h in some enumeration. The coefficients of in the expansion are found by solving a linear system of the form

$$G\vec{c} = B\vec{d}. \tag{2.15}$$

It is often the case that the projector Π is defined through the bilinear form a. This projector $\Pi_a : \mathcal{X}_h(\mathsf{P}) \to [\mathbb{P}_k(\mathsf{P})]^N$ when applied to a function $x_h \in \mathcal{X}_h(\mathsf{P})$ is given as the solution to

$$\forall q \in [\mathbb{P}_k(\mathsf{P})]^N: \quad a(\Pi_a x_h - x_h, q) = 0. \tag{2.16}$$

In this case we would use

$$G = \begin{pmatrix} P_0(p_1) & P_0(p_2) & P_0(p_3) & \ldots & P_0(p_n) \\ a(p_1, p_1) & a(p_1, p_2) & a(p_1, p_3) & \ldots & a(p_1, p_n) \\ \vdots & \vdots & \ddots & \vdots & \\ a(p_n, p_1) & a(p_n, p_2) & a(p_n, p_3) & \ldots & a(p_n, p_n) \end{pmatrix}, \quad B_{i,j} = a(x_h^i, p_j). \tag{2.17}$$

The function P_0 is used to fix the kernel of a. In the case that $\text{Ker}(a) \neq \{0\}$ some of the rows of G, as defined in (2.17) will be entirely populated by zeroes, in this case we omit them and replace them with those involving P_0 to guarantee that G is square and invertible. In the case that $\text{Ker}(a) = \{0\}$ the use of P_0 can be omitted. Computing each of the components of B must be explained in a case by case basis. Computing $a(p_i, p_j)$ usually boils down to computing integrals of polynomials over the polygon/polyhedron P. Due to the generality of the geometry of P it is not practical to develop quadrature rules. There are specialized techniques aimed at solving these sorts of problems. The first involves using Green's Theorem recursively to write volume/area integrals as line integrals across the edges of the cells where quadrature rules are available, see [33] for the original idea, and for applications of this method [4, 74]. Another technique is presented in [82, 83] and involves reducing volume/area integrals to one dimensional by introducing special lines supported by Gauss's integration points. In [84] the same authors use a compression technique to reduce the number of quadrature points necessary. This method is very general and allows for computations over cells with curved edges or faces, see [46] for an application in the VEM. The technique used in the implementations of this manuscript is the following: decompose P into a number of triangles/tetrahedrons. Then, using quadrature rules for these shapes, add the contributions of each of the pieces.

In any case, when we apply the matrix $\Pi_*^M := G^{-1}B$ to a vector of degrees of freedom, the output will be the array of coefficients in the expansion (2.14) as evidenced by (2.15). In practice we are much more interested in the vector of degrees of freedom of the projection rather than in the coefficients in the polynomial expansion. Hence, we define the matrix $\Pi^M = D\Pi_*^M$ where

$$D_{i,j} = \text{dof}_i(p_j). \tag{2.18}$$

Thus, multiplying the array of degrees of freedom of x_h by Π^M will yield the array of degrees of freedom of Πx_h.

Finally, we can define the matrix

$$A = \Pi_*^{M,T} H \Pi_*^{M,T} + |P|(I - \Pi^M)(I - \Pi^M). \tag{2.19}$$

where $|\mathsf{P}|$ is the volume/area of P and the entries of H are given by

$$H_{i,j} = a(p_i, p_j). \tag{2.20}$$

The definition of a_h is given by

$$\forall x_h, y_h \in \mathcal{X}_h(\mathsf{P}): \quad a_h(x_h, y_h) = x_h^T A y_h. \tag{2.21}$$

2.4 Mesh Assumptions

In this section we present the assumptions that we will make on the mesh. The main property that we want to preserve is regularity, we require that there exists $\rho \geq 0$ independent of the mesh size $h > 0$ such that

(M1) (*star-shapedness*): every polygonal cell P of every mesh Ω_h is star-shaped with respect to every point of a disk of radius ρh_{P};

(M2) (*uniform scaling*): every edge $\mathsf{e} \in \partial\mathsf{P}$ of cell $\mathsf{P} \in \Omega_h$ satisfies $h_{\mathsf{e}} \geq \rho h_{\mathsf{P}}$.

In 3D we add the following assumption:

(M3) (*uniform scaling*) Every face f and every edge e of f satisfies $h_{\mathsf{e}} \geq \rho h_{\mathsf{f}}$.

The regularity assumptions **(M1)**-**(M2)** in 2D or **(M1)** $-$ **(M3)** in 3D allow us to use meshes with cells having quite general geometric shapes. For example, non-convex cells or cells with hanging nodes on their edges are admissible. Nonetheless, these assumptions have some important implications such as: (i) every polygonal element is *simply connected*; (ii) the number of edges

of each polygonal cell in the mesh family $\{\Omega_h\}_h$ is uniformly bounded; (iii) a polygonal element cannot have *arbitrarily small* edges with respect to its diameter $h_{\mathsf{P}} \leq h$ for $h \to 0$ and inequality $h_{\mathsf{P}}^2 \leq C(\rho)|\mathsf{P}|h_{\mathsf{P}}^2$ holds, with the obvious dependence of constant $C(\rho)$ on the mesh regularity factor ρ. It is worth mentioning that virtual element methods on polygonal or polyhedral meshes possibly containing "small edges" in 2D or "small faces" in 3D have been considered in [25] for the numerical approximation of the Poisson problem. The work in [25] extends the results in [13] for the original two-dimensional virtual element method to the version of the virtual element method in [2] that can also be applied to problems in three dimensions. Finally, we note that assumptions **(M1)**-**(M2)** above also imply that the classical polynomial approximation theory in Sobolev spaces holds [24].

3. KINEMATICS

3.1 Introduction

When studying the kinematics of MHD we assume that the flow is controlled by some external source. Then, we proceed to predict the behavior of the electric and magnetic fields. Thus, we will consider that $\boldsymbol{u}$, the velocity of the flow is known exactly. The main topic we tackle in this chapter regards the construction of a VEM for a model in kinematics. In Section 3.2 we derive the model from physical principles. Then, in Section 3.3 we present a VEM for the derived model. In presenting this discretization we will introduce two virtual element spaces, their definition is a topic for Sections 3.4,3.5. In Section 3.6 we define a third space that, although it does not appear in the virtual element formulation, it is important for the purposes of analysis. We note that these spaces were initially conceived in the mimetic finite difference (MFD) framework and taken from [43]. The re-framing into VEM was done using the results found in [16]. These three sections are structured in a similar manner we will pick one of the cells in the mesh, denoted as P. Over this cell we will define the local spaces shape functions, their properties and geometries. The definitions of the individual spaces only say half of the story, the other half is told by their relationship. In Section 3.7 we show that these three spaces form a commuting De-Rham complex that guarantees a close mimicry of the continuum. Then, in Section 3.8 we will briefly mention how to extend this VEM to high orders in space. Next, in Section 3.9 we present some stability estimates in the L^2 norm that are satisfied by the continuous problem and their discrete mimicry. In Section 2.3 we presented a method for computing inner products in virtual element space. This method relies on first computing a series of projectors. To compute the inner product in the space presented in 3.4 we do not introduce a particular projector rather we describe criteria to construct one. Thus, we will finish this chapter with Section 3.11 where we present three examples of projectors satisfying these criteria as well as how they can be implemented. Finally,

in Section 3.12 we present the conclusions of this chapter.

3.2 The Electromagnetic Model

The contents of this section come from very well-known results in electromagnetics. Any book centered on the physics will contain the material here. We recommend the exposition in [51, 73].

There are two main quantities that drive the evolution of an electromagnetic system. They are the electric and magnetic field, in this manuscript we denote them as $\boldsymbol{E}$ and $\boldsymbol{B}$ respectively. Any charged particle that enters a region permeated by these fields will experience a force, the **Lorentz force**. We can quantify this value by using the expression

$$\boldsymbol{f} = q\boldsymbol{E} + q\boldsymbol{u} \times \boldsymbol{B}. \tag{3.1}$$

Here q represents the charge of the particle, $\boldsymbol{f}$ is the force experienced and $\boldsymbol{u}$ is the velocity with respect to the frame of reference that the viewer is taking. In the section about fluid flow the discussion will center around two types of frames of reference. If a particle is moving in a laboratory then the scientist will view from the **Eulerian** frame of reference. If, by some trick, we could mount the particle and ride along then we would be viewing **Lagrangian** frame of reference. The main difference in the two perspectives is the velocity of the particle. In the Eulerian frame of reference the velocity of the particle will be given as $\boldsymbol{u}_E$. Whereas, in the Lagrangian point of view the velocity is exactly zero. This implies that, apparently, the particle experiences two different forces, they are

$$\boldsymbol{f}_E = q\boldsymbol{E}_E + q\boldsymbol{u}_E \times \boldsymbol{B}_E, \text{ and } \boldsymbol{f}_L = q\boldsymbol{E}_L. \tag{3.2}$$

Here, the subscripts indicate which frame of reference is taken, ”E” for Eulerian and ”L” for

Lagrangian These two forces not independent, their relationship is given by a different set of rules depending on the size of the velocity $\boldsymbol{u}_E$. Very large velocities are ruled by Einstein's Theory of Relativity. These models are outside the scope of this manuscript. We will consider slower speeds for which Galilean relativity applies. This theory dictates that the force experienced should be the same independent of the frame of reference we take. Hence, $\boldsymbol{f}_L = \boldsymbol{f}_E$ or equivalently

$$\boldsymbol{E}_L = \boldsymbol{E}_E + \boldsymbol{u}_E \times \boldsymbol{B}_E. \tag{3.3}$$

The expression for the Lorentz force that we have been discussing is true for a single particle. In MHD, we are interested in a charged fluid made of an infinite number of particles. In this case, the net force is not very informative about the behavior of the system. Instead we consider a force density or force per unit volume. The expression is in the Eulerian coordinates is

$$\boldsymbol{F} = \rho_E \boldsymbol{E} + \rho_E \boldsymbol{u} \times \boldsymbol{B} = \rho_E \boldsymbol{E} + \boldsymbol{J} \times \boldsymbol{B}. \tag{3.4}$$

The variable ρ_E is the charge density and $\boldsymbol{J} = \rho_E \boldsymbol{u}_E$ is the electric current density. The Lorentz force is useful when we are studying the behavior of a charged particle in the presence of electric and magnetic fields. However, it does not say much about how electric and magnetic fields behave. Hence, the next item of business is to study the Electric and magnetic fields, their relationship and what we can do to predict them. These are described in partly by **Maxwell's system**. The full system is

$$\text{Ampere-Maxwell's law:} \quad \mu \left[\epsilon \frac{\partial}{\partial t} \boldsymbol{E} + \boldsymbol{J} \right] = \nabla \times \boldsymbol{B}, \tag{3.5a}$$

$$\text{Faraday's law:} \quad \frac{\partial}{\partial t} \boldsymbol{B} = -\nabla \times \boldsymbol{E}, \tag{3.5b}$$

$$\text{Gauss's laws:} \quad \nabla \cdot \boldsymbol{E} = \rho_E / \epsilon, \quad \nabla \cdot \boldsymbol{B} = 0. \tag{3.5c}$$

The variable ρ_E refers to the electric charge density, $\boldsymbol{J}$ is the electric current density and ϵ, μ are

the permittivity and permeability of the medium. A more intuitive interpretation of this system will come from its integral form. Consider sample volume V, arbitrarily, and take the integral over this volume on both sides of Gauss's Laws. An application of the Divergence Theorem will reveal that

$$\int_{\partial V} \boldsymbol{B} \cdot \boldsymbol{n} dS = 0 \quad \text{and} \quad \int_{\partial V} \boldsymbol{E} \cdot \boldsymbol{n} dS = \frac{1}{\epsilon} \int_V \rho_E dV. \tag{3.6}$$

Gauss's Law for the magnetic field implies that the flux across a closed surface must necessarily be null. This means that every magnetic field line that enters a surface must also leave at some other point along said surface. Turning to Gauss's law for the electric field, note that the volumetric integral of the charge density is the net charge in the volume. Hence, the flux of the electric field is directly proportional to the charge encapsulated within said volume. The constant of proportionality is related to the material properties of the medium.

Ampere-Maxwell and Faraday's laws also convey an interesting story. Consider a sample surface, S, compute the flux of the right and left hand sides of both Faraday's and Ampere-Maxwell's Law and apply Stoke's Theorem. The result is

$$\text{Ampere-Maxwell's Law:} \quad \mu\epsilon \frac{\partial}{\partial t} \int_S \boldsymbol{E} \cdot \boldsymbol{n} dS + \mu \int_S \boldsymbol{J} \cdot \boldsymbol{n} dS = \int_{\partial S} \boldsymbol{B} \cdot \boldsymbol{t} d\ell, \tag{3.7a}$$

$$\text{Faraday's Law:} \quad \frac{\partial}{\partial t} \int_S \boldsymbol{B} \cdot \boldsymbol{n} dS = -\int_{\partial S} \boldsymbol{E} \cdot \boldsymbol{t} d\ell. \tag{3.7b}$$

Thus, in this form Faraday's Law reveals the source of changes in the flux of the magnetic field across a surface, it is a circulation of the electric field along the path that the boundary of the surface defines. Likewise Ampere-Maxwell's Law reveals that a circulation of the magnetic field can generate a flux in two quantities, the electric current density and the electric field. Together they convey that changing electric fields or motion of charges will generate magnetic fields. In turn, changing magnetic fields will generate electric fields. Thus, the pattern continues and the cycle repeats. If we consider the cases when there are no charged particles in a region then we obtain waves, electromagnetic waves or light. This is not the case in MHD, rather we are considering a

fluid that is charged in itself. What is interesting to note is that in this situation the contribution of the time derivative of the electric field in Ampere-Maxwell in negligible. To see this, we must introduce another principle, the law of **conservation of charge** which states that charge cannot be created nor destroyed. Thus, if we consider a sample volume V then the rate of change of charge contained within that volume should correspond to the outward flux in electric current across the boundary of V. This is to say that

$$\frac{\partial}{\partial t}\int_V \rho_E dV = -\int_{\partial V} \boldsymbol{J}\cdot\boldsymbol{n}dS. \tag{3.8}$$

An application of the Divergence Theorem will reveal the differential form of this law, it is

$$-\frac{\partial}{\partial t}\rho_E = \nabla\cdot\boldsymbol{J}. \tag{3.9}$$

In in the static case, charged particles will quickly gather around the surface of the conducting solid they are in. This implies that the density of the charge is nearly zero. In MHD, since the fluid is itself in motion some charge is allowed to remain in the interior of the fluid. However, experiments show that the amount is minimal, so much so that the contribution of $\rho_E\boldsymbol{E}$ to the Lorentz force (3.4) is negligible. Thus, models in MHD generally use the expression

$$\boldsymbol{F} = \boldsymbol{J}\times\boldsymbol{B}. \tag{3.10}$$

Moreover, experiments also show that charges in the interior position themselves in the volume in very short time scales of the order of $10^{-18}s$. Generally, in MHD we are interested in timescales much larger than that, hence we may take the time derivative of the charge density to be minimal. From the statement of conservation of charge (3.9) this implies that

$$\nabla\cdot\boldsymbol{J} = 0. \tag{3.11}$$

Hence, the current density should be nearly divergence free. Consider taking the divergence on both sides of Ampere-Maxwell's law (3.5a). If we note that the divergence of the curl of any quantity is always zero then we arrive at

$$-\nabla \cdot \boldsymbol{J} = \epsilon \frac{\partial}{\partial t} \boldsymbol{E}. \tag{3.12}$$

Hence, the time derivative of the electric field is, as a consequence of (3.11), negligible. Hence, in MHD we use

$$\mu \boldsymbol{J} = \nabla \times \boldsymbol{B}. \tag{3.13}$$

This identity is called Ampere's law. Finally, to finish describing the kinematics of MHD we must also consider the behavior of the material itself. Experiments show that charged particles in conductors move in the direction of the force that is applied to them. Recalling the expression of the Lorentz force in equation (3.2), we find that the direction, in the Eulerian coordinate system, is the same as the direction of the vector $\boldsymbol{E} + \boldsymbol{u} \times \boldsymbol{B}$. Thus, this principle is posed as

$$\boldsymbol{J} = \sigma(\boldsymbol{E} + \boldsymbol{u} \times \boldsymbol{B}), \tag{3.14}$$

The constant of proportionality, σ is called the conductivity and depends on the medium itself. This expression goes by the name of **Ohm's law**. When combining the expressions of Ampere's law and Ohm's law into a single identity that we call **Ampere-Ohm's law**,

$$\eta^{-1}\boldsymbol{E} + \eta^{-1}\boldsymbol{u} \times \boldsymbol{B} - \nabla \times \boldsymbol{B} = \boldsymbol{0}, \quad \eta = \frac{1}{\mu\sigma}, \tag{3.15}$$

where η is called the magnetic diffusivity.

Now we have all the tools we require to come up with a model for the kinematics of MHD. Consider a bounded, polygonal domain Ω that contains a magnetized fluid. Further consider that the fluid flow is prescribed by some external agent that provides us with the exact velocity field

$\boldsymbol{u}$. In this case, the electric and magnetic fields are completely described by Faraday and Ampere-Ohm's law, (3.5b) and (3.15). We are interested in the dimensionless form of these equations. To arrive at this form we make the substitutions

$$\frac{\partial}{\partial t'} = T\frac{\partial}{\partial t}\,, \quad \nabla' = L\nabla\,, \quad \boldsymbol{u}' = \frac{\boldsymbol{u}}{U}\,, \quad \boldsymbol{B}' = \frac{\boldsymbol{B}}{B}\,, \quad \boldsymbol{E}' = \frac{\boldsymbol{E}}{E}, \tag{3.16}$$

where U, B and E are characteristic values of the velocity, magnetic and electric fields respectively and L is a characteristic length of the domain, while $T = L/U$ a the characteristic time scale. The resulting model is given by

$$\frac{\partial}{\partial t'}\boldsymbol{B}' + \nabla' \times \boldsymbol{E}' = \boldsymbol{0}, \tag{3.17a}$$

$$\boldsymbol{E}' + \boldsymbol{u}' \times \boldsymbol{B}' - R_m^{-1}\nabla' \times \boldsymbol{B}' = \boldsymbol{0}, \tag{3.17b}$$

where $R_m = UL/\eta$ is the magnetic Reynold's number. We will henceforth refer only to the dimensionless quantities and operators we introduced. In order to avoid cluttering the notation we will drop the prime.

Note that by taking the divergence of both sides in Ampere-Ohm's law (3.17b) and applying Ohm's law we retrieve the statement that the current density must be null, implying the law of conservation of charge. Moreover, we should see Gauss's law (3.5c) as constraints rather than as a part of the model. For the electric field, this law will predict the charge density distribution. Whereas, Gauss's law for the magnetic field is a consequence of Faraday's law (3.17a). To see this, we take divergence on both sides of this law, then

$$\frac{\partial}{\partial t}\left[\nabla \cdot \boldsymbol{B}\right] = \nabla \cdot \left[\frac{\partial}{\partial t}\boldsymbol{B}\right] = -\nabla \cdot \nabla \times \boldsymbol{E} = 0. \tag{3.18}$$

This implies that the divergence of the magnetic field will not change in time. In other words, if the initial conditions are divergence free then this property will be preserved for all time. Thus,

we will pick initial conditions $\boldsymbol{B}_0$ that come from a realistic magnetic field, hence $\boldsymbol{B}_0$ will be solenoidal.

$$\boldsymbol{B}(0) = \boldsymbol{B}_0 \quad \text{with} \quad \nabla \cdot \boldsymbol{B}_0 = 0. \tag{3.19}$$

To close the system we also consider that the electric field in known along the boundary $\partial\Omega$,

$$\boldsymbol{E} = \boldsymbol{E}_b \quad \text{along} \quad \partial\Omega. \tag{3.20}$$

3.3 The Continuous and Discrete Variational Formulations

The virtual element method we will be developing will include a key simplification in our MHD model. We will consider that the first two components of the electric field are zero, likewise we will assume that the last component of the magnetic field is zero. This, in effect, will reduce the dimensionality of the problem from a 3D problem to a 2D problem. Abusing the notation we will denote the two dimensional magnetic field as $\boldsymbol{B}$, the one dimensional electric field as E and the two dimensional computational domain as Ω. Following this trend we define the rotational and divergence operators

$$\mathbf{rot}\, E = \begin{pmatrix} \frac{\partial}{\partial y} E \\ -\frac{\partial}{\partial x} E \end{pmatrix}, \quad \text{rot}\, \boldsymbol{B} = \frac{\partial}{\partial x} B_y - \frac{\partial}{\partial y} B_x, \tag{3.21}$$

$$\text{div}\, \boldsymbol{B} = \frac{\partial}{\partial x} B_x + \frac{\partial}{\partial y} B_y. \tag{3.22}$$

With this notation we introduce the reduced model as finding $\boldsymbol{B}$ and E such that

$$\frac{\partial}{\partial t}\boldsymbol{B} + \mathbf{rot}\, E = \mathbf{0} \quad \text{in} \quad \Omega, \tag{3.23a}$$

$$E + \boldsymbol{u} \times \boldsymbol{B} - R_m^{-1}\text{rot}\, \boldsymbol{B} = 0 \quad \text{in} \quad \Omega, \tag{3.23b}$$

$$\boldsymbol{B}(0) = \boldsymbol{B}_0 \quad \text{in} \quad \Omega \tag{3.23c}$$

$$E \equiv E_b \quad \text{along} \quad \partial\Omega. \tag{3.23d}$$

The initial and boundary conditions, as well as the velocity field $\boldsymbol{u}$, are assumed to be known. The differential form presented in (3.23) is not very useful for a virtual element discretization. Instead we must pose the problem of finding E and $\boldsymbol{B}$ as a variational statement in a functional space. Thus, as is the case in most problems in electromagnetics we will assume some regularity on the solutions, specifically we will assume that at $E \in C\left([0,T], H(\mathbf{rot};\Omega)\right)$ and $\boldsymbol{B} \in C^1\left([0,T], H(\text{div};\Omega)\right)$ for

$$H(\mathbf{rot};\Omega) := \left\{ D \in L^2(\Omega) : \mathbf{rot}\, D \in \left[L^2(\Omega)\right]^2 \right\}, \tag{3.24a}$$

$$H(\text{div};\Omega) := \left\{ \boldsymbol{C} \in \left[L^2(\Omega)\right]^2 : \text{div}\, \boldsymbol{C} \in L^2(\Omega) \right\}, \tag{3.24b}$$

$$C\left([0,T], H(\mathbf{rot};\Omega)\right) := \left\{ E : [0,T] \to H(\mathbf{rot};\Omega) : E \text{ is continuous} \right\}, \tag{3.24c}$$

$$C^1\left([0,T], H(\text{div};\Omega)\right) = \left\{ \boldsymbol{B} : [0,T] \to H(\text{div};\Omega) : \boldsymbol{B}, \frac{\partial}{\partial t}\boldsymbol{B} \text{ are continuous} \right\}. \tag{3.24d}$$

The spaces where we look for solutions is called the **trial spaces**. There is a second set of spaces that concerns any variational formulation and they are the **test spaces**. These, in our case, will be $H(\text{div};\Omega)$ and $H_0(\mathbf{rot};\Omega)$ for

$$H_0(\mathbf{rot};\Omega) = \left\{ D \in H(\mathbf{rot};\Omega) : D \equiv 0 \text{ along } \partial\Omega \right\}. \tag{3.25}$$

If we pick, arbitrarily, a function $\boldsymbol{C} \in H(\text{div};\Omega)$ and multiply it on both sides of (3.23a) and integrate, we obtain

$$\big(\frac{\partial}{\partial t}\boldsymbol{B},\boldsymbol{C}\big) + \big(\mathbf{rot}\, E,\boldsymbol{C}\big) = 0. \tag{3.26}$$

Likewise we pick $D \in H_0(\mathbf{rot};\Omega)$ and multiply it on both sides of equation (3.17b). Then, we apply the integration by parts formula

$$\big(\text{rot}\,\boldsymbol{B},D\big) = \big(\boldsymbol{B},\mathbf{rot}\, D\big). \tag{3.27}$$

We obtain the expression

$$\big(E,D\big) + \big(\boldsymbol{u}\times\boldsymbol{B},D\big) - \big(\boldsymbol{B},\mathbf{rot}\, D\big) = 0. \tag{3.28}$$

Hence, putting equations (3.26) and (3.28) together we can pose the variational form of system (3.23). Thus, we want to *find* $(\boldsymbol{B},E) \in C^1\left([0,T],H(\textit{div};\Omega)\right)\times C\left([0,T],H(\textbf{\textit{rot}};\Omega)\right)$*, such that:*

$$\Big(\frac{\partial}{\partial t}\boldsymbol{B},\boldsymbol{C}\Big) + \Big(\mathbf{rot}\, E,\boldsymbol{C}\Big) = 0 \qquad \forall \boldsymbol{C} \in H(\text{div};\Omega), \tag{3.29a}$$

$$R_m\Big(E,D\Big) + R_m\Big(\boldsymbol{u}\times\boldsymbol{B},D\Big) - \Big(\boldsymbol{B},\mathbf{rot}\, D\Big) = 0 \qquad \forall v \in H_0(\mathbf{rot};\Omega), \tag{3.29b}$$

$$\boldsymbol{B}(0) = \boldsymbol{B}^0 \;\text{ with }\; \text{div}\,\boldsymbol{B}^0 = 0. \tag{3.29c}$$

Implicit in the above formulation is that $E = E_b$ along the boundary of Ω. In order to come up with a discrete formulation of (3.29) we must introduce a mesh Ω_h with mesh size $h > 0$. We can use this mesh to define subspaces of $H(\text{div};\Omega)$, $H(\mathbf{rot};\Omega)$ and $H_0(\mathbf{rot};\Omega)$ which we will denote as $\mathcal{E}_h$, $\mathcal{V}_h$ and $\mathcal{V}_{h,0}$. As the mesh size shrinks to zero, the dimension of $\mathcal{V}_h$ and $\mathcal{E}_h$ skyrocket to infinity and their approximation power grows. The precise definition of these spaces is very technical and will be left for Sections 3.4 and 3.5. We can also define mappings $\mathcal{I}^{\mathcal{V}_h} : H(\mathbf{rot};\Omega) \to \mathcal{V}_h$ and

$\mathcal{I}^{\mathcal{E}_h} : H(\text{div};\Omega) \to \mathcal{E}_h$ to interpolate every function in the continuous modeling spaces. Finally, in these spaces there is an inner product that gives a notion of geometry, and we denote by

$$\forall E, D \in H(\mathbf{rot};\Omega): \quad \Big(\mathcal{I}^{\mathcal{V}_h}(E), \mathcal{I}^{\mathcal{V}_h}(D)\Big)_{\mathcal{V}_h} \approx \big(E, D\big), \tag{3.30a}$$

$$\forall \boldsymbol{B}, \boldsymbol{C} \in H(\text{div};\Omega): \quad \Big(\mathcal{I}^{\mathcal{E}_h}(\boldsymbol{B}), \mathcal{I}^{\mathcal{E}_h}(\boldsymbol{C})\Big)_{\mathcal{E}_h} \approx \big(\boldsymbol{B}, \boldsymbol{C}\big). \tag{3.30b}$$

Thus, the virtual element formulation of system (3.29) is: *find* $\big\{\boldsymbol{B}_h^n\big\}_{n=0}^N \subset \mathcal{E}_h$ *and* $\big\{E_h^{n+\theta}\big\}_{n=0}^{N-1} \subset \mathcal{V}_h$ *such that for all* $(\boldsymbol{C}_h, D_h) \in \mathcal{E}_h \times \mathcal{V}_{h,0}$ *it holds that:*

$$\Big(\frac{\boldsymbol{B}_h^{n+1} - \boldsymbol{B}_h^n}{\Delta t}, \boldsymbol{C}_h\Big)_{\mathcal{E}_h} + \Big(\mathbf{rot}\, E_h^{n+\theta}, \boldsymbol{C}_h\Big)_{\mathcal{E}_h} = 0 \tag{3.31a}$$

$$R_m\big(E_h^{n+\theta}, D_h\big)_{\mathcal{V}_h} + R_m\big(\mathcal{I}^{\mathcal{V}_h}\big(\boldsymbol{u} \times \Pi^{RT}\boldsymbol{B}_h^{n+\theta}\big), D_h\big)_{\mathcal{V}_h} - \big(\boldsymbol{B}_h^{n+\theta}, \mathbf{rot}\, D_h\big)_{\mathcal{E}_h} = 0 \tag{3.31b}$$

$$\boldsymbol{B}_h^{n+\theta} = \theta\boldsymbol{B}_h^{n+1} + (1-\theta)\boldsymbol{B}_h^n, \tag{3.31c}$$

$$\boldsymbol{B}_h(\cdot, 0) = \mathcal{I}^{\mathcal{E}_h}\big(\boldsymbol{B}^0\big) \quad \text{with} \quad \text{div}\, \boldsymbol{B}^0 = 0. \tag{3.31d}$$

As before, in the above it is implicit that $E_h \equiv \mathcal{I}^{\mathcal{V}_h}(E_b)$ along the boundary of the computational domain. This formulation uses a leap-frog time scheme in which we use $\theta \in [0, 1]$.

3.4 The Nodal Space

The formal definition of the local nodal space is

$$\mathcal{V}_h(P) := \Big\{ D_h \in H(\mathbf{rot};\mathsf{P}) : \text{rot}\,\mathbf{rot}\, D_h = 0, \;\; D_h \in C(\partial\mathsf{P}), \\ \forall \mathsf{e} \in \partial\mathsf{P} \;\; D_h \in \mathbb{P}_1(\mathsf{e})\Big\}. \tag{3.32}$$

For any $D_h \in \mathcal{V}_h(\mathsf{P})$ we assign the degrees of freedom

V The evaluation $D_h(\mathsf{v})$ for every node v of the cell P.

As in the classic finite element method a space of shape functions endowed with a set of degrees of freedom is not very useful unless it is **unisolvent**. This is to say that for every function in $\mathcal{V}_h(\mathsf{P})$ there is one and only one set of degrees of freedom. And conversely, for every set of degrees of freedom there is one and only one function in $\mathcal{V}_h(\mathsf{P})$ that has that set assigned. Thus, the next result we present addresses this property in the particular case of $\mathcal{V}_h(\mathsf{P})$. We note that a proof in full generality can be found in [16]. In order to prove this result we will introduce the $\cdot^I$ notation. If $D_h \in \mathcal{V}_h(\mathsf{P})$ then D_h^I is the array of degrees of freedom of D_h, meaning

$$D_h^I = \Big(D_h(\mathsf{v}_1), \ldots, D_h(\mathsf{v}_N)\Big)^T. \tag{3.33}$$

Thus, unisolvency refers to the bijectivity of the map $\cdot^I$.

Theorem 3.40.1 *The finite element composed by the domain P, the spaces $\mathsf{v}_h(P)$ and the degrees of freedom **V** is unisolvent.*

Proof. Let $\{\mathsf{v}_i : 1 \leq i \leq N\}$ be the set of vertices of P. Consider the set of functions $\mathcal{B} = \{D_h^i : 1 \leq i \leq N_\mathsf{v}\}$ each defined as the solution to

$$\begin{aligned} -\triangle D_h^i = \operatorname{rot}\mathbf{rot}\, D_h^i = 0 \quad \text{in} \quad \mathsf{P}, \\ D_h^i(\mathsf{v}_j) = \delta_{ij}, \quad \forall \mathsf{e} \in \partial\mathsf{P} \;\; D_h^i \in \mathbb{P}_1(\mathsf{e}), \end{aligned} \tag{3.34}$$

where δ_{ij} represents the Kronecker delta meaning that

$$\delta_{ij} = \begin{cases} 1 \quad \text{if} \quad i = j, \\ 0 \quad \text{otherwise.} \end{cases} \tag{3.35}$$

It is well-known that the problem presented in (3.34) is well-posed, see [26, 56, 81]. This result guarantees the existence of the functions in $\mathcal{B}$. It is also immediate to check that $\mathcal{B} \subset \mathcal{V}_h(\mathsf{P})$

is a basis for $\mathcal{V}_h(\mathsf{P})$. Therefore, the dimension of $\mathcal{V}_h(\mathsf{P})$ is exactly the number of vertices in P implying that the domain and range of $\cdot^I$ have the same dimension. To finish the proof we will show that $\cdot^I$ is injective. Consider $D_h \in \mathcal{V}_h(\mathsf{P})$ such that $D_h^I = \mathbf{0}$. Then, by definition D_h must solve

$$\begin{aligned} -\triangle D_h = \operatorname{rot} \mathbf{rot}\, D_h = 0 \quad \text{in} \quad \mathsf{P}, \\ D_h = 0 \quad \text{along} \quad \partial\mathsf{P}. \end{aligned} \tag{3.36}$$

A problem for which the only solution is $D_h = 0$. □

The result of Theorem 3.40.1 allows us to identify each function in $\mathcal{V}_h(\mathsf{P})$ with its degrees of freedom and allows us to formally define the mapping $\mathcal{I}_{\mathsf{P}}^{\mathcal{V}_h} : H(\mathbf{rot}; \mathsf{P}) \to \mathcal{V}_h(\mathsf{P})$ by requiring that $\mathcal{I}_{\mathsf{P}}^{\mathcal{V}_h} D$ have the same set of degrees of freedom as those of D.

The next step is building a sense of geometry in $\mathcal{V}_h(\mathsf{P})$. We do this by defining an inner product. Generally, in the literature on the VEM, inner products are defined through a projector the L^2-orthogonal projection $\Pi^0 : \mathcal{V}_h(\mathsf{P}) \to \mathbb{P}_1(\mathsf{P})$. Unfortunately, this projector is not computable from the degrees of freedom in $\mathcal{V}_h(\mathsf{P})$ alone. The solution typically provided involves enhancing the space $\mathcal{V}_h(\mathsf{P})$ into another where such a projector is computable, see [3, 15, 16]. We will take a different approach. Instead we will construct an oblique projector $\Pi : \mathcal{V}_h(\mathsf{P}) \to \mathbb{P}_1(\mathsf{P})$ satisfying:

P1 The projection ΠD_h is computable from the degrees of freedom of D_h.

P2 If $D_h \in \mathbb{P}_1(\mathsf{P})$ then $\Pi D_h = D_h$.

P3 There exists a constant $C > 0$ independent of mesh-size and time-step such that

$$\|\Pi D_h\|_{0,\mathsf{P}} \leq C \|D_h\|_{0,\mathsf{P}}. \tag{3.37}$$

The reason we do this will be clear in Section 3.7. We have three examples of these types of projectors which can be found in Section 3.11. For now assume that such Π is given to us. Then,

following the construction in Section 2.3 we define

$$\Big(E_h, D_h\Big)_{\mathcal{V}_h(\mathsf{P})} = \big(\Pi E_h, \Pi D_h\big) + \mathcal{S}^{\mathsf{v}}((1-\Pi)E_h, (1-\Pi)D_h). \tag{3.38}$$

The bilinear form $\mathcal{S}^{\mathsf{v}}$ is picked such that

$$\exists s_*, s^* > 0 \quad \forall D_h \in \ker\Pi \cap \mathcal{V}_h(\mathsf{P}): \quad s_*\|D_h\|^2_{0,\mathsf{P}} \leq \mathcal{S}^{\mathsf{v}}(D_h, D_h) \leq s^*\|D_h\|_{0,\mathsf{P}}. \tag{3.39}$$

The value of the constants s_* and s^* should not depend on the characteristics of the mesh. We pick a canonical choice in Section 2.3. However, readers are referred to [49, 71] for more examples. This inner product defines a norm in $\mathcal{V}_h(\mathsf{P})$ by $|||D_h|||_{\mathcal{V}_h(\mathsf{P})} = \big(D_h, D_h\big)^{1/2}_{\mathcal{V}_h(\mathsf{P})}$. It turns out that when Π satisfies properties **P1**-**P3** the inner product in equation (3.38) will obtain two properties. These are summarized in the next theorem.

Theorem 3.40.2 *The inner product defined in equation* (3.38) *has first order* ***polynomial accuracy****. This is to say that*

$$\forall p, q \in \mathbb{P}_1(\mathsf{P}) \subset \mathcal{V}_h(\mathsf{P}): \quad \Big(p, q\Big)_{\mathcal{V}_h(\mathsf{P})} = \big(p, q\big). \tag{3.40}$$

Moreover, this inner product also satisfies the following ***stability*** *property. There exists constants $C_*, C^* > 0$ independent of the mesh-size and time-step such that*

$$\forall D_h \in \mathcal{V}_h(\mathsf{P})^2: \quad \alpha_*\|D_h\|^2_{0,\mathsf{P}} \leq |||D_h|||^2_{\mathcal{V}_h(\mathsf{P})} \leq \alpha^*\|D_h\|^2_{0,\mathsf{P}} \tag{3.41}$$

Proof. To check the property in (3.40) pick $p, q \in \mathbb{P}_1(\mathsf{P})$ then by property **P2** we have that

$$\Pi p = p \text{ and } \Pi q = q. \tag{3.42}$$

This implies that the right hand side of (3.38) is simply $\big(p, q\big)$. The proof of (3.41) is a bit more

involved. First, we note that

$$\|D_h\|_{0,\mathsf{P}}^2 = \left(\|\Pi D_h\|_{0,\mathsf{P}} + \|1-\Pi D_h\|_{0,\mathsf{P}}\right)^2 \leq$$
$$2\left(\|\Pi \boldsymbol{v}_h\|_{0,\mathsf{P}}^2 + \|1-\Pi D_h\|_{0,\mathsf{P}}^2\right) \leq (\alpha_*)^{-1}|||D_h|||_{\mathcal{V}_h(P)}, \tag{3.43}$$

where $\alpha_* = (\max\{s^*, 2\})^{-1}$. To attain the upper bound of (3.41) we use

$$|||D_h|||_{\mathcal{V}_h(\mathsf{P})} \leq \|\Pi D_h\|_{0,\mathsf{P}}^2 + s^*\|(1-\Pi)D_h\|_{0,\mathsf{P}}^2 \tag{3.44}$$
$$\leq \|\Pi\|^2\|D_h\|_{0,\mathsf{P}}^2 + s^*\|1-\Pi\|^2\|D_h\|_{0,\mathsf{P}}^2 \tag{3.45}$$
$$\leq \alpha^*\|D_h\|_{0,\mathsf{P}}^2, \tag{3.46}$$

where $\alpha^* = \max\{\|\Pi\|^2, s^*\|I-\Pi\|^2\}$. We note property **P3** gives a bound for $\|\Pi\|$ that is independent from the mesh-size and time-step. □

Having defined the nodal space locally and endowed it with an inner product we proceed to do the same at the global scale. Consider a mesh Ω_h made of polygons satisfying the assumptions in Section 2.4. Over this space we define the global nodal space as the set of all functions then when restricted to each cell will belong to the local nodal space. Formally this is to say that

$$\mathcal{V}_h = \left\{D_h \in H(\mathbf{rot};\Omega) : \forall \mathsf{P} \in \Omega_h \quad D_{h|\mathsf{P}} \in \mathcal{V}_h(\mathsf{P})\right\}. \tag{3.47}$$

Likewise, we define the global inner product as the sum of the local contributions, i.e.

$$\forall E_h, D_h \in \mathcal{V}_h : \quad \Big(E_h, D_h\Big)_{\mathcal{V}_h} = \sum_{\mathsf{P}\in\Omega_h} \big(E_{h|\mathsf{P}}, D_{h|\mathsf{P}}\big)_{\mathcal{V}_h(\mathsf{P})}. \tag{3.48}$$

The global norm is then defined as

$$\forall D_h \in \mathcal{V}_h : \quad \|D_h\|_{\mathcal{V}_h} = \Big(D_h, D_h\Big)^{1/2}. \tag{3.49}$$

Due to the fact that each of the local contributions satisfies an accuracy and stability property as evidenced in Theorem 3.40.2, the global inner product will also inherit these properties. For future reference we summarize them in the following Theorem.

Corollary 3.40.1 *The inner product defined in* (3.48) *satisfies the* ***accuracy*** *property for piecewise-linear polynomials. If for every* $\mathsf{P} \in \Omega_h$ *it is the case that* $p_{|\mathsf{P}}, q_{|\mathsf{P}} \in \mathbb{P}_1(\mathsf{P})$ *then*

$$\big(p, q\big)_{\mathcal{V}_h} = \big(p, q\big). \tag{3.50}$$

The following ***stability*** *condition is also satisfied*

$$\exists \beta_*, \beta^* > 0 \; \forall D_h \in \mathcal{V}_h : \quad \beta_* \|D_h\|_{0,\Omega}^2 \leq |||D_h|||_{\mathcal{V}_h}^2 \leq \beta^* \|D_h\|_{0,\Omega}^2. \tag{3.51}$$

The constants β_* *and* β^* *are independent of the mesh-size and time-step.*

Proof. The result in (3.50) follows immediately from (3.40). By adding the local contributions in (3.41) we obtain (3.51). The value of the constants is

$$\beta_* = \min\{\alpha_*\} \quad \text{and} \quad \beta^* = \max\{\alpha^*\}. \tag{3.52}$$

The extrema above are taken over the elements. According to Theorem 3.40.2 each element defines a pair α_* and α^*. □

The final definition we need involves the Fortin operator $\mathcal{I}^{\mathcal{V}_h} : H(\mathbf{rot}; \Omega) \to \mathcal{V}_h$. We define it as the pasting together of the local $\mathcal{I}_{\mathsf{P}}^{\mathcal{V}_h}$ previously defined. Thus

$$\forall D_h \in \mathcal{V}_h \; \forall \mathsf{P} \in \Omega_h : \quad \mathcal{I}^{\mathcal{V}_h}(D_h)_{|\mathsf{P}} = \mathcal{I}_{\mathsf{P}}^{\mathcal{V}_h}(D_{h|\mathsf{P}}). \tag{3.53}$$

3.5 The Edge Space

The next space we tackle will, in some sense, be the discretization of the larger space $H(\mathrm{div};\Omega)$. Like before, we begin by defining a local space over a cell P. The formal definition is

$$\mathcal{E}_h(\mathsf{P}) := \Big\{ \boldsymbol{C}_h \in H(\mathrm{div};\mathsf{P}) \cap H(\mathrm{rot};\mathsf{P}) \,:\mathrm{div}\, \boldsymbol{C}_h \in \mathbb{P}_0(\mathsf{P}),\ \ \mathrm{rot}\, \boldsymbol{C}_h = 0, \\ \forall \mathsf{e} \in \partial\mathsf{P} \quad \boldsymbol{C}_{h|\mathsf{e}} \cdot \boldsymbol{n} \in \mathbb{P}_0(\mathsf{e}) \Big\}. \tag{3.54}$$

For a function $\boldsymbol{C}_h \in \mathcal{E}_h(\mathsf{P})$ we will associate the degrees of freedom

E Fluxes across each edge, meaning the quantities

$$\forall \mathsf{e} \in \partial\mathsf{P}: \quad \frac{1}{|\mathsf{e}|}\int_{\mathsf{e}} \boldsymbol{C}_h \cdot \boldsymbol{n} d\ell. \tag{3.55}$$

Next we will discuss the unisolvency of $\mathcal{E}_h(\mathsf{P})$ with the degrees of freedom **E**. Like before, we need to introduce the notation

$$\forall \boldsymbol{C}_h \in \mathcal{E}_h(\mathsf{P}): \quad \boldsymbol{C}_h^I = \left(\frac{1}{|\mathsf{e}_1|}\int_{\mathsf{e}_1} \boldsymbol{C}_h \cdot \boldsymbol{n} d\ell, \ldots, \frac{1}{|\mathsf{e}_N|}\int_{\mathsf{e}_N} \boldsymbol{C}_h \cdot \boldsymbol{n} d\ell \right)^T. \tag{3.56}$$

Unisolvency is settled in the following theorem.

Theorem 3.50.1 *The finite element defined by the domain P, the space of shape functions $\mathcal{E}_h(\mathsf{P})$ and the degrees of freedom $\boldsymbol{E}$ is unisolvent.*

Proof. This proof is very similar to that of Theorem 3.40.1. First we construct a basis for $\mathcal{E}_h(\mathsf{P})$ as a vector space. We enumerate the edges $\{\mathsf{e}_i : 1 \le i \le N\}$ and define the set $\mathcal{B} := \{\boldsymbol{C}_h^1, \ldots, \boldsymbol{C}_h^N\}$

each function defined as the solution to the problems

$$\begin{aligned} &\operatorname{div} \boldsymbol{C}_h^i = \frac{|\mathsf{e}_i|}{|\mathsf{P}|}, \quad \operatorname{rot} \boldsymbol{C}_h^i = 0 \quad \text{in} \quad \mathsf{P}, \\ &\boldsymbol{C}_h^i \cdot \boldsymbol{n}_{\mathsf{e}_j} = \delta_{i,j}. \end{aligned} \tag{3.57}$$

Again, $\delta_{i,j}$ is the Kronecker delta, defined as

$$\delta_{i,j} = \begin{cases} 1 & i = j \\ 0 & \text{otherwise} \end{cases}. \tag{3.58}$$

The well-posedness of div-curl systems is guaranteed by the discussion in [6], which means that the functions in $\mathcal{B}$ in fact exist. Like before, the set $\mathcal{B}$ is in fact a basis for $\mathcal{E}_h(\mathsf{P})$. This implies that the dimension of $\mathcal{E}_h(\mathsf{P})$ is the number of edges along $\partial\mathsf{P}$. In order to finish the proof we only require a proof that $\cdot^I$ is injective. Pick $\boldsymbol{C}_h$ such that $\boldsymbol{C}_h^I = \mathbf{0}$. In this case $\boldsymbol{C}_h$ must be a solution to the system

$$\begin{aligned} &\operatorname{div} \boldsymbol{C}_h = 0, \quad \operatorname{rot} \boldsymbol{C}_h = 0 \quad \text{in} \quad \mathsf{P}, \\ &\boldsymbol{C}_h \cdot \boldsymbol{n} = 0 \quad \text{along} \quad \partial\mathsf{P}. \end{aligned} \tag{3.59}$$

Since the solution to this system must be unique and $\boldsymbol{C}_h = \mathbf{0}$ is a solution then this must be the only solution. □

With a result stating the unisolvency of $\mathcal{E}_h(\mathsf{P})$ we can define the Fortin projector $\mathcal{I}_{\mathsf{P}}^{\mathcal{E}_h} : H(\operatorname{div};\mathsf{P}) \to \mathcal{E}_h(\mathsf{P})$ by enforcing that for any $\boldsymbol{C}_h \in H(\operatorname{div};\mathsf{P})$ the image $\mathcal{I}_{\mathsf{P}}^{\mathcal{E}_h}(\boldsymbol{C}_h)$ and the primitive $\boldsymbol{C}_h$ share the same value for their degrees of freedom $\mathbf{E}$. Next, we define a pair of important projectors in the space $\mathcal{E}_h(\mathsf{P})$. They are the following L^2-orthogonal projections $\Pi^0 : \mathcal{E}_h(\mathsf{P}) \to \mathbb{P}_0(\mathsf{P})$, $\Pi_{\mathsf{P}}^{RT} : \mathcal{E}_h(\mathsf{P}) \to \mathrm{RT}_0(\mathsf{P})$ whose images are defined as the solution to the

variational problems

$$\forall \boldsymbol{C}_h \in \mathcal{E}_h(\mathsf{P}) \;\; \forall \boldsymbol{q} \in [\mathbb{P}_0(\mathsf{P})]^2 : \quad \left(\boldsymbol{C}_h - \Pi^0 \boldsymbol{C}_h, \boldsymbol{q}\right) = 0, \tag{3.60}$$

$$\forall \boldsymbol{q} \in \mathrm{RT}_0(\mathsf{P}) : \quad \left(\boldsymbol{C}_h - \Pi^{RT}_{\mathsf{P}} \boldsymbol{C}_h, \boldsymbol{q}\right) = 0 \tag{3.61}$$

where the space $\mathrm{RT}_0(\mathsf{P})$ is defined as

$$\mathrm{RT}_0(\mathsf{P}) = \left\{ a \begin{pmatrix} 1 \\ 0 \end{pmatrix} + b \begin{pmatrix} 0 \\ 1 \end{pmatrix} + c \begin{pmatrix} x \\ y \end{pmatrix} : \quad a, b, c \in \mathbb{R} \right\}. \tag{3.62}$$

We note that these projectors are computable using the degrees of freedom **E**. Pick $\boldsymbol{q} \in [\mathrm{RT}_0(\mathsf{P})]^2$ and find $p \in \mathbb{P}_1(\mathsf{P})$ such that $\nabla p = \boldsymbol{q}$. Then, applying the Green's Theorem we find that

$$\forall \boldsymbol{C}_h \in \mathcal{E}_h(\mathsf{P}) : \quad \int_{\mathsf{P}} \boldsymbol{C}_h \cdot \boldsymbol{q} dA = \int_{\partial \mathsf{P}} p \boldsymbol{C}_h \cdot \boldsymbol{n} d\ell - \int_{\mathsf{P}} (\operatorname{div} \boldsymbol{C}_h) p dA. \tag{3.63}$$

Note that since $\operatorname{div} \boldsymbol{C}_h \in \mathbb{P}_0(\mathsf{P})$ then it can be reconstructed from the Divergence Theorem

$$\operatorname{div} \boldsymbol{C}_h = \frac{1}{|\mathsf{P}|} \int_{\partial \mathsf{e}} \boldsymbol{C}_h \cdot \boldsymbol{n} d\ell = \frac{1}{|\mathsf{P}|} \sum_{\mathsf{e} \in \partial \mathsf{P}} \int_{\partial \mathsf{e}} \boldsymbol{C}_h \cdot \boldsymbol{n} d\ell. \tag{3.64}$$

Thus the area integral in the right hand side of (3.63) can be computed using only the degrees of freedom **E**. This is also the case for the line integral in the same expression (3.63) since

$$\int_{\partial \mathsf{P}} \boldsymbol{C}_h \cdot \boldsymbol{n} p d\ell = \sum_{\mathsf{e} \in \partial \mathsf{P}} \boldsymbol{C}_h \cdot \boldsymbol{n} \int_{\mathsf{e}} p d\ell. \tag{3.65}$$

Hence, the information necessary about the functions in the space $\mathcal{E}_h(\mathsf{P})$ can be read off the degrees of freedom. Note that in the case that we are constructing Π^0 and $\boldsymbol{q} \in \mathbb{P}_0(\mathsf{P}) \subset \mathrm{RT}_0(\mathsf{P})$ the we can pick p such that $\int_{\mathsf{P}} p dA = 0$. Using this trick we can make the area integral vanish

since

$$\forall \boldsymbol{C}_h \in \mathcal{E}_h(\mathsf{P}): \quad \int_{\mathsf{P}} (\operatorname{div} \boldsymbol{C}_h) p dA = (\operatorname{div} \boldsymbol{C}_h) \int_{\mathsf{P}} p dA = 0. \tag{3.66}$$

In the above we used that, by definition, $\operatorname{div} \boldsymbol{C}_h \in \mathbb{P}_0(\mathsf{P})$. Either projector can be used to define an inner product. In this manuscript we will choose to use Π^0 to define the inner product and Π^{RT} to approximate the term "$\boldsymbol{u} \times \boldsymbol{B}$" as can be evidenced in the discrete variational formulation (3.31). The main conflict with the aforementioned term is that, for the magnetic field, we only have access to its fluxes across the edges while the inner product in the variational formulation requires nodal evaluations. We amend this inconsistency by projecting the magnetic field onto a polynomial space and extract the necessary evaluations from this projection. Thus, any of the two projectors can fulfill this job. However, more complex MHD models have terms of the form

$$\big((\mathbf{rot}\, \boldsymbol{B}) \times \boldsymbol{B}, D\big). \tag{3.67}$$

Such a quantity cannot be estimated using Π^0 since the codomain of this projector is the space of constants and their curl is always zero. In this case using the projector Π^{RT} is ideal for low order approximations.

Having defined the necessary projectors in this space we introduce the following inner product

$$\forall \boldsymbol{B}_h, \boldsymbol{C}_h \in \mathcal{E}_h(\mathsf{P}): \quad \big(\boldsymbol{B}_h, \boldsymbol{C}_h\big)_{\mathcal{E}_h(\mathsf{P})} = \big(\Pi^0 \boldsymbol{B}_h, \Pi^0 \boldsymbol{C}_h\big) + \mathcal{S}^{\mathsf{e}}((\mathcal{I} - \Pi^0)\boldsymbol{B}_h, (\mathcal{I} - \Pi^0)\boldsymbol{C}_h). \tag{3.68}$$

As before we require that $\mathcal{S}^{\mathsf{e}}$ be a continuous bilinear form satisfying

$$\exists s_*, s^* > 0 \quad \forall \boldsymbol{C}_h \in \ker \Pi^0 \cap \mathcal{E}_h(\mathsf{P}): \quad s_* \|\boldsymbol{C}_h\|^2_{0,\mathsf{P}} \leq \mathcal{S}^{\mathsf{e}}(\boldsymbol{C}_h, \boldsymbol{C}_h) \leq s^* \|\boldsymbol{C}_h\|^2_{0,\mathsf{P}}. \tag{3.69}$$

We remind the reader that the canonical choice is described in Section 2.3. Check [49, 71] for more examples. The value of the constants s_*, s^* need not be the same as those in equation (3.39),

they are generic constants. Like before, this inner product defines a norm

$$\forall \boldsymbol{C}_h \in \mathcal{E}_h(\mathsf{P}): \quad |||\boldsymbol{C}_h|||_{\mathcal{E}_h(\mathsf{P})} = \big(\boldsymbol{C}_h, \boldsymbol{C}_h\big)^{1/2}_{\mathcal{E}_h(\mathsf{P})}. \tag{3.70}$$

This norm satisfies a set of properties regarding its accuracy and stability. They are summarized in the Theorem below

Theorem 3.50.2 *The inner product defined in* (3.68) *satisfies the* ***accuracy*** *property over the space of constants. Rigorously, what we mean is that if* $\boldsymbol{p}, \boldsymbol{q} \in [\mathbb{P}_0(\mathsf{P})]^2$ *then*

$$\big(\boldsymbol{p}, \boldsymbol{q}\big)_{\mathcal{E}_h(\mathsf{P})} = \big(\boldsymbol{p}, \boldsymbol{q}\big). \tag{3.71}$$

Moreover, the norm this inner product defines is stable with respect to the norm in $L^2(\mathsf{P})$*. Thus,*

$$\exists \gamma_*, \gamma^* > 0: \ \ \forall \boldsymbol{C}_h \in \mathcal{E}_h(\mathsf{P}): \quad \gamma_* \|\boldsymbol{C}_h\|^2_{0,\mathsf{P}} \leq |||\boldsymbol{C}_h|||^2_{\mathcal{E}_h(\mathsf{P})} \leq \gamma^* \|\boldsymbol{C}_h\|^2_{0,\mathsf{P}}. \tag{3.72}$$

The constants γ_*, γ^* *are independent of mesh-size and time-step.*

Proof. We omit most of the steps in the proof of this Theorem since it is essentially the same as the one presented for Theorem 3.40.2. However, we will show that Π^0 satisfies properties **P1**-**P3** in Section 3.4. Pick $\boldsymbol{C}_h \in \mathcal{E}_h(\mathsf{P})$ arbitrarily and consider a basis for $[\mathbb{P}_0(\mathsf{P})]^2$ with elements $\boldsymbol{b}_1$ and $\boldsymbol{b}_2$. Then, we know that

$$\Pi^0 \boldsymbol{C}_h = a\boldsymbol{b}_1 + b\boldsymbol{b}_2. \tag{3.73}$$

We can find the identity of the constants a and b as the solution to the system

$$\begin{pmatrix} \|\boldsymbol{b}_1\|^2_{0,\mathsf{P}} & \big(\boldsymbol{b}_1, \boldsymbol{b}_2\big) \\ \big(\boldsymbol{b}_2, \boldsymbol{b}_1\big) & \|\boldsymbol{b}_2\|^2_{0,\mathsf{P}} \end{pmatrix} \begin{pmatrix} a \\ b \end{pmatrix} = \begin{pmatrix} \big(\Pi^0 \boldsymbol{C}_h, \boldsymbol{b}_1\big) \\ \big(\Pi^0 \boldsymbol{C}_h, \boldsymbol{b}_2\big) \end{pmatrix}. \tag{3.74}$$

The necessary information to ensemble this system can be obtained from the definition of Π^0 in (3.60) and the formula in (3.63) thus Π^0 is computable and satisfies **P1**.

Any projector, by definition, satisfies **P2** in particular Π^0 satisfies it as well. Finally, since $\Pi^0 \boldsymbol{C}_h$ and $(\mathcal{I} - \Pi^0)\boldsymbol{C}_h$ are orthogonal then

$$\|\boldsymbol{C}_h\|_{0,\mathsf{P}} = \|\Pi^0 \boldsymbol{C}_h\|_{0,\mathsf{P}} + \|(\mathcal{I} - \Pi^0)\boldsymbol{C}_h\|_{0,\mathsf{P}}. \tag{3.75}$$

This implies that

$$\|\Pi^0 \boldsymbol{C}_h\|_{0,\mathsf{P}} \leq \|\boldsymbol{C}_h\|_{0,\mathsf{P}}. \tag{3.76}$$

Thus, Π^0 satisfies **P3**.

□

With Theorem 3.50.2 we conclude the construction of the notion of geometry in the space $\mathcal{E}_h(\mathsf{P})$. We proceed to present the global space $\mathcal{E}_h$. Consider a mesh Ω_h. Over each of the cells we can define a local space $\mathcal{E}_h(\mathsf{P})$. The global space is a "pasting together" of the functions in each of these global spaces. Formally,

$$\mathcal{E}_h = \left\{ \boldsymbol{C}_h \in H(\text{div}; \Omega) : \forall \mathsf{P} \in \Omega_h \quad \boldsymbol{C}_{h|\mathsf{P}} \in \mathcal{E}_h(\mathsf{P}) \right\}. \tag{3.77}$$

In this space we can define the inner product

$$\Big(\boldsymbol{B}_h, \boldsymbol{C}_h \Big)_{\mathcal{E}_h} = \sum_{\mathsf{P} \in \Omega_h} \Big(\boldsymbol{B}_{h|\mathsf{P}}, \boldsymbol{C}_{h|\mathsf{P}} \Big)_{\mathcal{E}_h(\mathsf{P})}. \tag{3.78}$$

And, the associated norm is

$$\forall \boldsymbol{C}_h \in \mathcal{E}_h : \quad |||\boldsymbol{C}_h|||_{\mathcal{E}_h} = \big(\boldsymbol{C}_h, \boldsymbol{C}_h \big)_{\mathcal{E}_h}^{1/2} \tag{3.79}$$

The inner product and norms defined also satisfy important properties that we list in the following corollary.

Corollary 3.50.1 *The inner product defined in* (3.78) *is exact for piecewise constant functions.This*

is to say that if $\boldsymbol{p}, \boldsymbol{q}$ *are such that for any cell* P *in the mesh* Ω_h *they satisfy* $\boldsymbol{p}_{|\mathsf{P}}, \boldsymbol{q}_{|\mathsf{P}} \in [\mathbb{P}_0(\mathsf{P})]^2$ *then*

$$\big(\boldsymbol{p}, \boldsymbol{q}\big)_{\mathcal{E}_h} = \big(\boldsymbol{p}, \boldsymbol{q}\big). \tag{3.80}$$

Moreover, the norm in (3.68) *is equivalent to the norm in the space* $L^2(\Omega)$*. This is to say that there exists constants* $\delta_*, \delta^* > 0$*, independent of the mesh-size and time-step such that*

$$\forall \boldsymbol{C}_h \in \mathcal{E}_h : \quad \delta_* \|\boldsymbol{C}_h\|_{0,\Omega}^2 \leq |||\boldsymbol{C}_h|||_{\mathcal{E}_h}^2 \leq \delta^* \|\boldsymbol{C}_h\|_{0,\Omega}^2. \tag{3.81}$$

We omit the proof of corollary since it is immediate from Theorem 3.50.2. The commentary in the proof of Corollary 3.40.1 applies here with the difference replacing the constants α_*, α^* being replaced by γ_*, γ^* and β_*, β^* replaced by δ_*, δ^* respectively.

We finish this section by extending the definition of the Fortin projector $\mathcal{I}_{\mathsf{P}}^{\mathcal{E}_h}$ and the orthogonal projector Π_{P}^{RT} which are defined for individual cells to the entire mesh. This is done by requiring that the restriction of the global operator agrees with the local operator. This is to say that for any $\boldsymbol{C}_h \in \mathcal{E}_h$ it is the case that

$$\forall \mathsf{P} \in \Omega_h : \quad \mathcal{I}^{\mathcal{E}_h}(\boldsymbol{C}_h)_{|\mathsf{P}} = \mathcal{I}_{\mathsf{P}}^{\mathcal{E}_h}(\boldsymbol{C}_{h|\mathsf{P}}) \quad \text{and} \quad (\Pi^{RT}\boldsymbol{C}_h)_{|\mathsf{P}} = \Pi_{\mathsf{P}}^{RT}(\boldsymbol{C}_{h|\mathsf{P}}). \tag{3.82}$$

3.6 The Cell Space

The final, and simplest, space that we need to define is the Cell space. It is the space of piecewise constants. Consider a mesh Ω_h then

$$\mathcal{P}_h = \Big\{ q_h \in L^2(\Omega) : \forall \mathsf{P} \in \Omega_h \quad q_{h|\mathsf{P}} \in \mathbb{P}_0(\mathsf{P}) \Big\}. \tag{3.83}$$

To every function $q \in \mathcal{P}_h$ we associate the degrees of freedom:

D Averages over the cells. Meaning the quantities

$$\forall \mathsf{P} \in \Omega_h : \quad \frac{1}{|P|} \int_{\mathsf{P}} q_h dA. \tag{3.84}$$

This space is trivially unisolvent since the constant value that comes as the restriction of a function to a cell is precisely the degree of freedom associated with said cell. We can define the Fortin projector as the operator $\mathcal{I}^{\mathcal{P}_h} : L^2(\Omega) \to \mathcal{P}_h$ such that

$$\forall q \in L^2(\Omega) \;\; \forall \mathsf{P} \in \Omega_h : \quad (\mathcal{I}^{\mathcal{P}_h} q)_{|\mathsf{P}} = \frac{1}{|\mathsf{P}|} \int_{\mathsf{P}} q_h dA. \tag{3.85}$$

We will endow this space with the following inner product

$$\forall p_h, q_h \in \mathcal{P}_h : \quad \big(p_h, q_h\big)_{\mathcal{P}_h} = \sum_{|\mathsf{P}|} p_{h|\mathsf{P}} |\mathsf{P}| q_{h|\mathsf{P}}. \tag{3.86}$$

A quick computation will show that this inner product is the exact $L^2(\Omega)$ inner product when restricted to $\mathcal{P}_h$. Indeed,

$$\forall p_h, q_h \in \mathcal{P}_h : \quad \big(p_h, q_h\big)_{\mathcal{P}_h} = \big(p_h, q_h\big). \tag{3.87}$$

Therefore, the associated norm, given by

$$\forall q_h \in \mathcal{P}_h : \quad |||q_h|||_{\mathcal{P}_h} = \big(q_h, q_h\big)^{1/2}_{\mathcal{P}_h}, \tag{3.88}$$

is in fact exactly the norm in the space $L^2(\Omega)$ when restricted to $\mathcal{P}_h$. Thus,

$$\forall q_h \in \mathcal{P}_h : \quad |||q_h|||_{\mathcal{P}_h} = \|q_h\|_{0,\Omega}. \tag{3.89}$$

3.7 The De-Rham Complex and the Condition on the Divergence of B_h

In previous sections we defined and studied each of the spaces $\mathcal{V}_h, \mathcal{E}_h$ and $\mathcal{P}_h$. Here we explore the relationships between these spaces. It is well-known that the spaces $H(\mathbf{rot}; \Omega), H(\text{div}; \Omega)$ and $L^2(\Omega)$ form a chain of the form

$$H(\mathbf{rot}; \Omega) \xrightarrow{\mathbf{rot}} H(\text{div}; \Omega) \xrightarrow{\text{div}} L^2(\Omega). \tag{3.90}$$

Moreover, in the case that Ω_h is simply connected, the chain above is exact. This is to say that

$$\mathbf{rot}\, H(\text{rot}; \Omega) = \{\boldsymbol{C} \in H(\text{div}; \Omega) : \text{div}\, \boldsymbol{C} = 0\}. \tag{3.91}$$

A formal proof of this fact can be found in [75]. In the spirit of constructing a discrete version of the continuous problem, the spaces $\mathcal{V}_h, \mathcal{E}_h$ and $\mathcal{P}_h$ also form a similar exact chain

$$\mathcal{V}_h \xrightarrow{\mathbf{rot}} \mathcal{E}_h \xrightarrow{\text{div}} \mathcal{P}_h. \tag{3.92}$$

Proving this result takes tools that we do not have currently. For now we prove that the chain above is well-defined.

Lemma 3.70.1 *The following statements hold*

$$\mathbf{rot}\, \mathcal{V}_h \subset \mathcal{E}_h \quad \textit{and} \quad \textit{div}\, \mathcal{E}_h \subset \mathcal{P}_h. \tag{3.93}$$

Therefore, the chain in (3.92) *is well defined.*

Proof. Let P be a cell in the mesh Ω_h and $D_h \in \Omega_h$ then by definition we have

$$\text{rot}\, \mathbf{rot}\, D_{h|\mathsf{P}} = 0. \tag{3.94}$$

Moreover,

$$\operatorname{div} \mathbf{rot}\, D_{h|\mathsf{P}} = 0 \in \mathbb{P}_0(\mathsf{P}). \tag{3.95}$$

Pick an edge of P, say e then since $D_h \in \mathbb{P}_1(\mathsf{e})$ it must also be the case that

$$\operatorname{rot} D_h \cdot \boldsymbol{n} = \nabla D_h \cdot \boldsymbol{t} \in \mathbb{P}_0(\mathsf{e}). \tag{3.96}$$

In the above $\boldsymbol{t}$ and $\boldsymbol{n}$ are a vector tangent and a vector normal to the edge e. The identity in (3.96) is true since if $\boldsymbol{n} = (n_1, n_2)$ is normal to e then $\boldsymbol{t} = (-n_2, n_1)$ is tangent to e, hence

$$\begin{aligned}\mathbf{rot}\, D_h \cdot \boldsymbol{n} = \begin{pmatrix} \frac{\partial}{\partial y} D_h \\ -\frac{\partial}{\partial x} D_h \end{pmatrix} \cdot \begin{pmatrix} n_1 \\ n_2 \end{pmatrix} = \frac{\partial}{\partial x} D_h(-n2) + \frac{\partial}{\partial y} D_h(n1) = \\ = \begin{pmatrix} \frac{\partial}{\partial x} D_h \\ \frac{\partial}{\partial y} D_h \end{pmatrix} \cdot \begin{pmatrix} -n_2 \\ n_1 \end{pmatrix} = \nabla D_h \cdot \boldsymbol{t}. \end{aligned} \tag{3.97}$$

Equations (3.94),(3.95) and (3.96) imply that $\mathbf{rot}\, D_{h|\mathsf{P}} \in \mathcal{E}_h(\mathsf{P})$ thus $\mathbf{rot}\, D_h \in \mathcal{E}_h$ proving the first containment in (3.93). To verify the second containment it suffices to note that, by definition, of the space $\mathcal{E}_h$ we have that any $\boldsymbol{C}_h \in \mathcal{E}_h$ verifies

$$\forall \mathsf{P} \in \Omega_h : \quad \operatorname{div} \boldsymbol{C}_{h|\mathsf{P}} \in \mathbb{P}_0(\mathsf{P}), \tag{3.98}$$

immediately implying that $\boldsymbol{C}_h \in \mathcal{P}_h$ and concluding the proof of (3.93). □

Thus, by Lemma 3.70.1 we know that if $D_h \in \mathcal{V}_h$ then $\mathbf{rot}\, D_h \in \mathcal{E}_h$. Thus, we can completely identify $\mathbf{rot}\, D_h$ if we find its degrees of freedom in $\mathcal{E}_h$. It turns out that they are computable from the degrees of freedom of $D_h \in \mathcal{V}_h$. Consider an edge e in one of the cells in the mesh Ω_h. Then, by the fundamental Theorem of line integrals we can compute

$$\frac{1}{|\mathsf{e}|} \int_{\mathsf{e}} \mathbf{rot}\, D_h \cdot \boldsymbol{n} d\ell = \frac{1}{|\mathsf{e}|} \int_{\mathsf{e}} \nabla D_h \cdot \boldsymbol{t} d\ell = \frac{D_h(\mathsf{v}_2) - D_h(\mathsf{v}1)}{|\mathsf{e}|}. \tag{3.99}$$

The points v_2 and v_1 are the endpoints of e, hence they are nodes of a cell. The identity used was proven in (3.97). Thus, from the degrees of freedom in $\mathcal{V}_h$ we can read the necessary information to completely identify the image of the rotational as a function in $\mathcal{E}_h$. The same is true about the divergence of a function in $\mathcal{E}_h$. Let $\boldsymbol{C}_h \in \mathcal{E}_h$ and pick a cell P in the mesh Ω_h. Then, by the Divergence Theorem we have that

$$\frac{1}{|\mathsf{P}|}\int_{\mathsf{P}} \operatorname{div} \boldsymbol{C}_h dA = \frac{1}{|\mathsf{P}|}\int_{\partial\mathsf{P}} \operatorname{div} \boldsymbol{C}_h dA = \frac{1}{|\mathsf{P}|}\sum_{\mathsf{e}\in\partial\mathsf{P}}\int_{\mathsf{e}} \boldsymbol{C}_h \cdot \boldsymbol{n} dA. \tag{3.100}$$

Hence, we can identify the divergence of a function in $\boldsymbol{C}_h$ based only on the degrees of freedom in $\mathcal{E}_h$.

The results summarized by equations (3.99) and (3.100) are essential in order to further study the spaces $\mathcal{V}_h, \mathcal{E}_h$ and $\mathcal{P}_h$ and their relationship with the larger spaces $H(\mathbf{rot};\Omega), H(\operatorname{div};\Omega)$ and $L^2(\Omega)$. These spaces form a diagram of the form

$$\begin{array}{ccccc} H(\mathbf{rot};\Omega) & \xrightarrow{\mathbf{rot}} & H(\operatorname{div};\Omega) & \xrightarrow{\operatorname{div}} & L^2(\Omega) \\ \downarrow{\scriptstyle \mathcal{I}^{\mathcal{V}_h}} & & \downarrow{\scriptstyle \mathcal{I}^{\mathcal{E}_h}} & & \downarrow{\scriptstyle \mathcal{I}^{\mathcal{P}_h}} \\ \mathcal{V}_h & \xrightarrow{\mathbf{rot}} & \mathcal{E}_h & \xrightarrow{\operatorname{div}} & \mathcal{P}_h. \end{array} \tag{3.101}$$

This diagram is commutative as we show in the following lemma.

Lemma 3.70.2 *The following identities hold*

$$\forall D \in H(\boldsymbol{rot};\Omega): \quad \mathcal{I}^{\mathcal{E}_h} \circ \mathbf{rot}\,(D) = \mathbf{rot}\, \circ \mathcal{I}^{\mathcal{V}_h}(D), \tag{3.102a}$$

$$\forall \boldsymbol{C} \in H(div;\Omega): \quad \mathcal{I}^{\mathcal{P}_h} \circ div\,(\boldsymbol{C}) = div\, \circ \mathcal{I}^{\mathcal{E}_h}(\boldsymbol{C}). \tag{3.102b}$$

Proof. Let $D \in H(\mathbf{rot};\Omega)$ we know that the functions lie in $\mathcal{E}_h$, hence in order to show that they are the same function we will show that they share the same value for their degrees of freedom. Let e be an edge in the mesh Ω_h with endpoints v_1 and v_2. Then, by definition the degree of

freedom associated with the function $\mathcal{I}^{\mathcal{E}_h} \circ \mathbf{rot}\,(D)$ is identical to that of $\mathbf{rot}\,D$, hence it is

$$\frac{1}{|\mathsf{e}|}\int_{\mathsf{e}} \mathbf{rot}\, D d\ell = \frac{D(\mathsf{v}_2) - D(\mathsf{v}_1)}{|\mathsf{e}|}. \tag{3.103}$$

Above we use the Fundamental Theorem of Line Integrals. On the other hand the degree of freedom associated with $\mathbf{rot}\, \circ \mathcal{I}^{\mathcal{V}_h}(D)$ is

$$\frac{1}{|\mathsf{e}|}\int_{\mathsf{e}} \mathbf{rot}\, \circ \mathcal{I}^{\mathcal{V}_h}(D) d\ell = \frac{\mathcal{I}^{\mathcal{V}_h} D(\mathsf{v}_2) - \mathcal{I}^{\mathcal{V}_h} D(\mathsf{v}_1)}{|\mathsf{e}|}. \tag{3.104}$$

Again, the above follows from the Fundamental Theorem of Line Integrals. By definition of the operator $\mathcal{I}^{\mathcal{V}_h}$ we have that

$$\mathcal{I}^{\mathcal{V}_h} D(\mathsf{v}_1) = D(\mathsf{v}_1) \quad \text{and} \quad \mathcal{I}^{\mathcal{V}_h} D_h(\mathsf{v}_2) = D(\mathsf{v}_2). \tag{3.105}$$

Thus, by equations (3.103) and (3.104) the two functions in question share degrees of freedom hence we verify (3.102a). Similarly, we will check that the functions on the right and left hand sides of (3.102b) share the same degrees of freedom in $\mathcal{P}_h$. Let P be a cell of the mesh Ω_h and $\boldsymbol{C} \in H(\text{div}; \Omega)$. Then, the degree of freedom associated with $\mathcal{I}^{\mathcal{P}_h} \circ \text{div}\,(\boldsymbol{C})$ is

$$\frac{1}{|\mathsf{P}|}\int_{\mathsf{P}} \text{div}\, \boldsymbol{C} dA = \frac{1}{|\mathsf{P}|}\sum_{\mathsf{e}\in\partial\mathsf{P}} \int_{\mathsf{e}} \boldsymbol{C}\cdot\boldsymbol{n} d\ell. \tag{3.106}$$

The above expression follows from the Divergence Theorem. The degree of freedom associated with $\text{div}\, \circ \mathcal{I}^{\mathcal{E}_h}(\boldsymbol{C})$ is

$$\frac{1}{|\mathsf{P}|}\int_{\mathsf{P}} \text{div}\, \mathcal{I}^{\mathcal{E}_h}(\boldsymbol{C}) dA = \frac{1}{|\mathsf{P}|}\sum_{\mathsf{e}\in\partial\mathsf{P}} \int_{\mathsf{e}} \mathcal{I}^{\mathcal{V}_h}(\boldsymbol{C})\cdot\boldsymbol{n} d\ell. \tag{3.107}$$

By definition of the operator $\mathcal{I}^{\mathcal{E}_h}$ we have that

$$\forall \mathsf{e} \in \partial \mathsf{P}: \quad \int_{\mathsf{e}} \mathcal{I}^{\mathcal{E}_h} \boldsymbol{C} \cdot \boldsymbol{n} d\ell = \int_{\mathsf{e}} \boldsymbol{C} \cdot \boldsymbol{n} d\ell. \tag{3.108}$$

Thus, equations (3.106) and (3.107) verify that both sides of (3.102b) share the same value for their degrees of freedom. □

We summarize our findings in the following theorem

Theorem 3.70.1 *The chain in* (3.92) *is well-defined and is exact. Moreover, the diagram in* (3.101) *is commutative.*

Proof. The well-definednes of (3.92) is proven in Lemma 3.70.1. The commutativity of the diagram in (3.101) was proven in Lemma 3.70.2. The only fact left to be proven is to show that (3.92) is exact. This is to say that

$$\mathbf{rot}\, \mathcal{V}_h = \ker \operatorname{div} = \{\boldsymbol{C}_h \in \mathcal{E}_h : \operatorname{div} \boldsymbol{C}_h = 0\}. \tag{3.109}$$

Let $D_h \in \mathcal{V}_h$ and then by Lemma 3.70.1 it is the case that $\mathbf{rot}\, D_h \in \mathcal{E}_h$. Moreover, we also have that

$$\operatorname{div} \mathbf{rot}\, D_h = 0. \tag{3.110}$$

Therefore, $\mathbf{rot}\, D_h \in \ker \operatorname{div}$ as defined in (3.109). Next consider $\boldsymbol{C}_h \in \mathcal{E}_h$ with $\operatorname{div} \boldsymbol{C}_h = 0$, since $\boldsymbol{C}_h \in H(\operatorname{div}; \Omega)$ and the chain (3.90) is exact there must exist $D \in H(\mathbf{rot};)$ such that $\mathbf{rot}\, D = \boldsymbol{C}_h$. Thus, $\mathcal{I}^{\mathcal{V}_h} D$ is a function, by definition, in $\mathcal{V}_h$ that verifies

$$\mathbf{rot} \circ \mathcal{I}^{\mathcal{V}_h} D = \mathcal{I}^{\mathcal{E}_h} \circ \mathbf{rot}\, D = \mathcal{I}^{\mathcal{E}_h} \boldsymbol{C}_h = \boldsymbol{C}_h, \tag{3.111}$$

completing the proof. □

The chain presented in Theorem 3.70.1 was first introduced in [47]. However, it was ex-

plored in much more detail and generality in [16].

Now that we have concluded our study of the space of shape functions that make up the variational formulation (3.31) we are ready to prove one of the most important properties of this numerical scheme: The continuous system naturally enforces Gauss's law for the magnetic field. This is a consequence of Faraday's law and was discussed in Section 3.2. Note that from (3.23a) it holds that

$$\frac{\partial}{\partial t}\text{div}\,\boldsymbol{B} = \text{div}\,\frac{\partial}{\partial t}\boldsymbol{B} = -\text{div}\,\mathbf{rot}\,E_h = 0. \tag{3.112}$$

Thus, since the initial conditions satisfy that

$$\text{div}\,\boldsymbol{B}_0 = 0, \tag{3.113}$$

then, this property is preserved throughout the evolution of this system. Discretizations will often fail to capture this property. The usual reason is that the discrete versions of the divergence and rotational operators do not annihilate each other completely leaving a remainder that gets compounded over time. The consequence of violating Gauss's law has been well-documented, see [21, 22]. Simulations that do not conserve this property will find significant errors, see [48, 88]. The conclusion in [48] is that these simulations experience fictitious forces.

It is of utmost importance for numerical methods to satisfy this property. Efforts have been devoted to "divergence cleaning" techniques; we mention three approaches. In [52] they add $\nabla \cdot \boldsymbol{B} = 0$ as an additional equation and add a Lagrange multiplier to the set of unknowns. A different approach involves the development of specialized flux limiters, see [64]. Finally, least squares finite element methods involve solving differential equations by minimizing energy functionals, one of which can involve the condition on the divergence of the magnetic field, see [60].

The VEM being developed in this manuscript preserves this property automatically, and with Theorem 3.70.1 we have the tools to prove it.

Theorem 3.70.2 *The solution to the variational formulation* (3.31) *satisfies*

$$\forall n \in \mathbb{N}: \quad \textit{div}\, \boldsymbol{B}_h^n = \textit{div}\, \boldsymbol{B}_h^0. \tag{3.114}$$

Proof. Pick $n \in \mathbb{N}$, then at the $n+1$-th time step we find that the discrete magnetic field satisfies

$$\forall \boldsymbol{C}_h \in \mathcal{E}_h: \quad \big(\frac{\boldsymbol{B}_h^{n+1} - \boldsymbol{B}_h^n}{\Delta t} - \mathbf{rot}\, E_h, \boldsymbol{C}_h\big)_{\mathcal{E}_h} = 0. \tag{3.115}$$

The above equation is the discrete version of Faraday's law. Since $\frac{\boldsymbol{B}_h^{n+1} - \boldsymbol{B}_h^n}{\Delta t} - \mathbf{rot}\, E_h \in \mathcal{E}_h$ then equation (3.115) implies that

$$\frac{\boldsymbol{B}_h^{n+1} - \boldsymbol{B}_h^n}{\Delta t} - \mathbf{rot}\, E_h = 0. \tag{3.116}$$

Taking divergence on both sides of (3.116) yields that

$$\operatorname{div} \boldsymbol{B}_h^{n+1} = \operatorname{div} \boldsymbol{B}_h^n. \tag{3.117}$$

An inductive argument will show that

$$\operatorname{div} \boldsymbol{B}_h^{n+1} = \operatorname{div} \boldsymbol{B}_h^0. \tag{3.118}$$

□

Theorem 3.70.2 guarantees that the scheme (3.31) will preserve the divergence of the initial conditions. However, it does not make a claim as to if the continuous initial conditions are divergence free then the discretization will be as well. This is settled in the following corollary.

Corollary 3.70.1 *The solution to the variational formulation* (3.31) *will satisfy*

$$\forall n \in \mathbb{N}: \quad \textit{div}\, \boldsymbol{B}_h^n = 0. \tag{3.119}$$

Proof. Taking the divergence of the discrete initial conditions and using (3.102b) from Lemma 3.70.2

we find that

$$\text{div}\, \boldsymbol{B}_h^0 = \text{div} \circ \mathcal{I}^{\mathcal{E}_h} \boldsymbol{B}_0 = \mathcal{I}^{\mathcal{P}_h} \circ \text{div}\, \boldsymbol{B}_0 = 0. \tag{3.120}$$

The above is true since $\text{div}\, \boldsymbol{B}_0 = 0$ by hypothesis. This result combined with Theorem 3.70.2 will yield the result. □

From the proof of Corollary 3.70.1 it is clear that the reason discretization (3.31) will satisfy Gauss's law is the commuting property described in Theorem 3.70.1. With this fact in mind we can discuss the reason we build an oblique projector to compute the inner product in $\mathcal{V}_h$. When the $L^2(\Omega)-$orthogonal projection onto a space of polynomials is not computable using on the degrees of freedom, the literature suggests to use an enhanced space where it is computable, see [3, 15, 16]. However, at the moment of the development of this method there was no guarantee that this enhanced space will satisfy a commuting diagram of the sort presented in Theorem 3.70.1. Therefore, in the case of MHD we would have no guarantee that our scheme preserves the divergence of the magnetic field. The solution we came up with was to use an oblique projector that satisfies properties **P1**-**P3** from Section 3.4. Recent discoveries in the theory of VEM have uncovered enhancements that do satisfy the desired commuting property, see [42]. This happened around the same time we came up we came up with the alternative of using oblique projectors. In principle using these elements should yield similar numerical results.

3.8 Extensions to Higher Order

In this section we will briefly mention upon the virtual elements that would be required for higher order discretizations, these are taken from [16] where are studied studied in greater detail. Let $k > 1$ and P is a cell in a mesh Ω_h, then the nodal space is given by

$$\mathcal{V}_h^k(\mathsf{P}) := \left\{ D_h \in \left[H^1(\mathsf{P})\right]^2 : \forall \mathsf{e} \in \partial \mathsf{P}\ D_{h|\mathsf{e}} \in \left[\mathbb{P}_k(\mathsf{e})\right]^2, \triangle D_h \in \mathbb{P}_{k-2}(\mathsf{P}) \right\}. \tag{3.121}$$

The set of degrees of freedom that we associate with each function $D_h \in \mathcal{V}_h^k$ are

$(\mathbf{D_1})$ The evaluations at each node of P.

$(\mathbf{D_2})$ A set of $k-1$ evaluations, equally spaced, along each edge of P.

$(\mathbf{D_3})$ The moments $\int_P v_h q$ for $q \in \mathbb{P}_{k-2}(\mathsf{P})$

$$\mathcal{E}_h^k(\mathsf{P}) := \Big\{ \boldsymbol{C}_h \in H(\mathrm{div};\mathsf{P}) \cap H(\mathrm{rot};\mathsf{P}) : \forall \mathsf{e} \in \partial\mathsf{P}\ \boldsymbol{C}_h \cdot \boldsymbol{n}_\mathsf{e} \in \mathbb{P}_k(\mathsf{e}), \\ \nabla \mathrm{div}\, \boldsymbol{C}_h \in G_{k-2}^2(\mathsf{P}),\ \text{and rot}\, \boldsymbol{w} \in \mathbb{P}_{k-1}(\mathsf{P}) \Big\}. \tag{3.122}$$

In this definition we use:

$$\forall k \in \mathbb{N}: \quad G_k(\mathsf{P}) = \nabla \mathbb{P}_{k+1}(\mathsf{P}), \\ G_k^\perp(\mathsf{P}) = \left\{ \boldsymbol{q} \in [\mathbb{P}_k(\mathsf{P})]^2 : \forall \boldsymbol{p} \in G_k(\mathsf{P}) \quad \int_P \boldsymbol{q} \cdot \boldsymbol{p}\, dV = 0 \right\}. \tag{3.123}$$

For a function $\boldsymbol{C}_h \in \mathcal{E}_h^k(\mathsf{P})$ the set of degrees of freedom are

$(\mathbf{E_1})$ For every edge $\int_\mathsf{e} \boldsymbol{C}_h \cdot \boldsymbol{n}\, q\, dS$, where $q \in \mathbb{P}_k(\mathsf{e})$.

$(\mathbf{E_2})$ The moments $\int_\mathsf{P} \boldsymbol{C}_h \cdot \boldsymbol{q}_h\, dV$ for $\boldsymbol{q}_h \in G_{k-2}(\mathsf{P})$.

$(\mathbf{E_3})$ The moments $\int_\mathsf{P} \boldsymbol{C}_h \cdot \boldsymbol{q}_h\, dV$ for $\boldsymbol{q}_h \in G_k^\perp(\mathsf{P})$.

Finally, the cell space $\mathcal{P}_h^k(\mathsf{P})$ is given as the space of polynomials $\mathbb{P}_k(\mathsf{P})$. The set of degrees of freedom for $p_h \in \mathcal{P}_h^k(\mathsf{P})$ is given by

$(\mathbf{P_1})$ The moments $\int_\mathsf{P} p_h q_h\, dV$ for $q_h \in \mathbb{P}_k(\mathsf{P})$.

Remark 1 *All of these spaces can be proven to be unisolvent with respect to the degrees of freedom presented. They also satisfy a commuting De-Rham complex of the type presented in Theorem 3.70.1. In [16] the authors also study the construction of the inner product in these spaces. In*

the case of $\mathcal{V}_h^k(\mathsf{P})$ the strategy involves an enhancement process that may invalidate the De-Rham complex and affect the divergence of the magnetic field. Instead we would generalize the oblique projectors presented in Section 3.11.

Remark 2 *We note that if we use the formulation in* (3.31) *we would achieve arbitrarily high speeds of convergence in space. However, in space the rate will be quadratic for $\theta = 1/2$ and linear for any other value of θ.*

Remark 3 *We note that the analysis done in Sections 5.5 and 3.10 will hold if we use the spaces defined in this section.*

3.9 Energy Stability Analysis

The continuous system (3.23) satisfies an important estimate in the L^2-norm. In this section we want to show that our discrete estimates (3.31) satisfy a similar estimate. First, note that, since the boundary conditions are given, the only unknowns to be solved for are the interior values of the electric field E_h. Thus, we decompose

$$E_h = \widehat{E} + E_b, \tag{3.124}$$

where $\widehat{E} \in H_0(\mathbf{rot}; \Omega)$.

Theorem 3.90.1 *Let $\boldsymbol{B}$ and $\widehat{E}$ solve* (3.31) *then*

$$\frac{d}{dt}\|\boldsymbol{B}\|_{0,\Omega}^2 + \frac{R_m}{2}\|\widehat{E}\|_{0,\Omega}^2 \leq \|E_b\|_{H_{R_m}(\mathbf{rot};\Omega)}^2 + \left(2R_m^2\|\boldsymbol{u}\|_\infty^2 + 1\right)\|\boldsymbol{B}\|_{0,\Omega}^2, \tag{3.125}$$

where $\|E\|_{H_{R_m}(\mathbf{rot};\Omega)}^2 = R_m\|E\|_{0,\Omega}^2 + \|\mathbf{rot}\, E\|_{0,\Omega}^2$. As a consequence there exists a bounded

function $\beta : [0,T] \to \mathbb{R}^+$ *such that*

$$\beta(t)\|\boldsymbol{B}(\cdot,t)\|_{0,\Omega}^2 + \frac{1}{2}\int_0^t \beta(\tau) R_m \|\widehat{E}(\cdot,\tau)\|_{0,\Omega}^2 \, d\tau \leq \\ \leq \int_0^t \beta(\tau)\|E_b(\cdot,\tau)\|^2_{H_{R_m}(\mathbf{rot}\,;\Omega)} \, d\tau + \|\boldsymbol{B}_0(\cdot,t)\|_{0,\Omega}^2. \quad (3.126)$$

Proof. Testing equation (3.29a) against $\boldsymbol{C} = \boldsymbol{B}$, equation (3.31b) against $D = \widehat{E}(\cdot,t)$ and adding the resulting expressions we find that

$$\frac{1}{2}\|\boldsymbol{B}\|_{0,\Omega}^2 + \|\sigma^{1/2}\widehat{E}\|_{0,\Omega}^2 \leq -R_m(\boldsymbol{u}\times\boldsymbol{B},\widehat{E}) - R_m(E_b,\widehat{E}) - (\mathbf{rot}\,E_b,\boldsymbol{B}). \quad (3.127)$$

We proceed to bound the right-hand side of (3.127) as follows

$$-R_m(\widehat{E},E_0) \leq R_m\|\widehat{E}\|_{0,\Omega}\|\sigma^{1/2}E_0\|_{0,\Omega} \leq \frac{R_m}{2}\|\widehat{E}\|_{0,\Omega}^2 + \frac{R_m}{2}\|E_0\|_{0,\Omega}^2, \quad (3.128)$$

$$-(\mathbf{rot}\,E_b,\boldsymbol{B}) \leq \|\mathbf{rot}\,E_b\|_{0,\Omega}\|\boldsymbol{B}\|_{0,\Omega} \leq \frac{1}{2}\|\mathbf{rot}\,E_b\|_{0,\Omega}^2 + \frac{1}{2}\|\boldsymbol{B}\|_{0,\Omega}^2, \quad (3.129)$$

$$-R_m(\boldsymbol{u}\times\boldsymbol{B},\widehat{E}) \leq R_m\|\boldsymbol{u}\times\boldsymbol{B}\|_{0,\Omega}\|\widehat{E}\|_{0,\Omega} \leq R_m\|\boldsymbol{u}\|_\infty^2\|\boldsymbol{B}\|_{0,\Omega}^2 + \frac{R_m}{4}\|\widehat{E}\|_{0,\Omega}^2. \quad (3.130)$$

Estimate (3.125) follows from (3.127), (3.128), (3.129) and (3.130). To prove (3.126) we define

$$\beta(t) = \exp\left(-\int_0^t \left(2R_m^2\|\boldsymbol{u}\|_\infty^2 + 1\right) d\tau\right). \quad (3.131)$$

Multiplication by β in (3.125) yields

$$\frac{d}{dt}\left(\beta\|\boldsymbol{B}\|_{0,\Omega}^2\right) + \frac{R_m\beta}{2}\|\widehat{E}\|_{0,\Omega}^2 \leq \beta\|E_b\|_{H_{R_m}(\mathbf{rot}\,;\Omega)}. \quad (3.132)$$

Integration in time gives (3.126). □

Consider the mapping L that provided the initial and boundary conditions $(\boldsymbol{B}_0, E_b)$ given

as an output of the solution to the variational problem (3.29):

$$L(\boldsymbol{B}_0, E_b) = (\boldsymbol{B}, \widehat{E}). \tag{3.133}$$

We note that since the variational problem (3.29) is linear then the function L will likewise be linear. Moreover, we could define a norm on the domain of L as the right hand side of (3.126), and, a norm on the codomain of L as the left hand side of (3.126). In this case, the statement of (3.126) can be interpreted as proof of the continuity of L. This gives some insight into the required regularity of solutions to problem (3.29). In the discrete realm, a result of this sort is a proof of stability. Before we proceed to show a discrete mimicry of Theorem 3.90.1 we require the following lemma.

Lemma 3.90.1 *There exists a real positive constant $\widetilde{C}$ independent of h (and Δt) that may depend on the continuity constants of $\mathcal{I}^{\mathcal{V}_h}$ and Π^{RT}, such that*

$$\forall \boldsymbol{C}_h \in \mathcal{E}_h, D_h \in \mathcal{V}_h : \quad \big(\mathcal{I}^{\mathcal{V}_h}\big(\boldsymbol{u} \times \Pi^{RT}\boldsymbol{C}_h\big), D_h\big)_{\mathcal{V}_h} \leq \widetilde{C}\|\boldsymbol{u}\|_\infty \|\boldsymbol{C}_h\|_{0,\Omega}\, \|D_h\|_{0,\Omega}, \tag{3.134}$$

assuming that $\boldsymbol{u} \in L^\infty(\Omega)$.

Proof.

$$\begin{aligned}
\big(\mathcal{I}^{\mathcal{V}_h}\big(\boldsymbol{u} \times \Pi^{RT}\boldsymbol{C}_h\big), D_h\big)_{\mathcal{V}_h} &\leq |||\mathcal{I}^{\mathcal{V}_h}\big(\boldsymbol{u} \times \Pi^{RT}\boldsymbol{C}_h\big)|||_{\mathcal{V}_h}\, |||D_h|||_{\mathcal{V}_h} && \text{[Cauchy-Swartz Ineq.]}\\
&\leq (\beta^*)^{\frac{1}{2}} \|\mathcal{I}^{\mathcal{V}_h}\big(\boldsymbol{u} \times \Pi^{RT}\boldsymbol{C}_h\big)\|_{0,\Omega}\, \|D_h\|_{0,\Omega} && \text{[use (3.51)]}\\
&\leq (\beta^*)^{\frac{1}{2}} \|\mathcal{I}^{\mathcal{V}_h}\|\, \|\boldsymbol{u} \times \Pi^{RT}\boldsymbol{C}_h\|_{0,\Omega}\, \|D_h\|_{0,\Omega} && \text{[note that } \|\boldsymbol{u}\|_\infty < \infty]\\
&\leq (\beta^*)^{\frac{1}{2}} \|\mathcal{I}^{\mathcal{V}_h}\|\, \|\boldsymbol{u}\|_\infty \|\Pi^{RT}\boldsymbol{C}_h\|_{0,\Omega}\, \|D_h\|_{0,\Omega} && \text{[note that } \|\Pi^{RT}\| \leq 1]\\
&\leq (\beta^*)^{\frac{1}{2}} \|\mathcal{I}^{\mathcal{V}_h}\|\, \|\boldsymbol{u}\|_\infty \|\boldsymbol{C}_h\|_{0,\Omega}\, \|D_h\|_{0,\Omega},
\end{aligned}$$

which is the assertion of the lemma after setting $\widetilde{C} = (\beta^*)^{\frac{1}{2}} \|\mathcal{I}^{\mathcal{V}_h}\|$. □

In order to present the discrete form of Theorem 3.90.1 we introduce the notation

$$E_h = \widehat{E}_h + \mathcal{I}^{\mathcal{V}_h}(E_b), \tag{3.135}$$

where $\widehat{E}_h \in \mathcal{V}_{h,0}$. We note that the proof of this theorem is essentially an application of the discrete form of Gronwall's Lemma. The techniques used are partially laid out in [55].

Theorem 3.90.2

(i) *Let $\theta \in [0,1]$. The solution of Scheme* (3.31) *satisfies*

$$\left(\theta - \frac{1}{2}\right) \frac{|||\boldsymbol{B}_h^{n+1} - \boldsymbol{B}_h^n|||^2_{\mathcal{E}_h}}{\Delta t} + \frac{|||\boldsymbol{B}_h^{n+1}|||^2_{\mathcal{E}_h} - |||\boldsymbol{B}_h^n|||^2_{\mathcal{E}_h}}{\Delta t} + \frac{1}{2}|||\widehat{E}_h^{n+\theta}|||^2_{\mathcal{V}_h} \tag{3.136}$$

$$\leq |||\mathcal{I}^{\mathcal{V}_h} E_b^{n+\theta}|||^2_{H(\boldsymbol{rot};\Omega)} + \frac{1}{2}\left(1 + 4\widetilde{C}\|\boldsymbol{u}\|^2_\infty\right)\left(\theta|||\boldsymbol{B}_h^{n+1}|||^2_{\mathcal{E}_h} + (1-\theta)|||\boldsymbol{B}_h^n|||^2_{\mathcal{E}_h}\right),$$

where $|||\mathcal{I}^{\mathcal{V}_h} E_b^{n+\theta}|||^2_{H(\boldsymbol{rot};\Omega)} = R_m|||\mathcal{I}^{\mathcal{V}_h} E_b^{n+\theta}|||^2_{\mathcal{V}_h} + |||\mathbf{rot}\,\mathcal{I}^{\mathcal{V}_h} E_b^{n+\theta}|||^2_{\mathcal{E}_h}$, and we recall that $\widetilde{C}$ is the constant introduced in Lemma 3.90.1.

(ii) *If $\theta \in \left[\frac{1}{2}, 1\right]$, then we can conclude that*

$$(\beta)^{n+1}|||\boldsymbol{B}_h^{n+1}|||^2_{\mathcal{E}_h} + \frac{R_m\gamma\Delta t}{2}\sum_{\ell=0}^{n}\beta^{n+1-\ell}|||\widehat{E}_h^{n-\ell+\theta}|||^2_{\mathcal{V}_h} \leq$$

$$|||\boldsymbol{B}_h^0|||^2_{\mathcal{E}_h} + \gamma\Delta t\sum_{\ell=0}^{n}\beta^{n+1-\ell}|||\mathcal{I}^{\mathcal{V}_h} E_b^{n-\ell+\theta}|||^2_{H(\boldsymbol{rot};\Omega)}, \tag{3.137}$$

where

$$\beta = \frac{\big(1 - Q\theta\big)}{\big(1 + Q(1-\theta)\big)}, \qquad \gamma = \frac{1}{\big(1 - Q\theta\big)} \qquad \textit{and } Q = \Delta t\big(1 + 4\widetilde{C}\|\boldsymbol{u}\|^2_\infty\big). \tag{3.138}$$

The coefficients in (3.137) *are guaranteed to be positive when*

$$\Delta t < \frac{1}{\theta\big(1+4\widetilde{C}\|\boldsymbol{u}\|_\infty^2\big)}. \tag{3.139}$$

Proof. (i). Testing equation (3.31a) against $\boldsymbol{C}_h = \boldsymbol{B}_h^{n+\theta} = \theta\boldsymbol{B}_h^{n+1} + (1-\theta)\boldsymbol{B}_h^n$ and equation (3.31b) against $D_h = \widehat{E}_h^{n+\theta}$ and adding them together we arrive at

$$\begin{aligned}
&\left(\frac{\boldsymbol{B}_h^{n+1}-\boldsymbol{B}_h^n}{\Delta t}, \boldsymbol{B}_h^{n+\theta}\right)_{\mathcal{E}_h} + R_m|||\widehat{E}_h^{n+\theta}|||_{\mathcal{V}_h}^2 \\
&= -\big(\mathbf{rot}\,\mathcal{I}^{\mathcal{V}_h}E_b^{n+\theta}, \boldsymbol{B}_h^{n+\theta}\big)_{\mathcal{E}_h} - R_m\big(\mathcal{I}^{\mathcal{V}_h}E_b^{n+\theta}, \widehat{E}_h^{n+\theta}\big)_{\mathcal{V}_h} - R_m\big(\mathcal{I}^{\mathcal{V}_h}\big(\boldsymbol{u}\times\Pi^{RT}\boldsymbol{B}_h^{n+\theta}\big), \widehat{E}_h^{n+\theta}\big)_{\mathcal{V}_h} \\
&= (\mathbf{T1}) + (\mathbf{T2}) + (\mathbf{T3}).
\end{aligned} \tag{3.140}$$

We transform the first term of the left-hand side of (3.140) using the identity

$$\boldsymbol{B}_h^{n+\theta} = \Delta t\left(\theta-\frac{1}{2}\right)\frac{\boldsymbol{B}_h^{n+1}-\boldsymbol{B}_h^n}{\Delta t} + \frac{\boldsymbol{B}_h^{n+1}+\boldsymbol{B}_h^n}{2}. \tag{3.141}$$

We obtain:

$$\begin{aligned}
\left(\frac{\boldsymbol{B}_h^{n+1}-\boldsymbol{B}_h^n}{\Delta t}, \boldsymbol{B}_h^{n+\theta}\right)_{\mathcal{E}_h} &= \Delta t\left(\theta-\frac{1}{2}\right)\left(\frac{\boldsymbol{B}_h^{n+1}-\boldsymbol{B}_h^n}{\Delta t}, \frac{\boldsymbol{B}_h^{n+1}-\boldsymbol{B}_h^n}{\Delta t}\right)_{\mathcal{E}_h} \\
&\quad + \left(\frac{\boldsymbol{B}_h^{n+1}-\boldsymbol{B}_h^n}{\Delta t}, \frac{\boldsymbol{B}_h^{n+1}+\boldsymbol{B}_h^n}{2}\right)_{\mathcal{E}_h} \\
&= \Delta t\left(\theta-\frac{1}{2}\right)\frac{|||\boldsymbol{B}_h^{n+1}-\boldsymbol{B}_h^n|||_{\mathcal{E}_h}^2}{\Delta t^2} + \frac{|||\boldsymbol{B}_h^{n+1}|||_{\mathcal{E}_h}^2 - |||\boldsymbol{B}_h^n|||_{\mathcal{E}_h}^2}{2\Delta t}.
\end{aligned} \tag{3.142}$$

Next, we bound the three terms in the right-hand side of (3.140) by using the Young inequality

with parameters ϵ_1, ϵ_2, and ϵ_1. For the first two terms we obtain the estimates:

$$\begin{aligned}(\mathbf{T1}) &\le \frac{\epsilon_1}{2}|||\mathbf{rot}\,\mathcal{I}^{\mathcal{V}_h}E_0^{n+\theta}|||_{\varepsilon_h}^2 + \frac{1}{2\epsilon_1}|||\boldsymbol{B}_h^{n+\theta}|||_{\varepsilon_h}^2 \\ &\le \frac{\epsilon_1}{2}|||\mathbf{rot}\,\mathcal{I}^{\mathcal{V}_h}E_0^{n+\theta}|||_{\varepsilon_h}^2 + \frac{1}{2\epsilon_1}\left(\theta^2|||\boldsymbol{B}_h^{n+1}|||_{\varepsilon_h}^2 + (1-\theta)^2|||\boldsymbol{B}_h^{n}|||_{\varepsilon_h}^2\right), \\ &\le \frac{\epsilon_1}{2}|||\mathbf{rot}\,\mathcal{I}^{\mathcal{V}_h}E_0^{n+\theta}|||_{\varepsilon_h}^2 + \frac{1}{\epsilon_1}\left(\theta|||\boldsymbol{B}_h^{n+1}|||_{\varepsilon_h}^2 + (1-\theta)|||\boldsymbol{B}_h^{n}|||_{\varepsilon_h}^2\right), \qquad (3.143)\\ (\mathbf{T2}) &\le \frac{\epsilon_2}{2}|||\mathcal{I}^{\mathcal{V}_h}E_0^{n+\theta}|||_{\mathcal{V}_h}^2 + \frac{1}{2\epsilon_2}|||\widehat{E}_h^{n+\theta}|||_{\mathcal{V}_h}^2. \qquad (3.144)\end{aligned}$$

The bound for the third term requires a bit more work. Since $\theta \in [0,1]$, we note that $\theta^2 \le \theta$ and $(1-\theta)^2 \le 1-\theta$. Therefore we have an estimate

$$\begin{aligned}|||\mathcal{I}^{\mathcal{V}_h}(\boldsymbol{u}\times\Pi^{RT}\boldsymbol{B}_h^{n+\theta})|||_{\mathcal{V}_h}^2 &\le C\|\boldsymbol{u}\|_\infty^2|||\theta\boldsymbol{B}_h^{n+1}+(1-\theta)\boldsymbol{B}_h^{n}|||_{\varepsilon_h}^2 \\ &\le 2C\|\boldsymbol{u}\|_\infty^2\left(\theta^2|||\boldsymbol{B}_h^{n+1}|||_{\varepsilon_h}^2 + (1-\theta)^2|||\boldsymbol{B}_h^{n}|||_{\varepsilon_h}^2\right) \\ &\le 2C\|\boldsymbol{u}\|_\infty^2\left(\theta|||\boldsymbol{B}_h^{n+1}|||_{\varepsilon_h}^2 + (1-\theta)|||\boldsymbol{B}_h^{n}|||_{\varepsilon_h}^2\right). \qquad (3.145)\end{aligned}$$

Next we again use the Young's inequality

$$\begin{aligned}(\mathbf{T3}) &\le \frac{\epsilon_3}{2}|||\mathcal{I}^{\mathcal{V}_h}(\boldsymbol{u}\times\theta\boldsymbol{B}_h^{n+\theta})|||_{\mathcal{V}_h}^2 + \frac{1}{2\epsilon_3}|||\widehat{E}_h^{n+\theta}|||_{\mathcal{V}_h}^2 + \\ &\le C\epsilon_3\|\boldsymbol{u}\|_\infty^2\left(\theta|||\boldsymbol{B}_h^{n+1}|||_{\varepsilon_h}^2 + (1-\theta)|||\boldsymbol{B}_h^{n}|||_{\varepsilon_h}^2\right) + \frac{1}{2\epsilon_3}|||\widehat{E}_h^{n+\theta}|||_{\mathcal{V}_h}^2. \qquad (3.146)\end{aligned}$$

Setting $\epsilon_1 = \epsilon_2 = \epsilon_3 = 2$, combining (3.140) with the estimates of $(\mathbf{T1})$, $(\mathbf{T2})$, and $(\mathbf{T3})$, and finally noting that $|||\mathcal{I}^{\mathcal{V}_h}E_b^{n+\theta}|||_{H(\mathbf{rot};\Omega)}^2 = |||\mathcal{I}^{\mathcal{V}_h}E_0^{n+\theta}|||_{\mathcal{V}_h}^2 + |||\mathbf{rot}\,\mathcal{I}^{\mathcal{V}_h}E_0^{n+\theta}|||_{\varepsilon_h}^2$ yields (3.136), which is the first assertion of the theorem.

(ii). If $\theta \in [1/2, 1]$, the coefficient in the first term on the left hand side of (3.136) is positive and

we can write

$$|||\boldsymbol{B}_h^{n+1}|||_{\mathcal{E}_h}^2 - |||\boldsymbol{B}_h^{n}|||_{\mathcal{E}_h}^2 \leq \Delta t \left(-\frac{R_m}{2} |||\widehat{E}_h^{n+\theta}|||_{\mathcal{V}_h}^2 + |||\mathcal{I}^{\mathcal{V}_h} E_b^{n+\theta}|||_{H(\mathbf{rot};\Omega)}^2 \right) + \Delta t\big(1 + 4\widetilde{C}\|\boldsymbol{u}\|_\infty^2\big) \left(\theta |||\boldsymbol{B}_h^{n+1}|||_{\mathcal{E}_h}^2 + (1-\theta)|||\boldsymbol{B}_h^{n}|||_{\mathcal{E}_h}^2 \right). \tag{3.147}$$

To simplify the notation, let $Q = \Delta t\big(1 + 4\widetilde{C}\|\boldsymbol{u}\|_\infty^2\big)$ and

$$\mathcal{F}^{n+\theta}(\widehat{E}_h, E_b) = \Delta t \left(-\frac{R_m}{2} |||\widehat{E}_h^{n+\theta}|||_{\mathcal{V}_h}^2 + |||\mathcal{I}^{\mathcal{V}_h} E_b^{n+\theta}|||_{H(\mathbf{rot};\Omega)}^2 \right). \tag{3.148}$$

Rearranging the terms and dividing by $\big(1 - Q\theta\big)$ we find:

$$|||\boldsymbol{B}_h^{n+1}|||_{\mathcal{E}_h}^2 - \frac{\big(1 + Q(1-\theta)\big)}{\big(1 - Q\theta\big)} |||\boldsymbol{B}_h^{n}|||_{\mathcal{E}_h}^2 \leq \frac{1}{\big(1 - Q\theta\big)} \mathcal{F}(\widehat{E}_h, E_b)^{n+\theta}. \tag{3.149}$$

Now, we introduce the quantities

$$\alpha = \frac{\big(1 + Q(1-\theta)\big)}{\big(1 - Q\theta\big)}, \qquad \gamma = \frac{1}{\big(1 - Q\theta\big)}, \tag{3.150}$$

and note that quantity α is well-defined and strictly positive since Assumption (3.139) guarantees that $1 - Q\theta > 0$, and $Q > 0$ implies $\big(1 + Q(1 - (1-\theta)\big) \leq 1$ for $\theta \in [0, 1]$, so that $\alpha > 0$. We rewrite (3.149) as

$$|||\boldsymbol{B}_h^{n+1}|||_{\mathcal{E}_h}^2 - \alpha |||\boldsymbol{B}_h^{n}|||_{\mathcal{E}_h}^2 \leq \gamma \mathcal{F}^{n+\theta}(\widehat{E}_h, E_b). \tag{3.151}$$

Such an inequality must be true for any index $n \geq 0$. We express this fact by keeping n fixed and introducing the index $\ell = 0, \ldots, n$ such that

$$|||\boldsymbol{B}_h^{n+1-\ell}|||_{\mathcal{E}_h}^2 - \alpha |||\boldsymbol{B}_h^{n-\ell}|||_{\mathcal{E}_h}^2 \leq \gamma \mathcal{F}^{n-\ell+\theta}(\widehat{E}_h, E_b). \tag{3.152}$$

Then, we multiply by α^ℓ and adding all the resulting inequalities we find a telescopic sum where all intermediate terms like $\boldsymbol{B}_h^{n-\ell}$ cancel. We illustrate this fact by writing the first four inequalities for $\ell = 0, \ldots, 3$:

$$\begin{aligned}
&\text{for } \ell = 0: && |||\boldsymbol{B}_h^{n+1}|||_{\mathcal{E}_h}^2 && -\alpha|||\boldsymbol{B}_h^{n}|||_{\mathcal{E}_h}^2 && \leq \gamma \mathcal{F}^{n+\theta}(\widehat{E}_h, E_b) && \big[\text{multiply by } 1\,\big],\\
&\text{for } \ell = 1: && |||\boldsymbol{B}_h^{n}|||_{\mathcal{E}_h}^2 && -\alpha|||\boldsymbol{B}_h^{n-1}|||_{\mathcal{E}_h}^2 && \leq \gamma \mathcal{F}^{n-1+\theta}(\widehat{E}_h, E_b) && \big[\text{multiply by } \alpha\,\big],\\
&\text{for } \ell = 2: && |||\boldsymbol{B}_h^{n-1}|||_{\mathcal{E}_h}^2 && -\alpha|||\boldsymbol{B}_h^{n-2}|||_{\mathcal{E}_h}^2 && \leq \gamma \mathcal{F}^{n-2+\theta}(\widehat{E}_h, E_b) && \big[\text{multiply by } \alpha^2\big],\\
&\text{for } \ell = 3: && |||\boldsymbol{B}_h^{n-2}|||_{\mathcal{E}_h}^2 && -\alpha|||\boldsymbol{B}_h^{n-3}|||_{\mathcal{E}_h}^2 && \leq \gamma \mathcal{F}^{n-3+\theta}(\widehat{E}_h, E_b) && \big[\text{multiply by } \alpha^3\big],\\
&\quad \ldots && \quad \ldots
\end{aligned} \tag{3.153}$$

The sum of these expressions (with coefficients indicated on the right) gives:

$$|||\boldsymbol{B}_h^{n+1}|||_{\mathcal{E}_h}^2 - \alpha^4|||\boldsymbol{B}_h^{n-3}|||_{\mathcal{E}_h}^2 \leq \gamma \sum_{\ell=0}^{3} \alpha^\ell \mathcal{F}^{n-\ell+\theta}(\widehat{E}_h, E_b). \tag{3.154}$$

Adding all inequalities for $\ell = 0, \ldots, n$ yields

$$|||\boldsymbol{B}_h^{n+1}|||_{\mathcal{E}_h}^2 - \alpha^{n+1}|||\boldsymbol{B}_h^{0}|||_{\mathcal{E}_h}^2 \leq \gamma \sum_{\ell=0}^{n} \alpha^\ell \mathcal{F}^{n-\ell+\theta}(\widehat{E}_h, E_b). \tag{3.155}$$

Finally, we substitute back the expression for $\mathcal{F}$ and γ, multiply both sides by $\beta^{n+1} = \alpha^{-(n+1)}$, rearrange the terms and obtain the second assertion of the theorem. □

As we did in the continuous case, we can interpret the statement of (3.137) as the continuity of the mapping that takes initial and boundary data and outputs the discrete solution to (3.31). Thus, our proof provides evidence of conditional stability. However, numerical experiments show that for $\theta \in [1/2, 1]$ stability is unconditional.

Remark 4 *Analysis of the case when $\theta \in [0, 1/2)$ requires the use of an inverse inequality of the*

sort

$$\exists C > 0 \; \forall E_h \in \mathcal{V}_h : \; |||\mathbf{rot}\, E_h|||_{\mathcal{E}_h} \leq \frac{C}{h} |||E_h|||_{\mathcal{V}_h}. \tag{3.156}$$

This inequality is classic in the finite element method, see for example [20, 32], but its extension to the VEM is highly non-trivial. In [23] the authors present a possible extension, however it is not clear how it can be used in the proof above.

3.10 Well-Posedness and Stability of the Linear Solve

In order to solve (3.31) we must, at each time step, solve following linear problem: *Find* $(\boldsymbol{B}_h^{n+1}, \widehat{E}_h^{n+\theta}) \in \mathcal{E}_h \times \mathcal{V}_{h,0}$ *such that for all* $(\boldsymbol{C}_h, D_h) \in \mathcal{E}_h \times \mathcal{V}_{h,0}$ *it holds:*

$$\Delta t^{-1} \big(\boldsymbol{B}_h^{n+1}, \boldsymbol{C}_h\big)_{\mathcal{E}_h} + \big(\mathbf{rot}\, \widehat{E}_h^{n+\theta}, \boldsymbol{C}_h\big)_{\mathcal{E}_h} = \big(\boldsymbol{F}, \boldsymbol{C}_h\big)_{\mathcal{E}_h}, \tag{3.157a}$$

$$R_m\big(\widehat{E}_h^{n+\theta}, D_h\big)_{\mathcal{V}_h} + \theta R_m\big(\mathcal{I}^{\mathcal{V}_h}\big(\boldsymbol{u} \times \Pi^{RT} \boldsymbol{B}_h^{n+1}\big), D_h\big)_{\mathcal{V}_h} - \theta \big(\boldsymbol{B}_h^{n+1}, \mathbf{rot}\, D_h\big)_{\mathcal{E}_h} = \\ = \big\langle g, D_h \big\rangle, \tag{3.157b}$$

where we define

$$\boldsymbol{F} = \Delta t^{-1} \boldsymbol{B}_h^n + \mathbf{rot}\, \big(\mathcal{I}^{\mathcal{V}_h} E_b^{n+\theta}\big), \tag{3.158}$$

$$\big\langle g, D_h \big\rangle = (1-\theta) \Big(\big(\boldsymbol{B}_h^n, \mathbf{rot}\, D_h\big)_{\mathcal{E}_h} - R_m\big(\mathcal{I}^{\mathcal{V}_h}\big(\boldsymbol{u} \times \Pi^{RT} \boldsymbol{B}_h^n\big), D_h\big)_{\mathcal{V}_h} \Big) - \\ - R_m\big(\mathcal{I}^{\mathcal{V}_h} E_b^{n+\theta}, D_h\big)_{\mathcal{V}_h}. \tag{3.159}$$

This system is obtained when we put every known quantity on the right hand side and every unknown quantity on the left hand side of (3.31). The main result will show that the solution to problem (3.157) exists, it is unique and there is a continuous dependence and the mapping that sends the right hand side to the solution of the system is continuous. The techniques we use are inspired by those in [59].

Let us begin by defining the space that will serve as setting for two variational problems. We define

$$\mathcal{X}_h := E_h \times \mathcal{V}_{h,0}. \tag{3.160}$$

We equip $\mathcal{X}_h$ with the norm

$$|||\xi|||^2_{\mathcal{X}_h} := |||D_h|||^2_{\Delta t,\mathbf{rot}} + |||\boldsymbol{C}_h|||^2_{\Delta t,\mathrm{div}}\,, \tag{3.161}$$

where

$$|||D_h|||^2_{\Delta t,\mathbf{rot}} := |||D_h|||^2_{\mathcal{V}_h} + \Delta t|||\mathbf{rot}\, D_h|||^2_{\mathcal{E}_h}, \tag{3.162}$$

$$|||\boldsymbol{C}_h|||^2_{\Delta t,\mathrm{div}} := \Delta t^{-1}|||\boldsymbol{C}_h|||^2_{\mathcal{E}_h} + |||\mathrm{div}\, \boldsymbol{C}_h|||^2_{\mathcal{P}_h}. \tag{3.163}$$

In this space we define two bilinear forms $a_h, a_{h,0} : \mathcal{X}_h \times \mathcal{X}_h \to \mathbb{R}$. When we evaluate $(\boldsymbol{B}, E_h) = \xi \in \mathcal{X}_h$ and $(\boldsymbol{C}_h, D_h) = \eta \in \mathcal{X}_h$, we obtain

$$\begin{aligned} a_h(\xi,\eta) = \\ = \big(\Delta t^{-1}\boldsymbol{B}_h + \mathbf{rot}\, E_h, \boldsymbol{C}_h\big)_{\mathcal{E}_h} + R_m\big(E_h + \theta\mathcal{I}^{\mathcal{V}_h}\big(\boldsymbol{u}\times\Pi^{RT}\boldsymbol{B}_h\big), D_h\big)_{\mathcal{V}_h} - \\ - \theta\big(\boldsymbol{B}_h, \mathbf{rot}\, D_h\big)_{\mathcal{E}_h} \end{aligned} \tag{3.164}$$

and

$$a_{h,0}(\xi,\eta) = a_h(\xi,\eta) + \big(\mathrm{div}\, \boldsymbol{B}_h, \mathrm{div}\, \boldsymbol{C}_h\big)_{\mathcal{P}_h}. \tag{3.165}$$

The two variational problems are

Problem 3.100.1 Find $(\boldsymbol{B}_h^{n+1}, \widehat{E}_h^{n+\theta}) = \xi \in \mathcal{X}_h$ such that for any $(\boldsymbol{C}_h, D_h) = \eta \in \mathcal{X}_h$ it holds:

$$a_h(\xi,\eta) = \big(\boldsymbol{F}, \boldsymbol{C}_h\big)_{\mathcal{E}_h} + \big\langle g, D_h\big\rangle, \tag{3.166}$$

assuming that $\boldsymbol{B}_h^n$ *(such that div* $\boldsymbol{B}_h^n = 0$*) is known*

and

Problem 3.100.2 Find $(\boldsymbol{B}_h^{n+1}, \widehat{E}_h^{n+\theta}) = \xi \in \mathcal{X}_h$ such that for any $(\boldsymbol{C}_h, D_h) = \eta \in \mathcal{X}_h$:

$$a_{h,0}(\xi, \eta) = \big(\boldsymbol{F}, \boldsymbol{C}_h\big)_{\mathcal{E}_h} + \big\langle g, D_h \big\rangle. \tag{3.167}$$

assuming that $\boldsymbol{B}_h^n$ *(such that div* $\boldsymbol{B}_h^n = 0$*) is known.*

In Problems 3.100.1 and 3.100.2 we use $\boldsymbol{F}$ and $\big\langle g, D_h \big\rangle$ as given by (3.158) and (3.159). It is immediate to check finding a solution to the linear system (3.157) is equivalent to solving Problem 3.100.1. Later we will show that Problems 3.100.1 and 3.100.2 are equivalent. Then, we will show that Problem 3.100.2 is well-posed. This will follow from Theorem 2.20.1. Thus, since all three problems are equivalent, this well-posedness result will transfer over to Problem 3.100.1 yielding the result that we are looking for.

In order to establish the equivalency that we are looking for we present the following result.

Theorem 3.100.3 . *If* $\xi = (\boldsymbol{B}_h^{n+1}, \widehat{E}_h^{n+\theta})$ *solves Problem 3.100.2, then div* $\boldsymbol{B}_h^{n+1} = 0$.

Proof. Test (3.167) against $\eta = (\boldsymbol{C}_h, D_h)$ with $D_h = 0$, while leaving $\boldsymbol{C}_h \in \mathcal{E}_h$ undefined for the moment. Using definitions (3.164), (3.165), (3.158), and (3.159), and rearranging the terms, we obtain the identity:

$$\big(\boldsymbol{F}^n - \Delta t^{-1} \boldsymbol{B}_h^{n+1} - \mathbf{rot}\, E_h^{n+\theta}, \boldsymbol{C}_h\big)_{\mathcal{E}_h} = \big(\operatorname{div} \boldsymbol{B}_h^{n+1}, \operatorname{div} \boldsymbol{C}_h\big)_{\mathcal{P}_h}. \tag{3.168}$$

Now, we set

$$\boldsymbol{C}_h = \boldsymbol{F}^n - \Delta t^{-1} \boldsymbol{B}_h^{n+1} - \mathbf{rot}\ E_h^{n+\theta}. \tag{3.169}$$

Since $\operatorname{div} \boldsymbol{B}_h^n = 0$ by hypothesis and $\operatorname{div} \circ \mathbf{rot} = 0$ we find that

$$\operatorname{div} \boldsymbol{F}^n = \Delta t^{-1} \operatorname{div} \boldsymbol{B}_h^n + \operatorname{div} \left(\mathbf{rot}\, \widehat{E}_h^{n-1+\theta} \right) = 0 \qquad \text{and} \quad \operatorname{div} \left(\mathbf{rot}\, E_h^{n+\theta} \right) = 0, \tag{3.170}$$

so that

$$\operatorname{div} \boldsymbol{C}_h = \operatorname{div} \left(\boldsymbol{F}^n - \Delta t^{-1} \boldsymbol{B}_h^{n+1} - \mathbf{rot}\, \widehat{E}_h^{n+\theta} \right) = -\Delta t^{-1} \operatorname{div} \boldsymbol{B}_h^{n+1}. \tag{3.171}$$

Substituting the expressions of $\boldsymbol{w}$ and $\operatorname{div} \boldsymbol{w}$ in (3.168) yields

$$0 \leq |||\boldsymbol{C}_h|||_{\mathcal{E}_h}^2 = -\Delta t^{-1} |||\operatorname{div} \boldsymbol{B}_h^{n+1}|||_{\mathcal{P}_h}^2, \tag{3.172}$$

which implies that $|||\operatorname{div} \boldsymbol{B}_h^{n+1}|||_{\mathcal{P}_h} \leq 0$, and, thus, the proposition. □

We are ready to show that the aforementioned problems are all equivalent.

Lemma 3.100.1 *The linear system* (3.157)*, Problem 3.100.1 and Problem 3.100.2 all have the same solution.*

Proof. As a consequence of Theorem 3.100.3 if $(\boldsymbol{B}_h^{n+1}, E_h^{n+\theta}) = \xi \in \mathcal{X}_h$ solves Problem 3.100.2 then

$$\forall \eta \in \mathcal{X}_h : \quad a_h(\xi, \eta) = a_{h,0}(\xi, \eta). \tag{3.173}$$

This implies that the solution to Problem 3.100.1 and Problem 3.100.2 are one and the same. Next we note that by adding both equations in the system (3.157) we obtain (3.166). Moreover, if we test (3.166) against $\eta = (\boldsymbol{C}_h, 0)$ we obtain (3.157a). Likewise, testing this problem against $\eta = (\mathbf{0}, D_h)$ will yield (3.157b). □

The following lemmas will show that Problem 3.100.2 satisfies the hypothesis of Theorem 2.20.1, we will conclude its well-posedness.

Lemma 3.100.2 *There exists a constant $C > 0$, independent of h and Δt, such that*

$$\forall \xi, \eta \in \mathcal{X}_h : \quad a_{h,0}(\xi, \eta) \leq C |||\xi|||_{\mathcal{X}_h} \, |||\eta|||_{\mathcal{X}_h} . \tag{3.174}$$

Proof. Let $\xi = (\boldsymbol{B}_h, E_h)$ and $\eta = (\boldsymbol{C}_h, D_h)$ be arbitrary elements in $\mathcal{X}_h$. A systematic application of the Cauchy Schwartz inequality yields that

$$\Delta t^{-1} \big(\boldsymbol{B}_h, \boldsymbol{C}_h\big)_{\mathcal{E}_h} \leq \Delta t^{-\frac{1}{2}} |||\boldsymbol{B}_h|||_{\mathcal{E}_h} \, \Delta t^{-\frac{1}{2}} |||\boldsymbol{C}_h|||_{\mathcal{E}_h} \leq |||\boldsymbol{B}_h|||_{\Delta t,\mathrm{div}} \, |||\boldsymbol{C}_h|||_{\Delta t,\mathrm{div}} , \tag{3.175}$$

$$\big(\mathbf{rot}\, E_h, \boldsymbol{C}_h\big)_{\mathcal{E}_h} \leq \Delta t^{\frac{1}{2}} |||\mathbf{rot}\, E_h|||_{\mathcal{E}_h} \, \Delta t^{-\frac{1}{2}} |||\boldsymbol{C}_h|||_{\mathcal{E}_h} \leq |||E_h|||_{\Delta t,\mathbf{rot}} \, |||\boldsymbol{C}_h|||_{\Delta t,\mathrm{div}} , \tag{3.176}$$

$$\big(E_h, D_h\big)_{\mathcal{V}_h} \leq |||E_h|||_{\mathcal{V}_h} \, |||D_h|||_{\mathcal{V}_h} \leq |||E_h|||_{\Delta t,\mathbf{rot}} \, |||D_h|||_{\Delta t,\mathbf{rot}} , \tag{3.177}$$

$$\big(\mathrm{div}\, \boldsymbol{B}_h, \mathrm{div}\, \boldsymbol{D}_h\big)_{\mathcal{P}_h} \leq |||\mathrm{div}\, \boldsymbol{B}_h|||_{\mathcal{P}_h} \, \|\mathrm{div}\, \boldsymbol{D}_h\|_{\mathcal{P}_h} \leq |||\boldsymbol{B}_h|||_{\Delta t,\mathrm{div}} \, |||\boldsymbol{D}_h|||_{\Delta t,\mathrm{div}} . \tag{3.178}$$

We recall that the Friedrichs-Poincaré inequality holds so that $\|D_h\|_{0,\Omega} \leq C \|\nabla D_h\|_{0,\Omega}$ for every $D_h \in \mathcal{V}_{h,0} \subset H_0^1(\Omega)$ and note that $\|\nabla D_h\|_{0,\Omega} = \|\mathbf{rot}\, D_h\|_{0,\Omega}$. In view of Lemma 3.90.1, we find that

$$\begin{aligned}
\big(\mathcal{I}^{\mathcal{V}_h}\big(\boldsymbol{u} \times \Pi^{RT} \boldsymbol{B}_h\big), D_h\big)_{\mathcal{V}_h} &\leq \widetilde{C} \|\boldsymbol{u}\|_\infty \|\boldsymbol{B}_h\|_{0,\Omega} \, \|D_h\|_{0,\Omega} && \text{[use Poincaré inequality]} \\
&\leq \widetilde{C} \|\boldsymbol{u}\|_\infty \|\boldsymbol{B}_h\|_{0,\Omega} \, \|\mathbf{rot}\, D_h\|_{0,\Omega} && \text{[use stability condition (3.81)]} \\
&\leq \widetilde{C} \|\boldsymbol{u}\|_\infty |||\boldsymbol{B}_h|||_{\mathcal{E}_h} \, |||\mathbf{rot}\, D_h|||_{\mathcal{E}_h} && \text{[multiply and divide by } \Delta t^{\frac{1}{2}}\text{]} \\
&\leq \widetilde{C} \|\boldsymbol{u}\|_\infty \Delta t^{-\frac{1}{2}} |||\boldsymbol{B}_h|||_{\mathcal{E}_h} \, \Delta t^{\frac{1}{2}} |||\mathbf{rot}\, D_h|||_{\mathcal{E}_h} && \text{[use definitions (3.162) and (3.163)]} \\
&\leq \widetilde{C} \|\boldsymbol{u}\|_\infty |||\boldsymbol{B}_h|||_{\Delta t,\mathrm{div}} \, |||D_h|||_{\Delta t,\mathbf{rot}} && \text{[use definition (3.161)]} \\
&\leq \widetilde{C} \|\boldsymbol{u}\|_\infty |||\xi|||_{\mathcal{X}_h} \, \|\eta\|_{\mathcal{X}_h} .
\end{aligned} \tag{3.179}$$

The assertion of the lemma follows from the definition of the norm in $\mathcal{X}_h$ and the above estimates.

□

Lemma 3.100.3 *Let $\theta > 0$. Then, for a sufficiently small Δt, there exists a real positive constant $\widehat{C}$, independent of h and Δt, such that:*

$$\inf_{\xi\in\mathcal{X}_h}\sup_{\eta\in\mathcal{X}_h}\frac{a_{h,0}(\xi,\eta)}{|||\xi|||_{\mathcal{X}_h}|||\eta|||_{\mathcal{X}_h}} \geq \widehat{C} > 0. \tag{3.180}$$

The constant $\widehat{C}$ depends on parameter θ (and the mesh regularity parameter ρ).

Proof. The assertion of the lemma follows from proving that for every $\xi = (\boldsymbol{B}_h, E_h) \in \mathcal{X}_h$ there exists a $\eta_\xi \in \mathcal{X}_h$ such that $|||\eta_\xi|||_{\mathcal{X}_h} \leq C|||\xi|||_{\mathcal{X}_h}$, and

$$a_{h,0}(\xi,\eta_\xi) \geq \widehat{C}|||\xi|||_{\mathcal{X}_h}|||\eta_\xi|||_{\mathcal{X}_h}, \tag{3.181}$$

where both C and $\widehat{C}$ are real positive constants independent of h and Δt. To this end, we first split the bilinear form in (3.165) as follows

$$a_{h,0}(\xi,\eta) = (\mathbf{T1}) + (\mathbf{T2}), \tag{3.182}$$

where

$$(\mathbf{T1}) = \big(\Delta t^{-1}\boldsymbol{B}_h + \mathbf{rot}\, E_h, \boldsymbol{C}_h\big)_{\mathcal{E}_h} + \big(\mathrm{div}\,\boldsymbol{B}_h, \mathrm{div}\,\boldsymbol{C}_h\big)_{\mathcal{P}_h}, \tag{3.183}$$

$$(\mathbf{T2}) = R_m\big(E_h + \theta\mathcal{I}^{\mathcal{V}_h}\big(\boldsymbol{u}\times\Pi^{RT}\boldsymbol{B}_h\big), D_h\big)_{\mathcal{V}_h} - \theta\big(\boldsymbol{B}_h, \mathbf{rot}\, D_h\big)_{\mathcal{E}_h}. \tag{3.184}$$

Then, for an arbitrary pair $\big(\boldsymbol{B}_h, E_h\big) = \xi \in \mathcal{X}_h$, we consider the pair $\big(\boldsymbol{C}_h, D_h\big) = \eta_\xi \in \mathcal{X}_h$ with $\boldsymbol{C}_h = (\theta/2)\big(\boldsymbol{B}_h + \Delta t\mathbf{rot}\, E_h\big)$ and $D_h = E_h$. Note that $\mathrm{div}\,\boldsymbol{C}_h = (\theta/2)\mathrm{div}\,\boldsymbol{B}_h$ because

$\operatorname{div}(\mathbf{rot}\, E_h) = 0$. Substituting ξ and η we transform the first term in (3.182) as follows:

$$(\mathbf{T1}) = \frac{\theta}{2}\Big(\big(\Delta t^{-1}\boldsymbol{B}_h + \mathbf{rot}\, E_h, \boldsymbol{B}_h + \Delta t \mathbf{rot}\, E_h\big)_{\mathcal{E}_h} + \big(\operatorname{div}\boldsymbol{B}_h, \operatorname{div}\boldsymbol{B}_h\big)\Big) \tag{3.185}$$

$$= \frac{\theta}{2}\Big(\Delta t^{-1}|||\boldsymbol{B}_h|||^2_{\mathcal{E}_h} + \Delta t|||\mathbf{rot}\, E_h|||^2_{\mathcal{E}_h} + 2\big(\boldsymbol{B}_h, \mathbf{rot}\, E_h\big)_{\mathcal{E}_h} + \|\operatorname{div}\boldsymbol{B}_h\|^2_{0,\Omega}\Big) \tag{3.186}$$

$$= \frac{\theta}{2}|||\boldsymbol{B}_h|||^2_{\Delta t,\operatorname{div}} + \frac{\theta}{2}\Delta t|||\mathbf{rot}\, E_h|||^2_{\mathcal{E}_h} + \theta\big(\boldsymbol{B}_h, \mathbf{rot}\, E_h\big)_{\mathcal{E}_h}. \tag{3.187}$$

Similarly, we transform the second term in (3.182) as follows:

$$(\mathbf{T2}) = R_m\big(E_h, E_h\big)_{\mathcal{V}_h} + R_m\theta\big(\mathcal{I}^{\mathcal{V}_h}\big(\boldsymbol{u}\times\Pi^{RT}\boldsymbol{B}_h\big), E_h\big)_{\mathcal{V}_h} - \theta\big(\boldsymbol{B}_h, \mathbf{rot}\, E_h\big)_{\mathcal{E}_h} \tag{3.188}$$

$$= R_m|||E_h|||^2_{\mathcal{V}_h} + R_m\theta\big(\mathcal{I}^{\mathcal{V}_h}\big(\boldsymbol{u}\times\Pi^{RT}\boldsymbol{B}_h\big), E_h\big)_{\mathcal{V}_h} - \theta\big(\boldsymbol{B}_h, \mathbf{rot}\, E_h\big)_{\mathcal{E}_h}. \tag{3.189}$$

Adding $(\mathbf{T1})$ and $(\mathbf{T2})$ we find that

$$\begin{aligned} a_{h,0}(\xi,\eta) &= \frac{\theta}{2}|||\boldsymbol{B}_h|||^2_{\Delta t,\operatorname{div}} + \frac{\theta}{2}\Delta t|||\mathbf{rot}\, E_h|||^2_{\mathcal{E}_h} + R_m|||E_h|||^2_{\mathcal{V}_h} + R_m\theta\big(\mathcal{I}^{\mathcal{V}_h}\big(\boldsymbol{u}\times\Pi^{RT}\boldsymbol{B}_h\big), E_h\big)_{\mathcal{V}_h} \\ &\geq K\theta\left(\frac{1}{2}|||\boldsymbol{B}_h|||^2_{\Delta t,\operatorname{div}} + \frac{1}{2}|||E_h|||^2_{\Delta t,\mathbf{rot}} + \big(\mathcal{I}^{\mathcal{V}_h}\big(\boldsymbol{u}\times\Pi^{RT}\boldsymbol{B}_h\big), E_h\big)_{\mathcal{V}_h}\right), \end{aligned} \tag{3.190}$$

where $K = \min\{1, R_m\}$. Now, we prove that the right hand side of (3.190) can be bounded from below by $|||\xi|||^2_{\mathcal{X}_h}$ for a suitable choice of Δt. Using the results of the Lemma 3.90.1 as an upper bound estimate we have

$$\begin{aligned} \big(\mathcal{I}^{\mathcal{V}_h}\big(\boldsymbol{u}\times\Pi^{RT}\boldsymbol{B}_h\big), E_h\big)_{\mathcal{V}_h} &\geq -\widetilde{C}\|\boldsymbol{u}\|_\infty\|\boldsymbol{B}_h\|_{0,\Omega}\,\|E_h\|_{0,\Omega} && \text{[multiply and divide by } \Delta t^{\frac{1}{2}}\text{]} \\ &\geq -\widetilde{C}\|\boldsymbol{u}\|_\infty\Delta t^{\frac{1}{2}}\Delta t^{-\frac{1}{2}}\,\|\boldsymbol{B}_h\|_{0,\Omega}\,\|E_h\|_{0,\Omega} && \text{[use Young's inequality]} \\ &\geq -\widetilde{C}\|\boldsymbol{u}\|_\infty\Delta t^{\frac{1}{2}}\left(\tfrac{1}{2}\Delta t^{-1}\|\boldsymbol{B}_h\|^2_{\mathcal{E}_h} + \tfrac{1}{2}\|E_h\|^2_{\mathcal{V}_h}\right) && \text{[use definitions (3.162) and (3.163)]} \\ &\geq -\widetilde{C}\|\boldsymbol{u}\|_\infty\left(\tfrac{1}{2}|||\boldsymbol{B}_h|||^2_{\Delta t,\operatorname{div}} + \tfrac{1}{2}|||E_h|||^2_{\Delta t,\mathbf{rot}}\right), \end{aligned} \tag{3.191}$$

where we note that $\widetilde{C} = (\beta^*)^{\frac{1}{2}} \|\mathcal{I}^{\mathcal{V}_h}\|$ is the constant from Lemma 3.90.1. We choose Δt sufficiently small so that $C = K(1 - \widetilde{C}\|\boldsymbol{u}\|_\infty \Delta t^{\frac{1}{2}}) > 0$ and we write

$$a_{h,0}(\xi,\eta) \geq \frac{K\theta}{2}\left(1 - \widetilde{C}\|\boldsymbol{u}\|_\infty \Delta t^{\frac{1}{2}}\right)\left(|||\boldsymbol{B}_h|||^2_{\Delta t,\mathrm{div}} + |||E_h|||^2_{\Delta t,\mathbf{rot}}\right) \geq C\frac{\theta}{2}|||\xi|||^2_{\mathcal{X}_h}. \quad (3.192)$$

Finally, we note that

$$\begin{aligned}
|||\eta_\xi|||^2_{\mathcal{X}_h} &= |||(\theta/2)\left(\boldsymbol{B}_h + \Delta t\ \mathbf{rot}\, E_h\right)|||^2_{\Delta t,\mathrm{div}} + |||E_h|||^2_{\Delta t,\mathbf{rot}} \\
&= \frac{\theta^2}{4}\left(\Delta t^{-1}|||\boldsymbol{B}_h + \Delta t\mathbf{rot}\, E_h|||^2_{\mathcal{E}_h} + \|\mathrm{div}\,\boldsymbol{B}_h\|^2_{0,\Omega}\right) + |||E_h|||^2_{\Delta t,\mathbf{rot}} \\
&= \frac{\theta^2}{4}\left(\Delta t^{-1}|||\boldsymbol{B}_h|||^2_{\mathcal{E}_h} + \Delta t|||\mathbf{rot}\, E_h|||^2_{\mathcal{E}_h} + 2\Big(\boldsymbol{B}_h, \mathbf{rot}\, E_h\Big)_{\mathcal{E}_h} + \|\mathrm{div}\,\boldsymbol{B}_h\|^2_{0,\Omega}\right) \\
&\qquad + |||E_h|||^2_{\Delta t,\mathbf{rot}} \\
&= \frac{\theta^2}{4}\left(\Delta t^{-1}|||\boldsymbol{B}_h|||^2_{\mathcal{E}_h} + \|\mathrm{div}\,\boldsymbol{B}_h\|^2_{0,\Omega} + 2\Big(\Delta t^{-1/2}\boldsymbol{B}_h, \Delta t^{1/2}\mathbf{rot}\, E_h\Big)_{\mathcal{E}_h} + \Delta t|||\mathbf{rot}\, E_h|||^2_{\mathcal{E}_h}\right) \\
&\qquad + |||E_h|||^2_{\Delta t,\mathbf{rot}} \\
&\leq \frac{\theta^2}{4}\left(2\Delta t^{-1}|||\boldsymbol{B}_h|||^2_{\mathcal{E}_h} + \|\mathrm{div}\,\boldsymbol{B}_h\|^2_{0,\Omega} + 2\Delta t|||\mathbf{rot}\, E_h|||^2_{\mathcal{E}_h}\right) + |||E_h|||^2_{\Delta t,\mathbf{rot}} \\
&\leq \frac{\theta^2}{2}|||\boldsymbol{B}_h|||^2_{\Delta t,\mathrm{div}} + \left(1 + \frac{\theta^2}{2}\right)|||E_h|||^2_{\Delta t,\mathbf{rot}} \\
&\leq \left(1 + \frac{\theta^2}{2}\right)|||\xi|||^2_{\mathcal{X}_h}.
\end{aligned}$$

The last inequality implies that

$$\forall \xi \in \mathcal{X}_h\ \ \exists \eta \in \mathcal{X}_h : \quad a_{h,0}(\xi,\eta) \geq K\widehat{C}|||\xi|||_{\mathcal{X}_h}|||\eta|||_{\mathcal{X}_h}, \qquad \widehat{C} = C\frac{\theta}{2}\left(1 + \frac{\theta^2}{2}\right)^{-\frac{1}{2}}, \quad (3.193)$$

from which the *inf-sup* condition stated in the lemma follows immediately. Note that for Δt sufficiently small, we have $0 < C < 1$. Hence, we can just set $C = 1$. □

Having collected the necessary results we present the main Theorem of this section.

Theorem 3.100.4 *The linear system described in* (3.157) *is well-posed.*

Proof. Lemmas 3.100.3 and 3.100.2 show that problem 3.100.2 satisfies the hypothesis of Theorem 2.20.1. Moreover, by Lemma 3.100.1 we know that system (3.157) and Problem 3.100.1 are equivalent. □

3.11 The Oblique Projectors in $\mathcal{V}_h(\mathsf{P})$

In Section 3.4 we presented criteria for an admissible oblique projector. In this section we present three different choices together with an explanation on how they can be computed.

3.111 The Elliptic Projector

The elliptic projector is denoted $\Pi^{\nabla}_{\mathsf{P}}$. For $D_h \in \mathcal{V}_h(\mathsf{P})$ the elliptic projector is the solution to the variational problem

$$\forall q \in \mathbb{P}_1(\mathsf{P}): \quad \int_{\mathsf{P}} \mathbf{rot}\ \left(D_h - \Pi^{\nabla}_{\mathsf{P}} D_h\right) \cdot \mathbf{rot}\, q dA = 0, \tag{3.194a}$$

$$\mathsf{P}_0(D_h - \Pi^{\nabla}_{\mathsf{P}} D_h) = 0, \tag{3.194b}$$

where,

$$P_0(D_h) = \sum_{\mathsf{v}} D_h(\mathsf{v}). \tag{3.195}$$

Note that in the case that D_h is a constant, the variational definition in (3.194a) is simply the statement that zero must equal zero which does not yield a means to define $\Pi^{\nabla}_{\mathsf{P}}$. We use P_0 precisely to fix the value of constants.

Following the framework of Section 2.3 all that is required to compute the elliptic projector is a means of attaining the quantities

$$\forall q \in \mathbb{P}_1(\mathsf{P}): \quad \int_{\mathsf{P}} \mathbf{rot}\, D_h \cdot \mathbf{rot}\, q dA. \tag{3.196}$$

We will use Green's Theorem:

$$\int_{\mathsf{P}} \mathbf{rot}\, D_h \cdot \mathbf{rot}\, q dA = \int_{\mathsf{P}} D_h \mathrm{rot}\, \mathbf{rot}\, q dA - \int_{\partial \mathsf{P}} (D_h \times \mathbf{rot}\, q) \cdot \boldsymbol{n} d\ell \tag{3.197}$$

From the definition of $\mathcal{V}_h(\mathsf{P})$ we know that $\mathrm{rot}\, \mathbf{rot}\, D_h = 0$. Moreover, using the identity

$$D_h \times \mathbf{rot}\, q \cdot \boldsymbol{n} = D_h \mathbf{rot}\, q \times \boldsymbol{n} = -D_h \mathbf{rot}\, q \cdot \boldsymbol{t}, \tag{3.198}$$

where, $\boldsymbol{n} = (n_1, n_2)$ and $\boldsymbol{t} = (-n_2, n_1)$. Thus, we arrive at the formula

$$\int_{\mathsf{P}} \mathbf{rot}\, D_h \cdot \mathbf{rot}\, q dA = \sum_{\mathsf{e} \in \partial \mathsf{P}} \int_{\mathsf{e}} D_h \mathbf{rot}\, q \cdot \boldsymbol{t} d\ell. \tag{3.199}$$

Note, that by definition $D_h \in \mathbb{P}_1(\mathsf{e})$ for every edge in P. Since we know two evaluations of D_h then we can reconstruct the function and compute the right hand side of (3.199).

Consider the basis for $\mathbb{P}_1(\mathsf{P})$ given by $\{m_1, m_2, m_3\}$ for

$$\forall (x, y) \in \mathsf{P}: \quad m_1(x, y) = 1, \quad m_2(x, y) = x - x_{\mathsf{P}} \quad \text{and} \quad m_3(x, y) = y - y_{\mathsf{P}}. \tag{3.200}$$

In the above $(x_{\mathsf{P}}, y_{\mathsf{P}})$ is the centroid of the cell P. In this case we can use the following formulas to compute the matrices G and H in Section 2.3:

$$\|\mathbf{rot}\, m_2\|_{L^2} = \|\mathbf{rot}\, m_3\|_{L^2} = |\mathsf{P}|, \quad \Big(m_2, m_3\Big) = 0. \tag{3.201}$$

Moreover, consider a basis consistent with the degrees of freedom for the space $\mathcal{V}_h(\mathsf{P})$, say $\{D_h^i : 1 \leq i \leq N\}$. We can use (3.199) in order to prove the identities

$$P_0 D_h^i = \frac{1}{N}, \quad \left(\mathbf{rot}\, m_2, \mathbf{rot}\, D_h^i\right) = \frac{1}{2}\left(|\mathsf{e}_k| t_{k,y} + |\mathsf{e}_j| t_{j,y}\right),$$
$$\left(\mathbf{rot}\, m_3, \mathbf{rot}\, D_h^i\right) = -\frac{1}{2}\left(|\mathsf{e}_k| t_{k,x} + |\mathsf{e}_j| t_{j,x}\right). \tag{3.202}$$

Here e_k and e_j are edges that have that have the $i-$th node as an endpoint. Vectors tangent to each of these edges are $(t_{k,x}, t_{k,y})$ and $(t_{j,x}, t_{j,y})$ respectively. We can use these formulas to compute the matrix B in Section 2.3.

3.112 The Least Squares Projector

The second projector we consider is Π^{LS}_{P}. For a function $D_h \in \mathcal{V}_h(\mathsf{P})$ we define $\Pi^{LS}_{\mathsf{P}} D_h$ as the first degree polynomial whose evaluations at the nodes of P are the closest, in Euclidean norm, to those of D_h. Let us consider the basis for $\mathbb{P}_1(\mathsf{P})$ denoted by $\{m_1, m_2, m_3\}$ and given by

$$\forall (x,y) \in \mathsf{P}: \quad m_1(x,y) = 1, \quad m_2(x,y) = x - x_{\mathsf{P}} \quad \text{and} \quad m_3(x,y) = y - y_{\mathsf{P}}. \tag{3.203}$$

Let $\{\mathsf{v}_i : 1 \leq i \leq N\}$ be the set of nodes of P. Then, we can write

$$\forall (x,y) \in \mathsf{P}: \quad \Pi^{LS}_{\mathsf{P}} D_h(x,y) = a m_1(x,y) + b m_2(x,y) + c m_3(x,y), \tag{3.204}$$

where the coefficients a, b, c are given as the least squares solution to the system $Ax = b$, amd where

$$A = \begin{pmatrix} m_1(\mathsf{v}_1) & m_2(\mathsf{v}_1) & m_3(\mathsf{v}_1) \\ m_1(\mathsf{v}_2) & m_2(\mathsf{v}_2) & m_3(\mathsf{v}_2) \\ \vdots & \vdots & \vdots \\ m_1(\mathsf{v}_N) & m_2(\mathsf{v}_N) & m_3(\mathsf{v}_N) \end{pmatrix}, \quad b = \begin{pmatrix} D_h(\mathsf{v}_0) \\ D_h(\mathsf{v}_2) \\ \vdots \\ D_h(\mathsf{v}_N) \end{pmatrix}. \tag{3.205}$$

Thus, in the notation of Section 2.3 we can consider $G = (A^T A)^{-1} A^T$.

3.113 The Galerkin Interpolator

The final projector that we present is denoted as Π^{pw}_{P}. This projector is experimental in the sense that its codomain is the space of piecewise polynomials. We consider a point $\mathsf{v}*$ in the interior of the cell P. Consider that

$$\mathsf{v}* = \sum_{\mathsf{v}} \alpha_{\mathsf{v}} \mathsf{v}. \tag{3.206}$$

For a function $D_h \in \mathcal{V}_h(\mathsf{P})$ we define

$$\Pi_{\mathsf{P}}^{pw} D_h(\mathsf{v}*) = \sum_{\mathsf{v}} \alpha_{\mathsf{v}} D_h(\mathsf{v}), \quad \Pi_{\mathsf{P}}^{pw} D_h(\mathsf{v}) = D_h(\mathsf{v}). \tag{3.207}$$

We further require that P be star shaped with respect to to $\mathsf{v}*$. This assumption is laid out in Section 2.4. Thus, we can connect $\mathsf{v}*$ with the vertices v to divide P into triangles, $\{T_i : 1 \leq i \leq N\}$. If $\mathsf{v}_1, \mathsf{v}_2$ and $\mathsf{v}*$ are the vertices of one of these triangles then we define the restriction of $\Pi_{\mathsf{P}}^{pw} D_h$ to this triangle as the first degree polynomial that agrees with the evaluations presented in (3.207).

Now we turn our attention to the details that are involved in the implementation of this projector. In this manuscript we will consider implementations only in convex cells. In this case we can use

$$\mathsf{v}* = \sum_{\mathsf{v}} \frac{1}{N} \mathsf{v}. \tag{3.208}$$

Recall that convex cells are, by definition, star-shaped with respect to every point in its interior. Next, let us consider

$$V = \{\phi_{\mathsf{v}} : \mathsf{v} \text{ is node of P}\} \cup \{\phi_{\mathsf{v}*}\} \tag{3.209}$$

as a basis for the codomain of Π_{P}^{pw}. The function Φ_{v} evaluates to 1 over the node v and zero over every other node including. The projector can be computed as

$$\Pi_{\mathsf{P}}^{pw} D_h = \frac{\sum_{v \in \partial P} D_h(\mathsf{v})}{N} \phi_{\mathsf{v}*} + \sum_{\mathsf{v}} D_h(\mathsf{v}) \phi_{\mathsf{v}}. \tag{3.210}$$

Therefore, in the notation of Section 2.3 we can use

$$\Pi_*^M = \begin{pmatrix} 1 & 0 & \dots & 0 \\ 0 & 1 & \dots & 0 \\ \vdots & \vdots & \ddots & \vdots \\ \frac{1}{N} & \frac{1}{N} & \dots & \frac{1}{N} \end{pmatrix}. \tag{3.211}$$

The matrix H requires a different definition. We use

$$H = \begin{pmatrix} \left(\phi_{\mathsf{v}_1}, \phi_{\mathsf{v}_1}\right) & \left(\phi_{\mathsf{v}_1}, \phi_{\mathsf{v}_2}\right) & \dots & \left(\phi_{\mathsf{v}_1}, \phi_{\mathsf{v}*}\right) \\ \vdots & \vdots & \ddots & \vdots \\ \left(\phi_{\mathsf{v}*}, \phi_{\mathsf{v}_1}\right) & \left(\phi_{\mathsf{v}*}, \phi_{\mathsf{v}_2}\right) & \dots & \left(\phi_{\mathsf{v}*}, \phi_{\mathsf{v}*}\right). \end{pmatrix} \tag{3.212}$$

To compute these integrals we use the reference element method. All of our computations will be done over the triangle T_0 with vertices at $(1,0),(0,0),(0,1)$. We define a series of affine transformations to translate computations over T_0 to those over some other triangle T. If the triangle T has vertices $v = (v_x, v_y), w = (w_x, w_y), z = (z_x, z_y)$ then the affine transformation that sends T_0 to T is given by

$$L(x,y) = \begin{pmatrix} w_x - v_x & z_x - v_x \\ w_y - v_y & z_y - v_y \end{pmatrix} \begin{pmatrix} x \\ y \end{pmatrix} + \begin{pmatrix} v_x \\ v_y \end{pmatrix}. \tag{3.213}$$

This transformation satisfies

$$L(0,0) = v, \quad L(1,0) = w \quad \text{and} \quad L(0,1) = z. \tag{3.214}$$

Thus, an affine transformation that sends T to T_0 is given by $K = L^{-1}$. An affine transformation

that sends the triangle T to the standard triangle T_0 is given by $L^{-1} = K$ which is

$$K(x,y) = \frac{\begin{pmatrix} z_y - v_y & v_x - z_x \\ v_y - w_y & w_x - v_x \end{pmatrix} \begin{pmatrix} x - v_x \\ y - v_y \end{pmatrix}}{(w_x - v_x)(z_y - v_y) - (w_y - v_y)(z_x - v_x)}. \tag{3.215}$$

Further, over the triangle T_0 we can define the basis $\{\psi_1, \psi_2, \psi_3\}$ as

$$\psi_1(x,y) = 1 - x - y, \quad \psi_2(x,y) = y \quad \text{and} \quad \psi_3(x,y) = x. \tag{3.216}$$

Thus, computations follow from the Change of Variables Theorem:

$$\begin{aligned} \int_T \phi_i \phi_j = \int_T \psi_m \circ K \psi_n \circ K = \\ = [(w_x - v_x)(z_y - v_y) - (w_y - v_y)(z_x - v_x)] \int_{T_0} \psi_m \psi_n. \end{aligned} \tag{3.217}$$

3.12 Conclusions

In this chapter, in Section 3.2 we came up with a model for the evolution of the electric and magnetic fields generated by a magnetized fluid. We assumed that the velocity of the flow was prescribed and known. Then, in Section 3.3 we presented a variational formulation of the aforementioned model and a VEM for the model. Sections 3.4, 3.5 and 3.6 present the spaces that appear in the variational formulation as well as the operators that act on functions from these spaces. In these sections the spaces are studied on an individual basis whereas in Section 3.7 we show that they form a commuting De-Rham complex. It is this De-Rham complex that guarantees that the magnetic field is divergence free. This condition is the statement of Gauss's Law presented in Section 3.2. Its violation will yield simulations that experience fictitious forces that will render them unfaithful to real MHD phenomena. A more complete discussion is presented

at the concluding remarks of Section 3.7. We also showed that the linear VEM developed satisfies a series of energy inequalities that show this method is stable, which was the main result of Section 3.9. Then, in Section 3.8 we extended the virtual elements introduced to arbitrary order. Implementations of this method will have to solve a linear system at each time step. We show that this system is well-posed in Section 3.10. We finish with Section 3.11 with a discussion about the construction of an important projectors in the nodal space presented in Section 3.4.

4. KINEMATICS IN 3D

4.1 Introduction

This chapter is dedicated to extending the VEM developed in chapter 3. to three dimensions. The main difference is lies in the virtual elements that are used. The derivation of the model and its mathematical formulation are essentially the same. Hence, readers interested in some discussion about the physical principles are referred to 3.2. In Section 4.2 we will briefly recall the mathematical formulation. Then, in Section 4.3 we present the three dimensional virtual elements. First is the analog to the nodal space in Section 3.4; this space is denoted $\mathcal{V}_h$. Similar to the situation in two dimensions the orthogonal projection in this space is not computable. Thus, in this section we will also propose an oblique projector. The second space is the analog of the edge space of Section 3.5 denoted $\mathcal{E}_h$. The computation of the orthogonal projection in this space is possible; we will present a procedure to do so. In the study of each of these we must introduce some important polynomial spaces. We also include bases for each of these spaces which will be important when computing the degrees of freedom of a function. These spaces form a De-Rham complex which can be used to prove that the scheme will respect the divergence of the magnetic field at the discrete level. These results are presented in Section 4.4. Using this complex we can show that the magnetic field at the discrete level will be solenoidal, a result that we present in the same section. The final result of Section 4.4 regards the curl of a function in the space $\mathcal{V}_h$. We can show that if $\boldsymbol{D}_h \in \mathcal{V}_h$ then $\nabla \times \boldsymbol{D}_h \in \mathcal{E}_h$. Hence, in order to identify $\nabla \times \boldsymbol{D}_h$ we will present a method to compute its degrees of freedom. Then, in Section 4.5 we will briefly discuss some extensions to higher orders. Finally, in Section 4.6 we will present some concluding remarks about this chapter.

4.2 Mathematical Formulation

The mathematical formulation is no different than the one presented in Section 3.3. For the sake of completeness we will briefly go over it.

Consider a polyhedral domain $\Omega \subset \mathbb{R}^3$. The strong form of the system we are interested in is:

$$\frac{\partial}{\partial t}\boldsymbol{B} + \nabla \times \boldsymbol{E} = \boldsymbol{0} \quad \text{in} \quad \Omega, \tag{4.1a}$$

$$\boldsymbol{E} + \boldsymbol{u} \times \boldsymbol{B} - R_m^{-1}\nabla \times \boldsymbol{B} = \boldsymbol{0} \quad \text{in} \quad \Omega, \tag{4.1b}$$

$$\boldsymbol{B}(0) = \boldsymbol{B}_0 \quad \text{in} \quad \Omega \tag{4.1c}$$

$$\boldsymbol{E} \equiv \boldsymbol{E}_b \quad \text{along} \quad \partial\Omega. \tag{4.1d}$$

Like before we will assume that

$$\nabla \cdot \boldsymbol{B}_0 = 0. \tag{4.2}$$

We can prove that the solution to (4.1) is the same as the solution to the following variational formulation: *find* $(\boldsymbol{B}, \boldsymbol{E}) \in C^1\left([0,T], H(\nabla\cdot;\Omega)\right) \times C\left([0,T], H(\nabla\times;\Omega)\right)$*, such that:*

$$\Big(\frac{\partial}{\partial t}\boldsymbol{B}, \boldsymbol{C}\Big) + \Big(\nabla \times \boldsymbol{E}, \boldsymbol{C}\Big) = 0 \qquad \forall \boldsymbol{C} \in H(\nabla\cdot;\Omega), \tag{4.3a}$$

$$R_m\Big(\boldsymbol{E}, \boldsymbol{D}\Big) + R_m\Big(\boldsymbol{u} \times \boldsymbol{B}, \boldsymbol{D}\Big) - \Big(\boldsymbol{B}, \nabla \times \boldsymbol{D}\Big) = 0 \qquad \forall v \in H_0(\nabla\times;\Omega), \tag{4.3b}$$

$$\boldsymbol{B}(0) = \boldsymbol{B}^0 \;\; \text{with} \;\; \operatorname{div} \boldsymbol{B}^0 = 0. \tag{4.3c}$$

We introduce two spaces of shape functions $\mathcal{V}_h$ and $\mathcal{E}_h$. These spaces are finite dimensional and approximate $H(\nabla\times;\Omega)$ and $H(\nabla\cdot;\Omega)$ respectively. We will formally define these spaces in Section 4.3. The discrete variational formulation of system (4.3) is given by *find* $\left\{\boldsymbol{B}_h^n\right\}_{n=0}^{N} \subset \mathcal{E}_h$ *and* $\left\{\boldsymbol{E}_h^{n+\theta}\right\}_{n=0}^{N-1} \subset \mathcal{V}_h$ *such that for all* $(\boldsymbol{C}_h, D_h) \in \mathcal{E}_h \times \mathcal{V}_{h,0}$ *it holds that:*

$$\Big(\frac{\boldsymbol{B}_h^{n+1}-\boldsymbol{B}_h^n}{\Delta t},\boldsymbol{C}_h\Big)_{\mathcal{E}_h}+\Big(\nabla\times\boldsymbol{E}_h^{n+\theta},\boldsymbol{C}_h\Big)_{\mathcal{E}_h}=0 \tag{4.4a}$$

$$R_m\big(\boldsymbol{E}_h^{n+\theta},\boldsymbol{D}_h\big)_{\mathcal{V}_h}+R_m\big(\mathcal{I}^{\mathcal{V}_h}\big(\boldsymbol{u}\times\Pi^{RT}\boldsymbol{B}_h^{n+\theta}\big),\boldsymbol{D}_h\big)_{\mathcal{V}_h}-\big(\boldsymbol{B}_h^{n+\theta},\mathbf{rot}\,\boldsymbol{D}_h\big)_{\mathcal{E}_h}=0 \tag{4.4b}$$

$$\boldsymbol{B}_h^{n+\theta}=\theta\boldsymbol{B}_h^{n+1}+(1-\theta)\boldsymbol{B}_h^n, \tag{4.4c}$$

$$\boldsymbol{B}_h(\cdot,0)=\mathcal{I}^{\mathcal{E}_h}\big(\boldsymbol{B}^0\big)\quad\text{with}\quad\operatorname{div}\boldsymbol{B}^0=0. \tag{4.4d}$$

4.3 The Virtual Elements

These finite elements are presented in [16]. For the space $\mathcal{V}_h$ we will use $k=2$, whereas for $\mathcal{E}_h$ element we will use $k=1$.

4.31 The Space $\mathcal{V}_h$

Consider a cell P in the mesh Ω_h. Let us introduce the following polynomial spaces

$$\boldsymbol{R}_k(\mathsf{P})=\nabla\times[\mathbb{P}_{k+1}(\mathsf{P})]^3,\quad \boldsymbol{R}_k(\mathsf{f})=\mathbf{rot}\,\mathbb{P}_{k+1}(\mathsf{f}). \tag{4.5}$$

We consider f to be a face of the cell P. We also define the orthogonal complements of these spaces as

$$\boldsymbol{R}_k(\mathsf{P})^\perp=\Big\{\boldsymbol{r}^\perp\in\mathbb{P}_k(\mathsf{P}):\forall\boldsymbol{r}\in\boldsymbol{R}_k(\mathsf{P})\quad\big(\boldsymbol{r}^\perp,\boldsymbol{r}\big)=0\Big\}, \tag{4.6}$$

$$\boldsymbol{R}_k(\mathsf{f})^\perp=\Big\{\boldsymbol{r}^\perp\in\mathbb{P}_k(\mathsf{f}):\forall\boldsymbol{r}\in\boldsymbol{R}_k(\mathsf{f})\quad\big(\boldsymbol{r}^\perp,\boldsymbol{r}\big)=0\Big\}. \tag{4.7}$$

Moreover, we denote the projection onto a face f as

$$\boldsymbol{D}_h^{\mathsf{f}}=\boldsymbol{D}_h-(\boldsymbol{D}_h\cdot\boldsymbol{n}_{\mathsf{f}})\boldsymbol{n}_{\mathsf{f}}. \tag{4.8}$$

A function $\boldsymbol{D}_h$ belongs to the local space $\mathcal{V}_h(\mathsf{P})$ if and only if it satisfies

- $\boldsymbol{D}_h \in H(\nabla\cdot;\mathsf{P}) \cap H(\nabla\times;\mathsf{P})$.
- For every face f: $\boldsymbol{D}_h^{\mathsf{f}} \in H(\mathrm{div};\mathsf{f}) \cap H(\mathrm{rot};\mathsf{f})$.
- For every face f: $\mathbf{rot}\,\mathrm{rot}\, D_h^{\mathsf{f}} \in \boldsymbol{R}_0(\mathsf{f})$.
- For every face f: $\mathrm{div}\,\boldsymbol{D}_h^{\mathsf{f}} \in \mathbb{P}_1(\mathsf{f})$.
- For every edge e: $\boldsymbol{D}_h \cdot \boldsymbol{t} \in \mathbb{P}_2(\mathsf{e})$.
- For every edge e: $\boldsymbol{D}_h \cdot \boldsymbol{t}_{\mathsf{f}_1} = \boldsymbol{D}_h \cdot \boldsymbol{t}_{\mathsf{f}_2}$ whenever e is a common edge of f_1 and f_2.
- $\mathrm{div}\,\boldsymbol{D}_h \in \mathbb{P}_1(\mathsf{P})$.
- $\nabla \times \nabla \times \boldsymbol{D}_h \in \boldsymbol{R}_0(\mathsf{P})$.

To a function $\boldsymbol{D}_h \in \mathcal{V}_h(\mathsf{P})$ we associate the following set of degrees of freedom:

- For every edge e: $\int_{\mathsf{e}} \boldsymbol{D}_h \cdot \boldsymbol{t} r d\ell,\ r \in \mathbb{P}_2(\mathsf{e})$.
- For every face f: $\int_{\mathsf{f}} \boldsymbol{D}_h \cdot \boldsymbol{r}^{\perp} dS,\ \boldsymbol{r}^{\perp} \in \boldsymbol{R}_2(\mathsf{f})^{\perp}$.
- For every face f: $\int_{\mathsf{f}} \boldsymbol{D}_h \cdot \boldsymbol{r}^{\perp} dS,\ \boldsymbol{r}^{\perp} \in \boldsymbol{R}_0(\mathsf{f})^{\perp}$.
- $\int_{\mathsf{P}} \boldsymbol{D}_h \cdot \boldsymbol{r}^{\perp} dV,\ \boldsymbol{r}^{\perp} \in \boldsymbol{R}_2(\mathsf{P})^{\perp}$.
- $\int_{\mathsf{P}} \boldsymbol{D}_h \cdot \boldsymbol{r}^{\perp} dV,\ \boldsymbol{r}^{\perp} \in \boldsymbol{R}_0(\mathsf{P})^{\perp}$.

It can be shown that the space $\mathcal{V}_h(\mathsf{P})$ is unisolvent when equipped with this set of degrees of freedom.

Theorem 4.31.1 *The finite element defined by the domain P, the space of shape functions $\mathcal{V}_h(\mathsf{P})$ and the degrees of freedom presented is unisolvent.*

Proof of the previous theorem is presented in [16]. We can use this result to define the interpolant $\mathcal{I}_{\mathsf{P}}^{\mathcal{V}_h} : H(\nabla\times;\mathsf{P}) \to \mathcal{V}_h(\mathsf{P})$ such that $\mathcal{I}_{\mathsf{P}}^{\mathcal{V}_h}\boldsymbol{D}$ and $\boldsymbol{D}$ share the same degrees of freedom.

Next we will consider the inner product. Like before we do this through a projector, ideally the orthogonal projector. However, this projector is not computable. So we will use an oblique projector $\Pi : \mathcal{V}_h(\mathsf{P}) \to [\mathbb{P}_2(\mathsf{P})]^3$ satisfying:

P1 The projection $\Pi \boldsymbol{D}_h$ is computable from the degrees of freedom of $\boldsymbol{D}_h$.

P2 If $\boldsymbol{D}_h \in [\mathbb{P}_2(\mathsf{P})]^3$ then $\Pi \boldsymbol{D}_h = \boldsymbol{D}_h$.

P3 There exists a constant $C > 0$ independent of mesh size and time step such that

$$\|\Pi \boldsymbol{D}_h\|_{0,\mathsf{P}} \leq C \|\boldsymbol{D}_h\|_{0,\mathsf{P}}. \tag{4.9}$$

These are the same criteria that we presented in Section 3.4. We will present an example of one of these projectors later in this section. The inner product is defined as

$$\forall \boldsymbol{E}_h, \boldsymbol{D}_h \in \mathcal{V}_h(\mathsf{P}): \quad \Big(\boldsymbol{E}_h, \boldsymbol{D}_h\Big)_{\mathcal{V}_h(\mathsf{P})} = \big(\Pi \boldsymbol{E}_h, \Pi \boldsymbol{D}_h\big) + \mathcal{S}^{\mathsf{v}}((1-\Pi)\boldsymbol{E}_h, (1-\Pi)\boldsymbol{D}_h). \tag{4.10}$$

The bilinear form $\mathcal{S}^{\mathsf{v}}$ is picked such that

$$\exists s_*, s^* > 0 \quad \forall D_h \in \ker \Pi \cap \mathcal{V}_h(\mathsf{P}): \quad s_* \|\boldsymbol{D}_h\|_{0,\mathsf{P}}^2 \leq \mathcal{S}^{\mathsf{v}}(\boldsymbol{D}_h, \boldsymbol{D}_h) \leq s^* \|\boldsymbol{D}_h\|_{0,\mathsf{P}}^2. \tag{4.11}$$

We can define the norm in $\mathcal{V}_h(\mathsf{P})$ as

$$\forall \boldsymbol{D}_h \in \mathcal{V}_h(\mathsf{P}): \quad |||\boldsymbol{D}_h|||_{\mathcal{V}_h(\mathsf{P})} = \big(\boldsymbol{D}_h, \boldsymbol{D}_h\big)_{\mathcal{V}_h(\mathsf{P})}^{1/2}. \tag{4.12}$$

This definition of an inner product satisfies the same consistency and stability conditions presented in Theorem 4.31.2. We present this result for the sake of completeness. The proof is essentially the same.

Theorem 4.31.2 *The inner product defined in equation* (3.38) *has first order* ***polynomial accu-***

***racy**. This is to say that*

$$\forall p, q \in \mathbb{P}_1(\mathsf{P}) \subset \mathcal{V}_h(\mathsf{P}): \quad \Big(p, q\Big)_{\mathcal{V}_h(\mathsf{P})} = \big(p, q\big). \tag{4.13}$$

*Moreover, this inner product also satisfies the following **stability** property. There exists constants $C_*, C^* > 0$ independent of the mesh-size and time-step such that*

$$\forall \boldsymbol{D}_h \in \mathcal{V}_h(\mathsf{P})^2: \quad \alpha_* \|\boldsymbol{D}_h\|_{0,\mathsf{P}}^2 \leq |||D_h|||_{\mathcal{V}_h(\mathsf{P})}^2 \leq \alpha^* \|\boldsymbol{D}_h\|_{0,\mathsf{P}}^2. \tag{4.14}$$

The global space is defined as

$$\mathcal{V}_h = \left\{ \boldsymbol{D}_h \in H(\nabla\times;\Omega) : \forall \mathsf{P} \in \Omega_h \quad \boldsymbol{D}_{h|\mathsf{P}} \in \mathcal{V}_h(\mathsf{P}) \right\}. \tag{4.15}$$

We equip this space with the inner product:

$$\forall \boldsymbol{E}_h, \boldsymbol{D}_h \in \mathcal{V}_h: \quad \big(\boldsymbol{E}_h, \boldsymbol{D}_h\big)_{\mathcal{V}_h} = \sum_{\mathsf{P}\in\Omega_h} \big(\boldsymbol{E}_{h|\mathsf{P}}, \boldsymbol{D}_{h|\mathsf{P}}\big)_{\mathcal{V}_h(\mathsf{P})}. \tag{4.16}$$

As a consequence of Theorem 4.31.2 the global inner product also satisfies some desirable properties. We present them in the following corollary:

Corollary 4.31.1 *The inner product defined in* (4.16) *satisfies the **accuracy** property for piecewise-linear polynomials. If for every $\mathsf{P} \in \Omega_h$ it is the case that $p_{|\mathsf{P}}, q_{|\mathsf{P}} \in \mathbb{P}_1(\mathsf{P})$ then*

$$\big(p, q\big)_{\mathcal{V}_h} = \big(p, q\big). \tag{4.17}$$

*The following **stability** condition is also satisfied*

$$\exists \beta_*, \beta^* > 0 \; \forall D_h \in \mathcal{V}_h: \quad \beta_* \|D_h\|_{0,\Omega}^2 \leq |||D_h|||_{\mathcal{V}_h}^2 \leq \beta^* \|D_h\|_{0,\Omega}^2, \tag{4.18}$$

where the constants β_* and β^* are independent of the mesh-size and time-step.

Finally, we define the global interpolant $\mathcal{I}^{\mathcal{V}_h} : H(\nabla\times;\Omega) \to \mathcal{V}_h$ such that when evaluated at $\boldsymbol{D}_h$ it satisfies:

$$\forall \boldsymbol{D} \in H(\nabla\times;\Omega): \quad (\mathcal{I}^{\mathcal{V}_h}\boldsymbol{D})_{|\mathsf{P}} = \mathcal{I}^{\mathcal{V}_h}_{\mathsf{P}}(\boldsymbol{D}_{|\mathsf{P}}). \tag{4.19}$$

The Oblique Projector: In principle we could generalize the projectors we presented in Section 3.11. However, here we will only present the least squares projector Π^{LS}_{P}. For a cell $\mathsf{P} \in \Omega_h$ and a function $\boldsymbol{D}_h \in \mathcal{V}_h(\mathsf{P})$ we define $\Pi^{LS}_{\mathsf{P}}\boldsymbol{D}_h \in [\mathbb{P}_2(\mathsf{P})]^3$ as the polynomial whose degrees of freedom is the closest to $\boldsymbol{D}_h$. If we consider a basis for $[\mathbb{P}_2(\mathsf{P})]^3$, say $\{\boldsymbol{q}_1,\dots,\boldsymbol{q}_N\}$, then

$$\Pi^{LS}_{\mathsf{P}}\boldsymbol{D}_h = \sum_{i=1}^{N} a_i \boldsymbol{q}_i. \tag{4.20}$$

The coefficients $\{a_i\}_{i=1}^N$ are given as the least square solution to the system $A\vec{x} = \vec{b}$ where

$$A = \begin{pmatrix} \text{DOF}_1(\boldsymbol{q}_1) & \text{DOF}_1(\boldsymbol{q}_2) & \dots & \text{DOF}_1(\boldsymbol{q}_N) \\ \text{DOF}_2(\boldsymbol{q}_1) & \text{DOF}_2(\boldsymbol{q}_2) & \dots & \text{DOF}_2(\boldsymbol{q}_N) \\ \vdots & \vdots & \ddots & \vdots \\ \text{DOF}_M(\boldsymbol{q}_1) & \text{DOF}_M(\boldsymbol{q}_2) & \dots & \text{DOF}_M(\boldsymbol{q}_N) \end{pmatrix} \quad \vec{b} = \begin{pmatrix} \text{DOF}_1(\boldsymbol{D}_h) \\ \text{DOF}_2(\boldsymbol{D}_h) \\ \vdots \\ \text{DOF}_M(\boldsymbol{D}_h) \end{pmatrix}. \tag{4.21}$$

In the notation of Section 2.3 we can use $G = (A^TA)^{-1}A^T$.

Some Important Basis

In order to implement this method we will need a particular set of bases. Firstly note that $\boldsymbol{R}_0(\mathsf{P}) = \mathbb{R}^3$, thus we can take as basis:

$$\begin{pmatrix} 1 \\ 0 \\ 0 \end{pmatrix} = \nabla\times\begin{pmatrix} 0 \\ 0 \\ y \end{pmatrix}, \quad \begin{pmatrix} 0 \\ 1 \\ 0 \end{pmatrix} = \nabla\times\begin{pmatrix} z \\ 0 \\ 0 \end{pmatrix}, \quad \begin{pmatrix} 0 \\ 0 \\ 1 \end{pmatrix} = \nabla\times\begin{pmatrix} 0 \\ x \\ 0 \end{pmatrix}. \tag{4.22}$$

Computing a basis for $\boldsymbol{R}_2(P)$ and $\boldsymbol{R}_2(P)^\perp$ is a bit more tricky. Firstly, note that $\boldsymbol{R}_2(P) = \text{Ker}\nabla\cdot$

when $\nabla\cdot$ is restricted to $\mathbb{P}_2(P)$, this is due to the fact that

$$\forall \boldsymbol{r} \in [\mathbb{P}_2(\mathsf{P})]^3 : \quad \left[\exists \boldsymbol{r}' \in [\mathbb{P}_3(\mathsf{P})]^3 \quad \boldsymbol{r} = \nabla \times \boldsymbol{r}'\right] \iff \nabla \cdot \boldsymbol{r} = 0. \tag{4.23}$$

From here we can conclude that $\nabla \cdot \boldsymbol{R}_2(P)^\perp =$ ran

$nabla\cdot$ and $\boldsymbol{R}_2(P) \cap$ ker$\nabla\cdot = \{\mathbf{0}\}$. This yields a means for a attaining a basis that is natural to the required spaces, let us pick an arbitrary $\boldsymbol{r} \in [\mathbb{P}_2(\mathsf{P})]^3$ say

$$\boldsymbol{r} = \begin{pmatrix} a_x x + b_x x^2 + c_x xy + d_x xz + q_x(y,z) \\ a_y y + b_y y^2 + c_y xy + d_y yz + q_y(x,z) \\ a_z z + b_z z^2 + c_z xz + d_z yz + q_z(x,y). \end{pmatrix} \tag{4.24}$$

Then since

$$\nabla \cdot \boldsymbol{r} = (a_x + a_y + a_z) + (2b_x + c_y + c_z)x + (c_x + 2b_y + d_z)y + (d_x + d_y + 2b_z)z \tag{4.25}$$

we can conclude that the range is four dimensional. As a consequence, we find that a basis for $\boldsymbol{R}_2(P)^\perp$ is given by $\{\boldsymbol{r}_0^\perp, \boldsymbol{r}_1^\perp, \boldsymbol{r}_2^\perp, \boldsymbol{r} \perp_3\}$ for

$$\boldsymbol{r}_0^\perp = \begin{pmatrix} x \\ 0 \\ 0 \end{pmatrix}, \ \boldsymbol{r}_1^\perp = \begin{pmatrix} x^2 \\ 0 \\ 0 \end{pmatrix}, \ \boldsymbol{r}_2^\perp = \begin{pmatrix} 0 \\ y^2 \\ 0 \end{pmatrix}, \ \boldsymbol{r}_3^\perp = \begin{pmatrix} 0 \\ 0 \\ z^2 \end{pmatrix}. \tag{4.26}$$

Moreover, a basis for $\boldsymbol{R}_2(P) = \text{Ker}\nabla\cdot$ is given by $B_R := \{\boldsymbol{r}_i : 0 \leq i \leq 25\}$ for

$$\boldsymbol{r}_0 = \begin{pmatrix} 1 \\ 0 \\ 0 \end{pmatrix} = \nabla \times \begin{pmatrix} 0 \\ 0 \\ y \end{pmatrix}, \ \boldsymbol{r}_1 = \begin{pmatrix} y \\ 0 \\ 0 \end{pmatrix} = \nabla \times \begin{pmatrix} 0 \\ 0 \\ y^2/2 \end{pmatrix}, \boldsymbol{r}_2 = \begin{pmatrix} z \\ 0 \\ 0 \end{pmatrix} = \nabla \times \begin{pmatrix} 0 \\ -z^2/2 \\ 0 \end{pmatrix},$$

$$\boldsymbol{r}_3 = \begin{pmatrix} 0 \\ 1 \\ 0 \end{pmatrix} = \nabla \times \begin{pmatrix} z \\ 0 \\ 0 \end{pmatrix}, \ \boldsymbol{r}_4 = \begin{pmatrix} 0 \\ z \\ 0 \end{pmatrix} = \nabla \times \begin{pmatrix} z^2/2 \\ 0 \\ 0 \end{pmatrix}, \ \boldsymbol{r}_5 = \begin{pmatrix} 0 \\ x \\ 0 \end{pmatrix} = \nabla \times \begin{pmatrix} 0 \\ 0 \\ -x^2/2 \end{pmatrix},$$

$$\boldsymbol{r}_6 = \begin{pmatrix} 0 \\ 0 \\ 1 \end{pmatrix} = \nabla \times \begin{pmatrix} 0 \\ x \\ 0 \end{pmatrix}, \ \boldsymbol{r}_7 = \begin{pmatrix} 0 \\ 0 \\ x \end{pmatrix} = \nabla \times \begin{pmatrix} 0 \\ x^2/2 \\ 0 \end{pmatrix}, \ \boldsymbol{r}_8 = \begin{pmatrix} 0 \\ 0 \\ y \end{pmatrix} = \nabla \times \begin{pmatrix} -y^2/2 \\ 0 \\ 0 \end{pmatrix},$$

$$\boldsymbol{r}_9 = \begin{pmatrix} yz \\ 0 \\ 0 \end{pmatrix} = \nabla \times \begin{pmatrix} 0 \\ 0 \\ y^2z/2 \end{pmatrix}, \boldsymbol{r}_{10} = \begin{pmatrix} 0 \\ xz \\ 0 \end{pmatrix} = \nabla \times \begin{pmatrix} xz^2/2 \\ 0 \\ 0 \end{pmatrix},$$

$$\boldsymbol{r}_{11} = \begin{pmatrix} 0 \\ 0 \\ xy \end{pmatrix} = \nabla \times \begin{pmatrix} 0 \\ x^2y/2 \\ 0 \end{pmatrix}, \boldsymbol{r}_{12} = \begin{pmatrix} y^2 \\ 0 \\ 0 \end{pmatrix} = \nabla \times \begin{pmatrix} 0 \\ 0 \\ y^3/3 \end{pmatrix},$$

$$\boldsymbol{r}_{13} = \begin{pmatrix} z^3 \\ 0 \\ 0 \end{pmatrix} = \nabla \times \begin{pmatrix} 0 \\ -z^3/3 \\ 0 \end{pmatrix}, \boldsymbol{r}_{14} = \begin{pmatrix} 0 \\ x^2 \\ 0 \end{pmatrix} = \nabla \times \begin{pmatrix} 0 \\ 0 \\ -x^3/3 \end{pmatrix},$$

$$\boldsymbol{r}_{15} = \begin{pmatrix} 0 \\ z^2 \\ 0 \end{pmatrix} = \nabla \times \begin{pmatrix} z^3/3 \\ 0 \\ 0 \end{pmatrix}, \boldsymbol{r}_{16} = \begin{pmatrix} 0 \\ 0 \\ x^2 \end{pmatrix} = \nabla \times \begin{pmatrix} 0 \\ x^3/3 \\ 0 \end{pmatrix},$$

$$\boldsymbol{r}_{17} = \begin{pmatrix} 0 \\ 0 \\ y^2 \end{pmatrix} = \nabla \times \begin{pmatrix} -y^3/3 \\ 0 \\ 0 \end{pmatrix}, \ \boldsymbol{r}_{18} = \begin{pmatrix} -x \\ y \\ 0 \end{pmatrix} = \nabla \times \begin{pmatrix} 0 \\ 0 \\ -xy \end{pmatrix},$$

$$\boldsymbol{r}_{19} = \begin{pmatrix} -x \\ 0 \\ z \end{pmatrix} = \nabla \times \begin{pmatrix} 0 \\ xz \\ 0 \end{pmatrix}, \ \boldsymbol{r}_{20} = \begin{pmatrix} -x^2 \\ 2xy \\ 0 \end{pmatrix} = \nabla \times \begin{pmatrix} 0 \\ 0 \\ -x^2 y \end{pmatrix},$$

$$\boldsymbol{r}_{21} = \begin{pmatrix} -x^2 \\ 0 \\ 2xz \end{pmatrix} = \nabla \times \begin{pmatrix} 0 \\ x^2 z \\ 0 \end{pmatrix}, \ \boldsymbol{r}_{22} = \begin{pmatrix} 2xy \\ -y^2 \\ 0 \end{pmatrix}, \ \nabla \times \begin{pmatrix} 0 \\ 0 \\ y^2 x \end{pmatrix},$$

$$\boldsymbol{r}_{23} = \begin{pmatrix} 0 \\ -y^2 \\ 2yz \end{pmatrix} = \nabla \times \begin{pmatrix} -y^2 z \\ 0 \\ 0 \end{pmatrix}, \ \boldsymbol{r}_{24} = \begin{pmatrix} 2xz \\ 0 \\ -z^2 \end{pmatrix} = \nabla \times \begin{pmatrix} 0 \\ -xz^2 \\ 0 \end{pmatrix},$$

$$\boldsymbol{r}_{25} = \begin{pmatrix} 0 \\ 2yz \\ -z^2 \end{pmatrix} = \nabla \times \begin{pmatrix} yz^2 \\ 0 \\ 0 \end{pmatrix}.$$

4.32 The Space $\mathcal{E}_h$

Next we present the space $\mathcal{E}_h$. Let us consider a cell $\mathsf{P} \in \Omega_h$, over this cell we can define the spaces:

$$\boldsymbol{G}_k(\mathsf{P}) = \nabla \mathbb{P}_{k+1}(\mathsf{P}), \quad \boldsymbol{G}_k(\mathsf{P})^{\perp} = \{\boldsymbol{g}^{\perp} \in [\mathbb{P}_k(\mathsf{P})]^3 : \forall \boldsymbol{g} \in \boldsymbol{G}_k(\mathsf{P}) \quad \left(\boldsymbol{g}^{\perp}, \boldsymbol{g}\right) = 0\}. \quad (4.27)$$

A function $\boldsymbol{C}_h$ belongs to the local virtual element space $\mathcal{E}_h(\mathsf{P})$ if and only if it satisfies the following criteria

- $\boldsymbol{C}_h \in H(\nabla\cdot;\mathsf{P}) \cap H(\nabla\times;\mathsf{P})$.
- For every face f: $\boldsymbol{C}_h \cdot \boldsymbol{n}_{\mathsf{f}} \in \mathbb{P}_1(\mathsf{f})$.
- $\nabla \left[\operatorname{div} \boldsymbol{C}_h\right] = \boldsymbol{0}$.

- $\nabla \times \boldsymbol{C}_h \in \boldsymbol{G}_0(\mathsf{P})$.

To a function $\boldsymbol{C}_h \in \mathcal{E}_h(\mathsf{P})$ we associate the following degrees of freedom:

- For every face f: $\int_{\mathsf{f}} \boldsymbol{C}_h \cdot \boldsymbol{n} q dS,\ q \in \mathbb{P}_1(\mathsf{f})$.
- $\int_{\mathsf{P}} \boldsymbol{C}_h \cdot \boldsymbol{g}^{\perp} dV,\ \boldsymbol{g}^{\perp} \in \boldsymbol{G}_1(\mathsf{P})^{\perp}$.

The space $\mathcal{E}_h(\mathsf{P})$ is unisolvent when endowed with this set of degrees of freedom. This allows us to define the interpolant $\mathcal{I}_{\mathsf{P}}^{\mathcal{E}_h} : H(\nabla\cdot;\mathsf{P}) \to \mathcal{E}_h(\mathsf{P})$. The evaluation of $\boldsymbol{C} \in H(\nabla\cdot;()\mathsf{P})$ is defined such that $\mathcal{I}_{\mathsf{P}}^{\mathcal{E}_h}\boldsymbol{C}$ and $\boldsymbol{C}$ share the same degrees of freedom.

In the space $\mathcal{E}_h(\mathsf{P})$ we can define orthogonal projection $\Pi^0 : \mathcal{E}_h(\mathsf{P}) \to [\mathbb{P}_1(\mathsf{P})]^3$ as the solution to the variational problem

$$\forall \boldsymbol{q} \in [\mathbb{P}_1(\mathsf{P})]^3 : \quad \big(\boldsymbol{C}_h - \Pi^0 \boldsymbol{C}_h, \boldsymbol{q}\big) = 0. \tag{4.28}$$

This projector is computable; we will show how later in this section. We can define the inner product in $\mathcal{E}_h(\mathsf{P})$ as

$$\forall \boldsymbol{B}_h, \boldsymbol{C}_h \in \mathcal{E}_h(\mathsf{P}) : \quad \big(\boldsymbol{B}_h, \boldsymbol{C}_h\big)_{\mathcal{E}_h(\mathsf{P})} = \big(\Pi^0 \boldsymbol{B}_h, \Pi^0 \boldsymbol{C}_h\big) + \mathcal{S}^{\mathsf{e}}((\mathcal{I} - \Pi^0)\boldsymbol{B}_h, (\mathcal{I} - \Pi^0)\boldsymbol{C}_h). \tag{4.29}$$

As before we require that $\mathcal{S}^{\mathsf{e}}$ be a continuous bilinear form satisfying

$$\exists s_*, s^* > 0 \quad \forall \boldsymbol{C}_h \in \ker \Pi^0 \cap \mathcal{E}_h(\mathsf{P}) : \quad s_* \|\boldsymbol{C}_h\|_{0,\mathsf{P}}^2 \leq \mathcal{S}^{\mathsf{e}}(\boldsymbol{C}_h, \boldsymbol{C}_h) \leq s^* \|\boldsymbol{C}_h\|_{0,\mathsf{P}}^2. \tag{4.30}$$

The norm in this space is given by

$$\forall \boldsymbol{C}_h \in \mathcal{E}_h(\mathsf{P}) : \quad |||\boldsymbol{C}_h|||_{\mathcal{E}_h(\mathsf{P})} = \big(\boldsymbol{C}_h, \boldsymbol{C}_h\big)_{\mathcal{E}_h(\mathsf{P})}^{1/2}. \tag{4.31}$$

This inner product satisfies the properties presented in the following theorem.

Theorem 4.32.1 *The inner product defined in* (3.68) *satisfies the* ***accuracy*** *property over the space of constants. Rigorously, what we mean is that if* $\boldsymbol{p}, \boldsymbol{q} \in [\mathbb{P}_0(\mathsf{P})]^2$ *then*

$$\big(\boldsymbol{p}, \boldsymbol{q}\big)_{\mathcal{E}_h(\mathsf{P})} = \big(\boldsymbol{p}, \boldsymbol{q}\big). \tag{4.32}$$

Moreover, the norm this inner product defines is stable with respect to the norm in $L^2(\mathsf{P})$*. Thus,*

$$\exists \gamma_*, \gamma^* > 0: \quad \forall \boldsymbol{C}_h \in \mathcal{E}_h(\mathsf{P}): \quad \gamma_* \|\boldsymbol{C}_h\|_{0,\mathsf{P}}^2 \leq |||\boldsymbol{C}_h|||_{\mathcal{E}_h(\mathsf{P})} \leq \gamma^* \|\boldsymbol{C}_h\|_{0,\mathsf{P}}^2, \tag{4.33}$$

where the constants γ_*, γ^* *are independent of the mesh-size and time-step.*

The proof of the above theorem is the same as the one presented for Theorem 3.50.2. Next we will define the global approximation space as

$$\mathcal{E}_h = \left\{ \boldsymbol{C}_h \in H(\nabla\cdot; \Omega) : \forall \mathsf{P} \in \Omega_h \quad \boldsymbol{C}_{h|\mathsf{P}} \in \mathcal{E}_h(\mathsf{P}) \right\}. \tag{4.34}$$

This space is equipped with the following inner product:

$$\Big(\boldsymbol{B}_h, \boldsymbol{C}_h\Big)_{\mathcal{E}_h} = \sum_{\mathsf{P} \in \Omega_h} \Big(\boldsymbol{B}_{h|\mathsf{P}}, \boldsymbol{C}_{h|\mathsf{P}}\Big)_{\mathcal{E}_h(\mathsf{P})}. \tag{4.35}$$

The associated norm is

$$\forall \boldsymbol{C}_h \in \mathcal{E}_h: \quad |||\boldsymbol{C}_h|||_{\mathcal{E}_h} = \big(\boldsymbol{C}_h, \boldsymbol{C}_h\big)_{\mathcal{E}_h}^{1/2}. \tag{4.36}$$

This norm inherits some accuracy and stability properties as a consequence of Theorem 4.32.1. These are laid out in the following corollary:

Corollary 4.32.1 *The inner product defined in* (4.35) *is exact for piecewise constant functions.This is to say that if* $\boldsymbol{p}, \boldsymbol{q}$ *are such that for any cell* P *in the mesh* Ω_h *they satisfy* $\boldsymbol{p}_{|\mathsf{P}}, \boldsymbol{q}_{|\mathsf{P}} \in [\mathbb{P}_0(\mathsf{P})]^2$ *then*

$$\big(\boldsymbol{p}, \boldsymbol{q}\big)_{\mathcal{E}_h} = \big(\boldsymbol{p}, \boldsymbol{q}\big). \tag{4.37}$$

Moreover, the norm in (4.29) *is equivalent to the norm in the space* $L^2(\Omega)$*. This is to say that there exists constants* $\delta_*, \delta^* > 0$*, independent of the mesh-size and time-step such that*

$$\forall \boldsymbol{C}_h \in \mathcal{E}_h : \quad \delta_* \|\boldsymbol{C}_h\|_{0,\Omega}^2 \leq |||\boldsymbol{C}_h|||_{\mathcal{E}_h}^2 \leq \delta^* \|\boldsymbol{C}_h\|_{0,\Omega}^2. \tag{4.38}$$

Finally, we define the global interpolant $\mathcal{I}^{\mathcal{E}_h} : H(\nabla\cdot;\Omega) \to \mathcal{E}_h$ by

$$\forall \boldsymbol{C} \in H(\nabla\cdot;\Omega) : \quad (\mathcal{I}^{\mathcal{E}_h}\boldsymbol{C})_{|\mathsf{P}} = \mathcal{I}_{\mathsf{P}}^{\mathcal{E}_h}(\boldsymbol{C}_{|\mathsf{P}}). \tag{4.39}$$

The Orthogonal Projection Following the framework laid out in Section 2.3 in order to compute the inner product we need only come up with a means of attaining the following quantities:

$$\int_{\mathsf{P}} \boldsymbol{C}_h \cdot \boldsymbol{q} dV, \quad \boldsymbol{q} \in \mathbb{P}_1(\mathsf{P}). \tag{4.40}$$

To do this first we decompose $\boldsymbol{q} = \nabla q + \boldsymbol{g}^\perp$ for $q \in \mathbb{P}_2(\mathsf{P})$ and $\boldsymbol{g}^\perp \in \boldsymbol{G}_1(P)^\perp$ yielding:

$$\int_{\mathsf{P}} \boldsymbol{C}_h \cdot \boldsymbol{q} dV = \int_{\mathsf{P}} \boldsymbol{C}_h \cdot \nabla q dV + \int_{\mathsf{P}} \boldsymbol{C}_h \cdot \boldsymbol{g}^\perp dV. \tag{4.41}$$

Note that $\int_{\mathsf{P}} \boldsymbol{C}_h \cdot \boldsymbol{g}^\perp dV$ can be read directly from the degrees of freedom. To compute the first integral, we integrate by parts

$$\int_{\mathsf{P}} \boldsymbol{C}_h \cdot \nabla q dV = \int_{\mathsf{P}} \nabla \cdot \boldsymbol{C}_h q dS - \sum_{\mathsf{f} \in \partial \mathsf{P}} \int_{\mathsf{f}} \boldsymbol{C}_h \cdot \boldsymbol{n} q dS. \tag{4.42}$$

Note that by definition $\nabla \cdot \boldsymbol{C}_h \in \mathbb{R}^3$. We can compute this quantity exactly using:

$$\nabla \cdot \boldsymbol{C}_h |\mathsf{P}| = \int_{\mathsf{P}} \nabla \cdot \boldsymbol{C}_h dV = \sum_{\mathsf{f} \in \partial \mathsf{P}} \int_{\mathsf{f}} \boldsymbol{C}_h \cdot \boldsymbol{n} dS. \tag{4.43}$$

The degrees of freedom of $\boldsymbol{C}_h$ on the faces of P give enough information to compute moments

against linear polynomials. However, $q \in \mathbb{P}_2(\mathsf{f})$ meaning that these quantities are not available. The solution is to realize that, since for every face f we have, by definition, that $\boldsymbol{C}_h \cdot \boldsymbol{n} \in \mathbb{P}_1(\mathsf{f})$ then the degrees of freedom allows us to reconstruct $\boldsymbol{C}_h \cdot \boldsymbol{n}$ exactly.

Some Useful Bases: To compute a basis for $\boldsymbol{G}_1(\mathsf{P})$ and $\boldsymbol{G}_1(\mathsf{P})^\perp$, we use a similar argument to the one used to compute those for $\boldsymbol{R}_2(\mathsf{P})$ and $\boldsymbol{R}_2(\mathsf{P})^\perp$. We can deduce that $\nabla \times \boldsymbol{G}_1(P)^\perp =$ ran$\nabla\times$ and $\boldsymbol{G}_1(\mathsf{P})^\perp \cap$ ker$\nabla\times$ is restricted to $\mathbb{P}_1^3(\mathsf{P})$. Thus, if we write

$$\boldsymbol{g}^\perp = \begin{pmatrix} a_0 + a_1 x_\mathsf{P} + a_2 y_\mathsf{P} + a_3 z_\mathsf{P} \\ b_0 + b_1 x_\mathsf{P} + b_2 y_\mathsf{P} + b_3 z_\mathsf{P} \\ c_0 + c_1 x_\mathsf{P} + c_2 y_\mathsf{P} + c_3 z_\mathsf{P}, \end{pmatrix} \tag{4.44}$$

where $(x_\mathsf{P}, y_\mathsf{P}, z_\mathsf{P})$ is the centroid of the cell P, then, from the fact that

$$\nabla \times \boldsymbol{g}^\perp = \begin{pmatrix} c_2 - b_3 \\ a_3 - c_1 \\ b_1 - a_2 \end{pmatrix} \tag{4.45}$$

we know that $\boldsymbol{G}_1(P)^\perp$ must be three dimensional. We can write a basis for it as $B_G^\perp = \{\boldsymbol{g}_0^\perp, \boldsymbol{g}_1^\perp, \boldsymbol{g}_2^\perp\}$ where

$$\boldsymbol{g}_0^\perp = \begin{pmatrix} 0 \\ 0 \\ y_\mathsf{P} \end{pmatrix}, \boldsymbol{g}_1^\perp = \begin{pmatrix} z_\mathsf{P} \\ 0 \\ 0 \end{pmatrix}, \boldsymbol{g}_2^\perp = \begin{pmatrix} 0 \\ x_\mathsf{P} \\ 0 \end{pmatrix}. \tag{4.46}$$

A basis for $\boldsymbol{G}_1(\mathsf{P})$ is given by the following set of functions:

$$\boldsymbol{g}_0 = \begin{pmatrix} 1 \\ 0 \\ 0 \end{pmatrix} = \nabla x, \quad \boldsymbol{g}_1 = \begin{pmatrix} x \\ 0 \\ 0 \end{pmatrix} = \frac{1}{2}\nabla x^2, \quad \boldsymbol{g}_2 = \begin{pmatrix} 0 \\ 1 \\ 0 \end{pmatrix} = \nabla y, \quad \boldsymbol{g}_3 = \begin{pmatrix} 0 \\ y \\ 0 \end{pmatrix} = \frac{1}{2}\nabla y^2,$$

$$\boldsymbol{g}_4 = \begin{pmatrix} 0 \\ 0 \\ 1 \end{pmatrix} = \nabla z, \quad \boldsymbol{g}_5 = \begin{pmatrix} 0 \\ 0 \\ z \end{pmatrix} = \frac{1}{2}\nabla z^2, \quad \boldsymbol{g}_6 = \begin{pmatrix} 0 \\ z \\ y \end{pmatrix} = \nabla yz, \quad \boldsymbol{g}_7 = \begin{pmatrix} z \\ 0 \\ x \end{pmatrix} = \nabla xz,$$

$$\boldsymbol{g}_8 = \begin{pmatrix} y \\ x \\ 0 \end{pmatrix} = \nabla xy.$$

4.4 The De-Rham Complex and the Condition on the Divergence of B_h

Similar to the case in two dimensions, the three dimensional spaces $H(\nabla\times;\Omega), H(\nabla\cdot;\Omega)$ and $L^2(\Omega)$ form a De-Rham complex of the form

$$H(\nabla\times;\Omega) \xrightarrow{\nabla\times} H(\nabla\cdot;\Omega) \xrightarrow{\nabla\cdot} L^2(\Omega). \tag{4.47}$$

The VEM we developed in this chapter will also form a similar chain. However, first we must introduce a discrete version of the space $L^2(\Omega)$ which we denote as $\mathcal{P}_h$. Locally, over a cell $\mathsf{P} \in \Omega_h$ the space is defined as $\mathcal{P}_h(\mathsf{P}) = \mathbb{P}_0(\mathsf{P})$. While globally we can define

$$\mathcal{P}_h = \left\{ q_h \in L^2(\Omega) : \forall \mathsf{P} \in \Omega_h \quad q_{h|\mathsf{P}} \in \mathcal{P}_h(\mathsf{P}) \right\}. \tag{4.48}$$

The set of degrees of freedom, the inner product and the interpolating operator in this space are the same as those presented in Section 3.6. The discrete form of the chain in (4.47) is given by

$$\mathcal{V}_h \xrightarrow{\nabla\times} \mathcal{E}_h \xrightarrow{\nabla\cdot} \mathcal{P}_h. \tag{4.49}$$

We summarize the main results of regarding this chain the following theorem.

Theorem 4.40.1 *The chain presented in* (4.49) *is exact. Moreover, the diagram*

$$\begin{array}{ccccc} H(\boldsymbol{rot};\Omega) & \xrightarrow{\nabla\times} & H(div;\Omega) & \xrightarrow{\nabla\cdot} & L^2(\Omega) \\ \downarrow{\scriptstyle \mathcal{I}^{\mathcal{V}_h}} & & \downarrow{\scriptstyle \mathcal{I}^{\mathcal{E}_h}} & & \downarrow{\scriptstyle \mathcal{I}^{\mathcal{P}_h}} \\ \mathcal{V}_h & \xrightarrow{\nabla\times} & \mathcal{E}_h & \xrightarrow{\nabla\cdot} & \mathcal{P}_h \end{array} \tag{4.50}$$

is commutative.

The proof of the above theorem is similar to the one presented for Theorem 3.70.1. We will omit this proof and refer interested readers to [16]. Using the result of Theorem 4.40.1 we can show that, at the discrete level, the divergence of the magnetic field will be zero.

Corollary 4.40.1 *The solution to the variational formulation* (4.4) *will satisfy*

$$\forall n \in \mathbb{N}: \quad div\, \boldsymbol{B}_h^n = 0. \tag{4.51}$$

The proof of this corollary is identical to the one presented for Corollary 3.70.1.

4.41 Computing the Curl

In this section we will characterize, for each cell P in Ω_h, the function $\nabla \times \boldsymbol{D}_h \in \mathcal{E}_h(\mathsf{P})$ with $\boldsymbol{D}_h \in \mathcal{V}_h(P)$. We can do this by computing its degrees of freedom. They are, in fact, computable from the degrees of freedom in $\mathcal{V}_h(P)$.

- **Degrees of Freedom over Faces**. Let $\mathsf{f} \in \partial\mathsf{P}$, $q \in \mathbb{P}_1(\mathsf{f})$ and note that Stokes's Theorem

yields the following integration by parts formula:

$$\int_{\mathsf{f}} q\nabla \times \boldsymbol{D}_h \cdot \boldsymbol{n} dS = \int_{\partial \mathsf{f}} q\boldsymbol{D}_h \cdot \boldsymbol{t} d\ell - \int_{\mathsf{f}} \nabla q \times \boldsymbol{D}_h \cdot \boldsymbol{n} dS. \tag{4.52}$$

The line integrals can be read from the degrees of freedom of $\boldsymbol{D}_h$. The identity

$$\int_{\mathsf{f}} \nabla r \times \boldsymbol{D}_h \cdot \boldsymbol{n} dS = \int_{\mathsf{f}} \boldsymbol{D}_h \cdot \nabla r \times \boldsymbol{n} dS, \tag{4.53}$$

reveals that, since $\nabla \mathbb{P}_2(\mathsf{f}) \subset [\mathbb{P}_1(\mathsf{f})]^2$, the second face integral can also be read from the degrees of freedom.

- **Degrees of Freedom over Cells** Let $\boldsymbol{g}^\perp \in \boldsymbol{G}_1(P)^\perp$ then from the following vector calculus identity

$$\nabla \cdot (\boldsymbol{D}_h \times \boldsymbol{g}^\perp) = (\nabla \boldsymbol{D}_h) \cdot \boldsymbol{g}^\perp - \boldsymbol{D}_h \cdot (\nabla \times \boldsymbol{g}^\perp), \tag{4.54}$$

we have that

$$\int_{\mathsf{P}} \nabla \times \boldsymbol{D}_h \cdot \boldsymbol{g}^\perp = \int_{\mathsf{P}} \boldsymbol{D}_h \cdot \nabla \times \boldsymbol{g}^\perp dV + \sum_{\mathsf{f} \in \partial \mathsf{P}} \int_{\mathsf{f}} \boldsymbol{D}_h \cdot \boldsymbol{g}^\perp \times \boldsymbol{n} dS. \tag{4.55}$$

Since $\nabla \times : \boldsymbol{G}_1(\mathsf{P})^\perp \to [\mathbb{P}_0(\mathsf{P})]^3$ is an isomorphism the volume integral in the right hand side can be read from the degrees of freedom of $\boldsymbol{D}_h$. To compute the surface integrals in (4.55) note that, since $\boldsymbol{g}^\perp \times \boldsymbol{n}$ lies on the plane f, we can decompose

$$\int_{\mathsf{f}} \boldsymbol{D}_h \cdot \boldsymbol{g}^\perp \times \boldsymbol{n} dS = \int_{\mathsf{f}} \boldsymbol{D}_h \cdot \mathbf{rot}\, r dS + \int_{\mathsf{f}} \boldsymbol{D}_h \cdot \boldsymbol{r}^\perp dS, \quad r \in \mathbb{P}_3(\mathsf{f}),\ \boldsymbol{r}^\perp \in \boldsymbol{R}_2(\mathsf{f}). \tag{4.56}$$

The integral $\int_{\mathsf{f}} \boldsymbol{D}_h \cdot \boldsymbol{r}^\perp dS$ is part of the degrees of freedom. To compute the first integral we need to reconstruct $\operatorname{rot} \boldsymbol{D}_h^{\mathsf{f}} \in \mathbb{P}_1(\mathsf{P})$. The coefficients necessary can be found after application of an integration by parts formula and the identity $\boldsymbol{D}_h \cdot \mathbf{rot}\, r = \boldsymbol{D}_h^{\mathsf{f}} \cdot \mathbf{rot}\, r$

yielding

$$\forall r \in \mathbb{P}_1(\mathsf{f}): \quad \int_{\mathsf{f}} \mathrm{rot}\, \boldsymbol{D}_h^{\mathsf{f}} r dS = \int_{\mathsf{f}} \boldsymbol{D}_h \cdot \mathbf{rot}\, r dS + \sum_{\mathsf{e}\in\partial\mathsf{f}} \int_{\mathsf{e}} \boldsymbol{D}_h^{\mathsf{f}} \cdot \boldsymbol{t} r d\ell. \tag{4.57}$$

Then, we can use the same formula

$$\forall r \in \mathbb{P}_3(\mathsf{f}): \quad \int_{\mathsf{f}} \boldsymbol{D}_h \cdot \mathbf{rot}\, r dS = \sum_{\mathsf{e}\in\partial\mathsf{f}} \int_{\mathsf{e}} \boldsymbol{D}_h^{\mathsf{f}} \cdot \boldsymbol{t} r dS - \int_{\mathsf{f}} \mathrm{rot}\, \boldsymbol{D}_h^{\mathsf{f}} r dS. \tag{4.58}$$

where each quantity is now computable.

4.5 Extensions To Higher Order

In this section we will briefly introduce the generalization to arbitrary orders of the virtual elements we presented in this section. In the above, and throughout this section f represents a face of the polyhedron P. The general form of the space $\mathcal{V}_h^k(\mathsf{P})$ is given by:

$$\mathcal{V}_h^k(\mathsf{P}) = \Big\{ \boldsymbol{D}_h \in H(\nabla\times;\mathsf{P}) \cap H(\nabla\cdot;\mathsf{P}) : \forall\, \mathsf{f} \in \partial\mathsf{P} \quad \boldsymbol{D}_{h|\mathsf{f}} \in B_k(\mathsf{f}) \\ \nabla\cdot\boldsymbol{v}_h \in \mathbb{P}_{k-1}(\mathsf{P}) \quad \text{and} \quad \nabla\times\nabla\times\boldsymbol{D}_h \in \boldsymbol{R}_{k-2}(\mathsf{P}) \Big\}, \tag{4.59}$$

where the boundary space $B_k(\partial\mathsf{P})$ is given by

$$B_k(\mathsf{f}) = \Big\{ \boldsymbol{D}_h \in H(\mathrm{div};\mathsf{f}) \cap H(\mathrm{rot};\mathsf{f}) : \forall\, \boldsymbol{D}_h\cdot\boldsymbol{t} \in \mathbb{P}_k(\mathsf{e}), \\ \mathrm{div}\, \boldsymbol{D}_h \in \mathbb{P}_{k-1}(\mathsf{f}) \quad \text{and} \quad \mathbf{rot}\, \mathrm{rot}\, \boldsymbol{D}_h \in \boldsymbol{R}_{k-2}(\mathsf{f}) \Big\}. \tag{4.60}$$

For a function $\boldsymbol{D}_h \in \mathcal{V}_h^k(\mathsf{P})$ the set of degrees of freedom are:

- For every face f, $\int_{\mathsf{f}} \boldsymbol{D}_h \cdot \boldsymbol{r}\, dS$ for $\boldsymbol{r} \in \boldsymbol{R}_k(\mathsf{f})^{\perp}$.
- For every face f, $\int_{\mathsf{f}} \boldsymbol{D}_h \cdot \boldsymbol{r}\, dS$ for $\boldsymbol{r} \in \boldsymbol{R}_{k-2}(\mathsf{f})$.

- The moments $\int_{\mathsf{P}} \boldsymbol{D}_h \cdot \boldsymbol{c}\, dV$ for $\boldsymbol{c} \in \boldsymbol{R}_k(\mathsf{P})^{\perp}$.
- The moments $\int_{\mathsf{P}} \boldsymbol{D}_h \cdot \boldsymbol{c}\, dV$ for $\boldsymbol{c} \in \boldsymbol{R}_{k-2}(\mathsf{P})$.

The second space in the chain, $\mathcal{E}_h^k(\mathsf{P})$, which will be used to approximate the magnetic field, is

$$\mathcal{E}_h^k(\mathsf{P}) = \Big\{ \boldsymbol{C}_h \in H(\nabla\cdot;\mathsf{P}) \cap H(\nabla\times;\mathsf{P}) : \forall \mathsf{f} \in \partial\mathsf{P} \quad \boldsymbol{C}_h \cdot \boldsymbol{n} \in \mathbb{P}_k(\mathsf{f}) \\ \nabla\nabla\cdot \boldsymbol{w}_h \in \boldsymbol{G}_{k-2}(\mathsf{P}) \quad \text{and} \quad \nabla \times \boldsymbol{D}_h \in \boldsymbol{R}_{k-1}(\mathsf{P}) \Big\}. \tag{4.61}$$

For a function $\boldsymbol{C}_h \in \mathcal{E}_h^k(\mathsf{P})$ the degrees of its freedom are:

- For every face f, $\int_{\mathsf{f}} \boldsymbol{C}_h \cdot \boldsymbol{n} q\, dS$, $q \in \mathbb{P}_k(\mathsf{f})$.
- The moments $\int_{\mathsf{P}} \boldsymbol{C}_h \cdot \boldsymbol{q}\, dV$, $\boldsymbol{q} \in \boldsymbol{G}_{k-2}(()\mathsf{P})$.
- The moments $\int_{\mathsf{P}} \boldsymbol{C}_h \cdot \boldsymbol{q}\, dV$, $\boldsymbol{q} \in Gk-2(\mathsf{P})^{\perp}$.

The final space is $\mathcal{P}_h^k(\mathsf{P}) := \mathbb{P}_k(\mathsf{P})$ along with the degrees of freedom given by the moments $\int_{\mathsf{P}} p_h q\, dV$ for $p_h \in \mathcal{P}_h^k(\mathsf{P})$ and $q \in \mathbb{P}_k(\mathsf{P})$.

Remark 5 *We note that the schemes developed using the virtual elements of this section are of k-th order for the electric field and $k-1$-th order for the magnetic field in space. The temporal convergence should be quadratic for $\theta = 1/2$ and linear otherwise. We note that higher order schemes in time can be achieved by using a Runge-Kutta method, for example. However, special care needs to be taken in order to guarantee that the divergence of the magnetic field remains within the machine epsilon. The precise conditions for high order schemes in time that also preserve this condition on the magnetic field are a topic of future research.*

4.6 Conclusions

In this chapter we developed a VEM for the three dimensional system modeling the kinematics of MHD. In Section 4.3 we presented each of the virtual element spaces that are necessary

as well as methods for computing important projectors in each of these spaces. In the process of defining each of these we introduced several polynomial spaces and their bases. These are important when computing the set of degrees of freedom. Next, in Section 4.4 we showed that these spaces form a commuting De-Rham complex. Using this result we were able to prove that our scheme will, at the discrete level, provide us with solenoidal magnetic fields. Furthermore, this diagram also allows us to come up with a means of characterizing the curl of a function in $\mathcal{V}_h$. We closed this chapter with Section 4.5, a brief discussion about the general form of these virtual element spaces. These are useful for higher order methods.

In this chapter we did not present much analysis of the VEM. However, the energy and well-posedness results of Sections 3.9 and 3.10 are valid for the elements we presented here as well.

5. COUPLING THE FLUID FLOW

5.1 Introduction

In Chapter 3., we considered a numerical discretization for the electromagnetic sub-model of MHD. In this chapter we will couple the electromagentic sub-model with a model for the fluid flow, and we will extend the numerical discretization from Chapter 3. to obtain a complete simulation of MHD in two dimensions.

In Section 5.2 we derive from physical principles the set of equations that will describe the mechanical behavior of a magnetized fluid. This section should be read in conjunction with Section 3.2 where the electromagnetic model is presented. Having derived a model we proceed in Section 5.3 to present the continuous and discrete variational formulations. The definition of the spaces and operators in the discrete variational formulation are a topic for Section 5.4. Here we will also describe how the inner product in these spaces is computed. Next, in Section 5.5 we show that the discrete system satisfies desirable energy estimates. This problem is non-linear therefore we must come up with a linearization strategy to approximate the solution. This strategy is presented in Section 5.6 where we also show that the linearization does not alter the divergence-free nature of the magnetic field. This condition was first introduced in Gauss's Law in Section 3.2. Its importance is laid out in the concluding remarks of Section 3.7. The linearization will lead to solving a series of linear systems at every time step. We will show that this linear problem is well-posed in Section 5.7. We note that the contents of Section 5.5 and 5.7 are generalizations of the results in Sections 3.9 and 3.10. We finish this chapter with Section 5.8, a summary of the conclusions that we can draw from the results presented throughout this chapter.

5.2 The Mechanical Model

In this section we derive a model that describes the mechanics of a magnetized fluid. This derivation is very standard; interested readers are referred to [51, 73] for a wider discussion in MHD. For a discussion on fluid mechanics in general see [8] for a beginner's introduction, [65] for a more advanced exposition. For mathematicians or those interested in the mathematics of fluid mechanics, see [34].

Consider that a magnetized fluid is encapsulated by a domain Ωin three spatial dimensions. Let V be an arbitrary open set contained in Ω. In physics, the set V is referred to as a fluid parcel. First we will consider the **law of conservation of mass**. This principle claims that mass cannot be created nor destroyed. Thus, the mass of the fluid parcel V can only change if some of the fluid either escapes or enters through the boundary of V. In mathematical terms this implies that the rate of change of the mass in V is the flux of mass across the surface ∂V, or equivalently

$$\frac{\partial}{\partial t}\int_V \rho dV = -\int_{\partial V} \rho \boldsymbol{u}\cdot\boldsymbol{n} dS. \tag{5.1}$$

Here ρ is the mass density, $\boldsymbol{u}$ is the velocity profile of the fluid and $\boldsymbol{n}$ is a normal vector that points out of the parcel V. Passing the time derivative through the integral and applying the Divergence Theorem we obtain that

$$\int_V \left(\frac{\partial}{\partial t}\rho + \nabla\cdot(\rho\boldsymbol{u})\right) dV = 0. \tag{5.2}$$

Finally, since the above is true for every fluid parcel we can conclude that

$$\frac{\partial}{\partial t}\rho + \nabla\cdot(\rho\boldsymbol{u}) = 0. \tag{5.3}$$

Equation (5.3) is the first in our model. The second equation that we require in our model involves

a balance of forces in the parcel. First we introduce the momentum in V, it is given by

$$\boldsymbol{m} = \int_V \rho \boldsymbol{u} dV. \tag{5.4}$$

When we study the rate of change of M we must consider that there are two reasons why M changes. The first is because the integrand $\rho \boldsymbol{u}$ itself is changing. The second reason is because, as momentum changes, the shape of V is deformed. **Leibniz's rule** is designed to take both of these causes into consideration, thus we use

$$\frac{\partial}{\partial t}\boldsymbol{m} = \int_V \frac{\partial}{\partial t}\rho \boldsymbol{u} dV + \int_{\partial V} \rho \boldsymbol{u}(\boldsymbol{u}\cdot\boldsymbol{n}) dS. \tag{5.5}$$

Note that equation (5.5) is a vector identity. The $i-$th coordinate of the identity in (5.5) is given by

$$\frac{\partial}{\partial t} m_i = \int_V \frac{\partial}{\partial t}(\rho u_i) dV + \int_{\partial V} \rho u_i (\boldsymbol{u}\cdot\boldsymbol{n}) dS. \tag{5.6}$$

Next, we apply the Divergence Theorem to find that

$$\begin{aligned}\frac{\partial}{\partial t} m_i = \int_V \frac{\partial}{\partial t}(\rho u_i) + \nabla\cdot(\rho u_i \boldsymbol{u}) dV = \\ = \int_V \left[\left(\frac{\partial}{\partial t}\rho + \nabla\cdot(\rho \boldsymbol{u}) \right) u_i + \rho \frac{\partial}{\partial t} u_i + \rho \boldsymbol{u}\cdot\nabla u_i \right] dV.\end{aligned} \tag{5.7}$$

If we recall the statement of the law of conservation of mass (5.3) we obtain, in vector form the expression:

$$\frac{\partial}{\partial t}\boldsymbol{m} = \int_V \left(\rho \frac{\partial}{\partial t}\boldsymbol{u} + \rho(\boldsymbol{u}\cdot\nabla)\boldsymbol{u} \right) dV. \tag{5.8}$$

Equipped with a means of computing the time derivative of the momentum we now introduce **Newton's Second Law** which explains explains that momentum in a mechanical system changes only if a force is applied and the rate of change is the sum of the forces. In the fluid parcel we consider three forces. The first is the force that the electromagnetic field applies on V, this is given

by the Lorentz force and given by the expression

$$\boldsymbol{F}_1 = \int_V \boldsymbol{J} \times \boldsymbol{B} dV. \tag{5.9}$$

This force was discussed in detail in Section 3.2 thus we avoid the discussion here. The second force we consider is that of an external agent. We will assume the force density $\boldsymbol{f}$ is known to us, hence it is given by

$$\boldsymbol{F}_2 = \int_V \boldsymbol{f} dV. \tag{5.10}$$

The third force that we consider is the force that fluid parcels surrounding V exert on V. In this manuscript we will consider fluids that are Newtonian and isotropic. For these fluids we can consider that this force is given by

$$\boldsymbol{F}_3 = \int_{\partial V} (\mu \nabla \boldsymbol{u} - p\mathbb{I}) dS = \int_V (\mu \triangle \boldsymbol{u} - \nabla p)\, dV. \tag{5.11}$$

The constant μ is the viscosity of the fluid, p is the pressure applied to the fluid and $\mathbb{I}$ is the identity matrix. Thus, Newton's Second Law predicts that

$$\frac{\partial}{\partial t}\boldsymbol{m} = \boldsymbol{F}_1 + \boldsymbol{F}_2 + \boldsymbol{F}_3. \tag{5.12}$$

Putting (5.8), (5.9), (5.10), (5.11) and (5.12) we arrive at

$$\int_V \left(\rho \frac{\partial}{\partial t}\boldsymbol{u} + \rho(\boldsymbol{u} \cdot \nabla)\boldsymbol{u} - \mu \triangle \boldsymbol{u} - \boldsymbol{J} \times \boldsymbol{B} + \nabla p \right) dV = \int_V \boldsymbol{f} dV. \tag{5.13}$$

Since the parcel V was selected arbitrarily then the following identity must hold

$$\rho \frac{\partial}{\partial t}\boldsymbol{u} + \rho(\boldsymbol{u} \cdot \nabla)\boldsymbol{u} - \mu \triangle \boldsymbol{u} - \boldsymbol{J} \times \boldsymbol{B} + \nabla p = \boldsymbol{f}. \tag{5.14}$$

Formally the model is the system

$$\rho\frac{\partial}{\partial t}\boldsymbol{u} + \rho(\boldsymbol{u}\cdot\nabla)\boldsymbol{u} - \mu\triangle\boldsymbol{u} - \boldsymbol{J}\times\boldsymbol{B} + \nabla p = \boldsymbol{f}, \tag{5.15a}$$

$$\frac{\partial}{\partial t}\rho + \nabla\cdot(\rho\boldsymbol{u}) = 0. \tag{5.15b}$$

We will make two final simplifications. The first is that we will consider that the mass density will remain constant implying that $\frac{\partial}{\partial t}\rho = 0$ yielding that the expression for conservation of mass (5.15b) is simply

$$\nabla\cdot\boldsymbol{u} = 0. \tag{5.16}$$

The second is that we will only consider slow flows. In this case the only term that is quadratic in the velocity, namely $(\boldsymbol{u}\cdot\nabla)\boldsymbol{u}$, is much smaller than the rest appearing in (5.15a). In this case we can simplify the expression in (5.15a) to

$$\rho\frac{\partial}{\partial t}\boldsymbol{u} - \mu\triangle\boldsymbol{u} - \boldsymbol{J}\times\boldsymbol{B} + \nabla p = \boldsymbol{f}. \tag{5.17}$$

We are interested in the dimensionless version of this model. To arrive at such an equation we make the substitutions

$$\boldsymbol{u}' = \frac{\boldsymbol{u}}{U}\,, \quad p' = \frac{p}{\rho U^2}\,, \quad \boldsymbol{f}' = \boldsymbol{f}\frac{\rho L}{U^2}\,, \quad \boldsymbol{J}' = \frac{\boldsymbol{J}}{J}\,, \quad \boldsymbol{B}' = \frac{\boldsymbol{B}}{B} \tag{5.18}$$

$$\frac{\partial}{\partial t'} = T\frac{\partial}{\partial t}\,, \quad \nabla' = L\nabla\,, \quad \triangle' = L^2\triangle \tag{5.19}$$

where U, B, J are the characteristic strengths of the velocity, magnetic field and current density respectively, and T, L are characteristic time and length scales, respectively. The resulting expression is

$$\frac{\partial}{\partial t'}\boldsymbol{u}' - R_e^{-1}\triangle'\boldsymbol{u}' - S\boldsymbol{J}'\times\boldsymbol{B}' + \nabla' p' = \boldsymbol{f}', \quad R_e = \frac{\rho LU}{\mu}, \quad S = \frac{\sigma BLJ}{\rho U^2}. \tag{5.20}$$

The constant σ is the electric conductivity of the medium. This constant was introduced in Section 3.2. The constants R_e and S are referred to as the viscous Reynold's number and the coupling number. We subsequently drop the prime notation.

5.3 The Continuous and Discrete Variational Formulations

Consider a bounded and open region of $\mathbb{R}^2$, denote this region by Ω. Further consider that in Ω there is a magnetized fluid. We combine the electromagnetic model derived in Section 3.2 together with the mechanical model presented in Section 5.2 to come up with a description of the flow of this fluid. The result is:

$$\text{Conservation of Momentum}: \quad \frac{\partial}{\partial t}\boldsymbol{u} - R_e^{-1}\triangle\boldsymbol{u} - J \times \boldsymbol{B} + \nabla p = \boldsymbol{f} \quad \text{in} \quad \Omega, \tag{5.21a}$$

$$\text{Faraday's Law}: \quad \frac{\partial}{\partial t}\boldsymbol{B} + \mathbf{rot}\, E = \mathbf{0} \quad \text{in} \quad \Omega, \tag{5.21b}$$

$$\text{Ohm's Law}: \quad J = E + \boldsymbol{u} \times \boldsymbol{B} \quad \text{in} \quad \Omega, \tag{5.21c}$$

$$\text{Ampere's Law}: \quad J - R_m^{-1}\text{rot}\, \boldsymbol{B} = \mathbf{0} \quad \text{in} \quad \Omega, \tag{5.21d}$$

$$\text{Conservation of Mass}: \quad \text{div}\, \boldsymbol{u} = 0 \quad \text{in} \quad \Omega. \tag{5.21e}$$

We note that in this model we are taking the particular case where $S = 1$. We consider the following initial conditions

$$\boldsymbol{u}(0) = \boldsymbol{u}_0, \quad \text{and} \quad \boldsymbol{B}(0) = \boldsymbol{B}_0 \quad \text{in} \quad \Omega. \tag{5.22}$$

As we discussed in Subsections 3.2 and 3.7 it is imperative that we satisfy Gauss's law for the magnetic field. According to Faraday's law, see Section 3.2, to do this we need only include the condition that

$$\text{div}\, \boldsymbol{B}_0 = 0. \tag{5.23}$$

We close the system by adding the boundary conditions

$$\boldsymbol{u} = \boldsymbol{u}_b \quad \text{and} \quad E = E_b \quad \text{along} \quad \partial\Omega. \tag{5.24}$$

Note that, according to the divergence Theorem and the law of conservation of mass (5.21e) we have that

$$\int_{\partial\Omega} \boldsymbol{u} \cdot \boldsymbol{n} d\ell = \int_{\Omega} \text{div}\, \boldsymbol{u} dA = 0. \tag{5.25}$$

So, in order to be consistent with this condition we will require that the boundary conditions on the velocity field satisfy

$$\int_{\partial\Omega} \boldsymbol{u}_b \cdot \boldsymbol{n} d\ell = 0. \tag{5.26}$$

Here, like we did in chapter 3, we will consider a two dimensional model. The velocity field and magnetic fields are two dimensional whereas the pressure, current density and electric fields are one dimensional.

The general strategy of the VEM requires a variational formulation the problem 5.21. Consider the spaces

$$H^1(\Omega) = \left\{ v \in L^2(\Omega) : \nabla v \in [L^2(\Omega)]^2 \right\}, \tag{5.27}$$

$$H_0^1(\Omega) = \left\{ v \in H^1 : v_{|\partial\Omega} = 0 \right\}, \tag{5.28}$$

$$L_0^2(\Omega) = \left\{ q \in L^2(\Omega) : \int_{\Omega} q dA = 0 \right\}, \tag{5.29}$$

$$C^1\left([0,T], \left[H^1(\Omega)\right]^2\right) = \left\{ \boldsymbol{v} : [0,T] \to \left[H^1(\Omega)\right]^2 : \boldsymbol{v} \text{ and } \frac{\partial}{\partial t}\boldsymbol{v} \text{ are continuous} \right\}, \tag{5.30}$$

$$C\left([0,T], L_0^2(\Omega)\right) = \left\{ q : [0,T] \to L_0^2(\Omega) : q \text{ is continuous} \right\}. \tag{5.31}$$

Then, the variational formulation of (5.21) is given by

Find $(\boldsymbol{u}, \boldsymbol{B}, E, p) \in C^1\left([0,T], \left[H^1(\Omega)\right]^2\right) \times C^1\left([0,T], H(\textit{div}; \Omega)\right) \times C\left([0,T], H_0(\textbf{\textit{rot}}; \Omega)\right) \times$

$C\left([0,T], L^2_0(\Omega)\right)$ *such that for any* $(\boldsymbol{v}, \boldsymbol{C}, D, q) \in \left[H^1_0(\Omega)\right]^2 \times H(\mathit{div};\Omega) \times H_0(\boldsymbol{rot};\Omega) \times L^2_0(\Omega)$ *it holds*

$$\Big(\frac{\partial}{\partial t}\boldsymbol{u}, \boldsymbol{v}\Big) + R_e^{-1}\Big(\nabla \boldsymbol{u}, \nabla \boldsymbol{v}\Big) - \Big(J \times \boldsymbol{B}, \boldsymbol{v}\Big) - \Big(p, \operatorname{div} \boldsymbol{v}\Big) = \Big(\boldsymbol{f}, \boldsymbol{v}\Big), \tag{5.32a}$$

$$\Big(\operatorname{div} \boldsymbol{u}, q\Big) = 0, \tag{5.32b}$$

$$\Big(\frac{\partial}{\partial t}\boldsymbol{B}, \boldsymbol{C}\Big) + \Big(\mathbf{rot}\, E, \boldsymbol{C}\Big) = 0, \tag{5.32c}$$

$$\Big(J, D\Big) - R_m^{-1}\Big(\boldsymbol{B}, \mathbf{rot}\, D\Big) = 0, \tag{5.32d}$$

$$J = E + \boldsymbol{u} \times \boldsymbol{B}, \quad \boldsymbol{u}(\cdot, 0) = \boldsymbol{u}_0, \quad \boldsymbol{B}(\cdot, 0) = \boldsymbol{B}_0 \text{ with } \operatorname{div} \boldsymbol{B}_0 = 0. \tag{5.32e}$$

Implicit above is the condition that the velocity and electric fields satisfy the boundary conditions (5.24) and that the condition on the velocity field satisfies (5.25). We note that many of the spaces in the formulation (5.32) spaces were introduced in Section 3.3.

The modeling spaces presented in the variational formulation (5.32) are infinite in dimension. This makes it impossible to compute the exact solution. Instead we introduce a mesh of the domain Ω denoted by Ω_h and with mesh size $h > 0$. On this mesh we can define the spaces $\mathcal{TV}_h, \mathcal{TV}_{h,0}, \mathcal{E}_h, \mathcal{V}_h, \mathcal{V}_{h,0}, \mathcal{P}_h$ and $\mathcal{P}_{h,0}$. The spaces $\mathcal{E}_h, \mathcal{V}_h, \mathcal{V}_{h,0}, \mathcal{P}_h$ were rigorously defined in Sections 3.5, 3.4 and 3.6 respectively. They serve as discrete versions of $H(\operatorname{div};\Omega), H(\mathbf{rot};\Omega)$, $H_0(\mathbf{rot};\Omega)$ and $L^2(\Omega)$ respectively. The newly introduced spaces are $\mathcal{TV}_h, \mathcal{TV}_{h,0}$ and $\mathcal{P}_{h,0}$. Their formal definition is the topic of Section 5.4. They are discrete versions of $\left[H^1(\Omega)\right]^2, \left[H^1_0(\Omega)\right]^2$ and $L^2_0(\Omega)$ respectively. Like their continuous counterparts these spaces satisfy

$$\mathcal{TV}_{h,0} \subset \mathcal{TV}_h, \quad \mathcal{V}_{h,0} \subset \mathcal{V}_h, \quad \mathcal{P}_{h,0} \subset \mathcal{P}_h. \tag{5.33}$$

These spaces are finite dimensional. However, their dimension is fully dependent on the mesh size, as $h \to 0$ their dimension skyrockets to infinity and they approach spaces that are dense in

their continuous counterparts.

There are mappings that embed the continuous spaces into their discrete versions, they are denoted as $\mathcal{I}^{\mathcal{TV}_h}, \mathcal{I}^{\mathcal{E}_h}, \mathcal{I}^{\mathcal{V}_h}$ and $\mathcal{I}^{\mathcal{P}_h}$. The geometry in these spaces is defined by an inner product that serves as an estimate to the $L^2(\Omega)$ inner product. They are

$$\big(\boldsymbol{u}_h, \boldsymbol{v}_h\big)_{\mathcal{TV}_h} \approx \big(\boldsymbol{u}_h, \boldsymbol{v}_h\big), \quad \Big[\boldsymbol{u}_h, \boldsymbol{v}_h\Big]_{\mathcal{TV}_h} \approx \big(\nabla \boldsymbol{u}_h, \nabla \boldsymbol{v}_h\big), \tag{5.34}$$

$$\big(\boldsymbol{B}_h, \boldsymbol{C}_h\big)_{\mathcal{E}_h} \approx \big(\boldsymbol{B}_h, \boldsymbol{C}_h\big), \quad \big(E_h, D_h\big)_{\mathcal{V}_h} \approx \big(E_h, D_h\big), \quad \big(p_h, q_h\big)_{\mathcal{P}_h} \approx \big(p_h, q_h\big). \tag{5.35}$$

Now we introduce the discrete variational formulation.

Find $\big\{(\boldsymbol{u}_h^n, \boldsymbol{B}_h^n)\big\}_{n=0}^{N} \subset \mathcal{TV}_h \times \mathcal{E}_h$ *and* $\big\{(E_h^{n+\theta}, p_h^{n+\theta}))\big\}_{n=0}^{N-1} \subset \mathcal{V}_h \times \mathcal{P}_{h,0}$ *such that for all* $(\boldsymbol{v}_h, \boldsymbol{C}_h, D_h, q_h) \in \mathcal{TV}_{h,0} \times \mathcal{E}_h \times \mathcal{V}_{h,0} \times \mathcal{P}_{h,0}$ *it holds:*

$$\Big(\frac{\boldsymbol{u}_h^{n+1} - \boldsymbol{u}_h^n}{\Delta t}, \boldsymbol{v}_h\Big)_{\mathcal{TV}_h} + R_e^{-1}\Big[\boldsymbol{u}_h^{n+\theta}, \boldsymbol{v}_h\Big]_{\mathcal{TV}_h} + \underbrace{\Big(J_h^{n+\theta}, \mathcal{I}^{\mathcal{V}_h}(\boldsymbol{v}_h \times \Pi^{RT} \boldsymbol{B}_h^{n+\theta})\Big)_{\mathcal{V}_h}}_{(1)} - \\ - \Big(\operatorname{div} \boldsymbol{v}_h, p_h^{n+\theta}\Big)_{\mathcal{P}_h} = \Big(\boldsymbol{f}_h, \boldsymbol{v}_h\Big)_{\mathcal{TV}_h}, \tag{5.36a}$$

$$\Big(\operatorname{div} \boldsymbol{u}_h^{n+\theta}, q_h\Big)_{\mathcal{P}_h} = 0, \tag{5.36b}$$

$$\Big(\frac{\boldsymbol{B}_h^{n+1} - \boldsymbol{B}_h^n}{\Delta t}, \boldsymbol{C}_h\Big)_{\mathcal{E}_h} + \Big(\mathbf{rot}\, E_h^{n+\theta}, \boldsymbol{C}_h\Big)_{\mathcal{E}_h} = 0, \tag{5.36c}$$

$$\big(J_h^{n+\theta}, D_h\big)_{\mathcal{V}_h} - R_m^{-1}\big(\boldsymbol{B}_h^{n+\theta}, \mathbf{rot}\, D_h\big)_{\mathcal{E}_h} = 0, \tag{5.36d}$$

$$\boldsymbol{u}_h^{n+\theta} = (1-\theta)\boldsymbol{u}_h^n + \theta \boldsymbol{u}_h^{n+1}, \quad \boldsymbol{B}_h^{n+\theta} = (1-\theta)\boldsymbol{B}_h^n + \theta \boldsymbol{B}_h^{n+1}, \tag{5.36e}$$

$$J_h^{n+\theta} = E_h^{n+\theta} + \mathcal{I}^{\mathcal{V}_h}(\boldsymbol{u}_h^{n+\theta} \times \Pi^{RT} \boldsymbol{B}_h^{n+\theta}), \tag{5.36f}$$

$$\boldsymbol{u}_h^0 = \mathcal{I}^{\mathcal{TV}_h}(\boldsymbol{u}_0), \quad \boldsymbol{B}_h^0 = \mathcal{I}^{\mathcal{E}_h}(\boldsymbol{B}_0) \text{ with } \operatorname{div} \boldsymbol{B}_0 = 0. \tag{5.36g}$$

As was the case in the continuous variational formulation. Here, we leave implicit that

$$E_h = \mathcal{I}^{\mathcal{V}_h}(E_b) \quad \text{and} \quad \boldsymbol{u}_h = \mathcal{I}^{\mathcal{TV}_h}(\boldsymbol{u}_b) \quad \text{along} \quad \partial\Omega. \tag{5.37}$$

The term labeled (1) in (5.36a) comes about from the approximation:

$$-\Big(J \times \boldsymbol{B}, \boldsymbol{v}\Big) = \Big(J, \boldsymbol{v} \times \boldsymbol{B}\Big) \approx \Big(J_h, \mathcal{I}^{\mathcal{V}_h}(\boldsymbol{v}_h \times \boldsymbol{B}_h)\Big)_{\mathcal{V}_h} \tag{5.38}$$

The reason we go through this trouble will become clear in Section 5.5 when we come up with stability estimates in the $L^2(\Omega)$ norm.

5.4 The Virtual Elements

The conforming virtual element space used in the discretization of the fluid-flow equations in (5.21) was originally proposed in [44, 45, 90], we note that there are VEMs for non-conforming approximations, see [29]. Here, we consider the enhanced formulation introduced in [90]. This formulation allows us to compute the L^2-orthogonal projection onto the largest polynomial subspace contained in the space of shape functions. Such operator is used in the construction of the approximate mass matrices.

The first, and simplest, space that we introduce is $\mathcal{P}_{h,0}$. This space is defined as

$$\mathcal{P}_{h,0} = \left\{ q_h \in \mathcal{P}_h : \int_\Omega q_h dA = 0 \right\}. \tag{5.39}$$

The construction of $\mathcal{P}_h$ is the topic of Section 3.6. To functions $q_h \in \mathcal{P}_{h,0}$ we associate the integral over every cell as the set of degrees of freedom, formally we refer to the quantities:

$$\forall \mathsf{P} \quad \in \Omega_h : \quad \int_{\mathsf{P}} q_h dA. \tag{5.40}$$

We note that they are equivalent to those in $\mathcal{P}_h$, we remind the reader that these were

$$\forall q_h \in \mathcal{P}_h \;\; \forall \mathsf{P} \in \Omega_h : \quad \frac{1}{|\mathsf{P}|} \int_{\mathsf{P}} q_h dA. \tag{5.41}$$

There is a simple correspondence between the two sets of degrees of freedom so that if one is known the other one can be immediately attained. We do this simply because computing the integral over $\mathcal{P}_{h,0}$ of a function $q_h \in \mathcal{P}_{h,0}$ is simpler with this set of degrees of freedom, it is the sum of them. This is to say that

$$\int_\Omega q_h dA = \sum_{i=0}^{N} \text{dof}_i(q_h). \tag{5.42}$$

Next we focus on the construction of the space we will use to approximate the velocity field. Consider a cell P in the mesh Ω_h. The construction of begins with the definition of the following sets:

$$\mathbb{B}\left(\partial\mathsf{P}\right) := \left\{v \in C^0(\partial\mathsf{P}) : \forall \mathsf{e} \in \partial\mathsf{P} \quad v_{|\mathsf{e}} \in \mathbb{P}_2(\mathsf{e})\right\}, \tag{5.43}$$

$$\mathbf{V}_h(\mathsf{P}) := \Big\{\boldsymbol{v}_h \in \left[H^1(\mathsf{P})\right]^2 \,:\, \boldsymbol{v}_{h|\partial\mathsf{P}} \in \left(\mathbb{B}\left(\partial\mathsf{P}\right)\right)^2, \operatorname{div} \boldsymbol{v}_h \in \mathbb{P}_0(\mathsf{P}), \\ -\triangle \boldsymbol{v}_h - \nabla s = \mathbf{0} \text{ for some } s \in L^2_0(\mathsf{P})\Big\}. \tag{5.44}$$

To a function $\boldsymbol{v}_h \in \mathbf{V}_h(\mathsf{P})$ we associate the following degrees of freedom

- $(\mathbf{D_1})$: pointwise evaluations of $\boldsymbol{v}_h$ at the vertices of P;
- $(\mathbf{D_2})$: pointwise evaluations at $\boldsymbol{v}_h$ at the midpoint of the edges of $\partial\mathsf{P}$.

We note that $\mathbf{V}_h(\mathsf{P})$ is unisolvent with this set of degrees of freedom. This result is documented in the following Theorem:

Theorem 5.40.1 Proof. *The domain P, the space of shape functions $\boldsymbol{V}_h(\mathsf{P})$ and the degrees of freedom $(\mathbf{D_1})$ and $(\mathbf{D_2})$ form a unisolvent finite element.*

Let $\{\mathsf{v}_i : 1 \leq i \leq n_\mathsf{v}\}$ and $\{\mathsf{v}_i^{1/2} : 1 \leq i \leq n_\mathsf{e}\}$ represent the set of vertices and midpoint of edges in P respectively. Consider $U := \{\boldsymbol{u}_h^i : 1 \leq i \leq 2n_\mathsf{v}\}$ and $V := \{\boldsymbol{v}_h^i : 1 \leq i \leq 2n_\mathsf{e}\}$ to be

defined as the solution to

$$
\begin{aligned}
&\triangle \boldsymbol{u}_h^i + \nabla p^i = \mathbf{0} \text{ in } \mathsf{P},\\
&\operatorname{div} \boldsymbol{u}_h^i = \int_{\partial P} \boldsymbol{u}_h^i ds \text{ in } \mathsf{P},\\
&\boldsymbol{u}_h^i(\mathsf{v}_j) = \begin{pmatrix} \delta_{i,j} \\ 0 \end{pmatrix}, \quad \boldsymbol{u}_h^i(\mathsf{v}_i^{1/2}) = \begin{pmatrix} 0 \\ 0 \end{pmatrix},\\
&\forall \mathsf{e} \in \partial \mathsf{P}: \quad \boldsymbol{u}_{h|\mathsf{e}} \in \mathbb{P}_2(\mathsf{e}),
\end{aligned}
$$

$$
\begin{aligned}
&\triangle \boldsymbol{u}_h^{i+n_\mathsf{v}} + \nabla p^{i+n_\mathsf{v}} = \mathbf{0} \text{ in } \mathsf{P},\\
&\operatorname{div} \boldsymbol{u}_h^{i+n_\mathsf{v}} = \int_{\partial P} \boldsymbol{u}_h^{i+n_\mathsf{v}} ds \text{ in } \mathsf{P},\\
&\boldsymbol{u}_h^{n_\mathsf{v}+i}(\mathsf{v}_j) = \begin{pmatrix} 0 \\ 0 \end{pmatrix}, \quad \boldsymbol{u}_h^{i+n_\mathsf{v}}(\mathsf{v}_i^{1/2}) = \begin{pmatrix} \delta_{i,j} \\ 0 \end{pmatrix},\\
&\forall \mathsf{e} \in \partial \mathsf{P}: \quad \boldsymbol{u}_{h|\mathsf{e}} \in \mathbb{P}_2(\mathsf{e}),
\end{aligned}
\tag{5.45}
$$

$$
\begin{aligned}
&\triangle \boldsymbol{v}_h^i + \nabla q^i = \mathbf{0} \text{ in } \mathsf{P},\\
&\operatorname{div} \boldsymbol{u}_h^i = \int_{\partial P} \boldsymbol{u}_h^i ds \text{ in } \mathsf{P},\\
&\boldsymbol{v}_h^i(\mathsf{v}_j) = \begin{pmatrix} 0 \\ \delta_{i,j} \end{pmatrix}, \quad \boldsymbol{u}_h^i(\mathsf{v}_i^{1/2}) = \begin{pmatrix} 0 \\ 0 \end{pmatrix},\\
&\forall \mathsf{e} \in \partial \mathsf{P}: \quad \boldsymbol{v}_{h|\mathsf{e}} \in \mathbb{P}_2(\mathsf{e}),
\end{aligned}
$$

$$
\begin{aligned}
&\triangle \boldsymbol{v}_h^{i+n_\mathsf{v}} + \nabla q^{i+n_\mathsf{v}} = \mathbf{0} \text{ in } \mathsf{P},\\
&\operatorname{div} \boldsymbol{v}_h^{i+n_\mathsf{v}} = \int_{\partial P} \boldsymbol{v}_h^{i+n_\mathsf{v}} ds \text{ in } \mathsf{P},\\
&\boldsymbol{v}_h^{n_\mathsf{v}+i}(\mathsf{v}_j) = \begin{pmatrix} 0 \\ 0 \end{pmatrix}, \quad \boldsymbol{v}_h^{i+n_\mathsf{v}}(\mathsf{v}_i^{1/2}) = \begin{pmatrix} 0 \\ \delta_{i,j} \end{pmatrix},\\
&\forall \mathsf{e} \in \partial \mathsf{P}: \quad \boldsymbol{u}_{h|\mathsf{e}} \in \mathbb{P}_2(\mathsf{e}).
\end{aligned}
$$

Here the $p^i, q^i \in L^2_0(\Omega)$ and

$$\delta_{i,j} = \begin{cases} 1 & \text{if } i = j, \\ 0 & \text{otherwise.} \end{cases} \tag{5.46}$$

The existence and uniqueness of these functions follow from the well-posedness of the differential equations presented, see [20]. The set $U \cup V$ makes a basis for $\mathbf{V}_h(\mathsf{P})$ proving that the dimension of the space $\mathbf{V}_h(\mathsf{P})$ agrees with the number of degrees of freedom. To check unisolvency we need only show that if the degrees of freedom of a function $\boldsymbol{u}_h \in \mathbf{V}_h(\mathsf{P})$ are all null then that function must be identically zero. For such a function, by definition, there exists $s \in L^2_0(\Omega)$ such that $\boldsymbol{u}_h$ and s satisfy

$$\triangle \boldsymbol{u}_h + \nabla s = \mathbf{0} \text{ in } \mathsf{P}, \tag{5.47a}$$

$$\operatorname{div} \boldsymbol{u}_h = 0 \text{ in } \mathsf{P}, \tag{5.47b}$$

$$\boldsymbol{u}_h = \mathbf{0} \text{ on } \partial\mathsf{P}. \tag{5.47c}$$

which is a problem whose unique solution is $\boldsymbol{u}_h \equiv \mathbf{0}$. This implies that the map that sends elements in $\mathcal{TV}_h(\mathsf{P})$ to its degrees of freedom has a trivial kernel, thus it is injective. And, any injective linear map whose domain and range have the same dimension must be in fact a bijection. □

In the space $\mathbf{V}_h(\mathsf{P})$ the stiffness matrix used to approximate the bilinear form

$$\forall \boldsymbol{u}, \boldsymbol{v} \in \left[H^1(\mathsf{P})\right]^2 : \quad a(\boldsymbol{u}, \boldsymbol{v}) = \int_{\mathsf{P}} \nabla \boldsymbol{u} \cdot \nabla \boldsymbol{v} dA \tag{5.48}$$

is computable. For us to show how this is done we begin by introducing the space of polynomials:

$$\mathbb{P}(\mathsf{P}) = \{q \in \mathbb{P}_2(\mathsf{P}) : \operatorname{div} q \in \mathbb{P}_0(\mathsf{P})\}. \tag{5.49}$$

Note that $[P(\mathsf{P})]^2$ is the largest polynomial space contained in $\mathbf{V}_h(\mathsf{P})$. Thus, following the

methodology laid out in Section 2.3 we define the projector $\Pi_{\mathsf{P}}^{\nabla} : \mathbf{V}_h(\mathsf{P}) \to [\mathbb{P}(\mathsf{P})]^2$ such that for $\boldsymbol{v}_h \in \mathbf{V}_h(\mathsf{P})$ the polynomial $\Pi_{\mathsf{P}}^{\nabla}\boldsymbol{v}_h$ is the solution to the following variational problem

$$\forall \boldsymbol{q} \in \left[\mathbb{P}(\mathsf{P})\right]^2 : \quad \int_{\mathsf{P}} \nabla \Pi_{\mathsf{P}}^{\nabla} \boldsymbol{v}_h \cdot \nabla \boldsymbol{q} dA = \int_{\mathsf{P}} \nabla \boldsymbol{v}_h \cdot \nabla \boldsymbol{q} dA, \tag{5.50a}$$

$$P_0\left(\Pi_{\mathsf{P}}^{\nabla} \boldsymbol{v}_h\right) = \mathsf{P}_0(\boldsymbol{v}_h). \tag{5.50b}$$

Where P_0 is given by

$$\forall \boldsymbol{v}_h \in \mathbf{V}_h : \quad P_0(\boldsymbol{v}_h) = \sum_{\mathsf{v}} \boldsymbol{v}_h(\mathsf{v}). \tag{5.51}$$

The sum above is taken over the nodes of P and the midpoint of every edge of $\partial\mathsf{P}$. To make computations using this projector a series of matrices need to be constructed, see Section 2.3. Most of these are standard for any bilinear form. However, the entries of the matrix B, in the notation of that chapter, requires that we compute the following quantities

$$\forall \boldsymbol{v}_h \in \mathbf{V}_h \forall \boldsymbol{q} \in [\mathbb{P}(\mathsf{P})]^2 : \quad a(\boldsymbol{u}_h, \boldsymbol{q}) = \int_{\Omega} \nabla \boldsymbol{v}_h \cdot \nabla \boldsymbol{q} dA \tag{5.52}$$

To do this note this we begin by applying Green's Theorem. Note that if $\boldsymbol{v}_h \in \mathbf{V}_h(\mathsf{P})$ and $\boldsymbol{q} \in [\mathbb{P}(\mathsf{P})]^2$ then

$$\int_P \nabla \boldsymbol{v}_h \cdot \nabla \boldsymbol{q} dA = \int_{\partial\mathsf{P}} \boldsymbol{v}_h \nabla \boldsymbol{q} \boldsymbol{n} d\ell - \int_P \boldsymbol{v}_h \cdot \triangle \boldsymbol{q} dA \tag{5.53}$$

Moreover, since $\triangle \boldsymbol{q} \in [\mathbb{P}_0(\mathsf{P})]^2$ then there exists $g \in \mathbb{P}_1(\mathsf{P})$ such that $\triangle \boldsymbol{q} = \nabla g$. We can substitute this identity back into equation (5.53) and apply Green's Theorem again to obtain

$$\begin{aligned}\int_{\mathsf{P}} \nabla \boldsymbol{v}_h \cdot \nabla \boldsymbol{q} dA &= \int_{\partial\mathsf{P}} \boldsymbol{v}_h \cdot \nabla \boldsymbol{q} \boldsymbol{n} d\ell - \int_P \boldsymbol{v}_h \cdot \triangle \boldsymbol{q} dA = \\ &= \int_{\partial\mathsf{P}} \boldsymbol{v}_h \cdot \nabla \boldsymbol{q} \boldsymbol{n} d\ell + \int_{\mathsf{P}} (\operatorname{div} \boldsymbol{v}_h) g dA - \int_{\partial\mathsf{P}} g \boldsymbol{v}_h \cdot \boldsymbol{n} d\ell = \\ &= (\mathbf{T1}) + (\mathbf{T2}) - (\mathbf{T3}).\end{aligned} \tag{5.54}$$

Note that along the each edge $\mathsf{e} \in \partial\mathsf{P}$ the function $\boldsymbol{v}_h$ must be a quadratic polynomial by definition. Hence the boundary integrals in terms $(\mathbf{T_1})$ and $(\mathbf{T_3})$ in equation (5.54) are integrals of polynomials. In this case we can find quadrature rules to compute them exactly using the evaluations found in the degrees of freedom $(\mathbf{D_1})$ and $(\mathbf{D_2})$. Regarding term $(\mathbf{T2})$ we will show that $\operatorname{div} \boldsymbol{v}_h \in \mathbb{P}_0(\mathsf{P})$ is computable using only the information obtained in the set of degrees of freedom. Note that in one hand

$$\int_{\mathsf{P}} \operatorname{div} \boldsymbol{v}_h = \operatorname{div} \boldsymbol{v}_h |\mathsf{P}|. \tag{5.55}$$

And, in the other hand

$$\int_{\mathsf{P}} \operatorname{div} \boldsymbol{v}_h = \int_{\partial\mathsf{P}} \boldsymbol{v}_h \cdot \boldsymbol{n} d\ell. \tag{5.56}$$

implying that

$$\operatorname{div} \boldsymbol{u}_h = \frac{1}{|\mathsf{P}|} \int_{\partial\mathsf{P}} \boldsymbol{v}_h \cdot \boldsymbol{n} d\ell. \tag{5.57}$$

We have arrived at a formula for computing the divergence of $\boldsymbol{v}_h$ that only requires boundary information. And, as we mentioned before, this information can be extracted from the degrees of freedom $(\mathbf{D_1})$ and $(\mathbf{D_2})$. Following the steps laid out in Section 2.3 we can construct an approximation to the bilinear from in (5.48). Since the bilinear form (5.54) can be approximated in $\mathbf{V}_h(\mathsf{P})$ then the space $\mathbf{V}_h(\mathsf{P})$ can be used to come up with approximations to the stationary Stokes equations:

$$-\triangle \boldsymbol{u} - \nabla p = \boldsymbol{f} \quad \text{in} \quad \Omega. \tag{5.58a}$$

$$\operatorname{div} \boldsymbol{u} = 0. \tag{5.58b}$$

For which the variational formulation is: *find* $(\boldsymbol{u}, p) \in C^1\left([0,T], \left[H^1(\Omega)\right]^2\right) \times C\left([0,T], L^2_0(\Omega)\right)$

such that

$$\forall \boldsymbol{v} \in \left[H^1(\Omega)\right]^2 : \quad \left(\nabla \boldsymbol{u}, \nabla \boldsymbol{v}\right) + \left(\operatorname{div} \boldsymbol{v}, p\right) = 0, \tag{5.59a}$$

$$\forall q \in L^2_0(\Omega) : \quad \left(\operatorname{div} \boldsymbol{u}, q\right) = 0. \tag{5.59b}$$

For further detail on how this is done we refer the reader to [44]. However, in the space $\mathbf{V}_h(\mathsf{P})$ it is not possible to compute the mass matrix used to compute the bilinear form

$$\forall \boldsymbol{u}, \boldsymbol{v} \in \left[H^1(\Omega)\right]^2 : \quad a(\boldsymbol{u}, \boldsymbol{v}) = \left(\boldsymbol{u}, \boldsymbol{v}\right). \tag{5.60}$$

Hence approximating the terms involving the time derivative of the velocity field in the variational formulation (5.32a) will require further treatment. We will apply the enhancement strategy in [90]. First, we introduce the spaces:

$$\mathcal{G}_2\left(\mathsf{P}\right) := \nabla \mathbb{P}_3(\mathsf{P}), \quad \mathcal{G}_2^{\perp}\left(\mathsf{P}\right) := \{\boldsymbol{g}^{\perp} \in [\mathbb{P}_2(\mathsf{P})]^2 : \forall \boldsymbol{g} \in \mathcal{G}_2\left(\mathsf{P}\right) \quad \left(\boldsymbol{g}^{\perp}, \boldsymbol{g}\right) = 0\}, \tag{5.61}$$

$$\mathbf{U}_h(\mathsf{P}) := \Bigg\{ \boldsymbol{v}_h \in \left[H^1(\mathsf{P})\right]^2 : \boldsymbol{v}_{h|\partial \mathsf{P}} \in \left[\mathbb{B}\left(\partial \mathsf{P}\right)\right]^2, \begin{cases} \exists s \in L^2_0(\mathsf{P}), \exists \boldsymbol{g}^{\perp} \in \mathcal{G}_2^{\perp}\left(\mathsf{P}\right) : \quad -\triangle \boldsymbol{v}_h - \nabla s = \boldsymbol{g}^{\perp}, \\ \operatorname{div} \boldsymbol{v}_h \in \mathbb{P}_0(\mathsf{P}) \end{cases} \Bigg\}. \tag{5.62}$$

We note that the projector $\Pi^{\nabla}_{\mathsf{P}}$ defined in (5.50) can be extended to $\mathbf{U}_h(\mathsf{P})$. And, it is computable using only the information in the degrees of freedom $(\mathbf{D_1})$ and $(\mathbf{D_2})$. In fact the same construction presented in the case of $\mathbf{V}_h(\mathsf{P})$ applies for $\mathbf{U}_h(\mathsf{P})$. However, the space $\mathbf{U}_h(\mathsf{P})$ is not unisolvent when equipped with these degrees of freedom. Thus, we consider a subspace of $\mathbf{U}_h(\mathsf{P})$, denoted $\mathcal{TV}_h(\mathsf{P})$, that is unisolvent. Formally $\mathcal{TV}_h(\mathsf{P})$ is defined as

$$\mathcal{TV}_h(\mathsf{P}) := \Big\{ \boldsymbol{v}_h \in \mathbf{U}_h(\mathsf{P}) : \forall \boldsymbol{g}^{\perp} \in \mathcal{G}_2^{\perp}\left(\mathsf{P}\right)/\mathbb{R}^2 \quad \left(\boldsymbol{v}_h - \Pi^{\nabla}_{\mathsf{P}} \boldsymbol{v}_h, \boldsymbol{g}^{\perp}\right) = 0 \Big\}. \tag{5.63}$$

This space is unisolvent if we equip it with the degrees of freedom $(\mathbf{D_1})$ and $(\mathbf{D_2})$. Hence we can define $\mathcal{I}^{\mathcal{TV}_h} : C^\infty(\Omega) \to \mathcal{TV}_h$ such that the degrees of freedom of $\boldsymbol{u} \in C^\infty(\Omega)$ and $\mathcal{I}_{\mathsf{P}}^{\mathcal{TV}_h}(\boldsymbol{u})$ agree. This map can be extended continuously to $\mathcal{I}_{\mathsf{P}}^{\mathcal{TV}_h} : \left[H^1(\Omega)\right]^2 \to \mathcal{TV}_h$.

In the space $\mathcal{TV}_h(\mathsf{P})$ we define the projector $\Pi^0_{\mathsf{P}} : \mathcal{TV}_h(\mathsf{P}) \to \mathbb{P}(\mathsf{P})$. When Π^0 is evaluated at a function $\boldsymbol{v}_h \in \mathcal{TV}_h(\mathsf{P})$ the resulting polynomial comes about as the solution to the variational problem

$$\forall \boldsymbol{q} \in \mathbb{P}(\mathsf{P}): \quad \left(\Pi^0_{\mathsf{P}} \boldsymbol{v}_h - \boldsymbol{v}_h, \boldsymbol{q}\right) = 0. \tag{5.64}$$

We can show that Π^0_{P} is computable using only $(\mathbf{D_1})$ and $(\mathbf{D_2})$. Let $\boldsymbol{v}_h \in \mathcal{TV}_h(\mathsf{P})$ and $\boldsymbol{q} \in \mathbb{P}(\mathsf{P})$. We can write

$$\boldsymbol{q} = \nabla g + \boldsymbol{g}^\perp \tag{5.65}$$

Where $g \in \mathbb{P}_3(\mathsf{P})$. Thus, we have that

$$\int_{\mathsf{P}} \boldsymbol{v}_h \cdot \boldsymbol{q} dA = \int_{\mathsf{P}} \boldsymbol{v}_h \cdot \nabla g dA + \int_{\mathsf{P}} \boldsymbol{v}_h \cdot \boldsymbol{g}^\perp dA. \tag{5.66}$$

We can use Green's Theorem to compute

$$\int_{\mathsf{P}} \boldsymbol{v}_h \cdot \nabla g dA = \int_{\partial \mathsf{P}} \boldsymbol{v}_h \cdot \boldsymbol{n} g d\ell - \int_{\mathsf{P}} \operatorname{div} \boldsymbol{v}_h g dA. \tag{5.67}$$

Since $\boldsymbol{v}_h$ is a polynomial when restricted to each edge then the boundary integral above is computable. Moreover, we can use (5.57) to compute the divergence of $\boldsymbol{v}_h$ and thus the area integral is also computable. We can also compute the second integral in (5.66) but first we write

$$\boldsymbol{g}^\perp = \boldsymbol{c} + (\boldsymbol{g}^\perp - \boldsymbol{c}), \quad \boldsymbol{c} = \frac{1}{|\mathsf{P}|} \int_{\mathsf{P}} \boldsymbol{g}^\perp dA. \tag{5.68}$$

Since $\boldsymbol{c} \in \mathbb{P}_0(\mathsf{P})$ then we can find $q \in \mathbb{P}_1(\mathsf{P})$ such that

$$\nabla q = \boldsymbol{c}. \tag{5.69}$$

So we can use the following formula.

$$\int_{\mathsf{P}} \boldsymbol{v}_h \cdot \boldsymbol{c} dA = \int_{\partial \mathsf{P}} q \boldsymbol{v}_h \cdot \boldsymbol{n} d\ell - \int_{\mathsf{P}} \operatorname{div} \boldsymbol{v}_h q dA. \tag{5.70}$$

Finally, we note that $\boldsymbol{g}^{\perp} - \boldsymbol{c} \in \mathcal{G}_2^{\perp}(\mathsf{P}) / \mathbb{R}^2$ so by definition of the space $\mathcal{TV}_h(\mathsf{P})$ we can use

$$\int_{\mathsf{P}} \boldsymbol{v}_h \cdot (\boldsymbol{g}^{\perp} - \boldsymbol{c}) dA = \int_{\mathsf{P}} \Pi_{\mathsf{P}}^{\nabla} \boldsymbol{v}_h \cdot (\boldsymbol{g}^{\perp} - \boldsymbol{c}) dA. \tag{5.71}$$

We note that in order to compute the necessary integrals necessary we can divide P into a series of triangles $\{\mathsf{T}_i\}$. Over each of these triangles we require a fourth order quadrature in order to compute the integrals above. We use the quadrature presented in [86].

Having defined and computed the projectors Π_{P}^0 and $\Pi_{\mathsf{P}}^{\nabla}$ in the space $\mathcal{TV}_h(\mathsf{P})$. We are ready to define the inner product and semi-inner product in $\mathcal{TV}_h(\mathsf{P})$ they are

$$\forall \boldsymbol{u}_h, \boldsymbol{v}_h \in \mathcal{TV}_h(\mathsf{P}) :$$

$$\left(\boldsymbol{u}_h, \boldsymbol{v}_h\right)_{\mathcal{TV}_h(\mathsf{P})} = \left(\Pi_{\mathsf{P}}^0 \boldsymbol{u}_h, \Pi_{\mathsf{P}}^0 \boldsymbol{v}_h\right) + \mathcal{S}_{\mathsf{P}}^{\mathcal{TV}_h}\left((\mathcal{I} - \Pi_{\mathsf{P}}^0)\boldsymbol{u}_h, (\mathcal{I} - \Pi_{\mathsf{P}}^0)\boldsymbol{v}_h\right), \tag{5.72}$$

$$\left[\boldsymbol{u}_h, \boldsymbol{v}_h\right]_{\mathcal{TV}_h(\mathsf{P})} = \left(\nabla \Pi_{\mathsf{P}}^{\nabla} \boldsymbol{u}_h, \nabla \Pi_{\mathsf{P}}^{\nabla} \boldsymbol{v}_h\right) + \mathcal{T}_{\mathsf{P}}^{\mathcal{TV}_h}\left(\nabla(\mathcal{I} - \Pi_{\mathsf{P}}^{\nabla})\boldsymbol{u}_h, \nabla(\mathcal{I} - \Pi_{\mathsf{P}}^{\nabla})\boldsymbol{v}_h\right). \tag{5.73}$$

The function $\mathcal{I}$ is the identity mapping. As was the case in the definition of the inner product in $\mathcal{V}_h(\mathsf{P})$ and $\mathcal{E}_h(\mathsf{P})$ we require that $\mathcal{S}_{\mathsf{P}}^{\mathcal{TV}_h}$ and $\mathcal{T}_{\mathsf{P}}^{\mathcal{TV}_h}$ be a continuous bilinear forms satisfying

$$\begin{aligned}
&\exists\ s_*,\ s^* > 0\ \ \forall \boldsymbol{v}_h \in \mathcal{TV}_h(\mathsf{P}) \cap \ker \Pi^0 : \quad s_* \|\boldsymbol{v}_h\|_{0,\Omega}^2 \leq \mathcal{S}_P^{\mathcal{TV}_h}(\boldsymbol{v}_h, \boldsymbol{v}_h) \leq s^* \|\boldsymbol{v}_h\|_{0,\Omega}^2, \\
&\exists\ t_*,\ t^* > 0\ \ \forall \boldsymbol{v}_h \in \mathcal{TV}_h(\mathsf{P}) \cap \ker \Pi_{\mathsf{P}}^{\nabla} : \quad t_* \|\nabla \boldsymbol{v}_h\|_{0,\Omega}^2 \leq \mathcal{T}_P^{\mathcal{TV}_h}(\nabla \boldsymbol{v}_h, \nabla \boldsymbol{v}_h) \leq t^* \|\nabla \boldsymbol{v}_h\|_{0,\Omega}^2.
\end{aligned} \tag{5.74}$$

Like before we refer the reader to [49, 71] for more examples of such bilinear forms. The inner and semi-inner products defined in (5.72) satisfy two fundamental properties: **consistency** and **stability**. These are presented in the following theorem:

Theorem 5.40.2 *Let* $\big(\cdot,\cdot\big)_{\mathcal{TV}_h(\mathsf{P})}$ *and* $\big[\cdot,\cdot\big]_{\mathcal{TV}_h(\mathsf{P})}$ *be the two inner and semi-inner products defined in* (5.72)*. The following two properties hold:*

- ***polynomial consistency****: for every* $\boldsymbol{v}_h \in \mathcal{TV}_h(\mathsf{P})$ *and vector polynomial* $\boldsymbol{q} \in [\mathbb{P}_2(\mathsf{P})]^2$ *it holds that:*

$$\big(\boldsymbol{v}_h, \boldsymbol{q}\big)_{\mathcal{TV}_h(\mathsf{P})} = \big(\boldsymbol{v}_h, \boldsymbol{q}\big), \quad \big[\boldsymbol{v}_h, \boldsymbol{q}\big]_{\mathcal{TV}_h(\mathsf{P})} = \big(\nabla \boldsymbol{v}_h, \nabla \boldsymbol{q}\big). \tag{5.75}$$

- ***stability****: there exists two pairs of positive real constants* (δ_*, δ^*) *and* (ϵ_*, ϵ^*)*, which are independent of mesh-size and time-step, such that for any* $\boldsymbol{v}_h \in \mathcal{TV}_h(\mathsf{P})$ *it holds that:*

$$\delta_* \|\boldsymbol{v}_h\|^2_{0,\mathsf{P}} \leq \Big(\boldsymbol{v}_h, \boldsymbol{v}_h\Big)_{\mathcal{TV}_h(\mathsf{P})} \leq \delta^* \|\boldsymbol{v}_h\|^2_{0,\mathsf{P}}, \tag{5.76}$$

and

$$\epsilon_* \|\nabla \boldsymbol{v}_h\|^2_{0,\mathsf{P}} \leq \Big[\boldsymbol{v}_h, \boldsymbol{v}_h\Big]_{\mathcal{TV}_h(\mathsf{P})} \leq \epsilon^* \|\gamma \boldsymbol{v}_h\|^2_{0,\mathsf{P}}. \tag{5.77}$$

Proof. The proof of the the above theorem is the same as the proof of Theorem 3.40.2. We note that we have already shown that the projectors $\Pi^{\nabla}_{\mathsf{P}}$ and Π^{0}_{P} satisfy properties **P1** and **P2** in Section 3.4. We can use the same arguments as we did in the proof of Theorem 3.50.2 to show that both projectors satisfy property **P3** as well. □

The global space $\mathcal{TV}_h$ is given by

$$\mathcal{TV}_h = \Big\{ \boldsymbol{v}_h \in \big[H^1(\Omega)\big]^2 : \forall \mathsf{P} \in \Omega_h \quad \boldsymbol{v}_{h|\mathsf{P}} \in \mathcal{TV}_h(\mathsf{P}) \Big\}. \tag{5.78}$$

In this space we define the the inner product and semi-inner product.

$$\forall \boldsymbol{u}_h, \boldsymbol{v}_h \in \mathcal{TV}_h :$$
$$\big(\boldsymbol{u}_h, \boldsymbol{v}_h\big)_{\mathcal{TV}_h} = \sum_{\mathsf{P}\in\Omega_h} \big(\boldsymbol{u}_{h|\mathsf{P}}, \boldsymbol{v}_{h|\mathsf{P}}\big)_{\mathcal{TV}_h(\mathsf{P})}, \quad \Big[\boldsymbol{u}_h, \boldsymbol{v}_h\Big]_{\mathcal{TV}_h} = \sum_{\mathsf{P}\in\Omega} \big[\boldsymbol{u}_{h|\mathsf{P}}, \boldsymbol{v}_{h|\mathsf{P}}\big]_{\mathcal{TV}_h(\mathsf{P})}. \quad (5.79)$$

We define the norms and semi-norm in the space $\mathcal{TV}_h$ as

$$|||\boldsymbol{v}_h|||_{\mathcal{TV}_h} = \big(\boldsymbol{v}_h, \boldsymbol{v}_h\big)^{1/2}_{\mathcal{TV}_h}, \quad \big|\boldsymbol{v}_h\big|_{\mathcal{TV}_h} = \big[\boldsymbol{v}_h, \boldsymbol{v}_h\big]^{1/2}_{\mathcal{TV}_h}, \quad (5.80a)$$

$$|||\boldsymbol{v}_h|||_{1,\mathcal{TV}_h} = \Big(|||\boldsymbol{v}_h|||^2_{\mathcal{TV}_h} + \big|\boldsymbol{v}_h\big|^2_{\mathcal{TV}_h}\Big)^{1/2}. \quad (5.80b)$$

The norm in the topological dual space of $\mathcal{TV}_{h,0}$ denoted by $\mathcal{TV}'_{h,0}$ is:

$$|||\boldsymbol{f}_h|||_{-1,\mathcal{TV}_h} = \sup_{\boldsymbol{v}_h\in\mathcal{TV}_{h,0}} \frac{\big(\boldsymbol{f}_h, \boldsymbol{v}_h\big)_{\mathcal{TV}_h}}{\big|\boldsymbol{v}_h\big|_{\mathcal{TV}_h}} \qquad \forall \boldsymbol{f}_h \in \mathcal{TV}'_{h,0}. \quad (5.81)$$

The global inner product, semi-inner product and the norms and semi-norm they define also satisfy the **consistency** and **stability** properties.

Corollary 5.40.1 *The norms and semi-norm in* (5.80) *are equivalent to the* $[L^2(\Omega)]^2$ *and* $\big[H^1(\Omega)\big]^2$ *inner products and semi-inner product respectively. In other words, there exists* $\eta_*, \eta^* > 0$ *independent of mesh-size and time-step such that for any* $\boldsymbol{v}_h \in \mathcal{TV}_h$ *it holds*

$$\eta_*\|\boldsymbol{v}_h\|^2_{0,\Omega} \leq |||\boldsymbol{v}_h|||^2_{\mathcal{TV}_h} \leq \eta^*\|\boldsymbol{v}_h\|^2_{0,\Omega}, \quad (5.82a)$$

$$\eta_*\|\nabla\boldsymbol{v}_h\|^2_{0,\Omega} \leq |||\boldsymbol{v}_h|||^{2,\nabla}_{\mathcal{TV}_h} \leq \eta^*\|\nabla\boldsymbol{v}_h\|^2_{0,\Omega}, \quad (5.82b)$$

$$\eta_*\|\boldsymbol{v}_h\|^2_{1,\Omega} \leq |||\boldsymbol{v}_h|||^2_{1,\mathcal{TV}_h} \leq \eta^*\|\boldsymbol{v}_h\|^2_{1,\Omega}. \quad (5.82c)$$

Proof. This result follows from Theorem 5.40.2. The techniques used are the same as those in the proof of Corollary 3.40.1. □

Finally, we can define the global Fortin projector $\mathcal{I}^{\mathcal{TV}_h}$ to satisfy

$$\forall \mathsf{P} \in \Omega_h \forall \boldsymbol{v}_h \in \mathcal{TV}_h : \quad \mathcal{I}^{\mathcal{TV}_h}(\boldsymbol{v}_h)_{|\mathsf{P}} = \mathcal{I}_{\mathsf{P}}^{\mathcal{TV}_h}\left(\boldsymbol{v}_{h|\mathsf{P}}\right). \tag{5.83}$$

Moreover, the space $\mathcal{TV}_{h,0}$ is set of functions in $\mathcal{TV}_h$ that, where restricted to the boundary, are null. This is to say that

$$\mathcal{TV}_{h,0} = \left\{\boldsymbol{v}_h \in \mathcal{TV}_h : \boldsymbol{v}_{h|\partial\Omega} \equiv \boldsymbol{0}\right\}. \tag{5.84}$$

Finally, the last result we present in this section regards the stability of approximations to problems in fluid flow of the spaces $\mathcal{TV}_h$ and $\mathcal{P}_{h,0}$. They are selected specifically to satisfy the following inf-sup condition. This is proven in proposition 4.3 of [44].

Theorem 5.40.3 *There exists a projector* $\Pi_h : \left[H_0^1(\Omega)\right]^2 \to \mathcal{TV}_{h,0}$ *that satisfies*

$$\forall q_h \in \mathcal{P}_{h,0} : \quad \left(div\, \Pi_h \boldsymbol{v}, q_h\right)_{\mathcal{P}_h} = \left(div\, \boldsymbol{v}, q_h\right)_{\mathcal{P}_h} \quad \textit{and} \quad |||\Pi_h \boldsymbol{v}|||_{1,\mathcal{TV}_h} \leq C_\pi \|\boldsymbol{v}\|_{1,\Omega}, \tag{5.85}$$

for every vector-valued field $\boldsymbol{v} \in \left[H_0^1(\Omega)\right]^2$ *and a real constant* $C_\pi > 0$ *that is independent of the mesh characteristics. Therefore, the spaces* $\mathcal{TV}_h$ *and* $\mathcal{P}_{h,0}$ *are a stable inf-sup pair and satisfy the relation:*

$$\inf_{q_h \in \mathcal{P}_{h,0}} \sup_{\boldsymbol{v}_h \in \mathcal{TV}_{h,0}} \frac{\left(div\, \boldsymbol{v}_h, q_h\right)_{\mathcal{P}_h}}{|||\boldsymbol{v}_h|||_{1,\mathcal{TV}_h} |||q_h|||_{\mathcal{P}_h}} > 0. \tag{5.86}$$

We finish this section by noting that pairs of finite elements that fail to satisfy the inf-sup condition presented in Theorem 5.40.3 will yield unstable simulations of fluid flow phenomena.

5.5 Energy Stability Estimates

The conforming nature of VEM allows us to mimic many properties that are present in the continuous scenario. One of the more important is preserving certain types of estimates in the

$L^2(\Omega)-$norm. These usually come about after testing the variational formulation against the exact solution and an application of Gronwall's Lemma. In this section, much like in Section 3.9, we present an estimate of this type true for the continuous system (5.21) and its discrete counterpart (6.3). We begin by presenting the decomposition

$$\boldsymbol{u} = \widehat{\boldsymbol{u}} + \boldsymbol{u}_b, \quad E = \widehat{E} + E_b, \tag{5.87}$$

where $\widehat{\boldsymbol{u}} \in \left[H_0^1(\Omega)\right]^2$ and $\widehat{E} \in H_0(\mathbf{rot};\Omega)$. The extension to the boundary condition on the velocity field is selected to satisfy

$$\operatorname{div} \boldsymbol{u}_b \equiv 0 \text{ in } \Omega, \quad \boldsymbol{u}_b(\boldsymbol{x}) = \mathbf{0} \text{ if } d(\boldsymbol{x}, \partial\Omega) \geq \epsilon. \tag{5.88}$$

For $h > \epsilon > 0$. We can do this by defining the domain $\Omega_\epsilon = \{\boldsymbol{x} \in \Omega : d(\boldsymbol{x}, \partial\Omega) < \epsilon\}$ and picking such an extension as the solution to

$$-\triangle \widehat{\boldsymbol{u}}_b + \nabla s = \mathbf{0} \text{ in } \Omega_\epsilon, \tag{5.89a}$$

$$\operatorname{div} \widehat{\boldsymbol{u}}_b = 0 \text{ in } \Omega_\epsilon, \tag{5.89b}$$

$$\widehat{\boldsymbol{u}}_b = \boldsymbol{u}_b \text{ on } \partial\Omega, \tag{5.89c}$$

$$\widehat{\boldsymbol{u}}_b = \mathbf{0} \text{ on } \partial(\Omega \setminus \Omega_\epsilon). \tag{5.89d}$$

which is well-posed by the discussion in [20]. Finally we define

$$\widehat{J} = \widehat{E} + \widehat{\boldsymbol{u}} \times \boldsymbol{B}, \quad J_b = E_b + \boldsymbol{u}_b \times \boldsymbol{B}. \tag{5.90}$$

We do this in order to reveal the boundary information. The following theorem gives the continuous energy estimate. Similar estimates are reported in [59, 67, 68].

Theorem 5.50.1 *Let* $(\boldsymbol{u}, \boldsymbol{B}, E, p)$ *solve the variational formulation* (5.32) *in the time interval*

$[0,T]$ *then*

$$\frac{1}{2}\frac{d}{dt}\|\widehat{\boldsymbol{u}}\|_{0,\Omega}^2+\frac{1}{2R_m}\frac{d}{dt}\|\boldsymbol{B}\|_{0,\Omega}^2+R_e^{-1}\|\nabla\widehat{\boldsymbol{u}}\|_{0,\Omega}^2+\|\widehat{J}\|_{0,\Omega}^2=$$
$$=\Big(\boldsymbol{f},\widehat{\boldsymbol{u}}\Big)-\Big(\frac{\partial}{\partial t}\boldsymbol{u}_b,\widehat{\boldsymbol{u}}\Big)-R_e^{-1}\Big(\nabla\boldsymbol{u}_b,\nabla\widehat{\boldsymbol{u}}\Big)-R_m^{-1}\Big(\mathbf{rot}\,E_b,\boldsymbol{B}\Big)-\Big(J_b,\widehat{J}\Big). \quad (5.91)$$

And, as a consequence it must be true that

$$\frac{e^{-T}}{2}\|\widehat{\boldsymbol{u}}(T)\|_{0,\Omega}^2+\frac{e^{-T}}{2R_m}\|\boldsymbol{B}(T)\|_{0,\Omega}^2+\int_0^T\left(\frac{e^{-t}}{2R_e}\|\nabla\widehat{\boldsymbol{u}}\|_{0,\Omega}^2+\frac{e^{-t}}{2}\|\widehat{J}\|_{0,\Omega}^2\right)dt\leq$$
$$\leq\frac{e^{-T}}{2}\|\widehat{\boldsymbol{u}}(0)\|_{0,\Omega}^2+\frac{e^{-T}}{2R_m}\|\boldsymbol{B}(0)\|_{0,\Omega}^2+$$
$$+\int_0^T\Big(e^{-t}R_e\|\boldsymbol{f}\|_{-1,\Omega}^2+\frac{e^{-t}}{2}\frac{d}{dt}\|\boldsymbol{u}_b\|_{0,\Omega}^2+R_e^{-1}e^{-t}\|\nabla\boldsymbol{u}_b\|_{0,\Omega}^2+$$
$$+\frac{e^{-t}}{2R_m}\|\mathbf{rot}\,E_b\|_{0,\Omega}^2+\frac{e^{-t}}{2}\|J_b\|_{0,\Omega}^2\Big)dt, \quad (5.92)$$

Proof. Taking the test function $(\boldsymbol{v},\boldsymbol{C},D,q)=(\widehat{\boldsymbol{u}},\boldsymbol{B},\widehat{E},p)$ in the variational formulation (5.32) yields

$$\frac{1}{2}\frac{d}{dt}\|\widehat{\boldsymbol{u}}\|_{0,\Omega}^2+R_e^{-1}\|\nabla\widehat{\boldsymbol{u}}\|_{0,\Omega}^2+\Big(\widehat{J},\widehat{\boldsymbol{u}}\times\boldsymbol{B}\Big)-\Big(\mathrm{div}\,\widehat{\boldsymbol{u}},p\Big)=$$
$$=\Big(\boldsymbol{f},\widehat{\boldsymbol{u}}\Big)-\Big(\frac{\partial}{\partial t}\boldsymbol{u}_b,\widehat{\boldsymbol{u}}\Big)-R_e^{-1}\Big(\nabla\boldsymbol{u}_b,\nabla\widehat{\boldsymbol{u}}\Big)-\Big(J_b,\widehat{\boldsymbol{u}}\times\boldsymbol{B}\Big), \quad (5.93a)$$

$$\Big(\mathrm{div}\,\widehat{\boldsymbol{u}},p\Big)=0, \quad (5.93b)$$

$$\frac{1}{2R_m}\frac{d}{dt}\|\boldsymbol{B}\|_{0,\Omega}^2+R_m^{-1}\Big(\mathbf{rot}\,\widehat{E},\boldsymbol{B}\Big)=-R_m^{-1}\Big(\mathbf{rot}\,E_b,\boldsymbol{B}\Big), \quad (5.93c)$$

$$\Big(\widehat{J},\widehat{E}\Big)-R_m^{-1}\Big(\boldsymbol{B},\mathbf{rot}\,\widehat{E}\Big)=-\Big(J_b,\widehat{E}\Big). \quad (5.93d)$$

In the above we used the identities

$$\Big(J \times \boldsymbol{B}, \widehat{\boldsymbol{u}}\Big) = -\Big(J, \widehat{\boldsymbol{u}} \times \boldsymbol{B}\Big), \quad \text{div}\, \boldsymbol{u}_b \equiv 0. \tag{5.94}$$

Adding the equations in (5.93) we arrive at (5.91). To obtain (5.92) we use

$$\Big|\Big(\frac{\partial}{\partial t}\boldsymbol{u}_b, \widehat{\boldsymbol{u}}\Big)\Big| \le \frac{d}{dt}\frac{1}{2}\big\|\boldsymbol{u}_b\big\|^2_{0,\Omega} + \frac{1}{2}\big\|\widehat{\boldsymbol{u}}\big\|^2_{0,\Omega}, \tag{5.95a}$$

$$\Big|\Big(\nabla \boldsymbol{u}_b, \nabla \widehat{\boldsymbol{u}}\Big)\Big| \le \big\|\nabla \boldsymbol{u}_b\big\|^2_{0,\Omega} + \frac{1}{4}\big\|\nabla \widehat{\boldsymbol{u}}\big\|^2_{0,\Omega}, \tag{5.95b}$$

$$\Big|\Big(\boldsymbol{f}, \widehat{\boldsymbol{u}}\Big)\Big| \le \|\boldsymbol{f}\|_{-1,\Omega}\|\nabla \widehat{\boldsymbol{u}}_h\|_{0,\Omega} \le R_e\|\boldsymbol{f}\|^2_{-1,\Omega} + \frac{1}{4R_e}\|\nabla \widehat{\boldsymbol{u}}_h\|^2_{0,\Omega} \tag{5.95c}$$

$$\Big|\Big(\mathbf{rot}\, E_b, \boldsymbol{B}\Big)\Big| \le \frac{1}{2}\big\|\mathbf{rot}\, E_b\big\|^2_{0,\Omega} + \frac{1}{2}\big\|\boldsymbol{B}\big\|^2_{0,\Omega}, \tag{5.95d}$$

$$\Big|\Big(J_b, \widehat{J}\Big)\Big| \le \frac{1}{2}\big\|J_b\big\|^2_{0,\Omega} + \frac{1}{2}\big\|\widehat{J}\big\|^2_{0,\Omega}, \tag{5.95e}$$

which combined with (5.91) yields

$$\frac{d}{dt}\left(\frac{1}{2}\big\|\widehat{\boldsymbol{u}}\big\|^2_{0,\Omega} + \frac{1}{2R_m}\big\|\boldsymbol{B}\big\|^2_{0,\Omega}\right) - \left(\frac{1}{2}\big\|\widehat{\boldsymbol{u}}\big\|^2_{0,\Omega} + \frac{1}{2R_m}\big\|\boldsymbol{B}\big\|^2_{0,\Omega}\right) + \frac{1}{2R_e}\big\|\nabla \widehat{\boldsymbol{u}}\big\|^2_{0,\Omega} + \frac{1}{2}\big\|\widehat{J}\big\|^2_{0,\Omega} \le$$

$$\le R_e\|\boldsymbol{f}\|^2_{-1,\Omega} + \frac{1}{2}\frac{d}{dt}\big\|\boldsymbol{u}_b\big\|^2_{0,\Omega} + R_e^{-1}\big\|\nabla \boldsymbol{u}_b\big\|^2_{0,\Omega} + \frac{1}{2R_m}\big\|\mathbf{rot}\, E_b\big\|^2_{0,\Omega} + \frac{1}{2}\big\|J_b\big\|^2_{0,\Omega}, \tag{5.96}$$

Multiply by e^{-t} to get

$$\frac{d}{dt}(e^{-t})\left(\frac{1}{2}\big\|\widehat{\boldsymbol{u}}\big\|^2_{0,\Omega} + \frac{1}{2R_m}\big\|\boldsymbol{B}\big\|^2_{0,\Omega}\right) + \frac{e^{-t}}{2R_e}\big\|\nabla \widehat{\boldsymbol{u}}\big\|^2_{0,\Omega} + \frac{e^{-t}}{2}\big\|\widehat{J}\big\|^2_{0,\Omega} \le$$

$$\le e^{-t}R_e\|\boldsymbol{f}\|^2_{-1,\Omega} + \frac{e^{-t}}{2}\frac{d}{dt}\big\|\boldsymbol{u}_b\big\|^2_{0,\Omega} + e^{-t}R_e^{-1}\big\|\nabla \boldsymbol{u}_b\big\|^2_{0,\Omega} + \frac{e^{-t}}{2R_m}\big\|\mathbf{rot}\, E_b\big\|^2_{0,\Omega} + \frac{e^{-t}}{2}\big\|J_b\big\|^2_{0,\Omega}, \tag{5.97}$$

integration over the time domain $[0, T]$ will yield estimate (5.92). □

To present the discrete version of the estimates presented in Theorem 5.50.1 we must decompose

$$\forall 0 \leq n \leq N-1: \quad E_h^{n+\theta} = \widehat{E}_h^{n+\theta} + \mathcal{I}^{\mathcal{V}_h}(E_b^{n+\theta}), \quad \boldsymbol{u}_h^{n+1} = \widehat{\boldsymbol{u}}_h^{n+1} + \mathcal{I}^{\mathcal{TV}_h}(\boldsymbol{u}_b^{n+1}). \quad (5.98)$$

where $(\widehat{E}_h^{n+\theta}, \widehat{\boldsymbol{u}}_h^{n+\theta}) \in \mathcal{V}_{h,0} \times \mathcal{TV}_{h,0}$ and $E_b, \boldsymbol{u}_b$ are picked such that its evaluations in $\Omega \setminus \Omega_\epsilon$ are identically zero. The condition on the boundary data is required to guarantee that the their degrees of freedom all lie along the boundary. Next, we define

$$\forall 1 \leq n \leq N: \quad \widehat{J}_h^{n+\theta} = \widehat{E}_h^{n+\theta} + \mathcal{I}^{\mathcal{V}_h}(\widehat{\boldsymbol{u}}_h^{n+\theta} \times \Pi^{RT} \boldsymbol{B}_h^{n+\theta}),$$
$$J_{h,b}^{n+\theta} = \mathcal{I}^{\mathcal{V}_h}(E_b^{n+\theta}) + \mathcal{I}^{\mathcal{V}_h}(\boldsymbol{u}_b^{n+\theta} \times \Pi^{RT} \boldsymbol{B}_h^{n+\theta}). \quad (5.99)$$

The next result is a discrete mimicry of Theorem 5.50.1.

Theorem 5.50.2 *Let* $\left\{(\boldsymbol{u}_h^n, \boldsymbol{B}_h^n)\right\}_{n=0}^N \subset \mathcal{TV}_h \times \mathcal{E}_h$ *and* $\left\{(E_h^{n+\theta}, p_h^{n+\theta}))\right\}_{n=0}^{N-1} \subset \mathcal{V}_h \times \mathcal{P}_{h,0}$ *solve the formulation* (6.3)*. Then, it holds that*

$$(\mathbf{L1}) + (\mathbf{L2}) = (\mathbf{R}), \quad (5.100)$$

where

$$(\mathbf{L1}) = \Delta t\big(\theta - 1/2\big) \left(\frac{|||\widehat{\boldsymbol{u}}_h^{n+1} - \widehat{\boldsymbol{u}}_h^n|||_{\mathcal{TV}_h}^2}{\Delta t^2} + \frac{|||\boldsymbol{B}_h^{n+1} - \boldsymbol{B}_h^n|||_{\mathcal{E}_h}^2}{\Delta t^2 R_m} \right) +$$
$$+ \left(\frac{|||\widehat{\boldsymbol{u}}_h^{n+1}|||_{\mathcal{TV}_h}^2 - |||\widehat{\boldsymbol{u}}_h^n|||_{\mathcal{TV}_h}^2}{2\Delta t} + \frac{|||\boldsymbol{B}_h^{n+1}|||_{\mathcal{E}_h}^2 - |||\boldsymbol{B}_h^n|||_{\mathcal{E}_h}^2}{2\Delta t R_m} \right), \quad (5.101)$$

$$(\mathbf{L2}) = R_e^{-1} \big|\widehat{\boldsymbol{u}}_h^{n+\theta}\big|_{\mathcal{TV}_h}^2 + |||\widehat{J}_h^{n+\theta}|||_{\mathcal{V}_h}^2 + \Big(div\, \mathcal{I}^{\mathcal{TV}_h} \boldsymbol{u}_b^{n+\theta}, p_h^{n+\theta}\Big)_{\mathcal{P}_h}, \quad (5.102)$$

$$(\mathbf{R}) = \Big(\boldsymbol{f}_h, \widehat{\boldsymbol{u}}_h^{n+\theta}\Big)_{\mathcal{TV}_h} - \Big(\frac{\mathcal{I}^{\mathcal{TV}_h}\boldsymbol{u}_b^{n+1} - \mathcal{I}^{\mathcal{TV}_h}\boldsymbol{u}_b^{n}}{\Delta t}, \widehat{\boldsymbol{u}}_h^{n+\theta}\Big)_{\mathcal{TV}_h} - R_e^{-1}\Big[\mathcal{I}^{\mathcal{TV}_h}\boldsymbol{u}_b^{n+\theta}, \widehat{\boldsymbol{u}}_h^{n+\theta}\Big]_{\mathcal{TV}_h} - \\ - \Big(J_{h,b}^{n+\theta}, \widehat{J}_h^{n+\theta}\Big)_{\mathcal{V}_h} - R_m^{-1}\Big(\mathbf{rot}\,\mathcal{I}^{\mathcal{V}_h}E_b^{n+\theta}, \boldsymbol{B}_h^{n+\theta}\Big)_{\mathcal{E}_h}. \quad (5.103)$$

In the case that $\theta \in [1/2, 1]$ then we can conclude that for any $\epsilon > 0$ we have

$$\alpha^N\Big(|||\widehat{\boldsymbol{u}}_h^N|||^2_{\mathcal{TV}_h} + R_m^{-1}|||\boldsymbol{B}_h^N|||^2_{\mathcal{E}_h}\Big) + \\ + \sum_{n=0}^{N}\gamma\alpha^n\Big(R_e^{-1}\big|\widehat{\boldsymbol{u}}_h^{n+\theta}\big|^2_{\mathcal{TV}_h} + |||\widehat{J}_h^{n+\theta}|||^2_{\mathcal{V}_h} - 2\epsilon|||p_h^{n+\theta}|||^2_{\mathcal{P}_h}\Big)\Delta t \leq \\ \leq \Big(|||\mathcal{I}^{\mathcal{TV}_h}(\boldsymbol{u}_0)|||^2_{\mathcal{TV}_h} + R_m^{-1}|||\mathcal{I}^{\mathcal{E}_h}(\boldsymbol{B}_0)|||^2_{\mathcal{E}_h}\Big) + \\ + \sum_{n=0}^{N}\gamma\alpha^n\big(R_e|||\boldsymbol{f}_h|||^2_{-1,\mathcal{TV}_h} + \Delta t^{-1}|||\mathcal{I}^{\mathcal{TV}_h}(\boldsymbol{u}_b^{n+1} - \boldsymbol{u}_b^n)|||^2_{\mathcal{TV}_h} + R_e^{-1}\big|\mathcal{I}^{\mathcal{V}_h}\boldsymbol{u}_b^{n+\theta}\big|^2_{\mathcal{TV}_h} + \\ + \frac{\eta^*}{2\epsilon}\left(\int_{\partial\Omega}\Big|\mathcal{I}^{\mathcal{TV}_h}\boldsymbol{u}_b^{n+\theta}\cdot\boldsymbol{n}\Big|\,ds\right)^2 + R_m^{-1}|||\mathbf{rot}\,\mathcal{I}^{\mathcal{V}_h}E_b^{n+\theta}|||^2_{\mathcal{E}_h} + |||J_{h,b}^{n+\theta}|||^2_{\mathcal{V}_h}\big)\Delta t, \quad (5.104)$$

where $\eta^* > 0$ is given in Theorem 5.40.1 and

$$\alpha = \frac{\theta}{1+\theta}, \quad \gamma = \frac{1}{1+\theta}. \quad (5.105)$$

In the case that walls of the domain are non-penetrating, meaning $\boldsymbol{u}_b \cdot \boldsymbol{n} \equiv 0$ along $\partial\Omega$, then we obtain our final energy stability estimate

$$\alpha^N\Big(|||\widehat{\boldsymbol{u}}_h^N|||^2_{\mathcal{TV}_h} + R_m^{-1}|||\boldsymbol{B}_h^N|||^2_{\mathcal{E}_h}\Big) + \sum_{n=0}^{N}\gamma\alpha^n\Big(R_e^{-1}\big|\widehat{\boldsymbol{u}}_h^{n+\theta}\big|^2_{\mathcal{TV}_h} + |||\widehat{J}_h^{n+\theta}|||^2_{\mathcal{V}_h}\Big) \leq \\ \leq \Big(|||\mathcal{I}^{\mathcal{TV}_h}(\boldsymbol{u}_0)|||^2_{\mathcal{TV}_h} + R_m^{-1}|||\mathcal{I}^{\mathcal{E}_h}(\boldsymbol{B}_0)|||^2_{\mathcal{E}_h}\Big) + \\ + \sum_{n=0}^{N}\gamma\alpha^n\big(R_e|||\boldsymbol{f}_h|||^2_{-1,\mathcal{TV}_h} + \Delta t^{-1}|||\mathcal{I}^{\mathcal{TV}_h}(\boldsymbol{u}_b^{n+1} - \boldsymbol{u}_b^n)|||^2_{\mathcal{TV}_h} + R_e^{-1}\big|\mathcal{I}^{\mathcal{V}_h}\boldsymbol{u}_b^{n+\theta}\big|^2_{\mathcal{TV}_h} + \\ + R_m^{-1}|||\mathbf{rot}\,\mathcal{I}^{\mathcal{V}_h}E_b^{n+\theta}|||^2_{\mathcal{E}_h} + |||J_{h,b}^{n+\theta}|||^2_{\mathcal{V}_h}\big)\Delta t. \quad (5.106)$$

Proof. Testing the formulation (6.3) against $(\boldsymbol{v}_h, \boldsymbol{C}_h, D_h, q_h) = (\widehat{\boldsymbol{u}}_h^{n+\theta}, \boldsymbol{B}_h^{n+\theta}, \widehat{E}_h^{n+\theta}, p_h^{n+\theta})$ we obtain

$$\Big(\frac{\widehat{\boldsymbol{u}}_h^{n+1}-\widehat{\boldsymbol{u}}_h^{n}}{\Delta t}, \widehat{\boldsymbol{u}}_h^{n+\theta}\Big)_{\mathcal{TV}_h} + R_e^{-1}\big|\widehat{\boldsymbol{u}}_h^{n+\theta}\big|^2_{\mathcal{TV}_h} + \Big(\widehat{J}_h^{n+\theta}, \mathcal{I}^{\mathcal{V}_h}(\widehat{\boldsymbol{u}}_h^{n+\theta}\times \boldsymbol{B}_h^{n+\theta})\Big)_{\mathcal{V}_h} -$$
$$- \Big(\operatorname{div}\widehat{\boldsymbol{u}}_h^{n+\theta}, p_h^{n+\theta}\Big)_{\mathcal{P}_h} = \Big(\boldsymbol{f}_h, \widehat{\boldsymbol{u}}_h^{n+\theta}\Big)_{\mathcal{TV}_h} - \Big(\frac{\mathcal{I}^{\mathcal{TV}_h}\boldsymbol{u}_b^{n+1}-\mathcal{I}^{\mathcal{TV}_h}\boldsymbol{u}_b^{n}}{\Delta t}, \widehat{\boldsymbol{u}}_h^{n+\theta}\Big)_{\mathcal{V}_h} -$$
$$- R_e^{-1}\Big[\mathcal{I}^{\mathcal{TV}_h}\boldsymbol{u}_b^{n+\theta}, \widehat{\boldsymbol{u}}_h^{n+\theta}\Big]_{\mathcal{TV}_h} - \Big(J_{h,b}^{n+\theta}, \mathcal{I}^{\mathcal{V}_h}(\widehat{\boldsymbol{u}}_h^{n+\theta}\times \Pi^{RT}\boldsymbol{B}_h^{n+\theta})\Big)_{\mathcal{TV}_h}, \tag{5.107a}$$

$$\Big(\operatorname{div}\widehat{\boldsymbol{u}}_h^{n+\theta}, q_h\Big)_{\mathcal{P}_h} = -\Big(\operatorname{div}\mathcal{I}^{\mathcal{TV}_h}\boldsymbol{u}_b^{n+\theta}, q_h\Big)_{\mathcal{P}_h}, \tag{5.107b}$$

$$R_m^{-1}\Big(\frac{\boldsymbol{B}_h^{n+1}-\boldsymbol{B}_h^{n}}{\Delta t}, \boldsymbol{B}_h^{n+\theta}\Big)_{\mathcal{E}_h} + R_m^{-1}\Big(\mathbf{rot}\,\widehat{E}_h^{n+\theta}, \boldsymbol{B}_h^{n+\theta}\Big)_{\mathcal{E}_h} =$$
$$- R_m^{-1}\Big(\mathbf{rot}\,\mathcal{I}^{\mathcal{V}_h}E_b^{n+\theta}, \boldsymbol{B}_h^{n+\theta}\Big)_{\mathcal{E}_h}, \tag{5.107c}$$

$$\Big(\widehat{J}_h^{n+\theta}, \widehat{E}_h^{n+\theta}\Big)_{\mathcal{V}_h} - R_m^{-1}\Big(\boldsymbol{B}_h^{n+\theta}, \mathbf{rot}\,\widehat{E}_h^{n+\theta}\Big)_{\mathcal{E}_h} = -\Big(J_{h,b}, \widehat{E}_h^{n+\theta}\Big)_{\mathcal{V}_h}. \tag{5.107d}$$

Next, note that

$$\boldsymbol{B}_h^{n+\theta} = \Delta t\big(\theta-1/2\big)\frac{\boldsymbol{B}_h^{n+1}-\boldsymbol{B}_h^{n}}{\Delta t} + \frac{\boldsymbol{B}_h^{n+1}+\boldsymbol{B}_h^{n}}{2}, \tag{5.108}$$

immediately gives that

$$\Big(\frac{\boldsymbol{B}_h^{n+1}-\boldsymbol{B}_h}{\Delta t}, \boldsymbol{B}_h^{n+\theta}\Big)_{\mathcal{E}_h} =$$
$$= \Delta t\big(\theta-1/2\big)\frac{|||\boldsymbol{B}_h^{n+1}-\boldsymbol{B}_h^{n}|||^2_{\mathcal{E}_h}}{\Delta t^2} + \frac{|||\boldsymbol{B}_h^{n+1}|||^2_{\mathcal{E}_h} - |||\boldsymbol{B}_h^{n}|||^2_{\mathcal{E}_h}}{2\Delta t}. \tag{5.109}$$

An analogous argument will yield

$$\Big(\frac{\widehat{\boldsymbol{u}}_h^{n+1}-\boldsymbol{B}_h}{\Delta t}, \widehat{\boldsymbol{u}}_h^{n+\theta}\Big)_{\mathcal{TV}_h} =$$
$$= \Delta t\big(\theta-1/2\big)\frac{|||\widehat{\boldsymbol{u}}_h^{n+1}-\widehat{\boldsymbol{u}}_h^{n}|||^2_{\mathcal{TV}_h}}{\Delta t^2} + \frac{|||\widehat{\boldsymbol{u}}_h^{n+1}|||^2_{\mathcal{TV}_h} - |||\widehat{\boldsymbol{u}}_h^{n}|||^2_{\mathcal{TV}_h}}{2\Delta t}. \tag{5.110}$$

We can use the identities (5.109) and (5.110) to transform the left hand side of (5.107a) and (5.107c) then adding the resulting equations with (5.107b) and (5.107d) will yield (5.100). To verify the estimate in (5.104) note that $\theta \in [1/2, 1]$ guarantees

$$(\mathbf{L1}) \geq \frac{|||\widehat{\boldsymbol{u}}_h^{n+1}|||^2_{\mathcal{TV}_h} - |||\widehat{\boldsymbol{u}}_h^{n}|||^2_{\mathcal{TV}_h}}{2\Delta t} + \frac{|||\boldsymbol{B}_h^{n+1}|||^2_{\mathcal{E}_h} - |||\boldsymbol{B}_h^{n}|||^2_{\mathcal{E}_h}}{2\Delta t}. \tag{5.111}$$

Next we apply the following estimates to the terms in $(\mathbf{R})$,

$$-\Big(\frac{\mathcal{I}^{\mathcal{TV}_h}\boldsymbol{u}_b^{n+1} - \mathcal{I}^{\mathcal{TV}_h}\boldsymbol{u}_b^{n}}{\Delta t}, \widehat{\boldsymbol{u}}_h^{n+\theta}\Big)_{\mathcal{TV}_h} \leq \tag{5.112a}$$

$$\leq \frac{1}{2\Delta t}|||\mathcal{I}^{\mathcal{TV}_h}(\boldsymbol{u}_b^{n+1} - \boldsymbol{u}_b^{n})|||^2_{\mathcal{TV}_h} + \frac{1}{2}|||\widehat{\boldsymbol{u}}_h^{n+\theta}|||^2_{\mathcal{TV}_h}, \tag{5.112b}$$

$$-\Big[\mathcal{I}^{\mathcal{TV}_h}\boldsymbol{u}_b^{n+\theta}, \widehat{\boldsymbol{u}}_h^{n+\theta}\Big]_{\mathcal{TV}_h} \leq \big|\mathcal{I}^{\mathcal{V}_h}\boldsymbol{u}_b^{n+\theta}\big|^2_{\mathcal{TV}_h} + \frac{1}{4}\big|\widehat{\boldsymbol{u}}_h^{n+\theta}\big|^2_{\mathcal{TV}_h}, \tag{5.112c}$$

$$\Big(\boldsymbol{f}_h, \widehat{\boldsymbol{u}}_h\Big)_{\mathcal{TV}_h} \leq R_e|||\boldsymbol{f}_h|||^2_{-1,\mathcal{TV}_h} + \frac{1}{4R_e}\big|\widehat{\boldsymbol{u}}_h\big|^2_{\mathcal{TV}_h}, \tag{5.112d}$$

$$-\Big(\operatorname{div}\mathcal{I}^{\mathcal{TV}_h}\boldsymbol{u}_b^{n+\theta}, p^{n+\theta}\Big)_{\mathcal{P}_h} \leq \frac{1}{4\epsilon}|||\operatorname{div}\mathcal{I}^{\mathcal{TV}_h}\boldsymbol{u}_b^{n+\theta}|||^2_{\mathcal{P}_h} + \epsilon|||p^{n+\theta}|||^2_{\mathcal{P}_h}, \tag{5.112e}$$

$$-\Big(\mathbf{rot}\,\mathcal{I}^{\mathcal{V}_h}E_b^{n+\theta}, \boldsymbol{B}_h^{n+\theta}\Big)_{\mathcal{E}_h} \leq \frac{1}{2}|||\mathbf{rot}\,\mathcal{I}^{\mathcal{V}_h}E_b^{n+\theta}|||^2_{\mathcal{E}_h} + \frac{1}{2}|||\boldsymbol{B}_h^{n+\theta}|||^2_{\mathcal{E}_h}, \tag{5.112f}$$

$$-\Big(J_{h,b}^{n+\theta}, \widehat{J}_h^{n+\theta}\Big)_{\mathcal{V}_h} \leq \frac{1}{2}|||J_{h,b}^{n+\theta}|||^2_{\mathcal{V}_h} + \frac{1}{2}|||\widehat{J}_h^{n+\theta}|||^2_{\mathcal{V}_h}, \tag{5.112g}$$

$$|||\boldsymbol{B}_h^{n+\theta}|||^2_{\mathcal{E}_h} \leq \theta|||\boldsymbol{B}_h^{n}|||^2_{\mathcal{E}_h} + (1-\theta)|||\boldsymbol{B}_h^{n+1}|||^2_{\mathcal{E}_h}, \tag{5.112h}$$

$$|||\widehat{\boldsymbol{u}}_h^{n+\theta}|||^2_{\mathcal{TV}_h} \leq \theta|||\widehat{\boldsymbol{u}}_h^{n}|||^2_{\mathcal{TV}_h} + (1-\theta)|||\widehat{\boldsymbol{u}}_h^{n+1}|||^2_{\mathcal{TV}_h}. \tag{5.112i}$$

To estimate $(\mathbf{L2})$ use

$$-\Big(\operatorname{div}\boldsymbol{u}_b^{n+\theta}, p_h^{n+\theta}\Big)_{\mathcal{P}_h} \leq \frac{1}{4\epsilon}|||\operatorname{div}\mathcal{I}^{\mathcal{TV}_h}\boldsymbol{u}_b^{n+\theta}|||^2_{\mathcal{P}_h} + \epsilon|||p_h^{n+\theta}|||^2_{\mathcal{P}_h}. \tag{5.113}$$

And, finally

$$\begin{aligned}
\left|\left|\left|\operatorname{div}\mathcal{I}^{\mathcal{TV}_h}\boldsymbol{u}_b^{n+\theta}\right|\right|\right|_{\mathcal{P}_h} &= \sum_{\mathsf{P}\in\partial\Omega_h} |||\operatorname{div}\mathcal{I}^{\mathcal{TV}_h}\boldsymbol{u}_b^{n+\theta}|||_{\mathcal{TV}_h(\mathsf{P})} \\
&\leq \sqrt{\eta^*}\sum_{\mathsf{P}\in\partial\Omega_h}\left|\operatorname{div}\mathcal{I}^{\mathcal{TV}_h}\boldsymbol{u}_b^{n+\theta}\right||\mathsf{P}| \\
&\leq \sqrt{\eta^*}\sum_{\mathsf{P}\in\partial\Omega_h}\left|\int_{\mathsf{P}\cap\partial\Omega}\mathcal{I}^{\mathcal{TV}_h}\boldsymbol{u}_b^{n+\theta}\cdot\boldsymbol{n}ds\right| \\
&\leq \sqrt{\eta^*}\sum_{\mathsf{P}\in\partial\Omega_h}\int_{\mathsf{P}\cap\partial\Omega}\left|\mathcal{I}^{\mathcal{TV}_h}\boldsymbol{u}_b^{n+\theta}\cdot\boldsymbol{n}\right|ds \\
&\leq \sqrt{\eta^*}\int_{\partial\Omega}\left|\mathcal{I}^{\mathcal{TV}_h}\boldsymbol{u}_b^{n+\theta}\cdot\boldsymbol{n}\right|ds
\end{aligned} \tag{5.114}$$

Where $\partial\Omega_h$ is defined as the set of elements that have an edge intersecting $\partial\Omega$ and the constant η^* is given by Theorem 5.40.1.

The result of applying estimates (5.111)-(5.114) is

$$\alpha\mathcal{A}^{n+1}(\widehat{\boldsymbol{u}}_h,\boldsymbol{B}_h)-\mathcal{A}^n(\widehat{\boldsymbol{u}}_h,\boldsymbol{B}_h)=\gamma\mathcal{F}^{n+\theta}(\widehat{\boldsymbol{u}}_h,\widehat{J}_h,p_h,\boldsymbol{u}_b,J_{h,b})\Delta t, \tag{5.115}$$

where

$$\alpha=\frac{\theta}{1+\theta},\quad \gamma=\frac{1}{1+\theta},\quad \mathcal{A}^n(\widehat{\boldsymbol{u}}_h,\boldsymbol{B}_h)=|||\widehat{\boldsymbol{u}}_h^n|||^2_{\mathcal{TV}_h}+R_m^{-1}|||\boldsymbol{B}_h^n|||^2_{\mathcal{E}_h} \tag{5.116}$$

and

$$\begin{aligned}
&\mathcal{F}^{n+\theta}(\widehat{\boldsymbol{u}}_h,\widehat{J}_h,p_h,\boldsymbol{u}_b,J_{h,b})= \\
&=R_e|||\boldsymbol{f}_h|||^2_{-1,\mathcal{TV}_h}+\frac{1}{\Delta t}|||\mathcal{I}^{\mathcal{TV}_h}(\boldsymbol{u}_b^{n+1}-\boldsymbol{u}_b^n)|||^2_{\mathcal{TV}_h}+\frac{1}{R_e}\left|\mathcal{I}^{\mathcal{V}_h}\boldsymbol{u}_b^{n+\theta}\right|^2_{\mathcal{TV}_h}+ \\
&\frac{\eta^*}{2\epsilon}\left(\int_{\partial\Omega}\left|\mathcal{I}^{\mathcal{TV}_h}\boldsymbol{u}_b^{n+\theta}\cdot\boldsymbol{n}\right|ds\right)^2+\frac{1}{R_m}|||\mathbf{rot}\,\mathcal{I}^{\mathcal{V}_h}E_b^{n+\theta}|||^2_{\mathcal{E}_h}+|||J_{h,b}^{n+\theta}|||^2_{\mathcal{V}_h}- \\
&-\frac{1}{2R_e}\left|\widehat{\boldsymbol{u}}_h^{n+\theta}\right|^2_{\mathcal{TV}_h}-|||\widehat{J}_h^{n+\theta}|||^2_{\mathcal{V}_h}+2\epsilon|||p_h^{n+\theta}|||^2_{\mathcal{P}_h}.
\end{aligned} \tag{5.117}$$

When multiplying the inequalities (5.115) for $0 \leq n \leq N$ by an appropriate power of $\alpha$and adding them together yields a telescoping sum, we illustrate this by writing the first 4 terms:

$$\begin{aligned}
&\text{for } n=0: && \alpha\mathcal{A}^1(\widehat{\boldsymbol{u}}_h, \boldsymbol{B}_h) && -\mathcal{A}^0(\widehat{\boldsymbol{u}}_h, \boldsymbol{B}_h) && \leq \gamma\mathcal{F}^{\theta}(\widehat{\boldsymbol{u}}_h, \widehat{J}_h, p_h, \boldsymbol{u}_b, J_{h,b})\Delta t,\\
&\text{for } n=1: && \alpha^2\mathcal{A}^2(\widehat{\boldsymbol{u}}_h, \boldsymbol{B}_h) && -\alpha\mathcal{A}^1(\widehat{\boldsymbol{u}}_h, \boldsymbol{B}_h) && \leq \gamma\alpha\mathcal{F}^{1+\theta}(\widehat{\boldsymbol{u}}_h, \widehat{J}_h, p_h, \boldsymbol{u}_b, J_{h,b})\Delta t,\\
&\text{for } n=2: && \alpha^3\mathcal{A}^3(\widehat{\boldsymbol{u}}_h, \boldsymbol{B}_h) && -\alpha^2\mathcal{A}^2(\widehat{\boldsymbol{u}}_h, \boldsymbol{B}_h) && \leq \gamma\alpha^2\mathcal{F}^{2+\theta}(\widehat{\boldsymbol{u}}_h, \widehat{J}_h, p_h, \boldsymbol{u}_b, J_{h,b})\Delta t,\\
&\text{for } n=3: && \alpha^4\mathcal{A}^4(\widehat{\boldsymbol{u}}_h, \boldsymbol{B}_h) && -\alpha^3\mathcal{A}^3(\widehat{\boldsymbol{u}}_h, \boldsymbol{B}_h) && \leq \gamma\alpha^3\mathcal{F}^{3+\theta}(\widehat{\boldsymbol{u}}_h, \widehat{J}_h, p_h, \boldsymbol{u}_b, J_{h,b})\Delta t,\\
&\quad \cdots && \quad \cdots
\end{aligned}$$

The result of this sum is (5.104). Finally, if we assume that $\boldsymbol{u}_b \cdot \boldsymbol{n} = 0$ along $\partial\Omega_h$ then since the quadrature is exact for constants

$$\int_{\partial\Omega} |\mathcal{I}^{\mathcal{V}_h}\boldsymbol{u}_b^{n+\theta} \cdot \boldsymbol{n}| ds = \int_{\partial\Omega} |\boldsymbol{u}_b^{n+\theta} \cdot \boldsymbol{n}| ds = 0, \tag{5.118}$$

This allows us to take $\epsilon \to 0$ in (5.104) to attain the final stability estimate (5.106). □

5.6 Linearization and the Condition on the Divergence of $\boldsymbol{B}_h$

This section takes inspiration from [31]. In this section we will mainly be concerned with the development of a solver for (6.3) at a single point in time. For this reason the values of $\theta > 0$ and n will remain fixed and thus we will omit them from the notation that we will introduce.

In practice, we will find arrays of degrees of freedom, to express this we will add a superscript I. This to say that, for example, $\boldsymbol{u}_h^I$ will refer to the array of degrees of freedom of $\boldsymbol{u}_h$.

To begin let us introduce the space

$$\mathcal{X}_{h,0} = \left\{(\boldsymbol{v}_h^I, \boldsymbol{C}_h^I, D_h^I, q_h^I) : (\boldsymbol{v}_h, \boldsymbol{C}_h, D_h, q_h) \in \mathcal{TV}_{h,0} \times \mathcal{E}_h \times \mathcal{V}_{h,0} \times \mathcal{P}_{h,0}\right\}. \tag{5.119}$$

We will equip this space with the ℓ_2 inner product. We do this mainly to conform to much of the literature on linear and nonlinear methods. We seek to pose the formulation (6.3) in the space $\mathcal{X}_h$. First we substitute (5.36c) with the equivalent expression

$$\theta R_m^{-1}\big(\frac{\boldsymbol{B}_h - \boldsymbol{B}_h^n}{\Delta t}, \boldsymbol{C}_h\big)_{\mathcal{E}_h} + \theta R_m^{-1}\big(\mathbf{rot}\, E_h, \boldsymbol{C}_h\big)_{\mathcal{E}_h} = 0 \tag{5.120}$$

and add it to (5.36a), (5.36b) and (5.36d). We define G in such a way that $G(\boldsymbol{x}_h)\cdot \boldsymbol{y}_h$ as the left hand side of the resulting expression. In doing this we are implying that $\boldsymbol{x}_h, \boldsymbol{y}_h \in \mathcal{X}_{h,0}$ with

$$\boldsymbol{x}_h = (\widehat{\boldsymbol{u}}_h^{n+1,I}, \boldsymbol{B}_h^{n+1,I}, \widehat{E}_h^{n+\theta,I}, p_h^{n+\theta,I}), \quad \boldsymbol{y}_h = (\boldsymbol{v}_h^I, \boldsymbol{C}_h^I, D_h^I, q_h^I). \tag{5.121}$$

Thus, solving the variational formulation (6.3) is equivalent to solving

Find $\boldsymbol{x}_h \in \mathcal{X}_h$ such that

$$G(\boldsymbol{x}_h) = \mathbf{0}. \tag{5.122}$$

Indeed, testing (5.122) against $\boldsymbol{y}_h = (\boldsymbol{v}_h, \mathbf{0}, 0, 0)$ we retrieve (5.36a), the three remaining equations can be attained similarly. This is the set up to apply a Jacobian-free Newton–Krylov method. This method is highly parallelizable and has optimal speed of convergence.

The Newton method will have us, at every iteration, update the estimate for the zeroes of G in accordance to

$$\boldsymbol{x}_h^0 = (\widehat{\boldsymbol{u}}_h^{n,I}, \boldsymbol{B}_h^{n,I}, \widehat{E}_h^{n-1+\theta,I}, p_h^{n-1+\theta,I}), \quad \boldsymbol{x}_h^{m+1} = \boldsymbol{x}_h^m + \delta\boldsymbol{x}_h^m, \quad \partial G(\boldsymbol{x}_h^m)\delta\boldsymbol{x}_h^m = -G(\boldsymbol{x}_h^m), \tag{5.123}$$

where $\partial G : \mathcal{X}_{h,0} \to \mathcal{L}(\mathcal{X}_{h,0})$ is the Jacobian of G, the space $\mathcal{L}(\mathcal{X}_{h,0})$ is the collection of linear operators from $\mathcal{X}_{h,0}$ to $\mathcal{X}'_{h,0}$. The reason we had to substitute (5.36c) with (5.120) is to attain some symmetry in the Jacobian matrix, this will be clear from the well-posedness analysis. This method, as described, will require that we compute and store the Jacobian matrix. This takes a good deal of memory and computational power. Instead, we will approximate the action of the

Jacobian matrix onto vectors using the finite difference approximation

$$DG(\boldsymbol{x}_h)\delta\boldsymbol{x}_h = \frac{G(\boldsymbol{x}_h + \epsilon\delta\boldsymbol{x}_h) - G(\boldsymbol{x}_h)}{\epsilon}, \quad \epsilon = 10^{-7}. \tag{5.124}$$

The value of ϵ is selected as a "sweet-spot" value for epsilon that makes for stable float point arithmetic and approximation accuracy. suggested in page 80 of [61]. The algorithm we propose by provides updates in accordance to

$$\forall 0 \leq m \leq M-1: \quad \boldsymbol{x}_h^{m+1} = \boldsymbol{x}_h^m + \delta\boldsymbol{x}_h^m, \quad DG(\boldsymbol{x}_h^m)\delta\boldsymbol{x}^m = -G(\boldsymbol{x}_h^m), \tag{5.125a}$$

$$\boldsymbol{x}_h^0 = \begin{cases} \left(\widehat{\boldsymbol{u}}_h^{n,I}, \boldsymbol{B}_h^{n,I}, \widehat{E}_h^{n-1+\theta,I}, p_h^{n-1+\theta,I}\right), & n > 0, \\ \left(\widehat{\boldsymbol{u}}_h^{0,I}, \boldsymbol{B}_h^{0,I}, 0, 0\right), & n = 0. \end{cases} \tag{5.125b}$$

We define $(\widehat{\boldsymbol{u}}_h^{n+1}, \boldsymbol{B}_h^{n+1}, \widehat{E}_h^{n+\theta}, p_h^{n+\theta})$ such that its array degrees of freedom is $\boldsymbol{x}_h^M$ whereas intermediate steps will be denoted as

$$\boldsymbol{x}_h^k = \left(\widehat{\boldsymbol{u}}_h^{n+1,k,I}, \boldsymbol{B}_h^{n+1,k,I}, \widehat{E}_h^{n+\theta,k,I}, p_h^{n+\theta,k,I}\right). \tag{5.126}$$

The routine we use to solve the linear system in (5.125) is the GMRES algorithm. This Krylov method will require a tolerance input which will be fixed to satisfy

$$\|DG(\boldsymbol{x}_h^m)\delta\boldsymbol{x}^m + G(\boldsymbol{x}_h^m)\|_2 \leq \eta_m \|G(\boldsymbol{x}_h^m)\|_2, \tag{5.127a}$$

$$\eta_m = \min\left\{\eta_{\max}, \max\left(\eta_m^B, \gamma\frac{\epsilon_t}{\|G(\boldsymbol{x}_h^m)\|_2}\right)\right\}, \tag{5.127b}$$

$$\eta_m^B = \min\left\{\eta_{\max}, \max\left(\eta_m^A, \gamma\eta_{m-1}^\alpha\right)\right\}, \quad \eta_m^A = \gamma\left(\frac{\|G(\boldsymbol{x}_h^m)\|_2}{\|G(\boldsymbol{x}_h^{m-1})\|_2}\right)^\alpha. \tag{5.127c}$$

with $\alpha = 1.5, \gamma = 0.9, \eta_{\max} = 0.8$. The value of ϵ_t is fixed to guarantee non-linear convergence

has been achieved.

$$\|G(\boldsymbol{x}_h^m)\|_2 < \epsilon_a + \epsilon_r \|G(\boldsymbol{x}_h^0)\|_2 = \epsilon_t, \quad \epsilon_a = \sqrt{\#dof} \times 10^{-15,}, \epsilon_r = 10^{-4}. \tag{5.128}$$

The particular choices for the constants are the same as in [31]. However, this strategy is much more general [54]. The guiding philosophy being a desire to guarantee super-linear convergence while simultaneously not over-solving with unnecessary GMRES iterations.

The non-linear nature of the inexact Newton steps may shed doubt as to whether or not this solver preserves the divergence free nature of the magnetic field. The following result arises from an understanding of how Faraday's Law is used to predict the magnetic field. The reality is that since this Law is linear then our finite difference approximation to its Jacobian will, in fact, be exact.

Theorem 5.60.1 *Suppose that $\delta \boldsymbol{x}_h$ solves*

$$DG(\boldsymbol{x}_h)\delta \boldsymbol{x}_h = -G(\boldsymbol{x}_h), \tag{5.129}$$

then

$$div\, \delta \boldsymbol{B}_h = div\, (\boldsymbol{B}_h^n - \boldsymbol{B}_h). \tag{5.130}$$

Proof. Testing (5.129) against $\boldsymbol{y}_h = (0, \boldsymbol{C}_h^I, 0, 0)$ yields

$$\Delta t^{-1} \Big(\delta \boldsymbol{B}_h, \boldsymbol{C}_h \Big)_{\mathcal{E}_h} + \Big(\mathbf{rot}\, \delta \widehat{E}_h, \boldsymbol{C}_h \Big)_{\mathcal{E}_h} = -\Big(\frac{\boldsymbol{B}_h - \boldsymbol{B}_h^n}{\Delta t}, \boldsymbol{C}_h \Big)_{\mathcal{E}_h} - \Big(\mathbf{rot}\, \widehat{E}_h, \boldsymbol{C}_h \Big)_{\mathcal{E}_h} \tag{5.131}$$

since $\boldsymbol{C}_h$ can be selected arbitrarily the above is equivalent to

$$\Delta t^{-1} \left[\delta \boldsymbol{B}_h + \boldsymbol{B}_h - \boldsymbol{B}_h^n \right] = -\mathbf{rot} \, \left(\delta \widehat{E}_h + \widehat{E}_h \right). \tag{5.132}$$

Taking divergence on both sides yields (5.130). □

Corollary 5.60.1 *If the initial conditions on the magnetic field* $\boldsymbol{B}_0$ *satisfy that div* $\boldsymbol{B}_0 = 0$ *then updates defined by* (5.125) *will satisfy that*

$$\forall 0 \leq n \leq N, 0 \leq m \leq M : \quad div\, \delta \boldsymbol{B}_h^{n,m} = 0. \tag{5.133}$$

Implying that

$$\forall 0 \leq n \leq N : \quad div\, \boldsymbol{B}_h^{n} = 0. \tag{5.134}$$

Proof. The divergence of the initial estimate can be computed using the commuting property of the diagram in Theorem 3.70.1. Indeed:

$$\text{div}\, \boldsymbol{B}_h^0 = \text{div}\, \mathcal{I}^{\mathcal{E}_h}(\boldsymbol{B}_0) = \mathcal{I}^{\mathcal{P}_h}(\text{div}\, \boldsymbol{B}_0) = 0 \tag{5.135}$$

Next, suppose that div $_h \boldsymbol{B}_h^n = 0$ then by definition div $\boldsymbol{B}_h^{n+1,0} = 0$. For the inductive step we can further assume that div $\boldsymbol{B}_h^{n+1,m} = 0$ thus from Theorem 5.60.1 we have that

$$\text{div}\, \boldsymbol{B}_h^{n+1,m+1} = \text{div}\, \boldsymbol{B}_h^{n+1,m} + \text{div}\, \delta \boldsymbol{B}_h^{n+1,m} = \text{div}\, (2\boldsymbol{B}_h^{n+1,m} - \boldsymbol{B}_h^{n}) = 0. \tag{5.136}$$

□

5.61 The Jacobian Matrix

In this subsection we will compute the action of the Jacobian at the point $\boldsymbol{x}_h$ on a vector $\delta \boldsymbol{x}_h$. We are referring to the quantities

$$\partial G(\boldsymbol{x}_h) \delta \boldsymbol{x}_h. \tag{5.137}$$

Then, we will use the expression attained to come up with a matrix representation for the Jacobian. To do this, first we must select a direction $\boldsymbol{y}_h \in \mathcal{X}_{h,0}$. Then by definition we have that

$$[\partial G(\boldsymbol{x}_h)\delta\boldsymbol{x}_h]\cdot\boldsymbol{y}_h = \lim_{\epsilon\to 0}\frac{G(\boldsymbol{x}_h+\epsilon\delta\boldsymbol{x}_h)\cdot\boldsymbol{y}_h - G(\boldsymbol{x}_h)\cdot\boldsymbol{y}_h}{\epsilon}. \tag{5.138}$$

The limit above yields

$$[\partial G(\boldsymbol{x}_h)\delta\boldsymbol{x}_h]\cdot\boldsymbol{y}_h = \ell_1(\boldsymbol{y}_h)+\ell_2(\boldsymbol{y}_h)+\ell_3(\boldsymbol{y}_h)+\ell_4(\boldsymbol{y}_h), \tag{5.139a}$$

$$\boldsymbol{x}_h = (\widehat{\boldsymbol{u}}_h^I, \boldsymbol{B}_h^I, \widehat{E}_h^I, p_h^I), \quad \delta\boldsymbol{x}_h = (\delta\widehat{\boldsymbol{u}}_h^I, \delta\boldsymbol{B}_h^I, \delta\widehat{E}_h^I, \delta p_h^I), \quad \boldsymbol{y}_h = (\boldsymbol{v}_h^I, \boldsymbol{C}_h^I, D_h^I, q_h^I), \tag{5.139b}$$

$$\begin{aligned}\ell_1(\boldsymbol{y}_h) = {}& \Delta t^{-1}\Big(\delta\widehat{\boldsymbol{u}}_h, \boldsymbol{v}_h\Big)_{\mathcal{TV}_h} + \theta R_e^{-1}\Big[\delta\widehat{\boldsymbol{u}}_h, \boldsymbol{v}_h\Big]_{\mathcal{TV}_h} + \\ & + \theta\Big(\widehat{E}_h, \mathcal{I}^{\mathcal{V}_h}(\boldsymbol{v}_h\times\Pi^{RT}\delta\boldsymbol{B}_h)\Big)_{\mathcal{V}_h} + \theta\Big(\delta\widehat{E}_h, \mathcal{I}^{\mathcal{V}_h}(\boldsymbol{v}_h\times\Pi^{RT}\boldsymbol{B}_h)\Big)_{\mathcal{V}_h} - \\ & - \Big(\operatorname{div}\boldsymbol{v}_h, p_h\Big)_{\mathcal{P}_h},\end{aligned} \tag{5.139c}$$

$$\ell_2(\boldsymbol{y}_h) = \theta\Big(\operatorname{div}\delta\widehat{\boldsymbol{u}}_h, q_h\Big)_{\mathcal{P}_h}, \quad \ell_3(\boldsymbol{y}_h) = \Delta t^{-1}\Big(\delta\boldsymbol{B}_h, \boldsymbol{C}_h\Big)_{\mathcal{E}_h} + \Big(\mathbf{rot}\,\delta E_h, \boldsymbol{C}_h\Big)_{\mathcal{E}_h}, \tag{5.139d}$$

$$\begin{aligned}\ell_4(\boldsymbol{y}_h) = {}& \Big(\delta\widehat{E}_h + \theta\mathcal{I}^{\mathcal{V}_h}(\widehat{\boldsymbol{u}}_h\times\Pi^{RT}\delta\boldsymbol{B}_h + \delta\widehat{\boldsymbol{u}}_h\times\Pi^{RT}\boldsymbol{B}_h), \boldsymbol{D}_h\Big)_{\mathcal{V}_h} + \\ & + R_m^{-1}\theta\big(\delta\boldsymbol{B}_h, \mathbf{rot}_h D_h\big)_{\mathcal{E}_h}.\end{aligned} \tag{5.139e}$$

Therefore, the matrix representation of the Jacobian is given by

$$\partial G(\boldsymbol{x}_h)\delta\boldsymbol{x}_h = \left[\begin{pmatrix}\mathbb{A} & 0 & \mathbb{B} & \mathbb{C}\\ 0 & \mathbb{D} & \mathbb{E} & 0\\ \mathbb{B}^T & \mathbb{E}^T & \mathbb{F} & 0\\ \mathbb{C}^T & 0 & 0 & 0\end{pmatrix} + \begin{pmatrix}0 & \mathbb{G}+\mathbb{I} & 0 & 0\\ 0 & 0 & 0 & 0\\ 0 & \mathbb{H} & 0 & 0\\ 0 & 0 & 0 & 0\end{pmatrix}\right]\begin{pmatrix}\delta\widehat{\boldsymbol{u}}_h^I\\ \delta\boldsymbol{B}_h^I\\ \delta\widehat{E}_h^I\\ \delta p_h^I\end{pmatrix} \tag{5.140}$$

The matrices above are given by

$$\mathbb{A} = \Delta t^{-1}\mathbb{M}_{\mathcal{TV}_h} + \theta R_e^{-1}\mathbb{S}_{\mathcal{TV}_h} + \theta^3\mathbb{M}_{\boldsymbol{B}}^T\mathbb{M}_{\mathcal{V}_h}\mathbb{M}_{\boldsymbol{B}}, \quad \mathbb{B} = \theta\mathbb{M}_{\boldsymbol{B}}^T\mathbb{M}_{\mathcal{V}_h}, \tag{5.141a}$$

$$\mathbb{C} = \operatorname{div}_h^T\mathbb{M}_{\mathcal{P}_h}, \mathbb{D} = \theta R_m^{-1}\Delta t^{-1}\mathbb{M}_{\mathcal{E}_h}, \quad \mathbb{E} = \theta R_m^{-1}\mathbb{M}_{\mathcal{E}_h}\mathbf{rot}_h, \quad \mathbb{F} = \mathbb{M}_{\mathcal{V}_h}, \tag{5.141b}$$

$$\mathbb{H} = \theta\mathbb{M}_{\mathcal{V}_h}\mathbb{M}_{\boldsymbol{u}}, \quad \mathbb{I} = \theta^3\mathbb{M}_{\boldsymbol{B}}^T\mathbb{M}_{\mathcal{V}_h}\mathbb{M}_{\boldsymbol{u}} \tag{5.141c}$$

where

$$\boldsymbol{v}_h^I \cdot \mathbb{M}_{\mathcal{TV}_h}\boldsymbol{u}_h^I = \Big(\boldsymbol{u}_h, \boldsymbol{v}_h\Big)_{\mathcal{TV}_h}, \quad \boldsymbol{v}_h^I \cdot \mathbb{S}_{\mathcal{TV}_h}\boldsymbol{u}_h^I = \Big[\boldsymbol{v}_h, \boldsymbol{u}_h\Big]_{\mathcal{TV}_h}, \tag{5.142a}$$

$$q_h^I \cdot \mathbb{M}_{\mathcal{P}_h}p_h^I = \Big(q_h, p_h\Big)_{\mathcal{P}_h}, \quad \boldsymbol{C}_h^I \cdot \mathbb{M}_{\mathcal{E}_h}\boldsymbol{B}_h^I = \Big(\boldsymbol{C}_h, \boldsymbol{B}_h\Big)_{\mathcal{E}_h}, \tag{5.142b}$$

$$D_h^I \cdot \mathbb{M}_{\mathcal{V}_h}E_h^I = \Big(D_h, E_h\Big)_{\mathcal{V}_h}, \quad \mathbf{rot}_h E_h^I = [\mathbf{rot}\, E_h]^I, \quad \operatorname{div}_h \boldsymbol{u}_h^I = [\operatorname{div}_h \boldsymbol{u}_h]^I, \tag{5.142c}$$

$$\mathbb{M}_{\boldsymbol{u}}\boldsymbol{B}_h^I = [\mathcal{I}^{\mathcal{TV}_h}(\widehat{\boldsymbol{u}}_h \times \Pi^{RT}\boldsymbol{B}_h)]^I, \mathbb{M}_{\boldsymbol{B}}\boldsymbol{u}_h^I = [\mathcal{I}^{\mathcal{TV}_h}(\widehat{\boldsymbol{u}}_h \times \Pi^{RT}\boldsymbol{B}_h)]^I. \tag{5.142d}$$

The matrix $\mathbb{G}$ can be computed by selecting a basis consistent with the degrees of freedom for $\mathcal{TV}_{h,0}$ and another one for $\mathcal{E}_h$, say $\{\boldsymbol{v}_h^j\}$ and $\{\boldsymbol{C}_h^i\}$ respectively then

$$\mathbb{G}_{i,j} = \theta\Big(\widehat{E}_h, \mathcal{I}^{\mathcal{V}_h}(\boldsymbol{v}_h^i \times \Pi^{RT}\boldsymbol{C}_h^j)\Big)_{\mathcal{V}_h} + \theta^3\Big(\mathcal{I}^{\mathcal{V}_h}(\widehat{\boldsymbol{u}}_h \times \Pi^{RT}\boldsymbol{B}_h), \mathcal{I}^{\mathcal{V}_h}(\boldsymbol{v}_h^i \times \Pi^{RT}\boldsymbol{C}_h^j)\Big)_{\mathcal{V}_h}. \tag{5.143}$$

5.7 Well-posedness and Stability of the Linear Solve

The linearization strategy laid out in Section 5.6 can be summarized as follows. We are given a set of initial conditions. Then, at each time step we perform a series of Newton Iterations. Each of these consists of solving a linear system that looks like: *Find* $\delta\boldsymbol{x}_h \in \mathcal{X}_{h,0}$ *such that given* $\boldsymbol{x}_h \in \mathcal{X}_{h,0}$ *we have that*

$$\partial G(\boldsymbol{x}_h)\delta\boldsymbol{x}_h = -G(\boldsymbol{x}_h). \tag{5.144}$$

In this section we will study the well-posedness of each of these linear systems. We will show that this linear problem is a saddle-point problem. Then, we will show that this problem satisfies the hypothesis of Theorem 2.20.2.

Let us define the space:

$$\mathfrak{X}_h = \mathcal{TV}_{h,0} \times \mathcal{E}_h \times \mathcal{V}_{h,0} \tag{5.145}$$

And, $a_h : \mathfrak{X}_h \times \mathfrak{X}_h \to \mathbb{R}$ whose evaluation at $\delta\boldsymbol{\xi}_h = (\delta\widehat{\boldsymbol{u}}_h, \delta\boldsymbol{B}_h, \delta\widehat{E}_h)$, $\boldsymbol{\eta}_h = (\boldsymbol{v}_h, \boldsymbol{C}_h, D_h)$ is given by $a_h(\delta\boldsymbol{\xi}_h, \boldsymbol{\eta}_h) = \ell_1(\boldsymbol{v}_h) + \ell_2(\boldsymbol{C}_h) + \ell_3(D_h)$ as they are defined in equations (5.139). Here, and for the remainder of the section, we have fixed the value of $\boldsymbol{x}_h = (\widehat{\boldsymbol{u}}_h, \boldsymbol{B}_h, \widehat{E}_h)$. We can present problem (5.144) as:

Find $(\delta\boldsymbol{\xi}_h, \delta p_h) \in \mathfrak{X}_h \times \mathcal{P}_{h,0}$ *such that for all* $(\boldsymbol{\eta}_h, q_h) \in \mathfrak{X}_h \times \mathcal{P}_{h,0}$ *it holds that*

$$a_h(\delta\boldsymbol{\xi}_h, \boldsymbol{\eta}_h) - b_h(\boldsymbol{v}_h, \delta p_h) = f(\boldsymbol{\eta}_h), \tag{5.146a}$$

$$b_h(\delta\widehat{\boldsymbol{u}}_h, q_h) = g(q_h). \tag{5.146b}$$

Where $f \in \mathfrak{X}_h'$ and $g \in \mathcal{P}_{h,0}'$ are some appropriate bounded linear functionals and

$$b_h(\boldsymbol{v}_h, q_h) = \Big(\operatorname{div} \boldsymbol{v}_h, q_h\Big)_{\mathcal{P}_h} \tag{5.147}$$

We will follow a similar strategy to the one presented in Section 3.10. First, we introduce problem an auxiliary problem. Then we will show that such a problem and (5.146) are equivalent. We conclude our proof by showing that the auxiliary problem is well posed.

The auxiliary problem is given by

Find $(\delta\boldsymbol{\xi}_h, \delta p_h) \in \mathfrak{X}_h \times \mathcal{P}_{h,0}$ *such that for all* $(\boldsymbol{\eta}_h, q_h) \in \mathfrak{X}_h \times \mathcal{P}_{h,0}$ *it holds that*

$$a_{h,0}(\delta\boldsymbol{\xi}_h, \boldsymbol{\eta}_h) - b_h(\boldsymbol{v}_h, \delta p_h) = f_h(\boldsymbol{\eta}_h), \tag{5.148a}$$

$$b_h(\delta\widehat{\boldsymbol{u}}_h, q_h) = g_h(q_h). \tag{5.148b}$$

The difference lies in that

$$a_{h,0}(\delta\boldsymbol{\xi}_h, \boldsymbol{\eta}_h) = a_h(\delta\boldsymbol{\xi}_h, \boldsymbol{\eta}_h) + \theta R_m^{-1}\Big(\operatorname{div}\delta\boldsymbol{B}_h, \operatorname{div}\boldsymbol{C}_h\Big)_{\mathcal{P}_h}. \tag{5.149}$$

To establish the equivalency between (5.146) and (5.148) first we must present the following theorem:

Theorem 5.70.1 *Let* $\delta\boldsymbol{\xi}_h = (\delta\widehat{\boldsymbol{u}}_h, \delta\boldsymbol{B}_h, \delta\widehat{E}_h) \in \mathfrak{X}_h$ *and* $p_h \in \mathcal{P}_{h,0}$ *solve* (5.148) *should the initial conditions on the magnetic field be divergence free then div* $\delta\boldsymbol{B}_h = 0$.

Proof. Testing (5.148) against $q_h = 0$, and $\eta = (\mathbf{0}, \boldsymbol{C}_h, 0)$ yields

$$\Delta t^{-1}\Big(\delta\boldsymbol{B}_h + \mathbf{rot}\,\delta E_h, \boldsymbol{C}_h\Big)_{\mathcal{E}_h} + \Big(\operatorname{div}\delta\boldsymbol{B}_h, \operatorname{div}\boldsymbol{C}_h\Big)_{\mathcal{P}_h} = -\Big(\frac{\boldsymbol{B}_h - \boldsymbol{B}_h^n}{\Delta t} + \mathbf{rot}\,E_h, \boldsymbol{C}_h\Big)_{\mathcal{E}_h} \tag{5.150}$$

or equivalently

$$\Delta t^{-1}\Big(\delta\boldsymbol{B}_h + \mathbf{rot}\,\delta E_h + \frac{\boldsymbol{B}_h^{n,m} - \boldsymbol{B}_h^n}{\Delta t} + \mathbf{rot}\,E_h, \boldsymbol{C}_h\Big)_{\mathcal{E}_h} = -\Big(\operatorname{div}\delta\boldsymbol{B}_h, \operatorname{div}\boldsymbol{C}_h\Big)_{\mathcal{E}_h}. \tag{5.151}$$

Therefore, making

$$\boldsymbol{C}_h = \delta\boldsymbol{B}_h + \mathbf{rot}\,\delta E_h + \frac{\boldsymbol{B}_h^{n,m} - \boldsymbol{B}_h^n}{\Delta t} + \mathbf{rot}\,E_h. \tag{5.152}$$

Note that if $\operatorname{div}\boldsymbol{B}_h^n = \operatorname{div}\boldsymbol{B}_h^{n,m} = 0$ then

$$\Delta t^{-1}|||\boldsymbol{C}_h|||_{\mathcal{E}_h}^2 = -|||\operatorname{div}\delta\boldsymbol{B}_h|||_{\mathcal{P}_h}^2 \tag{5.153}$$

As a consequence the only solution is that $\operatorname{div}\delta\boldsymbol{B}_h = 0$. □

The result of the above theorem can be leveraged to show that both problems (5.146) and (5.148) are in fact equivalent. We present this result in the following lemma:

Lemma 5.70.1 *The problems* (5.146) *and* (5.148) *are equivalent.*

Proof. If $\delta\boldsymbol{\xi}_h = (\boldsymbol{u}_h, \boldsymbol{B}_h, \widehat{E}_h)$ and $\delta p_h \in \mathcal{P}_{h,0}$ solve the linear system (5.146). Then, by Corollary 5.60.1 we know that div $\delta\boldsymbol{B}_h = 0$ and therefore

$$\forall \boldsymbol{\eta}_h \in \mathfrak{X}_{h,0} : \quad a_{h,0}(\delta\boldsymbol{\xi}_h, \boldsymbol{\eta}_h) = a_h(\delta\boldsymbol{\xi}_h, \boldsymbol{\eta}_h). \tag{5.154}$$

Implying that $\delta\boldsymbol{\xi}_h$ and δp_h solve (5.148).

Similarly, if $\delta\boldsymbol{\xi}_h = (\boldsymbol{u}_h, \boldsymbol{B}_h, \widehat{E}_h)$ and δp_h solve the linear system (5.148). Then, by Theorem 5.70.1 we know that div $\delta\boldsymbol{B}_h = 0$ and equation (5.154) is satisfied. This implies that $\delta\boldsymbol{x}_h$ and δp_h solve (5.146). □

Finally, we can present the well-posedness of (5.148). In the spirit of [59] we introduce the following norm on $\boldsymbol{\xi}_h = (\boldsymbol{u}_h, \boldsymbol{B}_h, E_h) \in \mathfrak{X}_{h,0}$ as

$$|||\boldsymbol{\xi}_h|||^2_{\mathfrak{X}_{h,0}} := |||\boldsymbol{v}_h|||^2_{\Delta t,\nabla} + |||E_h|||^2_{\Delta t,\mathbf{rot}} + |||\boldsymbol{B}_h|||^2_{\Delta t,\mathrm{div}}\,, \tag{5.155a}$$

$$|||\boldsymbol{u}_h|||^2_{\Delta t,\nabla} := \Delta t^{-1}|||\boldsymbol{u}_h|||^2_{\mathcal{TV}_h} + \left|\boldsymbol{u}_h\right|^2_{\mathcal{TV}_h} + \Delta t^{-1}|||\mathrm{div}\,\boldsymbol{u}_h|||^2_{\mathcal{P}_h}\,, \tag{5.155b}$$

$$|||\boldsymbol{B}_h|||^2_{\Delta t,\mathrm{div}} := \Delta t^{-1}|||\boldsymbol{B}_h|||^2_{\mathcal{E}_h} + |||\mathrm{div}\,\boldsymbol{B}_h|||^2_{\mathcal{P}_h}\,, \tag{5.155c}$$

$$|||E_h|||^2_{\Delta t,\mathbf{rot}} := |||E_h|||^2_{\mathcal{V}_h} + \Delta t|||\mathbf{rot}\,E_h|||^2_{\mathcal{E}_h}\,. \tag{5.155d}$$

Well-posedness relies on Theorem 2.20.2. The following two lemmas prove that (5.148) satisfies its hypothesis.

Lemma 5.70.2 *Suppose that* $\Delta t^{1/2}\widehat{\boldsymbol{u}}_h, \widehat{\boldsymbol{u}}_h, \boldsymbol{B}_h \in [L^\infty(\Omega)]^2$ *and* $\widehat{E}_h \in L^\infty(\Omega)$ *then bilinear form* $a_{h,0}$ *is continuous in the norms defined in* (5.155a)*.*

Proof. Let $\xi = (\boldsymbol{u}_h, \boldsymbol{B}_h, E_h)$ and $\eta = (\boldsymbol{v}_h, \boldsymbol{C}_h, E_h)$ be arbitrary elements in $\mathfrak{X}_h$. A series

of applications of the Cauchy-Schwartz inequality yields that

$$\Delta t^{-1}\Big(\delta \boldsymbol{u}_h, \boldsymbol{v}_h\Big)_{\mathcal{TV}_h} \leq \Delta t^{-1/2} |||\delta \boldsymbol{u}_h|||_{\mathcal{TV}_h} \Delta t^{-1/2} |||\boldsymbol{v}_h|||_{\mathcal{TV}_h} \leq |||\delta \boldsymbol{u}_h|||_{\Delta t,\nabla} |||\boldsymbol{v}_h|||_{\Delta t,\nabla}, \quad (5.156)$$

$$\Big[\delta \boldsymbol{u}_h, \boldsymbol{v}_h\Big]_{\mathcal{TV}_h} \leq \big|\delta \boldsymbol{u}_h\big|_{\mathcal{TV}_h} \big|\boldsymbol{v}_h\big|_{\mathcal{TV}_h} \leq |||\delta \boldsymbol{u}_h|||_{\Delta t,\nabla} |||\boldsymbol{v}_h|||_{\Delta t,\nabla} \quad (5.157)$$

$$\Delta t^{-1}\big(\delta \boldsymbol{B}_h, \boldsymbol{C}_h\big)_{\mathcal{E}_h} \leq \Delta t^{-\frac{1}{2}} |||\delta \boldsymbol{B}_h|||_{\mathcal{E}_h} \, \Delta t^{-\frac{1}{2}} |||\boldsymbol{C}_h|||_{\mathcal{E}_h} \leq |||\delta \boldsymbol{B}_h|||_{\Delta t,\mathrm{div}} \, |||\boldsymbol{C}_h|||_{\Delta t,\mathrm{div}}\,, \quad (5.158)$$

$$\big(\mathbf{rot}\, \delta E_h, \boldsymbol{C}_h\big)_{\mathcal{E}_h} \leq \Delta t^{\frac{1}{2}} |||\mathbf{rot}\, \delta E_h|||_{\mathcal{E}_h} \, \Delta t^{-\frac{1}{2}} |||\boldsymbol{C}_h|||_{\mathcal{E}_h} \leq |||\delta E_h|||_{\Delta t,\mathbf{rot}} \, |||\boldsymbol{C}_h|||_{\Delta t,\mathrm{div}}\,, \quad (5.159)$$

$$\big(\delta E_h, D_h\big)_{\mathcal{V}_h} \leq |||\delta E_h|||_{\mathcal{V}_h} \, |||D_h|||_{\mathcal{V}_h} \leq |||\delta E_h|||_{\Delta t,\mathbf{rot}} \, |||D_h|||_{\Delta t,\mathbf{rot}}\,, \quad (5.160)$$

$$\big(\mathrm{div}\, \delta \boldsymbol{B}_h, \mathrm{div}\, \boldsymbol{C}_h\big)_{\mathcal{P}_h} \leq |||\mathrm{div}\, \delta \boldsymbol{B}_h|||_{\mathcal{P}_h} \, |||\mathrm{div}\, \boldsymbol{C}_h|||_{\mathcal{P}_h} \leq |||\delta \boldsymbol{B}_h|||_{\Delta t,\mathrm{div}} \, |||\boldsymbol{C}_h|||_{\Delta t,\mathrm{div}}\,. \quad (5.161)$$

Continuity of the coupling terms comes about by similar arguments. Here, two representative terms. They rely on the Friedrichs-Poincaré inequality, recall that $\|E_h\|_{0,\Omega} \leq C\|\nabla E_h\|_{0,\Omega} = \|\mathbf{rot}\, E_h\|_{0,\Omega}$ and $\|\boldsymbol{v}_h\|_{0,\Omega} \leq C\|\nabla \boldsymbol{v}_h\|_{0,\Omega}$ holds for every $E_h \in \mathcal{V}_{h,0} \subset H_0^1(\Omega)$ and $\boldsymbol{v}_h \in \mathcal{TV}_{h,0} \subset H_0^1$ respectively. Thus,

$$\begin{aligned}
\big(\mathcal{I}^{\mathcal{V}_h}\big(\widehat{\boldsymbol{u}}_h \times \Pi^{RT} \delta \boldsymbol{B}_h\big), D_h\big)_{\mathcal{V}_h} &\leq C\|\mathcal{I}^{\mathcal{V}_h}\big(\widehat{\boldsymbol{u}}_h \times \Pi^{RT} \delta \boldsymbol{B}_h\big)\|_{0,\Omega} \|D_h\|_{0,\Omega} \\
&\leq C\|\widehat{\boldsymbol{u}}_h\|_\infty \|\delta \boldsymbol{B}_h\|_{0,\Omega} \|D_h\|_{0,\Omega} \\
&\leq C\|\widehat{\boldsymbol{u}}_h\|_\infty \|\delta \boldsymbol{B}_h\|_{0,\Omega} \|\mathbf{rot}\, D_h\|_{0,\Omega} \\
&\leq C\|\widehat{\boldsymbol{u}}_h\|_\infty \Delta t^{-1/2} |||\delta \boldsymbol{B}_h|||_{\mathcal{E}_h} \Delta t^{1/2} |||\mathbf{rot}\, D_h|||_{\mathcal{E}_h} \\
&\leq \widetilde{C} |||\delta \boldsymbol{B}_h|||_{\Delta t,\mathrm{div}} \, |||D_h|||_{\Delta t,\mathbf{rot}}\,. \qquad (5.162)
\end{aligned}$$

Finally, continuity of the second coupling term follows by

$$\begin{aligned}\Big(\mathcal{I}^{\mathcal{V}_h}(\widehat{\boldsymbol{u}}_h \times \Pi^{RT}\delta\boldsymbol{B}_h), \mathcal{I}^{\mathcal{V}_h}(\boldsymbol{v}_h \times \Pi^{RT}\boldsymbol{B}_h)\Big)_{\mathcal{V}_h} \leq \\ &\leq C\|\mathcal{I}^{\mathcal{V}_h}(\widehat{\boldsymbol{u}}_h \times \Pi^{RT}\delta\boldsymbol{B}_h)\|_{0,\Omega}\|\mathcal{I}^{\mathcal{V}_h}(\boldsymbol{v}_h \times \Pi^{RT}\boldsymbol{B}_h)\|_{0,\Omega} \\ &\leq C\|\widehat{\boldsymbol{u}}_h\|_\infty\|\Pi^{RT}\boldsymbol{B}_h\|_\infty\|\delta\boldsymbol{B}_h\|_{0,\Omega}\|\boldsymbol{v}_h\|_{0,\Omega} \\ &\leq C\|\Delta t^{1/2}\widehat{\boldsymbol{u}}_h\|_\infty\|\Pi^{RT}\boldsymbol{B}_h\|_\infty\Delta t^{-1/2}\|\delta\boldsymbol{B}_h\|_{0,\Omega}\|\nabla\boldsymbol{v}_h\|_{0,\Omega} \\ &\leq \widetilde{C}\|\Delta t^{1/2}\widehat{\boldsymbol{u}}_h\|_\infty\|\Pi^{RT}\boldsymbol{B}_h\|_\infty\Delta t^{-1/2}|||\delta\boldsymbol{B}_h|||_{\mathcal{E}_h}\big|\boldsymbol{v}_h\big|_{\mathcal{T}\mathcal{V}_h} \\ &\leq \widetilde{C}|||\delta\boldsymbol{B}_h|||_{\Delta t,\mathrm{div}}\,|||\boldsymbol{v}_h|||_{\Delta t,\nabla}. \end{aligned} \tag{5.163}$$

□

Next, we present a proof of the so-called inf-sup condition of the bilinear form $a_{h,0}$.

Lemma 5.70.3 *Let $\theta > 0$, and $\widehat{\boldsymbol{u}}_h, \boldsymbol{B}_h \in [L^\infty(\Omega)]^2$ and $\widehat{E}_h \in L^\infty(\Omega)$ In this case, for Δt is small enough then*

$$\inf_{\delta\boldsymbol{\xi}_h\in\mathfrak{X}_{h,0}}\sup_{\boldsymbol{\eta}_h\in\mathfrak{X}_{h,0}}\frac{a_{h,0}(\delta\boldsymbol{\xi}_h,\boldsymbol{\eta}_h)}{|||\delta\boldsymbol{\xi}_h|||_{\mathfrak{X}_h}|||\boldsymbol{\eta}_h|||_{\mathfrak{X}_h}} \geq C > 0, \quad \textit{where} \quad \mathfrak{X}_{h,0} = \{(\boldsymbol{v}_h, \boldsymbol{B}_h, E_h) : \textit{div}\,\boldsymbol{v}_h = 0\}. \tag{5.164}$$

Where C does not depend on h nor Δt.

Proof. Select $\boldsymbol{\xi}_h = (\delta\boldsymbol{u}_h, \delta\boldsymbol{B}_h, \delta E_h) \in \mathfrak{X}_{h,0}$ arbitrarily, proof of (5.164) would follow if we can show that there exists $\boldsymbol{\eta}_h \in \mathfrak{X}_{h,0}$ satisfying

$$a_{h,0}(\delta\boldsymbol{\xi}_h,\boldsymbol{\eta}_h) \geq C|||\delta\boldsymbol{\xi}_h|||_{\mathfrak{X}_h}|||\boldsymbol{\eta}_h|||_{\mathfrak{X}_h}. \tag{5.165}$$

We will do this by decomposing $a_{h,0}$ into

$$a_{h,0}(\delta\boldsymbol{\xi}_h,\boldsymbol{\eta}_h) = \ell_1(\boldsymbol{v}_h) + \ell_2^*(\boldsymbol{C}_h) + \ell_3(D_h), \tag{5.166}$$

where ℓ_1 and ℓ_3 are defined in (5.139) and

$$\ell_2^*(\boldsymbol{C}_h) = \ell_2(\boldsymbol{C}_h) + \Big(\operatorname{div}\delta\boldsymbol{B}_h, \operatorname{div}\boldsymbol{C}_h\Big). \tag{5.167}$$

Let us pick $\eta = (\boldsymbol{v}_h, \boldsymbol{C}_h, D_h)$ for

$$\boldsymbol{v}_h = \delta\widehat{\boldsymbol{u}}_h, \quad \boldsymbol{C}_h = \frac{1}{2}(\delta\boldsymbol{B}_h + \Delta t\mathbf{rot}\,\delta E_h), \quad D_h = \delta\widehat{E}_h. \tag{5.168}$$

Then,

$$\begin{aligned}
\ell_1(\boldsymbol{v}_h) &= \Delta t^{-1}|||\delta\widehat{\boldsymbol{u}}_h|||_{\mathcal{TV}_h} + R_e^{-1}\big|\delta\widehat{\boldsymbol{u}}_h\big|_{\mathcal{TV}_h} + \theta\Big(\widehat{E}_h, \mathcal{I}^{\mathcal{V}_h}(\delta\widehat{\boldsymbol{u}}_h \times \Pi^{RT}\delta\boldsymbol{B}_h)\Big)_{\mathcal{V}_h} + \\
&+ \theta^3\Big(\delta\widehat{E}_h, \mathcal{I}^{\mathcal{V}_h}(\delta\widehat{\boldsymbol{u}}_h \times \Pi^{RT}\boldsymbol{B}_h)\Big)_{\mathcal{V}_h} + \theta^3\Big(\mathcal{I}^{\mathcal{V}_h}(\widehat{\boldsymbol{u}}_h \times \Pi^{RT}\boldsymbol{B}_h), \mathcal{I}^{\mathcal{V}_h}(\delta\widehat{\boldsymbol{u}}_h \times \Pi^{RT}\delta\boldsymbol{B}_h)\Big)_{\mathcal{V}_h} + \\
&+ \theta^3\Big(\mathcal{I}^{\mathcal{V}_h}(\widehat{\boldsymbol{u}}_h \times \Pi^{RT}\delta\boldsymbol{B}_h), \mathcal{I}^{\mathcal{V}_h}(\delta\boldsymbol{u}_h \times \Pi^{RT}\boldsymbol{B}_h)\Big)_{\mathcal{V}_h} + \\
&+ \theta^3\Big(\mathcal{I}^{\mathcal{V}_h}(\delta\widehat{\boldsymbol{u}}_h \times \Pi^{RT}\boldsymbol{B}_h), \mathcal{I}^{\mathcal{V}_h}(\delta\widehat{\boldsymbol{u}}_h \times \Pi^{RT}\boldsymbol{B}_h)\Big)_{\mathcal{V}_h},
\end{aligned} \tag{5.169}$$

$$\begin{aligned}
\ell_2^*(\boldsymbol{C}_h) = \theta R_m^{-1}\frac{\Delta t^{-1}}{2}|||\delta\boldsymbol{B}_h|||_{\varepsilon_h}^2 + \theta\frac{R_m^{-1}}{2}|||\operatorname{div}\delta\boldsymbol{B}_h|||_{\varepsilon_h}^2 + \\
+ \theta\frac{R_m^{-1}\Delta t}{2}|||\mathbf{rot}\,\delta\widehat{E}_h|||_{\varepsilon_h}^2 + \theta R_m^{-1}\Big(\delta\boldsymbol{B}_h, \mathbf{rot}\,\delta\widehat{E}_h\Big)_{\mathcal{E}_h},
\end{aligned} \tag{5.170}$$

$$\begin{aligned}
\ell_3(D_h) = |||\delta\widehat{E}_h|||_{\mathcal{V}_h}^2 + \theta\Big(\mathcal{I}^{\mathcal{V}_h}(\widehat{\boldsymbol{u}}_h \times \Pi^{RT}\delta\boldsymbol{B}_h), \delta\widehat{E}_h\Big)_{\mathcal{V}_h} + \\
\theta\Big(\mathcal{I}^{\mathcal{V}_h}(\delta\widehat{\boldsymbol{u}}_h \times \Pi^{RT}\boldsymbol{B}_h), \delta\widehat{E}_h\Big)_{\mathcal{V}_h} - \theta R_m^{-1}\big(\delta\boldsymbol{B}_h, \mathbf{rot}_h\delta\widehat{E}_h\big)_{\mathcal{E}_h}.
\end{aligned} \tag{5.171}$$

Note that

$$\theta\Big(\widehat{E}_h, \mathcal{I}^{\mathcal{V}_h}(\delta\widehat{\boldsymbol{u}}_h \times \Pi^{RT}\delta\boldsymbol{B}_h)\Big)_{\mathcal{V}_h} + \theta^3\Big(\mathcal{I}^{\mathcal{V}_h}(\widehat{\boldsymbol{u}}_h \times \Pi^{RT}\boldsymbol{B}_h), \mathcal{I}^{\mathcal{V}_h}(\delta\widehat{\boldsymbol{u}}_h \times \Pi^{RT}\delta\boldsymbol{B}_h)\Big)_{\mathcal{V}_h} +$$
$$\theta^3\Big(\mathcal{I}^{\mathcal{V}_h}(\widehat{\boldsymbol{u}}_h \times \Pi^{RT}\delta\boldsymbol{B}_h, \mathcal{I}^{\mathcal{V}_h}(\delta\boldsymbol{u}_h \times \Pi^{RT}\boldsymbol{B}_h)\Big)_{\mathcal{V}_h} +$$
$$+ \theta^3\Big(\mathcal{I}^{\mathcal{V}_h}(\delta\widehat{\boldsymbol{u}}_h \times \Pi^{RT}\boldsymbol{B}_h), \mathcal{I}^{\mathcal{V}_h}(\delta\widehat{\boldsymbol{u}}_h \times \Pi^{RT}\boldsymbol{B}_h)\Big)_{\mathcal{V}_h} \geq$$
$$\geq -\widetilde{C}\Delta t\left(\Delta t^{-1}|||\delta\boldsymbol{B}_h|||^2_{\mathcal{E}_h} + \Delta t^{-1}|||\delta\widehat{\boldsymbol{u}}_h|||^2_{\mathcal{TV}_h}\right). \tag{5.172}$$

Where $\widetilde{C} > 0$ depends on θ, $\|\widehat{\boldsymbol{u}}_h\|_\infty$, $\|\boldsymbol{B}_h\|_\infty$ and $\|\widehat{E}_h\|_\infty$. We also note that

$$2\theta\Big(\delta\widehat{E}_h, \mathcal{I}^{\mathcal{V}_h}(\delta\widehat{\boldsymbol{u}}_h \times \Pi^{RT}\boldsymbol{B}_h)\Big)_{\mathcal{V}_h} + \theta\Big(\mathcal{I}^{\mathcal{V}_h}(\widehat{\boldsymbol{u}}_h \times \Pi^{RT}\delta\boldsymbol{B}_h), \delta\widehat{E}_h\Big)_{\mathcal{V}_h} \geq$$
$$\geq -C_1\Delta t(\Delta t^{-1}|||\delta\widehat{\boldsymbol{u}}_h|||_{\mathcal{TV}_h}) - C_2\Delta t(\Delta t^{-1}|||\delta\boldsymbol{B}_h|||_{\mathcal{E}_h}) - \frac{1}{2}|||\delta\widehat{E}_h|||^2_{\mathcal{V}_h}. \tag{5.173}$$

Here C_1 depends on $\|\Pi^{RT}\boldsymbol{B}_h\|_\infty$ and C_2 depends on $\|\widehat{\boldsymbol{u}}_h\|_\infty$. Putting these together we find that

$$a_{h,0}(\boldsymbol{\xi}_h, \boldsymbol{\eta}_h) \geq (1 - \widetilde{C}\Delta t - C_1\Delta t)\Delta t^{-1}|||\delta\widehat{\boldsymbol{u}}_h|||_{\mathcal{TV}_h} + R_e^{-1}\big|\delta\widehat{\boldsymbol{u}}_h\big|_{\mathcal{TV}_h} +$$
$$+ \left(\frac{R_m^{-1}}{2} - \widetilde{C}\Delta t - C_2\Delta t\right)\Delta t^{-1}|||\delta\boldsymbol{B}_h|||^2_{\mathcal{E}_h} + |||\operatorname{div}\delta\boldsymbol{B}_h|||^2_{\mathcal{E}_h} +$$
$$+ \frac{R_m^{-1}\Delta t}{2}|||\mathbf{rot}\,\delta\widehat{E}_h|||^2_{\mathcal{E}_h} + \frac{1}{2}|||\widehat{E}_h|||^2_{\mathcal{V}_h}. \tag{5.174}$$

We pick Δt in such a way that

$$1 - \widetilde{C}\Delta t - C_1\Delta t \geq \frac{1}{2}, \quad \frac{R_m^{-1}}{2} - \widetilde{C}\Delta t - C_2\Delta t \geq \frac{R_m^{-1}}{4}. \tag{5.175}$$

This gives that

$$a_{h,0}(\boldsymbol{\xi}_h,\boldsymbol{\eta}_h) \geq \min\left\{\frac{1}{2},R_e^{-1}\right\}|||\delta\widehat{\boldsymbol{u}}_h|||^2_{\Delta t,\nabla} + \min\left\{\frac{R_m^{-1}}{4},1\right\}|||\delta\boldsymbol{B}_h|||^2_{\Delta t,\mathrm{div}} +$$
$$+\min\left\{\frac{R_m^{-1}}{2},\frac{1}{2}\right\}|||\delta\widehat{E}_h|||^2_{\Delta t,\mathbf{rot}} \geq \min\left\{\frac{1}{2},R_e^{-1},\frac{R_m^{-1}}{4}\right\}|||\boldsymbol{\xi}_h|||^2_{\mathfrak{X}_h}. \qquad (5.176)$$

To finish, note that

$$\begin{aligned}
|||\eta_\xi|||^2_{\mathcal{X}_h} &= |||(\theta/2)\left(\boldsymbol{B}_h+\Delta t\,\mathbf{rot}\,E_h\right)|||^2_{\Delta t,\mathrm{div}} + |||E_h|||^2_{\Delta t,\mathbf{rot}}\\
&= \frac{\theta^2}{4}\left(\Delta t^{-1}|||\boldsymbol{B}_h+\Delta t\mathbf{rot}\,E_h|||^2_{\mathcal{E}_h}+\|\mathrm{div}\,\boldsymbol{B}_h\|^2_{0,\Omega}\right)+|||E_h|||^2_{\Delta t,\mathbf{rot}}\\
&= \frac{\theta^2}{4}\left(\Delta t^{-1}|||\boldsymbol{B}_h|||^2_{\mathcal{E}_h}+\Delta t|||\mathbf{rot}\,E_h|||^2_{\mathcal{E}_h}+2\Big(\boldsymbol{B}_h,\mathbf{rot}\,E_h\Big)_{\mathcal{E}_h}+\|\mathrm{div}\,\boldsymbol{B}_h\|^2_{0,\Omega}\right)\\
&\qquad\qquad +|||E_h|||^2_{\Delta t,\mathbf{rot}}\\
&= \frac{\theta^2}{4}\left(\Delta t^{-1}|||\boldsymbol{B}_h|||^2_{\mathcal{E}_h}+\|\mathrm{div}\,\boldsymbol{B}_h\|^2_{0,\Omega}+2\Big(\Delta t^{-1/2}\boldsymbol{B}_h,\Delta t^{1/2}\mathbf{rot}\,E_h\Big)_{\mathcal{E}_h}+\Delta t|||\mathbf{rot}\,E_h|||^2_{\mathcal{E}_h}\right)\\
&\qquad\qquad +|||E_h|||^2_{\Delta t,\mathbf{rot}}\\
&\leq \frac{\theta^2}{4}\left(2\Delta t^{-1}|||\boldsymbol{B}_h|||^2_{\mathcal{E}_h}+\|\mathrm{div}\,\boldsymbol{B}_h\|^2_{0,\Omega}+2\Delta t|||\mathbf{rot}\,E_h|||^2_{\mathcal{E}_h}\right)+|||E_h|||^2_{\Delta t,\mathbf{rot}}\\
&\leq \frac{\theta^2}{2}|||\boldsymbol{B}_h|||^2_{\Delta t,\mathrm{div}}+\left(1+\frac{\theta^2}{2}\right)|||E_h|||^2_{\Delta t,\mathbf{rot}}\\
&\leq \left(1+\frac{\theta^2}{2}\right)|||\xi|||^2_{\mathcal{X}_h}. \qquad (5.177)
\end{aligned}$$

□

Finally, we present the main result of this section.

Theorem 5.70.2 *Both problems* (5.146) *and* (5.148) *are well-posed.*

Proof. Lemmas 5.70.2,5.70.3, Theorem 5.40.3 prove that the hypothesis of Theorem 2.20.2 are satisfied yielding as a conclusion that (5.148) is well-posed. By Lemma 5.70.1 problems

(5.146) and (5.148) are equivalent. The well-posedness of one will imply the well-posedness of both. □

We note that this well-posedness result exposes the saddle-point nature of the linear system. This result can be leveraged to come up with efficient preconditioner following the framework laid out in [69]. This was done for a similar MHD system in [70] using a Picard fixed point iteration as the choice of linearization. Efficient implementation of this preconditioner will require a generalization of mass lumping. While it is unclear how this can be done in general, in [77] some strategies are laid out in the context of elastodynamics. We also note that these type of preconditioners have been used in 3D VEMs for problems in fluid flow as well as electromagnetics, see [50]. Other physics-based preconditioners have been developed, see [31, 39].

5.8 Conclusions

In this chapter we returned to the discretization presented in chapter 3.. This chapter was concerned with the development in 2D of a method for a model that predicts the evolution of the electric and magnetic fields assuming that the velocity field is prescribed. The novelty is that now we are including a model for the mechanics of a magnetized fluid. This model was derived in Section 5.2. With this model we can product the evolution of the velocity field and the pressure. Then, in Section 5.3 we came up with a variational formulation of the continuous system. In the same section we proposed a VEM to approximate the solution to the variational formulation. Some of the operators and spaces we used in presenting this variational formulation are defined and studied in Sections 3.4, 3.5, 3.6 and 3.7 in Chapter 3.. These are the spaces and operators that approximate the electromagnetics in the MHD model. Then, in Section 5.4 we introduced the spaces and operators that pertain to the approximation of the mechanics of the MHD model. In this section we showed that these spaces satisfy an important inf-sup condition that will guarantee that approximations of the fluid flow equations will be stable with the use of the virtual elements. Then,

in Section 5.5 we show a generalization of the energy estimates presented in 3.9. In this section we present the continuous version of these estimates and a discrete mimicry that leads to their discrete counterpart. The model that we presented in this chapter is non-linear. A linearization strategy was developed in Section 5.6. We also show that this linearization will not alter the divergence of the magnetic field. As we discussed in Section 3.2 this is required by Gauss's law. At each time step the linearization strategy will require the solution of a series of linear systems involving the Jacobian. Finally, in Section 5.7 we show that these linear systems are well-posed. This is done by writing these linear systems as saddle point problem. Then, we checked that the hypothesis of Theorem 2.20.2 are satisfied.

6. NUMERICAL EXPERIMENTS

6.1 Introduction

In this section we will summarize a series of numerical experiments. First we present experiments showing that the truncation error of the discrete form of the full MHD system presented in Chapter 5. shrinks to zero as the mesh size decays. This is the topic of Section 6.2. Then, we present a series of numerical experiments of the electromagnetic subsystem presented in Chapter 3.. In Section 6.3 we will test the convergence of our method and we will check that the divergence of the magnetic field will remain around machine epsilon. Then, in Section 6.4 we will perform a numerical exploration of the energy estimates we presented in Theorem 3.90.2. Then, in Section 6.5 we will test our VEM using a well-understood model, the model for Hartmann flow. The last experiment that we will perform will be presented in Section 6.6. Here we will present a model for a phenomenon characteristic to MHD, a model for magnetic reconnection. We finish this chapter with some concluding remarks, there will be compiled in Section 6.7.

6.2 Truncation Error

In this section we explore the trunction error for all four equations in the full system presented Chapter 5.. Our tests will be performed over the computational domain $[-1,1]^2$. We explore three different types of meshes, these are presented in Figure 6.1.

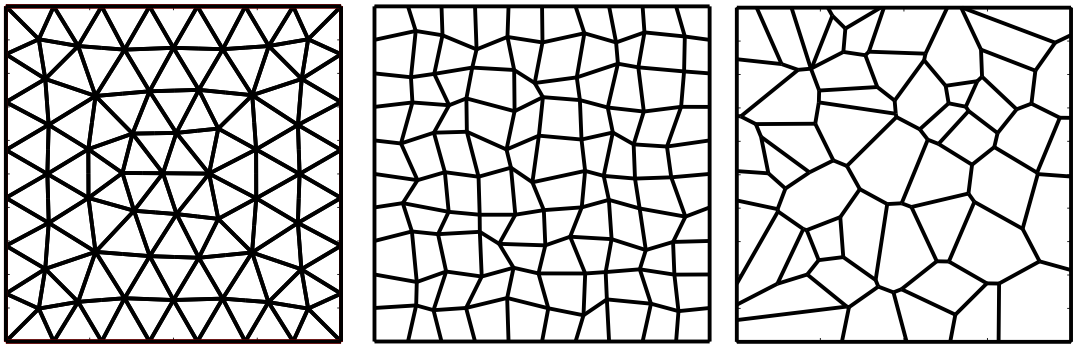

FIGURE 6.1: Illustration of the meshes used for testing the rate of convergence: triangular mesh (left panel), perturbed square mesh (central panel) and Voronoi tessellation (right panel).

To do this we introduce an exact solution to the continuous form of the equations as given by

$$\boldsymbol{u}(x,y,t) = \begin{pmatrix} e^t \cos y \\ 0 \end{pmatrix}, \quad \boldsymbol{B}(x,y,t) = \begin{pmatrix} 0 \\ \sin t \cos x \end{pmatrix}, \quad E(x,y,t) = \sin x, \quad p(x,y,t) = -x \cos y. \tag{6.1}$$

We select $\theta = 1/2$ and the boundary conditions, initial conditions and source functions set in accordance with this solution. Next we extract the degrees of freedom from each of the functions in equation (6.1) and consider functions in the respective discrete spaces that share these degrees of freedom. This test will consider only one time step which is selected to be of size $\Delta t = h^2$, where h is the mesh size. Thus, we need only consider the following:

$$\begin{aligned} &\boldsymbol{u}_h^1 = \mathcal{I}^{\mathcal{TV}_h}(\boldsymbol{u}(\Delta t)), \quad \boldsymbol{u}_h^0 = \mathcal{TV}_h(\boldsymbol{u}(0)), \quad \boldsymbol{B}_h^1 = \mathcal{I}^{\mathcal{E}_h}(\boldsymbol{B}(\Delta t)), \quad \boldsymbol{B}_h^0 \mathcal{I}^{\mathcal{E}_h}(\boldsymbol{B}(0)), \\ &E_h^\theta = \mathcal{I}^{\mathcal{V}_h}(E_h(\theta \Delta t)), \quad p_h^\theta = \mathcal{I}^{\mathcal{P}_h}(p_h(\theta \Delta t)). \end{aligned} \tag{6.2}$$

Then we plug these degrees of freedom into the discrete form of the equations. Since these functions are not a solution to the discrete equations then we will note that four remainders appear, one

for each equation. We denote them as $\boldsymbol{r}_{Mo}, r_{Ma}, \boldsymbol{r}_F$ and r_A and they satisfy:

$$\forall \boldsymbol{v}_h \in \mathcal{TV}_{h,0}: \quad \Big(\frac{\boldsymbol{u}_h^1 - \boldsymbol{u}_h^0}{\Delta t}, \boldsymbol{v}_h\Big)_{\mathcal{TV}_h} + R_e^{-1}\Big[\boldsymbol{u}_h^\theta, \boldsymbol{v}_h\Big]_{\mathcal{TV}_h} + \Big(J_h^\theta, \mathcal{I}^{\mathcal{V}_h}(\boldsymbol{v}_h \times \Pi^{RT}\boldsymbol{B}_h^\theta)\Big)_{\mathcal{V}_h} - \\ - \Big(\operatorname{div} \boldsymbol{v}_h, p_h^\theta\Big)_{\mathcal{P}_h} - \Big(\boldsymbol{f}_h, \boldsymbol{v}_h\Big)_{\mathcal{TV}_h} = \big(\boldsymbol{r}_{Mo}, \boldsymbol{v}_h\big)_{\mathcal{TV}_h}, \tag{6.3a}$$

$$\forall q_h \in \mathcal{P}_{h,0}: \quad \Big(\operatorname{div} \boldsymbol{u}_h^\theta, q_h\Big)_{\mathcal{P}_h} = \Big(r_{Ma}, q_h\Big)_{\mathcal{P}_h}, \tag{6.3b}$$

$$\forall \boldsymbol{C}_h \in \mathcal{E}_h: \quad \Big(\frac{\boldsymbol{B}_h^1 - \boldsymbol{B}_h^0}{\Delta t}, \boldsymbol{C}_h\Big)_{\mathcal{E}_h} + \Big(\mathbf{rot}\, E_h^\theta, \boldsymbol{C}_h\Big)_{\mathcal{E}_h} = \big(\boldsymbol{r}_F, \boldsymbol{C}_h\big)_{\mathcal{E}_h}, \tag{6.3c}$$

$$\forall D_h \in \mathcal{V}_{h,0}: \quad \big(J_h^\theta, D_h\big)_{\mathcal{V}_h} - R_m^{-1}\big(\boldsymbol{B}_h^\theta, \mathbf{rot}\, D_h\big)_{\mathcal{E}_h} - \big(h, D_h\big)_{\mathcal{V}_h} = \big(r_A, D_h\big)_{\mathcal{V}_h}, \tag{6.3d}$$

$$\boldsymbol{u}_h^\theta = (1-\theta)\boldsymbol{u}_h^0 + \theta \boldsymbol{u}_h^1, \quad \boldsymbol{B}_h^\theta = (1-\theta)\boldsymbol{B}_h^0 + \theta \boldsymbol{B}_h^1, \tag{6.3e}$$

$$J_h^\theta = E_h^\theta + \mathcal{I}^{\mathcal{V}_h}(\boldsymbol{u}_h^\theta \times \Pi^{RT}\boldsymbol{B}_h^\theta), \tag{6.3f}$$

We use the elliptic projector as defined in Section 3.11 to define the inner product in the space $\mathcal{V}_h$. We refer to equations (6.3a),(6.3b),(6.3c) and (6.3d) as cons. of momentum, cons. of mass, Faraday's law and Ampere-Ohm's law respectively. We compute each of these remainders and their respective norms. The results are summarized in Figure 6.2 where we evidence the norm of each remainder decays to zero as the mesh size shrinks. It is important to note that when observing the result for Faraday's law that the size of the norm is close to machine precision thus, after a certain mesh-size computations are not reliable yielding what would appear as ill- behavior. In the plot of the truncation error in Ampere-Ohm's law shows some irregularities when using Voronoi Tesselations. The reason is an open question but a hypothesis that is likely true regards the length of the edges of cells in Voronoi tesselations, if they are too short then it may cause undesired behavior in VEMs.

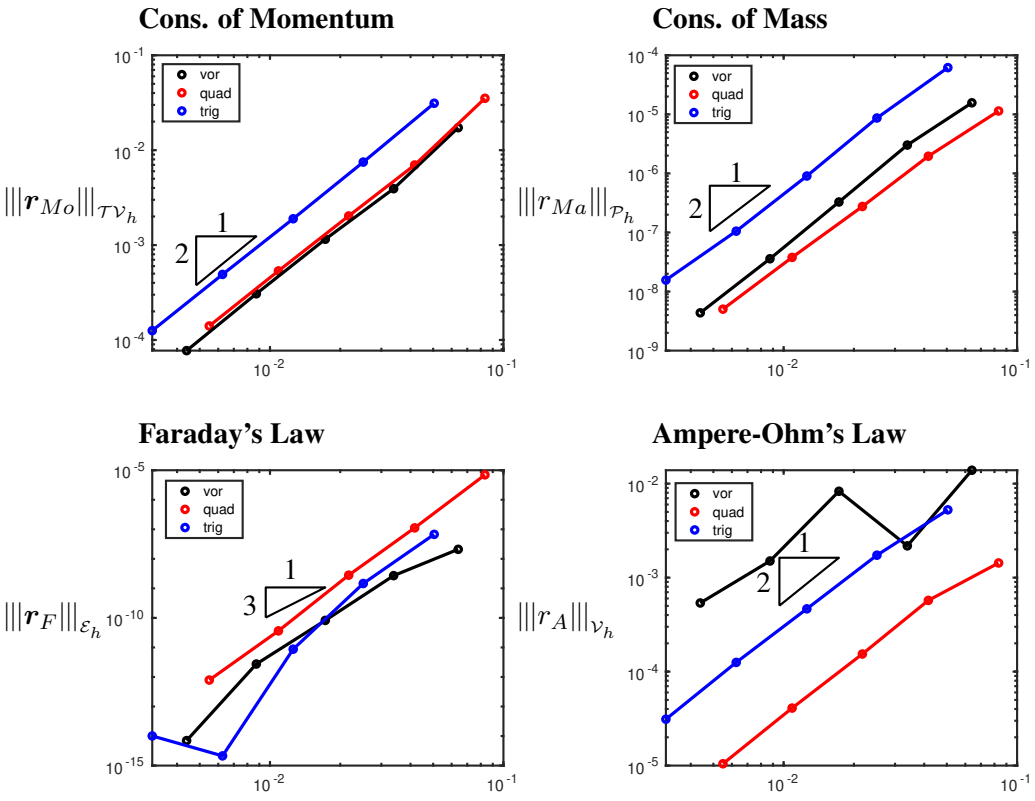

FIGURE 6.2: Plot of the truncation error of each of the equations in the full MHD system. Vor refers to Voronoi tessellations, quad to perturbed quadrilateals and trig to triangles, they allude to the type of mesh used.

6.3 Convergence Plots Of Kinematics

The first test that we perform regards the speed of convergence of the VEM. We consider the computational domain $\Omega = [-1, 1] \times [-1, 1]$. We will consider three different types of meshes. A sample of these meshes is presented in Figure 6.1. We use three types of meshes to check for convergence. These meshes are presented in Figure 6.1. We will also use the following exact solution to the kinematic system in Chapter 3.. We consider the velocity field $\boldsymbol{u} = (u_x, u_y)^T$

given by

$$u_x(x,y) = -\frac{(x^2+y^2-1)(\sin(xy)+\cos(xy)) - 100e^x + 100e^y}{2(50e^x - y\sin(xy) + y\cos(xy))}, \tag{6.4}$$

$$u_y(x,y) = \frac{(x^2+y^2-1)(\sin(xy)+\cos(xy)) - 100e^x + 100e^y}{2(50e^y + x\sin(xy) - x\cos(xy))} \tag{6.5}$$

and the initial and the boundary conditions are set in accordance with the exact solution of the electric and magnetic fields:

$$\boldsymbol{B}(x,y,t) = \begin{pmatrix} 50e^y + x\sin(xy) - x\cos(xy) \\ 50e^x - y\sin(xy) + y\cos(xy) \end{pmatrix} e^{-t}, \tag{6.6}$$

$$E(x,y,t) = -\big(50(e^x - e^y) + \cos(xy) + \sin(xy)\big)e^{-t}. \tag{6.7}$$

The simulation uses the time discretization given by $\theta = 1/2$. This is representative of the errors given by other values of θ, the main difference lies in the stability of the method. The final time is $T = 0.25$ and the time step is given by $\Delta t = 0.05h^2$. The errors we present are relative L^2 errors. They are the respective mesh dependent norms of the difference between the exact and numerical solutions divided by the norm of the exact solution. The results are shown in Figure 6.4. Each of these plots show three different convergence curves. These refer to the three different possibilities that we presented in Section 3.11 for the construction of the inner product in the space $\mathcal{V}_h$. These plots provide evidence that the speed convergence of the electric field is quadratic while the speed of convergence of the magnetic field is linear. We note that in the case of Voronoi tessellations the convergence plots associated with the inner product defined by the Galerkin interpolator (GI) show some irregular behavior. These types of meshes may have arbitrarily small edges conflating with the criteria laid out in Section 2.4. Another possible explanation may have to do with the G.I, note that this irregular behavior does not happen with the other two sample inner products. Further experimentation is required to fully understand this

behavior. An important feature of the VEM is that the divergence of the magnetic field should remain zero throughout the simulation. In Figure 6.3 we show plots of the evolution of the L^2-norm of the divergence of the magnetic field. These show that this quantity remains very close, in norm, to the machine epsilon.

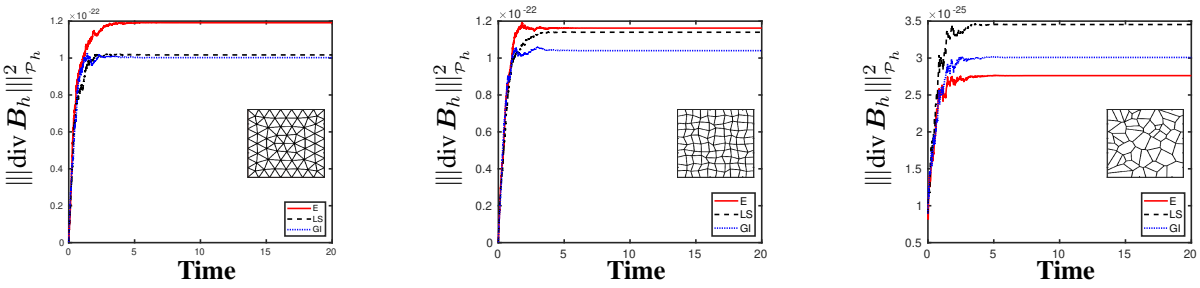

FIGURE 6.3: Plots of the time evolution of the square of the L^2 norm of the divergence of the numerical magnetic field. We present three different types of meshes, these are displayed in the lower right hand corner of each plot.

Remark 6 *The plots in Figure 6.3 show that the divergence of the magnetic field grows very rapidly then levels off at a very small value. This behavior is not entirely well understood. One hypothesis is that errors in the floating point arithmetic compound until they reach a threshold then stabilize at machine precision.*

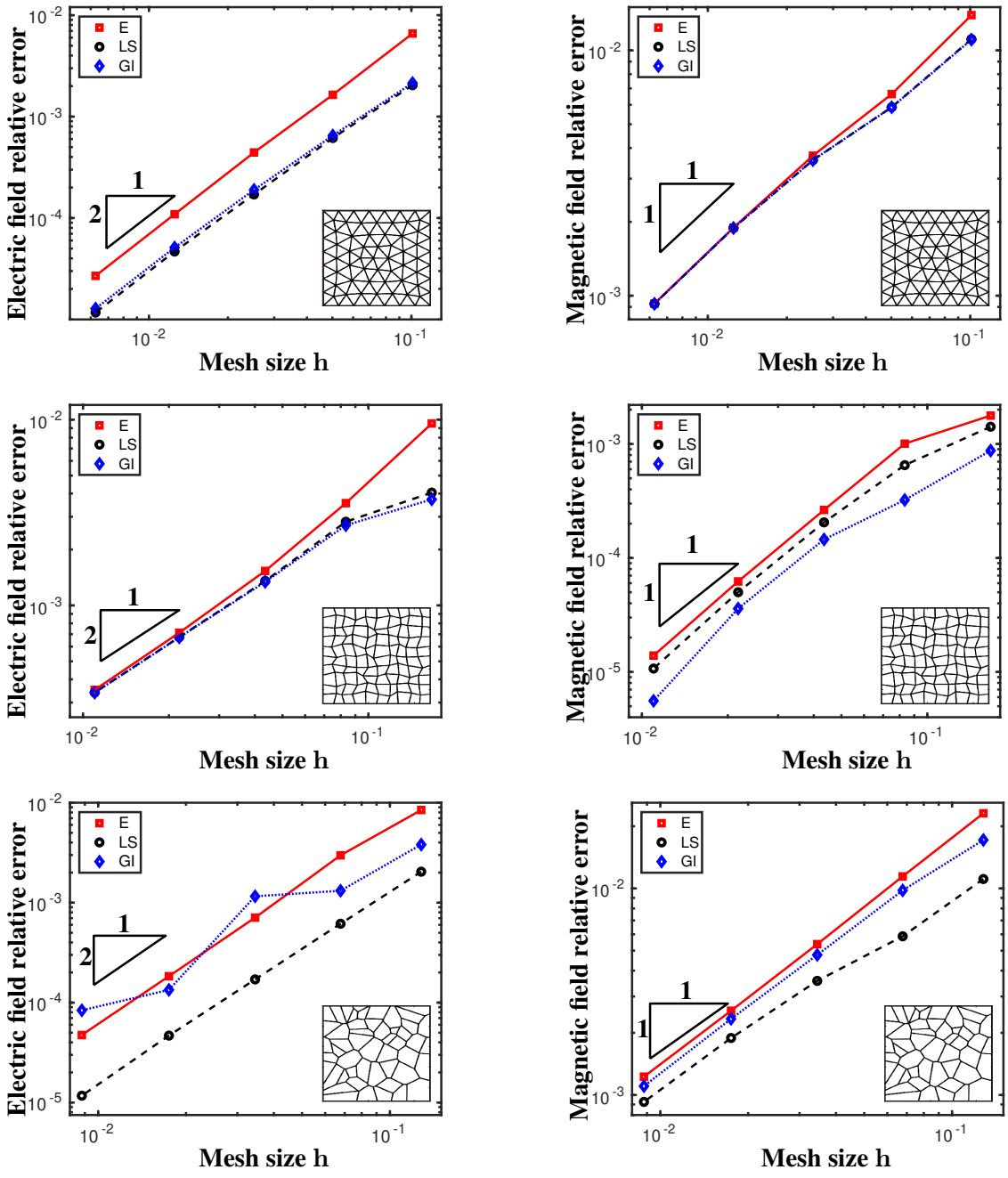

FIGURE 6.4: Convergence plots of the VEM developed in Chapter 3.. The type of mesh used in the simulation is portrayed in the lower right corner of each plot. The three convergence curves shown in each plot show the different performance between the three possibilities of the inner product in the space $\mathcal{V}_h$, see Section 3.11. Each of these inner products is associated with a projector, they are the elliptic projector (E), the least squares projector (LS) and the Galerkin interpolator (GI).

6.4 Experimental Analysis of Energy Estimates

In this section we will study, experimentally, the energy estimate presented in Theorem 3.90.2. Specifically we will look into inequality (3.137). We define the right and left hand sides of this inequality as

$$\mathcal{E}_R(n) = \frac{|||\boldsymbol{B}_h^0|||_{\mathcal{E}_h}^2 + \gamma\Delta t \sum_{\ell=0}^{n} \beta^{n+1-\ell} |||\mathcal{I}^{\mathcal{V}_h} E_0^{n-\ell+\theta}|||_{H(\mathbf{rot};\Omega)}^2}{|||\boldsymbol{B}_h^0|||_{\mathcal{E}_h}^2}, \tag{6.8}$$

$$\mathcal{E}_L(n) = \frac{(\beta)^{n+1} |||\boldsymbol{B}_h^{n+1}|||_{\mathcal{E}_h}^2 + \frac{\gamma\Delta t}{2} \sum_{\ell=0}^{n} \beta^{n+1-\ell} |||\widehat{E}_h^{n-\ell+\theta}|||_{\mathcal{V}_h}^2}{|||\boldsymbol{B}_h^0|||_{\mathcal{E}_h}^2}, \tag{6.9}$$

$$\mathcal{E}(n) = \mathcal{E}_R(n) - \mathcal{E}_L(n). \tag{6.10}$$

Thus, inequality 3.137 is equivalent to

$$\forall n \geq 1: \quad \mathcal{E}(n) \geq 0. \tag{6.11}$$

The value of β above is defined by the condition given in (3.139). This condition necessarily implies that $\beta \in (0, 1)$. Thus we can expect that $\mathcal{E}(n) \to 1$ as $n \to \infty$ unless the electric and magnetic fields grow fast enough to offset this decay. We introduce the parameter $C \in \mathbb{R}$ and the set of solutions

$$\boldsymbol{B}^C(x, y, t) = \begin{pmatrix} 50e^y - x\sin(xy) + x\cos(xy) \\ 50e^x + y\sin(xy) + y\cos(xy) \end{pmatrix} e^{Ct}, \tag{6.12}$$

$$E^C(x, y, t) = C\big(50(e^x - e^y) - \cos(xy) - \sin(xy)\big)e^{Ct} \tag{6.13}$$

The associated velocity field is given by $\boldsymbol{u}^C = (u_x^C, u_y^C)^T$ with

$$u_x^C(x,y) = -C\frac{(-x^2-y^2-1)(\sin(xy)+\cos(xy))}{2(50e^x + y\sin(xy) - y\cos(xy))}, \tag{6.14}$$

$$u_y^C(x,y) = C\frac{(-x^2-y^2-1)(\sin(xy)+\cos(xy))}{2(50e^y - x\sin(xy) + x\cos(xy))} \tag{6.15}$$

and define $R_m = 1/C$. Note that the Assumption (3.139) yields that $0 < Q < \theta^{-1}$. In Figure 6.5 we plot $\mathcal{E}$ field against the value of Q at time $T = 0.5$. The type of mesh or the alternative on the nodal mass matrix do not yield significant difference to the results in this figure. Thus, we present the results on Voronoi tessellations of the elliptic projector as a representative with mesh size $h = 0.0678$. The results of Figure 6.5 indicate that, in the case that the growth of the solution

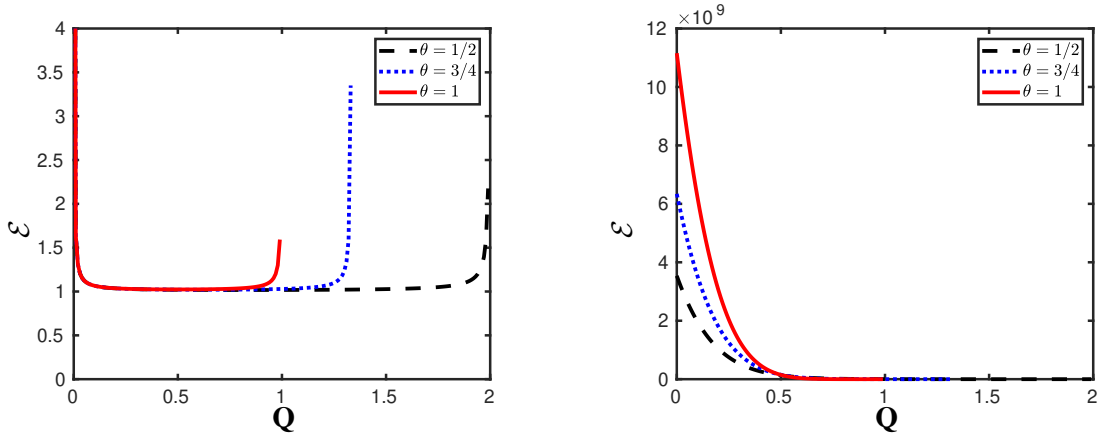

FIGURE 6.5: Plot of Q against the resulting energy inequality at $T = 0.5$. The initial and boundary information for the left plot is associated with $C = 0.1$ and time step $\Delta t = 0.001$. The results of the plot to the right are those associated with $C = 5$ and $\Delta t = 0.21$

is relatively small only the values of Q near zero yields $\beta \approx 1$ and the coefficients in $\mathcal{E}$ will show some exponential growth, if $Q \approx \theta^{-1}$ then the value of γ blows up yielding that $\mathcal{E}$ will be large. The rest of the values of Q will show convergence towards the norm of the initial conditions on the magnetic field. Since we normalized the error by this value we can expect a flat line of height one. If, however, the solution grows faster than the decay brought about by the coefficients in $\mathcal{E}$ then we

will see the energy blow up. Note that the growth in time, at least in our example, of $\mathcal{E}$ is mainly ruled by terms that look like $\beta^n e^{Cn\Delta t}$ were $t = n\Delta t$, hence a rule of thumb for checking whether the energy will grow or flatten is to check if $\ln \beta + C\Delta t$ is positive or negative respectively. This is the reason we picked such a small value for Δt in the right plot of Figure 6.5 since large values of C can yield overflow errors. In Figure 6.6 we can clearly see the two different types of behavior that the energy estimates present.

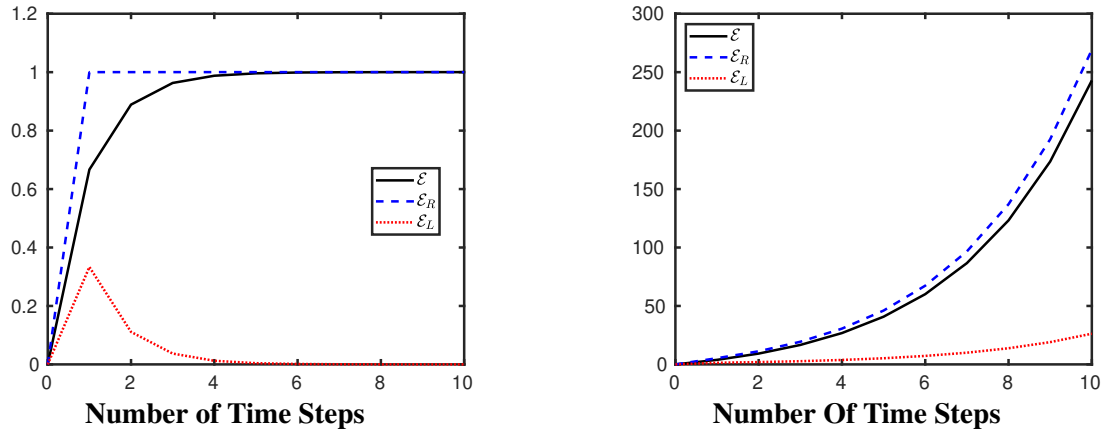

FIGURE 6.6: Energy Plots against number of time steps. The initial and boundary information used on the plots to the left are associated with $C = 0.1$ and time step $\Delta t = 0.001$. In the case of the plot to the right plot we use the information associated with $C = 5$ and $\Delta t = 0.21$. In both cases, $h = 0.0678$.

6.5 Hartmann Flow

In this section we consider a common problem in MHD used to assess numerical simulations, the Hartmann Flow problem. The set up is the following: consider a square duct of infinite length containing a conducting fluid. We subject this fluid to a magnetic field that runs along a direction perpendicular to the duct. The response of the fluid will depend on the ratio of the Laplace force and the viscous forces. This is a dimensionless quantity called the Hartmann number. There

is a set of known formulas that describes the solution to this problem, a proof of which can be found in [73]. This is one of the few problems in MHD where a formula for the exact solution can be found. For this reason researchers use the Hartmann flow problem to test the performance of their simulations, see [36, 59, 80].

In this section we consider a square computational domain $[-1,1]^2$ as cross section of the duct and consider a fluid with $R_m = 1$. The magnetic field is applied in the direction of the $y-$axis. Consider the case where the viscous forces and Laplace forces are of equal strength, so that the Hartmann number is 1. Then, we can expect the fluid to behave in accordance to the solution $\boldsymbol{B} = (B_x, 1, 0)$, $\boldsymbol{u} = (u_x, 0, 0)$ and $\boldsymbol{E} = (0, 0, E_z)$ with

$$\begin{aligned} u_x(x,y) &= \frac{\cosh 1/2 - \cosh y}{2\sinh 1/2}, \\ B_x(x,y) &= \frac{\sinh y - 2y\sinh 1/2}{2\sinh 1/2}, \\ E_z(x,y) &= \frac{2\sinh 1/2 - \cosh 1/2}{2\sinh 1/2} \approx -0.0820. \end{aligned} \tag{6.16}$$

Note that the $y-$component of the magnetic field is 1 by assumption. Therefore, we will check if we can recover the $x-$component. We use the exact solution extract the necessary initial and boundary conditions. Then, we evolve the system until $T = 10$ with step size $\Delta t = 0.005$. The result shown in Figure 6.7 provide evidence that the numerical and analytic solutions are close. We conducted a convergence test that verifies that every alternative to the mass matrix yields a close approximation and provides additional evidence that rate of convergence of the magnetic field is linear, these results are in Figure 6.8.

6.6 Magnetic Reconnection

The next experiment we will perform involves a characteristic feature of resistive MHD, the phenomenon of magnetic reconnection. At very large scales, usually in space physics, the behavior

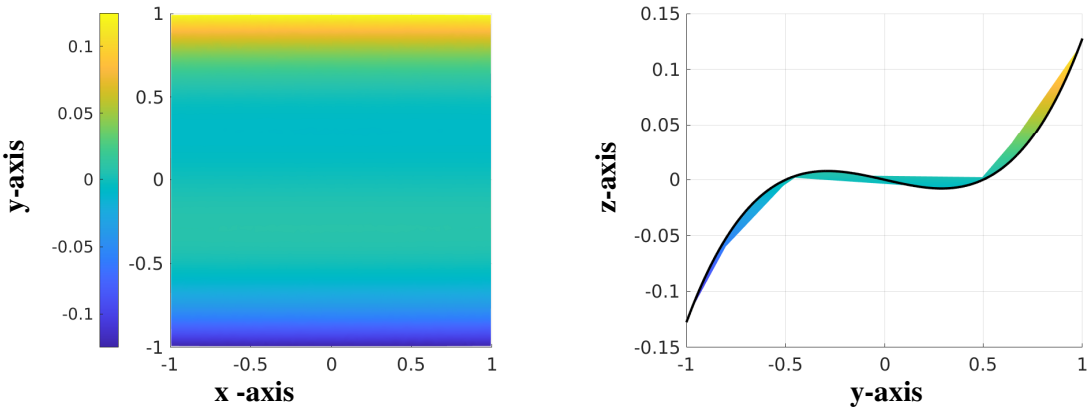

FIGURE 6.7: Pictures of the analytic and numerical solution for the $x-$component of the magnetic field, computed in a Voronoi tessellation of mesh size $h = 0.017$ using the elliptic projector as the alternative to the mass matrix. The plot on the left is of the numerical solution as viewed from above, whereas the plot on the right shows the numerical solution in a rainbow color bar overlaid with the exact solution in bold black, both are viewed from the side.

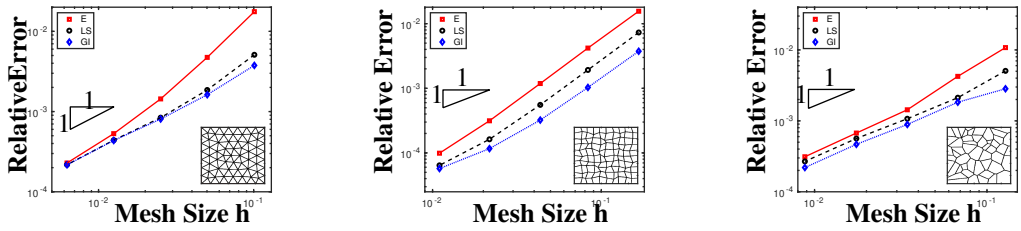

FIGURE 6.8: Convergence plots for the approximation of the magnetic field on the three different mesh families. As before, the symbols E,LS,GI refers to the three alternatives we have for constructing the nodal mass matrix; the elliptic projector (E), least squares projector (LS) and the Galerkin interpolator (GI) respectively. See section 3.11.

of plasmas can be well-approximated using ideal MHD. In this case, the magnetic field lines will advect with the fluid. This is often referred to as the "frozen-in" condition on the magnetic field and it is the statement of Alfven's Theorem. In certain regions of the earth's magnetosphere, namely the magneto pause and magneto tail, this process will lead to very thin current sheets that separate regions across which the magnetic field changes substantially. In this test we consider one Harris sheet constrained to the computational domain $\Omega = [-1, 1]^2$. The magnetic field in

this domain is given by

$$\boldsymbol{B}_0(x, y) = (\tanh y, 0). \tag{6.17}$$

The above expression will be the initial conditions on the magnetic field. This profile for the magnetic field was introduced in [57]. Its simplicity has made it a common choice in modeling magnetic reconnection. We will further assume that the particles in this sheet are subjected by some external agent to a flow described by

$$\boldsymbol{u}(x, y, t) = (-x, y). \tag{6.18}$$

This flow will force the magnetic field lines together at a single point making the current density grow. A tearing instability is formed and magnetic reconnection happens as a response. This process is described in detail in [63, 79]. We close this model by imposing the boundary conditions

$$\forall t > 0: \quad E_b(t) \in \mathbb{P}_0(\partial\Omega), \quad \text{and} \quad \int_{\partial\Omega} \boldsymbol{B}_b(t) \cdot \boldsymbol{n} d\ell = 0 \tag{6.19}$$

The mesh we are using is refined near the center of the domain Ω. This guarantees higher resolution where the phenomenon of magnetic reconnection occurs. The downside is that a series of hanging nodes are introduced. This is an example of a simulation where the versatility of the VEM yields advantages over more classical methods like FEM or FDM. In Figure 6.9 the reader will find a picture of the mesh used along with a summary of the numerical experiments.

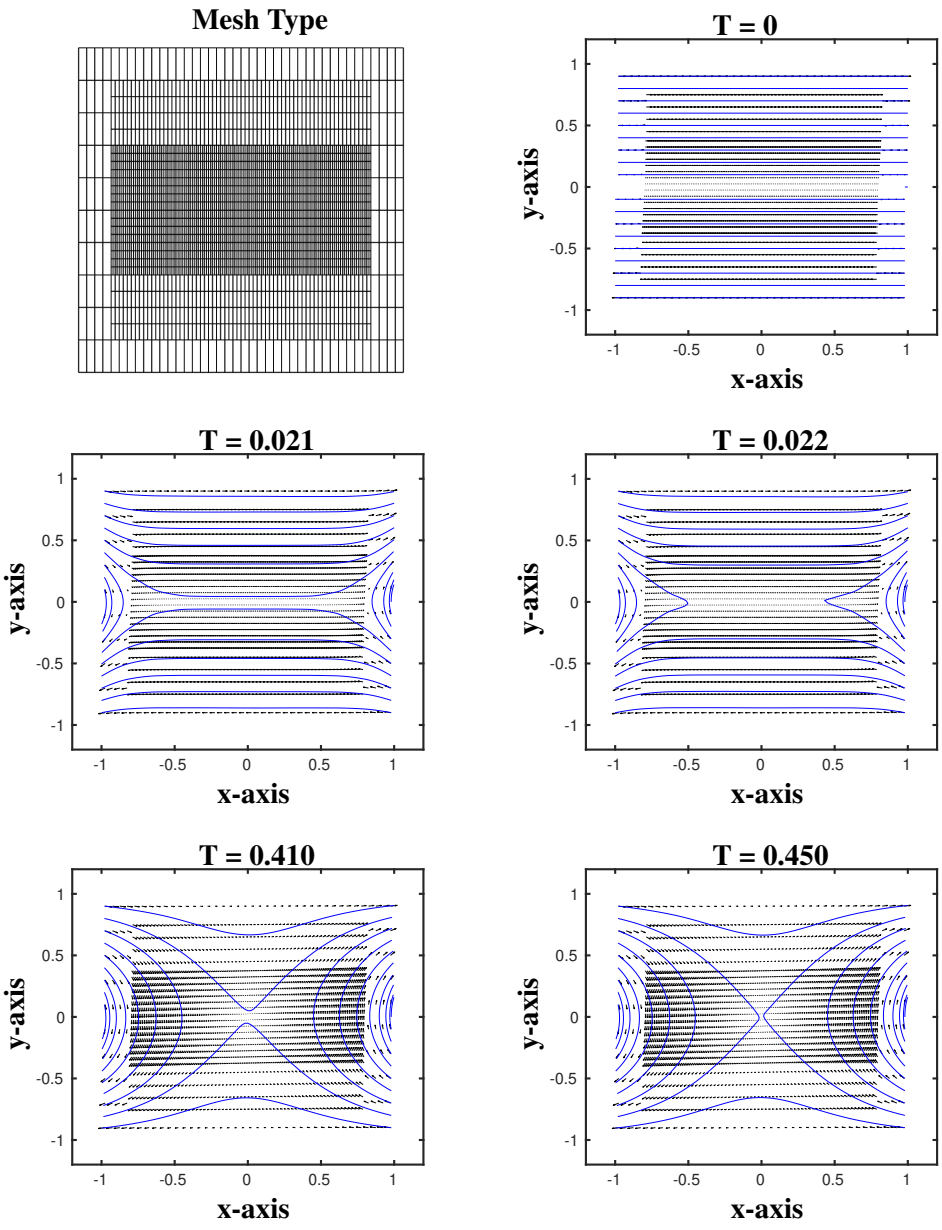

FIGURE 6.9: Frames displaying the evolution, in time, of the magnetic field. The phenomenon of magnetic reconnection begins right away and by T= 0.450 a steady state is achieved.

6.7 Conclusions

In Section 6.2 we noted that the truncation error of the discretization to the full MHD decays to zero as the mesh size shrinks. Then, in Section 6.3 we performed a convergence test for the kinematic subsystem describing the electromagnetics of MHD. This test revealed that the speed of convergence of our method is quadratic for the electric field and linear for the magnetic field. Moreover, we were also able to verify that the divergence of the discrete magnetic field is well beneath machine epsilon. Then, in Section 6.4 we verified that the estimates of Theorem 3.90.2 hold. Moreover, we discovered that there are two types of behavior. Either the overall energy goes to infinity or it decays to zero. In Section 6.5 we showed that our method can predict the evolution of a Hartmann flow. And, we once again verified that the speed of convergence of the magnetic field is quadratic. The last test that we perform was presented in Section 6.6. Here we proposed a model for magnetic reconnection happening at the center of the square $[-1, 1]\times[-1, 1]$. Hence, we used a mesh refined to provide higher resolution in near the center. In this process we introduced a series of hanging nodes. The results show that the VEM is capable of handling this type of refinement and the phenomenon is clearly visible.

7. MODELING OPINION DYNAMICS

7.1 Introduction

The development of the following chapter was supported by the Oregon State University National Research Trainee-ship in Risk and Uncertainty Quantification in Marine Science (OSU NRT). This is a program funded by the National Science Foundation (NSF). The aim is to foster the training of trans-disciplinary professionals capable of ”identifying the response of marine systems to climate change and human pressures and to identify policy solutions for such responses”. As a requirement of the NRT program, students are placed into teams in which they would develop a Trans-disciplinary (TD) report based on collaborative research performed by the group. Then, each of the students will take part of the work done in this report and develop an interdisciplinary (ID) chapter in their dissertation.

The trans-disciplinary report was done in collaboration with the doctoral students Patricia Halleran from the OSU Department of Anthropology and Elena Tuttle from the OSU Department of Environmental Science. Our team periodically met with by Drew Gerkey, Dennis Albert, and Vrushali A. Bokil, who are the academic advisors of Patricia, Elena, and Sebastian, respectively, as well as Lorenzo Ciannelli, the OSU NRT representative. Our group studied cultural keystone species (CKS). These are species that are so important to a people’s culture that their extinction would collapse the people’s way of living. In order to protect these species and the people’s culture, we would list them as endangered. However, the criteria that are taken into account to list a species as endangered do not include its cultural importance. In order to make this change, we would require a vote from policy makers and have appropriate legislation passed. The aim of this chapter is in the development and study of mathematical models of deliberations between policy makers that incorporates mechanisms leading to a consensus in opinion or polarization. The models will aid in understanding the processes leading to passing legislation that would protect a

species based on their importance to a culture. Models in opinion dynamics will be the focal tool to study these debates.

There are two categories of models in opinion dynamics, namely space dependent and space independent models, see [10]. In spatial models the agents engaging in the debate are more likely to be influenced by the agents that are in close proximity to them as they themselves move within their community whereas in space independent models the position of the agents has no influence on the evolution of their opinions. Spatial models are effective in describing the opinion distribution in space of large communities since in this case individuals tend to update their beliefs based on the beliefs of the people that are in close proximity. Examples of these models are in [10, 35]. Many of these models, as in [35], are adapted from models of biological systems. In space independent models, agents seek to update their opinion based on the influence of another agent in a well-mixed setting meaning that they are willing to contact anyone regardless of spatial proximity. Examples of these types of models are those found in [9, 53].

There are major differences in the opinion dynamics in space dependent versus space independent models. The results in [10] show that the most likely long term behavior of space dependent models is that like-minded individuals will cluster and thus will only come in contact with individuals that hold similar opinions, what the authors call an echo-chamber and it leads to polarization. Whereas in [9], the authors show that if the agents are willing to update their status based on a random selection that disregards spatial location then the distribution of opinions will eventually arrive at a steady state, leading to a consensus.

In [9, 10] the authors begin by presenting a framework, or a theory, which can then be applied to construct space dependent and independent models. In our particular application we will assume that the policy decision makers, whose debate can lead to a possible policy change, seek to update their opinion based on the arguments they are presented with, rather than by the spatial location of those making the arguments and thus a space independent model suits our case best, where space is interpreted appropriately.

This chapter is organized as follows. We begin by exploring how the framework presented in [9, 10] can be used in the case of a debate where no policy decision maker is influenced by anyone other than decision makers within the debate. We make the appropriate definitions needed to derive a model for the temporal evolution of their opinion in the particular case of CKS. Once a model is derived we will study its dynamical behavior and then proceed to introduce an outside influence, that of pressure from the electorate. Finally, we conclude by exploring the amount of pressure that the communities need to exert in order for the debate to lead to policy change and consideration of the cultural importance of CKS when assessing the level of endangerment of these species.

In order to arrive at meaningful results, we will need to accept a series of assumptions aside the one we have already stated, namely that *spatial* proximity does not have an impact in debates among policy decision makers. We list these assumptions below:

(A1) There is equal probability of any individual being influenced by any other individual. This to say that the policy decision makers act in a professional manner and thus will always update their opinion based on the argument they are presented with rather than who presents the argument.

(A2) Every policy decision maker will update their opinion at the same time.

(A3) There are no closed minded policy decision makers, thus they are open to listening to the arguments of anyone else within the debate, or as the case may be, the electorate.

(A4) In [9] we are assured that the type of modeling, as mentioned before, will always lead to a consensus in the debate. We assume that the debate will be allowed to continue until a conclusion is reached.

The model that we present in this chapter is a system of ordinary differential equations. These cannot be solved exactly. The numerical experiments we present use Runge-Kutta discretizations in time. We note that this discretization strategy just like the VEM elsewhere in this

dissertation are constructed to enable discrete analogs of the continuous behavior In this sense, throughout this dissertation the discretization strategies that we pursue are all mimetic. In real world applications we are, usually, interested in the behavior of the exact solution. Having some guarantees that our approximations will mimic important continuum properties gives us a high degree of confidence when making decisions based on the discrete approximations.

7.2 Mathematical Background

In this chapter we will present some mathematical analysis of the existence and uniqueness of solutions to the ODE models that we will develop. These results will come as a consequence of the following Theorem, see [66, 85].

Theorem 7.20.1 *Let $\mathcal{D} \subset \mathbb{R}^N$ be a compact domain and $F : \mathcal{D} \times [0,T] \to \mathbb{R}^N$ be a Lipschitz function. i.e,*

$$\exists L > 0 \text{ such that } \forall t \in [0,t],\ \forall \boldsymbol{x}, \boldsymbol{y} \in \mathcal{D}, \quad \|F(\boldsymbol{x},t) - F(\boldsymbol{y},t)\| \leq L\|\boldsymbol{x} - \boldsymbol{y}\|. \tag{7.1}$$

Then, there exists a unique function $\boldsymbol{y} : [0,T] \to \mathcal{D}$ such that

$$\frac{d}{dt}\boldsymbol{y}(t) = F(\boldsymbol{y}(t), t). \tag{7.2}$$

From this theorem we can derive a corollary which will be key in studying the models that we will introduce.

Corollary 7.20.1 *Let $\mathcal{D} \subset \mathbb{R}^N$ be a compact domain and $F : \mathcal{D} \times [0,T] \to \mathbb{R}^N$. Further assume that*

$$\forall t \in [0,T],\ \forall 1 \leq i \leq N : \quad \frac{\partial}{\partial x_i} F \text{ exists and is continuous.} \tag{7.3}$$

Then, there exists a unique function $\boldsymbol{y} : [0, T] \to \mathbb{R}^N$ *such that*

$$\frac{d}{dt}\boldsymbol{y}(t) = F(\boldsymbol{y}(t), t). \tag{7.4}$$

Proof. Using the result in Theorem 7.20.1 we need only show that F is Lipschitz. Consider

$$\forall 1 \leq i \leq N : \quad L_i = \max_{\boldsymbol{x}\in\mathcal{D}, t\in[0,T]} \frac{\partial}{\partial x_i} F(\boldsymbol{x}, t). \tag{7.5}$$

These constants exist, by the Extreme Value Theorem, since the domain is compact. Define

$$L = \max\{L_1, \ldots, L_N\}. \tag{7.6}$$

Next, consider $t \in [0, T]$ and $\boldsymbol{x}, \boldsymbol{y} \in \mathcal{D}$. Then, by the Mean Value Theorem there must exist $\boldsymbol{w} \in \{\ell\boldsymbol{x} + (1 - \ell)\boldsymbol{y} : 0 \leq \ell \leq 1\}$ such that

$$\|F(\boldsymbol{x}, t) - F(\boldsymbol{y}, t)\| = \|\partial F(\boldsymbol{w}, t)(\boldsymbol{x} - \boldsymbol{y})\|, \tag{7.7}$$

where $\partial F(\boldsymbol{w}, t)$ is the Jacobian matrix at the point $(\boldsymbol{w}, t)$. Finally note that

$$\|\partial F(\boldsymbol{w}, t)(\boldsymbol{x} - \boldsymbol{y})\| \leq \|F(\boldsymbol{w}, t)\|\|\boldsymbol{x} - \boldsymbol{y}\| \leq NL\|\boldsymbol{x} - \boldsymbol{y}\|. \tag{7.8}$$

□

7.3 The Framework of a Debate Without Outside Influence

We begin by presenting the **attitude spectrum**, which is defined as the set:

$$\alpha = \{\pm 1, \pm 2\}. \tag{7.9}$$

Elements of of the attitude spectrum are called **attitudes**. In our framework, each policy decision maker will be assigned an attitude. The sign of an attitude symbolizes their opinion towards policy change, approving in case it is positive and disapproving in case it is negative. The absolute value of the attitude reflects the strength of their conviction. The set $\{-2,-1\}$ is called the **left side** of the attitude spectrum, $\{-1,+1\}$ is the **center** of the attitude spectrum, $\{+1,+2\}$ is the right side of the attitude spectrum, and $\{-2,+2\}$ is the **extremes** of the attitude spectrum. For a member of the debate, x, we denote by $A(x)$ their attitude. We will say that agent x has **strong left tendencies** or **strongly opposes** policy in the case that $A(x) = -2$, **slight 2 left tendency** or **slightly opposes** policy change if $A(x) = -1$. Analogously x **slightly favours** policy change or has **slight right tendency** when $A(x) = +1$, and finally x has **strong right tendency** or **strongly favours** policy change if $A(x) = +2$.

For $t \geq 0$ denote by $L_2(t), L_1(t), R_1(t)$, and $R_2(t)$ the proportion of policy decision makers who strongly oppose, slightly oppose, slightly favour and strongly favour policy change at time t respectively, i.e

$$L_2(t) = \frac{\ell_2(t)}{N}, \quad L_1(t) = \frac{\ell_1(t)}{N}, \quad R_1(t) = \frac{r_1(t)}{N}, \quad R_2(t) = \frac{r_2(t)}{N} \tag{7.10}$$

The value of N is the total number of legislators, whereas the values of $\ell_2(t), \ell_1(t), r_1(t)$ and $r_2(t)$ are the number of legislators that strongly oppose, slightly oppose, slightly favour and strongly favour policy change at time t. The quadruple $[L_2(t), L_1(t), R_1(t), R_2(t)]$ is referred to as the distribution of policy decision makers at time t. We may omit the dependence on time to ease the notation. Finally, the distribution of policy decision makers at time $t = 0$ provide the **initial conditions**.

We proceed to explain the mechanisms involved in opinion dynamics. At every time step every policy decision maker i, will telephone, with equal probability, a random policy decision maker, p. The attitude of i will be updated to reflect the influence of p as follows:

- If $A(i)$ and $A(p)$ have opposite signs then $A(i)$ will move one step towards the opposite

side of the attitude spectrum.

- If $A(i)$ and $A(p)$ have the same sign then there are three possible outcomes:

  (M1) If p has a stronger conviction than i then $A(i)$ will move one step towards $A(p)$.

  (M2) If the strength of the conviction of i and p agree, then with probability p_a individual i will amplify their attitude by moving one step towards more extreme conviction unless $A(i) = \pm 2$ in which case their opinion will be retained. If this is the case, then we say that i has **amplified their attitude** based on the opinion of p.

  (M3) With probability $1 - p_a$ individual i will not amplify their attitude moving one step towards the attitude of p. If these two agents share their conviction then this effect is nullified and i will retain their attitude.

This process takes place over a discrete length of time Δt. The model that we present results when we take the limit $\Delta t \to 0$.

The value p_a is the **probability of attitude amplification**. It is a measure of how trusting policy decision makers are of one another and thus we will refer to it as the **amplification parameter** or **degree of trust** of the policy decision makers. If $p_a = 0$, then we will say that the policy decision makers are **strongly distrusting** of each other. Note that in this case they never amplify their opinion based on that of others. Likewise, the case $p_a = 1$ will be referred to by saying that the policy decision makers are **strongly trusting** of each other, since this implies that the members of the debate will be swayed to amplify their opinion at every chance. In case $p_a = 0.5$, we say that is that of policy decision makers are **wary of each other**.

7.4 The Model for a Debate Without Outside Influence

The purpose of this section is to construct a dynamic mathematical model to describe the evolution through time of the distribution of policy decision makers into the components

L_2, L_1, R_1, R_2 previously described. We begin by exploring the evolution of the proportion of the policy decision makers that strongly oppose policy change i.e, L_2. In order to model the rate of change of L_2 we must study the interactions that generate loss and gain in attitudes.. If i is an individual that interacts with p then Table 7.1 summarizes the different scenarios in which the update of $A(i)$ will cause a change in the proportion L_2.

Interaction Type	Attitude of i	Attitude of p	Rate of Interaction
Loss $(\mathbf{L1})$	$A(i) = -2$	$A(p) = -1$, non-amplifying	$(1 - p_a)L_2L_1$
Loss $(\mathbf{L2})$	$A(i) = -2$	$A(p) = +1$	L_2R_1
Loss $(\mathbf{L3})$	$A(i) = -2$	$A(p) = +2$	L_2R_2
Gain $(\mathbf{G1})$	$A(i) = -1$	$A(p) = -2$	L_2L_1
Gain $(\mathbf{G2})$	$A(i) = -1$	$A(p) = -1$, with amplification	$p_aL_1L_1$

TABLE 7.1: Summary of the interactions between policy decision makers that will cause a change in the percentage of them that strongly oppose policy change.

The rate of change of L_2 is therefore,

$$\frac{dL_2}{dt} = (\mathbf{G1}) + (\mathbf{G2}) - ((\mathbf{L_1}) + (\mathbf{L_2}) + (\mathbf{L_3})) \,. \tag{7.11}$$

or equivalently

$$\frac{dL_2}{dt} = L_1 \left[L_2 + p_aL_1\right] - L_2 \left[(1 - p_a)L_1 + R_1 + R_2\right] . \tag{7.12}$$

Now we explore the temporal evolution of the percentage of policy decision makers with slight left tendency. We employ the same technique: we pick a policy decision maker i and have them interact with a random member of the debate p, Table 7.2 summarizes all the interactions that can make a change in L_1. The resulting non-linear differential equation is

$$\frac{dL_1}{dt} = L_1 \left[1 - L_2 - p_aL_1\right] + R_1 \left[L_1 + L_2\right] - L_1 \left[1 - (1 - p_a)L_1\right] . \tag{7.13}$$

This, again, is but the statement that the rate of change of L_1 is the sum of the rates of the gain

Interaction Type	Attitude of i	Attitude of p	Rate of Interaction
Loss	$A(i) = -1$	$A(p) = -2$	$L_2 L_1$
Loss	$A(i) = -1$	$A(p) = -1$, with amplification	$p_a L_1 L_1$
Loss	$A(i) = -1$	$A(p) = +1$	$L_1 R_1$
Loss	$A(i) = -1$	$A(p) = +2$	$L_1 R_2$
Gain	$A(i) = -2$	$A(p) = -1$, non-amplifying	$(1 - p_a) L_2 L_1$
Gain	$A(i) = +1$	$A(p) = -1$	$R_1 L_1$
Gain	$A(i) = +1$	$A(p) = -1$	$R_1 L_2$
Gain	$A(i) = -2$	$A(p) = +1$	$L_2 R_1$
Gain	$A(i) = -2$	$A(p) = +2$	$L_2 R_2$

TABLE 7.2: Summary of the interactions between policy decision makers that will cause a change in the percentage of them that slightly oppose policy change.

minus the sum of the rates of loss.

We now turn our attention to the percentage of policy decision makers that have slight right tendency. If the focal policy decision maker i interacts with another random agent labeled p then the possible changes in R_1 are summarized by Table 7.3 below A balance between rates of gain and rates of loss leads to the following non-linear ODE:

$$\frac{dR_1}{dt} = R_2 \left[1 - R_2 - p_a R_1\right] + L_1 \left[R_1 + R_2\right] - R_1 \left[1 - R_2 - p_a R_1\right]. \tag{7.14}$$

And, finally when regarding how the interaction between the policy decision makers i and p affects the value of the percentage of policy decision makers who strongly support policy change Table7.4 presents all the possibilities

Which leads to the following non-linear ODE:

$$\frac{dR_2}{dt} = R_1 \left[R_2 + p_a R_1\right] - R_2 \left[(1 - p_a) R_1 + L_1 + L_2\right]. \tag{7.15}$$

In summary, the evolution in the debate can be summarized bu the following non-linear ODE

Interaction Type	Attitude of i	Attitude of p	Rate of Interaction
Loss	$A(i) = +1$	$A(p) = +2$	$R_2 R_1$
Loss	$A(i) = +1$	$A(p) = +1$, with amplification	$p_a R_1 R_1$
Loss	$A(i) = +1$	$A(p) = -2$	$R_1 L_2$
Loss	$A(i) = -1$	$A(p) = +2$	$L_1 R_2$
Gain	$A(i) = +2$	$A(p) = +1$, non-amplifying	$(1 - p_a) R_2 R_1$
Gain	$A(i) = -1$	$A(p) = +1$	$L_1 R_1$
Gain	$A(i) = -1$	$A(p) = +2$	$L_1 R_2$
Gain	$A(i) = +2$	$A(p) = -1$	$R_2 L_1$
Gain	$A(i) = +2$	$A(p) = -2$	$R_2 L_2$

TABLE 7.3: Summary of the interactions between policy decision makers that will cause a change in the percentage of them that slightly favor policy change.

Interaction Type	Attitude of i	Attitude of p	Rate of Interaction
Loss	$A(i) = +2$	$A(p) = +1$, non-amplifying	$(1 - p_a) R_2 R_1$
Loss	$A(i) = +2$	$A(p) = -1$	$R_2 L_1$
Loss	$A(i) = +2$	$A(p) = -2$	$R_2 L_2$
Gain	$A(i) = +1$	$A(p) = +2$	$R_1 R_2$
Gain	$A(i) = +1$	$A(p) = +1$, with amplification	$p_a R_1 R_1$

TABLE 7.4: Summary of the interactions between policy decision makers that will cause a change in the percentage of them that strongly favor policy change.

system:

$$\frac{L_2}{dt} = L_1 \left[L_2 + p_a L_1 \right] - L_2 \left[(1 - p_a) L_1 + R_1 + R_2 \right], \tag{7.16a}$$

$$\frac{dL_1}{dt} = L_1 \left[1 - L_2 - p_a L_1 \right] + R_1 \left[L_1 + L_2 \right] - L_1 \left[1 - (1 - p_a) L_1 \right], \tag{7.16b}$$

$$\frac{dR_1}{dt} = R_2 \left[1 - R_2 - p_a R_1 \right] + L_1 \left[R_1 + R_2 \right] - R_1 \left[1 - R_2 - p_a R_1 \right], \tag{7.16c}$$

$$\frac{dR_2}{dt} = R_1 \left[R_2 + p_a R_1 \right] - R_2 \left[(1 - p_a) R_1 + L_1 + L_2 \right]. \tag{7.16d}$$

We note that the solution to this system exists and is unique. We present this result in the following theorem:

Theorem 7.40.1 *There exists a unique* $\boldsymbol{y} : [0, T] \to [0, 1]^4$ *such that*

$$\frac{\partial}{\partial t}\boldsymbol{y}(t) = F(\boldsymbol{y}(t), t). \tag{7.17}$$

Where

$$\forall \boldsymbol{y} = (R_1, R_2, L_1, L_2) \in [0, 1]^4,\ \forall t \in [0, T]:$$

$$F(\boldsymbol{y}, t) = \begin{pmatrix} L_1\left[L_2 + p_a L_1\right] - L_2\left[(1 - p_a)L_1 + R_1 + R_2\right] \\ R_2\left[1 - R_2 - p_a R_1\right] + L_1\left[R_1 + R_2\right] - R_1\left[1 - R_2 - p_a R_1\right] \\ R_2\left[1 - R_2 - p_a R_1\right] + L_1\left[R_1 + R_2\right] - R_1 \\ R_1\left[R_2 + p_a R_1\right] - R_2\left[(1 - p_a)R_1 + L_1 + L_2\right] \end{pmatrix} \tag{7.18}$$

Proof. Note that the components of F are polynomials which implies that they are infinitely differentiable and all of their derivatives are continuous. This result follows from Corollary 7.20.1. □

We will refer to this system as the **model for a debate without outside influence** or simply as the model if it is clear from context. We say that the **debate reaches a conclusion** if there exists a moment $T > 0$ for which the distribution of policy decision makers stays constant past that moment. In other words a conclusion is a steady state or equilibrium of the dynamical system. This is to say that for any $t \geq T$ the rates of change to the distribution of policy decision makers is null, or

$$\frac{dL_2}{dt} = \frac{dL_1}{dt} = \frac{dR_1}{dt} = \frac{dR_2}{dt} = 0. \tag{7.19}$$

In this case, we will say that the **conclusion of the debate** is the constant distribution of the attitudes of the policy decision makers, the time independent quadruple. Moreover, if the conclusion

of a debate has more policy decision makers whose attitude lies in the left side of the spectrum we will that the **left won the debate**. Similarly, if said distribution has more policy decision makers in the right side of the spectrum we will say that the **right won the debate**. If there are the same number of policy decision makers on the left and the right then we will say that **no side won the debate**. If $[0, 0, 0, 1]$ is the conclusion of the debate then the debate reached a **positive consensus** and similarly if it is $[1, 0, 0, 0]$ then the debate reached a **negative consensus**. In [9] the authors provide numerical evidence to support the claim that *open debates without outside influence reach a conclusion regardless of the value of the amplification parameter nor the initial conditions*. We will focus on studying when the conclusion is a consensus.

7.5 Numerical Sensitivity Analysis of the Debate Without Outside Influence

In this section we are interested in exploring how the initial conditions and the amplification parameter influence the eventual consensus. To do this we present a series of numerical experiments. All computations were done using the ode45 function from the ODE suite of Matlab.

7.51 The Balanced Case

The first experiment that we will perform will explore what happens when the initial conditions are **balanced**, meaning that the same number of policy decision makers hold a particular attitude as those that hold the symmetric opposite attitude. Generally,

$$L_2(0) + L_1(0) = R_1(0) + R_2(0). \tag{7.20}$$

We will use the initial conditions $[0.25, 0.25, 0.25, 0.25]$. We begin with exploring the case that the policy decision makers are highly distrusting of one another.

As shown in Figure 7.1 the case where the amplification parameter p_a is zero leads to an endless debate where no consensus is reached, although the extremes of the attitude spectrum

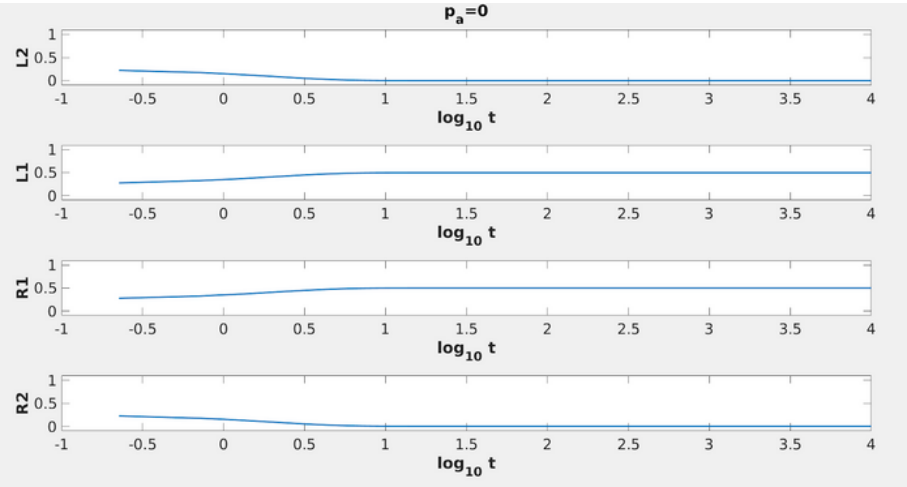

FIGURE 7.1: The evolution of the distribution of policy decision makers with balanced initial conditions in the case that they are strongly distrusting of each other, the conclusion [0,0.5,0.5,0] is reached, no side won the debate.

are not present, all the policy decision makers continue their debate from the center. Now let us explore what happens if the policy decision makers are wary of each other. As is presented in Figure 7.2, again, no consensus arises but although the center of the attitude spectrum lost some policy decision makers, they now take part in the extreme. Finally we explore what happens when the policy decision makers strongly trust each other. As Figure 7.3 shows, although each policy decision maker will continue to update their opinion, the number of people holding each attitude will remain the same. The conclusion is that the more trusting the agents are to one another, the closer the debate will be to an equilibrium where one fourth of all policy decision makers will have each of the four attitudes. Further numerical experimentation shows that if the initial conditions are balanced then consensus does not arise.

7.52 The Slightly Unbalanced Case

In this section, we explore the consequences of a slight perturbation of the balanced case. Note that if we permute the roles of L_2 and R_2 and also the roles of L_1 and R_1 then the model for an open debate without outside influence remains unaltered. This implies that when permuting the roles, the policy decision makers who strongly oppose and strongly favor and those who slightly

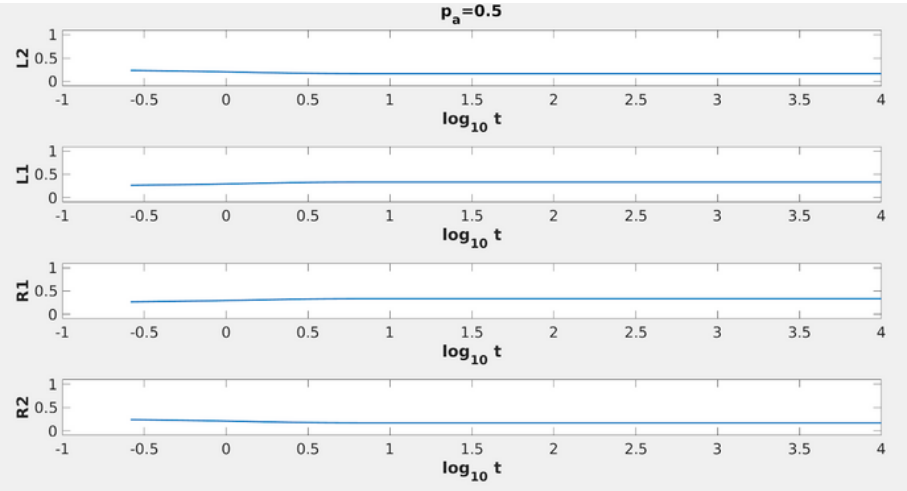

FIGURE 7.2: The evolution of the distribution of policy decision makers with balanced initial conditions in the case that they are wary of each other, the conclusion $[1/6, 1/3, 1/3, 1/6]$ is reached and no side won the debate.

oppose and slightly favor policy change makes no difference regarding the evolution in time of the distribution of policy decision makers. A moment's thought reveals that an imbalance to the initial conditions towards one side or another of the attitude spectrum results in identical results.

The **unbalanced case** will have the initial conditions

$$[L_2(0), L_1(0), R_1(0), R_2(0)] = [0.26, 0.25, 0.25, 0.24]. \tag{7.21}$$

We begin with exploring the results of the debate when the policy decision makers are highly distrusting of each other. As Figure 7.4 shows, consensus is not reached but unlike the balanced case one of the sides does win the debate, although not by a large margin. Now let us explore what happens when the policy decision makers strongly trust each other. In this case we see, in Figure 7.5, that the slight initial advantage tips the scale to the left and every policy decision maker eventually agrees with the initial majority. Let us explore what the level of trust must be in order for the policy decision makers to arrive at a consensus. To do this, we treat p_a as a bifurcation parameter and perform a numerical bifurcation analysis. We mesh this parameter and plot it against the equilibrial or steady state values of L_2, the proportion of policy decision makers

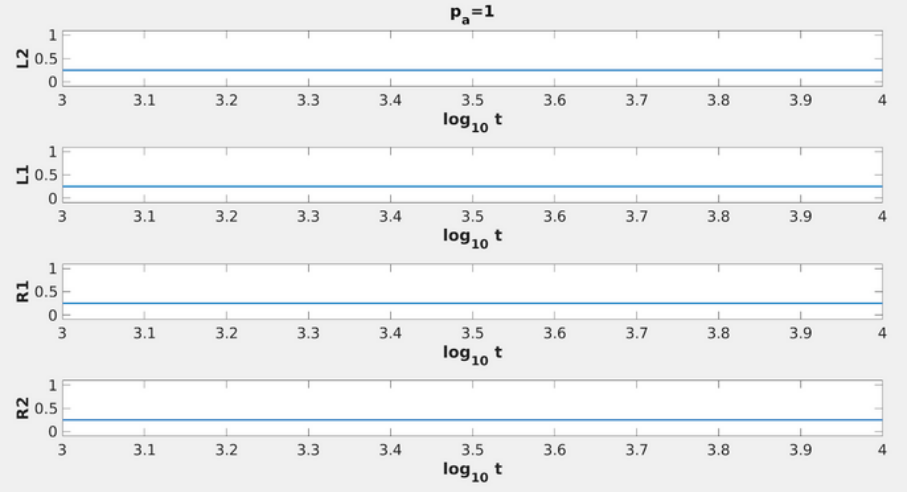

FIGURE 7.3: The evolution of the distribution of policy decision makers with balanced initial conditions in the case that they strongly trust of each other, the conclusion $[0.25, 0.25, 0.25, 0.25]$ is reached, and no side won the debate .

that strongly oppose policy change. To do this we mesh the amplification parameter p_a and plot it against the value of the policy decision makers that are strongly opposed to policy change in the conclusion of the debate. An interesting observation from Figure 7.6 is that it is only required for less than 10% of the policy decision makers to amplify their views based on their level of trust in their fellow policy decision makers to make the slight initial imbalance to tip the scale towards the side that had the initial advantage. Further numerical experimentation reveals that this behavior is the norm. Debates without outside influence generally conclude with a consensus that favors the side with the initial advantage, as in the balanced case unless the policy decision makers strongly distrust each other, even then the conclusion favors the side with the initial majority.

7.6 Framework for a Debate With Outside Influence

We now introduce an outside influence into the debate from the electorate and their supporters who will be represented by I. We will be working in the same framework as before, our

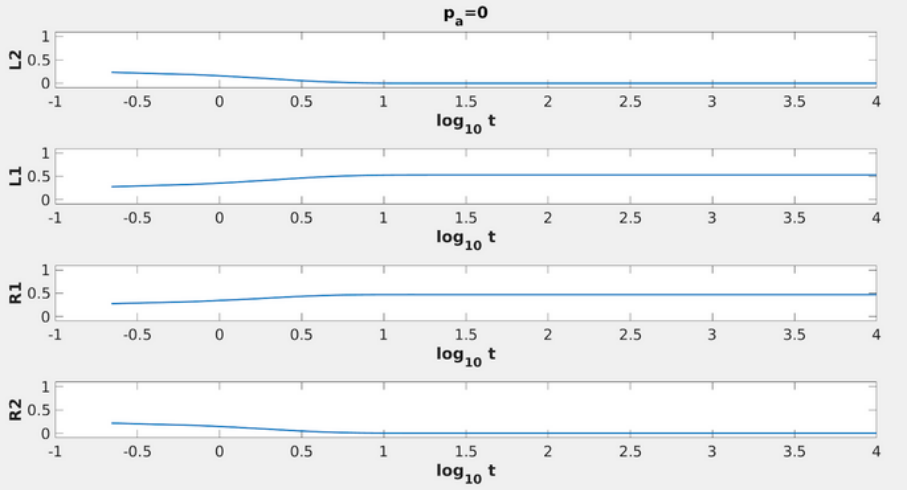

FIGURE 7.4: The evolution of the distribution of policy decision makers with unbalanced initial conditions in the case that they strongly distrust each other. The conclusion $[0, 0.53, 0.47, 0]$ is reached and the left wins the debate.

attitude spectrum is

$$\alpha = \{\pm 1, \pm 2\}. \tag{7.22}$$

The proportion of policy decision makers with each of the four attitudes will, as before, be denoted L_2, L_1, R_1 and R_2. However, the electorate I will be introduced with $A(I) = +2$. We will further assume that I is firm in their belief and cannot be influenced by policy decision makers within the debate. In a similar manner as before at every time step each policy decision maker, i, chooses an agent, p, and updates their attitude based on the guidelines presented in Section 7.3. The difference in this model from the previous one is that with probability p_I the policy decision maker i will interact with the electorate I. This implies that with probability $1 - p_I$ the policy decision maker i will interact with another within the debate. The parameter p_I will be referred to as the **social activism parameter**, and it is a measure of the amount of pressure the policy decision makers in the debate are subjected to by the electorate. The social activism parameter can also be interpreted as the proportion of policy decision makers that, at every time step, will be influenced by the social activists.

To explore the evolution in time of the distribution of policy decision makers we will use

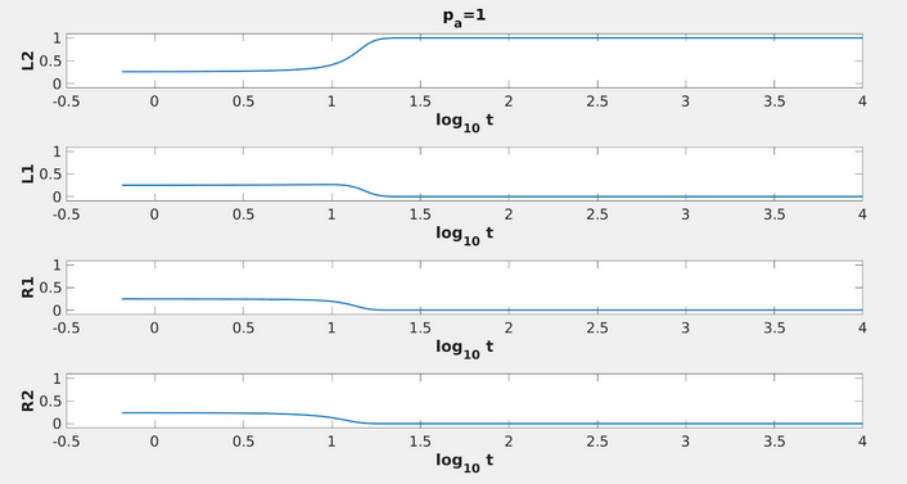

FIGURE 7.5: The evolution of the distribution of policy decision makers with unbalanced initial conditions in the case that they strongly trust each other. A negative consensus is reached.

the same strategy as before, looking for the rates of gain and loss of the different attitudes within the policy decision makers in the debate. Since this strategy was presented in Section 7.3 we will present the four tables and quickly jump to the model for a debate with outside influence. In each table the focal policy decision maker i seeks to update their opinion based on the agent p. A

Interaction Type	attitude of i	Attitude of p	Rate of Interaction
Loss	$A(i) = -2$	$A(p) = -1$, non-amplifying	$(1 - p_a)(1 - p_I)R_2R_1$
Loss	$A(i) = -2$	$A(p) = +1$	$(1 - p_I)L_2R_1$
Loss	$A(i) = -2$	$A(p) = +2$	$(1 - p_I)L_2R_2$
Loss	$A(i) = -2$	$p = I$	p_IL_2
Gain	$A(i) = -1$	$A(p) = -2$	$(1 - p_I)L_2L_1$
Gain	$A(i) = -1$	$A(p) = -1$, with amplification	$(1 - p_I)p_aL_1L_1$

TABLE 7.5: The interactions that, at each instant, affect the number of policy decision makers with strong left tendency.

balance statement based on Table 7.5 will yield the following statement for the rate of change L_2:

$$\frac{dL_2}{dt} = (1 - p_I)L_1 \left[L_2 + p_aL_1\right] - (1 - p_I)L_2 \left[(1 - p_a)L_1 + R_1 + R_2\right] - p_IL_2. \tag{7.23}$$

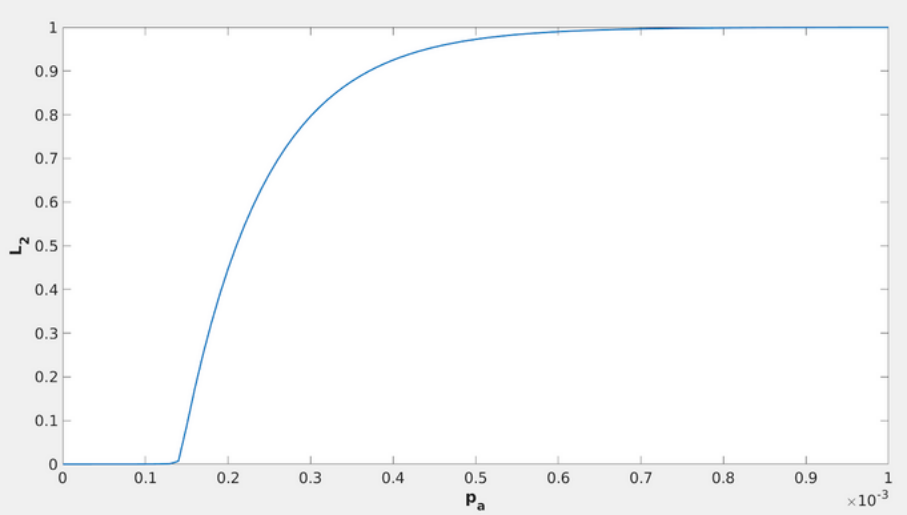

FIGURE 7.6: The equilibrial proportion of policy decision makers that strongly oppose policy change at the conclusion of a debate with unbalanced initial conditions plotted against the amplification parameter.

According to Table 7.6 the rate of change of L_1 is given by the non-linear ODE:

$$\frac{dL_1}{dt} = p_I L_2 + (1-p_I)\left[L_2R_2 + 2L_2R_1 + R_1L_1 + (1-p_a)L_2L_1\right] - \\ - (1-p_I)L_1\left[L_2 + p_aL_1 + R_1 + R_2\right] - p_IL_1. \quad (7.24)$$

The analysis in Table 7.7 leads to following non-linear ODE for the rate of change of R_1.

$$\frac{dR_1}{dt} = p_I L_1 + (1-p_I)\left[R_2L_2 + 2R_2L_1 + L_1R_1 + (1-p_a)L_2L_1\right] - \\ - (1-p_I)R_1\left[R_2 + p_aR_1 + L_1 + L_2\right] - p_IR_1. \quad (7.25)$$

By Table 7.8 the final non-linear ODE in our system is:

$$\frac{dR_2}{dt} = p_I R_1 + (1-p_I)R_1\left[R_2 + p_aR_1\right] - (1-p_I)R_2\left[(1-p_a)R_2 + L_1 + L_2\right]. \quad (7.26)$$

In summary, the model for the debate with outside influence is the coupling of equations (7.23),

Interaction Type	Attitude of i	Attitude of p	Rate of Interaction
Loss	$A(i) = -1$	$A(p) = -2$	$(1 - p_I)L_2L_1$
Loss	$A(i) = -1$	$A(p) = -1$, with amplification	$p_a(1 - p_I)L_1L_1$
Loss	$A(i) = -1$	$A(p) = +1$	$(1 - p_I)L_1R_1$
Loss	$A(i) = -1$	$A(p) = +2$	$(1 - p_I)L_1R_2$
Loss	$A(i) = -1$	$p = I$	p_IL_1
Gain	$A(i) = -2$	$A(p) = -1$, non-amplifying	$(1 - p_a)L_2L_1$
Gain	$A(i) = +1$	$A(p) = -1$	$(1 - p_I)R_1L_1$
Gain	$A(i) = +1$	$A(p) = -2$	$(1 - p_I)R_1L_2$
Gain	$A(i) = -2$	$A(p) = +2$	$(1 - p_I)L_2R_2$
Gain	$A(i) = -2$	$p = I$	p_IL_2

TABLE 7.6: The interactions that, at each instant, affect the number of policy decision makers with slight left tendency.

(7.24), (7.25) and (7.26). It is important to note that in the case $p_I = 0$, this model reduces to that of a debate without outside influence, as expected. As before we can show that the solution to this model exist and is unique. We present this result in the following theorem:

Theorem 7.60.1 *There exists a unique* $\boldsymbol{y} : [0, T] \to [0, 1]^4$ *such that*

$$\frac{\partial}{\partial t}\boldsymbol{y}(t) = F(\boldsymbol{y}(t), t), \tag{7.27}$$

where each of the components of F *are the right-hand side of equations* (7.23)*,*(7.24)*,*(7.25) *and* (7.26)*.*

Proof. The components of F are polynomials. Therefore they satisfy the hypothesis of Corollary 7.20.1. □

An immediate conclusion about our new model is that $[1, 0, 0, 0]$ is no longer a steady state

Interaction Type	Attitude of i	Attitude of p	Rate of Interaction
Loss	$A(i) = +1$	$A(p) = +2$	$(1 - p_I)R_2R_1$
Loss	$A(i) = +1$	$A(p) = +1$, with amplification	$p_a(1 - p_I)R_1R_1$
Loss	$A(i) = +1$	$A(p) = -1$	$(1 - p_I)R_1L_1$
Loss	$A(i) = +1$	$A(p) = -2$	$(1 - p_I)R_1L_2$
Loss	$A(i) = +1$	$p = I$	p_IR_1
Gain	$A(i) = +2$	$A(p) = +1$, non-amplifying	$(1 - p_a)R_2R_1$
Gain	$A(i) = -1$	$A(p) = +1$	$(1 - p_I)L_1R_1$
Gain	$A(i) = -1$	$A(p) = +12$	$(1 - p_I)R_2L_1$
Gain	$A(i) = +2$	$A(p) = -1$	$(1 - p_I)R_2L_1$
Gain	$A(i) = +2$	$A(p) = -2$	$(1 - p_I)R_2L_2L_1$
Gain	$A(i) = -1$	$p = I$	p_IL_1

TABLE 7.7: The interactions that, at each instant, affect the number of policy decision makers that slightly favor policy change.

of this dynamical system since in this case

$$\frac{dL_2}{dt} = -p_I. \tag{7.28}$$

This implies that the conclusion of the debate will never be a negative consensus. Should consensus arise it shall be a positive one.

Remark 7 *We note that more advanced models for the influence of the electorate over the point of view of legislators can be studied more in depth using the the framework of optimal control theory [18].*

Interaction Type	Attitude of i	Attitude of p	Rate of Interaction
Loss	$A(i) = +2$	$A(p) = +1$ non-amplifying	$(1 - p_a)(1 - p_I)R_2R_1$
Loss	$A(i) = +2$	$A(p) = -1$	$(1 - p_I)R_2L_1$
Loss	$A(i) = +2$	$A(p) = -2$	$(1 - p_I)R_2L_2$
Gain	$A(i) = +1$	$p = I$	p_IR_1
Gain	$A(i) = +1$	$A(p) = +2$	$(1 - p_I)R_1R_2$
Gain	$A(i) = +1$	$A(p) = +1$ with amplification	$(1 - p_I)p_aR_1R_1$

TABLE 7.8: The interactions that affect, at each time step, the number of policy decision makers that strongly favor policy change.

7.7 Influence in the Worst Case Scenario

The purpose of this section is to numerically explore the proportion of policy decision makers that need to be influenced by the indigenous communities in order for the debate to arrive at a positive consensus. We will do this under *worst case scenario conditions*, this is to say that throughout this section the initial conditions are $[1, 0, 0, 0]$, meaning that all the policy decision makers strongly oppose policy change initially. We proceed to perform a numerical two parameter analysis with the parameters p_a and p_I. To do this we mesh the equilibrial amplification and the social influence parameters and for each pair we find the proportion, at the conclusion of the debate, of policy decision makers that have strong right tendency. We observe in Figure 7.7, that there are two distinct regions one where positive consensus is reached and another where the value of the proportion of policy decision makers with strong right tendency is essentially zero. We proceed to explore how the degree of trust of the policy decision makers influences the conclusion of the debate. To do this, we will vary the social influence parameter while keeping the amplification parameter constant, i.e, we conduct a one parameter bifurcation analysis by fixing the value of the other parameter. Looking at Figure 7.8, we can verify two important behaviors of our model for debates with outside influence. One is that there is a well-defined **bifurcation value of** p_I that separates the region in which positive consensus arise and where it does not. The second

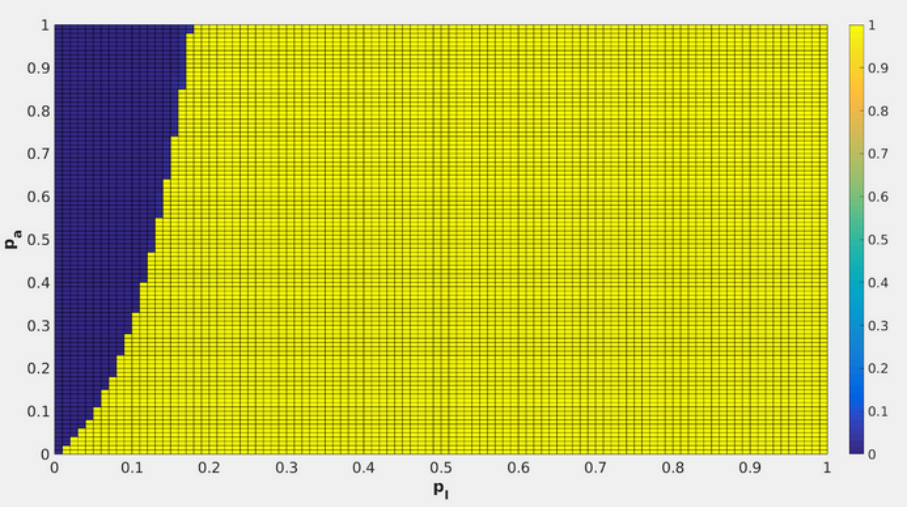

FIGURE 7.7: A numerical bifurcation plot. The horizontal axis represents the social activism parameter, the vertical axis the amplification parameter and the color represents the value, at the conclusion of the debate, of the equilibrial proportion of policy decision makers that strongly favor policy change.

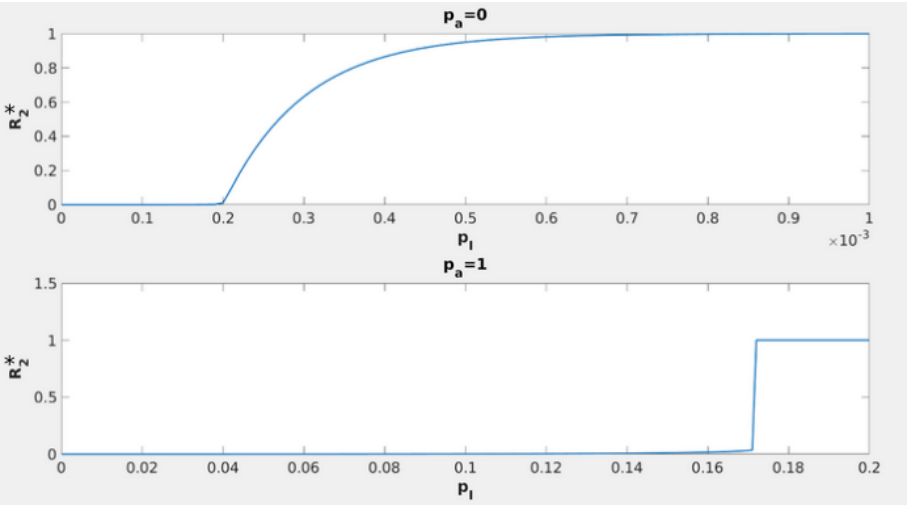

FIGURE 7.8: Numerical bifurcation plot of the social influence parameter in the horizontal axis and the equilibrial value of the proportion of policy decision makers with strong right tendency in the vertical axis under worst case scenario conditions. The top graph represents the case in which policy decision makers strongly distrust each other while the lower graph shows the case in which they strongly trust each other.

is that this value is dependent upon p_a. In Figure 7.9, the bifurcation value of the social influence

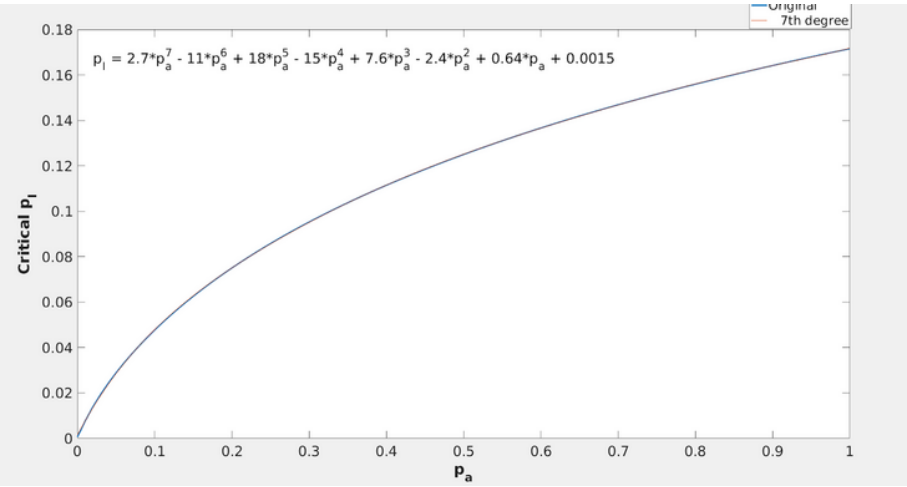

FIGURE 7.9: Plot of the amplification parameter in the horizontal axis and the critical value of the social activism parameter that separates the region where positive consensus is the conclusion of the debate and the region where it is not under worst case scenario conditions. A best fit 7th degree polynomial is also presented. This curve is a fit of the boundary between the two colored regions in Figure 7.7

parameter that separates the two regions presented in Figure 7.9 is evidenced. An immediate observation that we can draw is that the bifurcation value of the social influence parameter depends monotonically on the degree of trust of the policy decision makers in the debate. This is to say that when all of the policy decision makers initially oppose policy change then the more they trust their fellow policy decision makers the stronger the pressure from the electorate needs to be in order to sway their opinion.

Another conclusion we can draw from Figure 7.9, is that if $p_I = 0.1716$ then regardless of the degree of trust of the policy decision makers the debate will always end in a positive consensus.

7.8 Mathematical Modeling and Protecting CKS

In this section, we will present ideas about how we can use mathematical modeling to create strategies and influence policies to protect CKS. The process of arriving at the mathematical

model requires a collaboration between a team of diverse scientists including anthropologists, ecological and environmental scientists, mathematical modelers and computational scientist. A possible series of steps in arriving at a mathematical model to inform policy decision making for CKS are as follows:

1. **Identify CKS:** Information about these species tends to be held by indigenous communities. Unfortunately, the history of the United States demonstrates a disregard for the cultural values and traditions of the native tribes. These communities have been devastated by famines, plagues, sickness and even genocide. As a response to these injustices indigenous communities have become distrustful of the general population. Therefore, in identifying CKS we would need the help of an anthropologist with specialty in communicating with the American indigenous communities. The anthropologist will be crucial in generating trust between our team and the communities that will be impacted by the extinction of a CKS.

2. **Design strategies to protect the CKS:** Once the CKS are identified then we need to study the factors that are contributing to their extinction. The reasons may be convoluted. They could be affected by pollution, deforestation, invasive species or their source of food may be disappearing. Often times addressing these species are affected involves the consideration of multiple factors. Here, the expertise of a team of environmental scientist is best fit to this task.

3. **Draft legislation:** The best avenue to enforce the strategies designed by our team in step 2 are the governmental institutions. Thus, we need to draft legislation using legal language in order to guarantee enforcement by system of courts. This can be done at the municipal, state or federal level depending on the scope of our strategies and the availability of resources. We also need to make sure that the indigenous communities agree to these laws. A collaboration between a team of lawyers to draft the legal language, a team of environmental scientist to convey the strategies and a team of anthropologists to communicate the legislation back to the communities and get feedback.

4. **Design a simulation of debates between policy makers:** A bill will only become law after a vote from policy decision makers. However, their deliberation can, to a degree, be predicted using mathematical modeling First, we need to figure out the initial conditions. This is to say that we need to know where each of the policy decision makers stand with respect to policy change. There are political analysts that study the behavior of these politicians and follow their decisions closely. Then, we need to know how strongly they are influenced by other policy decision makers, an estimate for p_I, to arrive at an estimate for p_a. And, finally we need to estimate how much influence to pass legislation will come from the electorate. For this task we can refer back to our team of anthropologists or sociologists. With this information we need to design a model for the debate between the policy decision makers. Our models took the form of a system of non-linear ODEs. More complete models may use a continuum to model the attitudes of the legislators and stochastic processes to account for the uncertainty that may arise. Then, we need to come up with compatible discretizations of the models. The design and discretization of the model will be the job for a team of mathematicians. Finally, the implementation of the discretization will likely need to be done in a high performance cluster. Engineers and computer scientist may be the best fit to create a robust parallel code.

5. **Influence the electorate:** In the case that our simulations show that legislation is unlikely to pass, then we need to influence the electorate to pressure the legislators. We will need a publicity plan that will convey to the public that we will all benefit from this legislation in one way or another. This step is best suited by a team of publicists, artist and social communicators.

6. **Poll the electorate**: After our publicity campaign we need to assess its effectiveness. This is done to update the parameters of our models. We recommend a team of statisticians and mathematicians for this task.

7.9 Conclusions

In this chapter, we explored how we can use mathematical modeling to help protect CKS. Change will only be enforced if legislation is passed. We can use mathematical modeling to predict the outcomes of debates between policy decision makers. We have presented two models one in which the electorate do not pressure the legislators and another in which they do. These two models are called the models for debates without and with outside influence respectively. From the analysis in [9] we are assured that debates without outside influence will always arrive at a conclusion. Although we have no guarantee that the time to conclusion will be reasonable, this question is left for future research. A reasonable starting point may lie in the following references [91, 92]

From the analysis presented in Section 7.5, we find that the conclusion is strongly dependent upon the initial conditions and the amplification parameter. If the initial conditions of the debate are balanced, meaning that the same number of policy decision makers hold a particular attitude as those that hold the symmetric opposite attitude, then although a conclusion to the debate will arise, it will never be a consensus. Moreover, no side will win the debate. The outcome of debates with balanced initial conditions will differ depending on the degree of trust among the policy decision makers. If they are strongly distrusting of one another then, as shown in Figure 7.1, the conclusion will favor the center of the attitude spectrum. This is due to the fact that policy decision makers are not likely to amplify their views based on that of others within the debate. As the degree of trust increases, however, there will be policy decision makers whose attitudes lie in the extreme end of the spectrum, testament to which are the results presented in Figures 7.2,7.3.

If the initial conditions are unbalanced, meaning that there is an initial majority, however slight, between the policy decision makers whose attitudes lie on the left side of the spectrum and those on the right, then the conclusion tends to favor the initial majority. A major difference between the balanced and unbalanced case is that the unbalanced case will, almost always, lead

to the conclusion of the debate being a consensus. This depends on the degree of trust among the policy decision makers. This was evidenced by the fact that in Figure 7.4, debates with unbalanced initial conditions where the policy decision makers strongly distrust each other lead to a conclusion that was not a consensus, whereas in Figure 7.5, when they are strongly trusting of each other the debate terminated with a consensus. In each case the conclusion favored the initial majority. Further exploration on the degree of trust that is necessary to arrive at consensus showed that if the policy decision makers are willing to amplify their attitude based on that of others at least 0.1% of the time then consensus arises. This was the take away from Figure 7.6, and thus when there is an initial majority very little trust is necessary to tip the scale in its favor.

Finally, when in the debate, we include the pressure from indigenous communities then the first conclusion that we arrive at is that the debate will never end with a negative consensus. If consensus arises then it will be a positive consensus. In order to find some estimates as to what proportion of policy decision makers need to be influenced in order for positive consensus to be the conclusion of the debate we need to consider the worst case scenario conditions, when initially all of the policy decision makers strongly oppose policy change. Should positive consensus arise under the worst case scenario conditions then we can be assured that the conclusion of the debate will be the same under any initial conditions.

Under the worst case scenario conditions we find, in Figure 7.7, that there are two important regions of the amplification and social activism parameters, one for which positive consensus will arise and one where it will not. Moreover from Figure 7.8, we learn that the effect that these two parameters have on the number of policy decision makers that strongly support policy change at the conclusion of the debate is not gradual, rather, for every degree of trust there exists a critical value of the social activism parameter with the property that any debate with a lower one will lead to no consensus and any debate with a larger one will arrive at a positive consensus. In Figure 7.9, we find that this dependence can be computed with an error of less than 0.001 by the seventh

degree polynomial

$$p_I = 2.7p_a^7 - 11p_a^6 - 15p_a^4 + 7.6p_a^3 - 2.4p_a^2 + 0.64p_a + 0.0015. \tag{7.29}$$

This polynomial is monotone and therefore the higher the degree of trust among the policy decision makers the higher the proportion of them that need to be influenced by the indigenous communities in order to lead to a positive consensus. Moreover, if the measure of the degree of trust is not available then, as a rule of thumb, if the we can influence at least 17.16% of the policy decision makers then the debate will end with a positive consensus in any circumstance.

Finally, in Section 7.8, we present a set of ideas regarding how we can use models like the one developed in the chapter to drive policy change.

8. CONCLUSIONS

In this thesis, we considered the numerical discretization of mathematical models in MHD. As discussed in the introduction, this is an important area of research with applications that have broad impacts to society. We also considered an application of mathematical modeling and simulation to the social sciences, as part of a trans-disciplinary research project involving the intersection of conservation ecology, public policy and the mathematical sciences.

In this chapter, we outline the major novel contributions presented in this dissertation. In Chapters 3.,4. we prescribed the flow of a magnetized fluid (MHD kinematics) and derived a model for the evolution of the electric and magnetic fields from Maxwell's equations. This was done in two and three dimensions respectively. A variational formulation of this model revealed the chain of spaces.

$$H(\mathbf{rot};\Omega) \xrightarrow{\mathbf{rot}} H(\mathrm{div};\Omega) \xrightarrow{\mathrm{div}} L^2(\Omega). \tag{8.1}$$

In developing a VEM we first defined a discrete version of these spaces. Their discrete versions also form a chain:

$$\mathcal{V}_h \xrightarrow{\mathbf{rot}} \mathcal{E}_h \xrightarrow{\mathrm{div}} \mathcal{P}_h. \tag{8.2}$$

These spaces were introduced in [16]. We can define Fortin projectors making the following diagram commute

$$\begin{array}{ccccc} H(\mathbf{rot};\Omega) & \xrightarrow{\mathbf{rot}} & H(\mathrm{div};\Omega) & \xrightarrow{\mathrm{div}} & L^2(\Omega) \\ \downarrow{\scriptstyle \mathcal{I}^{\mathcal{V}_h}} & & \downarrow{\scriptstyle \mathcal{I}^{\mathcal{E}_h}} & & \downarrow{\scriptstyle \mathcal{I}^{\mathcal{P}_h}} \\ \mathcal{V}_h & \xrightarrow{\mathbf{rot}} & \mathcal{E}_h & \xrightarrow{\mathrm{div}} & \mathcal{P}_h \end{array} \tag{8.3}$$

This commuting property is the central result needed to prove that the discrete approximations

to the magnetic field are divergence free. In order to approximate the inner product terms in the variational formulation we define inner products that are equivalent to those associated with their continuous counterparts. Following the framework laid out in [16], we do this by defining L^2-orthogonal projections onto polynomial spaces. Unfortunately this projector is not computable in $\mathcal{V}_h$. A novel aspect in the formulation presented is that this inner product is constructed via an oblique projector.

In Chapter 5., we dropped the assumption that the flow was known to us and developed a model that predicts the velocity field as well as the pressure of a magnetized fluid. This model was coupled with our previous model for a complete simulation of a magnetized fluid that includes both the electromagnetic and fluid mechanical phenomena. In developing a VEM we considered the two dimensional case. The variational formulation of this coupled model reveals two chains of spaces, the first is associated with the electromagnetics. This chain is (8.1) which we approximate using the same spaces presented in (8.2). The second is the chain associated with the fluid flow and is given by

$$\left[H^1(\Omega)\right]^2 \xrightarrow{\text{div}} L^2(\Omega). \tag{8.4}$$

We use $\mathcal{P}_h$ to approximate $L^2(\Omega)$ and introduce the space $\mathcal{TV}_h$ forming the chain.

$$\mathcal{TV}_h \xrightarrow{\text{div}} \mathcal{P}_h. \tag{8.5}$$

These spaces are borrowed from [90]. Similar to the case presented in the spaces in (8.2), we develop an inner product in $\mathcal{TV}_h$ that is equivalent to its continuous counterpart. These spaces form a inf-sup stable stokes pair. The coupling in this system is non-linear. Thus, we develop a linearization strategy. We can show that this strategy will provide approximations to the magnetic field that remain divergence-free.

For all of the VEMs that we developed throughout this dissertation we were able to obtain

important energy estimates that attest to their stability. Simulations based on these methods will, at each time step, solve one or more linear systems. We were able to identify these as well-posed saddle-point problems.

The series of simulations that we presented provide evidence about the rate of convergence of the electric and magnetic fields, they are quadratic and linear respectively. We show that some of the energy estimates do in fact hold. We also provide a model for magnetic reconnection. The computational domain is the square $[-1, 1] \times [-1, 1]$. The phenomenon happens near the center of the domain. To show the versatility of the VEM we use an adaptively refined mesh to provide higher resolution in this region. This mesh introduces a series of hanging nodes which would make it difficult for other methods to provide formulations. However, this mesh agrees with the assumptions we made on the mesh and the VEM provides approximations without any complications.

This work presented is only meant to be a first step into research in this area and leaves a series of open questions that we document in what follows.

(Q1) How to we develop and implement efficient preconditioners? As we mentioned before, at each time step a linear system needs to be solved. This is a rather slow process without a preconditioner to speed up an iterative solver like GMRES. This result can be leveraged to come up with efficient preconditioner following the framework laid out in [69]. This was done for a similar MHD system in [70] using a Picard fixed point iteration as the choice of linearization. Efficient implementation of this preconditioner will require a generalization of mass lumping. While it is unclear how this can be done in general, in [77] some strategies are laid out in the context of elastodynamics. We also note that these type of preconditioners have been used in 3D VEMs for problems in fluid flow as well as electromagnetics, see [50]. Other physics-based preconditioners have been developed, see [31, 39].

(Q2) How do we parallelize the VEMs developed? We have not addressed the implementation aspects of the VEM. Although the similarities between FEM and VEM do imply that many

of the techniques currently in use for FEMs can be imported over the extent to which this is the case has yet to be studied.

(Q3) Why should the numerical approximations converge to the exact solutions as the mesh size shrinks? Although we did provide evidence in the form of numerical experiments, see Chapter 6., a formal proof of convergence is left for future work.

In Chapter 7., that comprises the OSU NRT interdisciplinary chapter, we introduced the concept of CKS, species of utmost importance to a people's culture, and an approach that utilizes mathematical modeling of opinion dynamics to understand how opinions can be influenced to develop policy that will protect CKS. This is presented in Section 7.8. Central to this idea is the development of a model for debates between legislators. In this chapter, we developed a mathematical model based on a non-linear system of ODEs.

The main conclusion that we can draw from the analysis in this chapter is that, if the electorate influences at least 17.16% of the legislators then appropriate legislation is guaranteed to pass. Thus, the modeling gives a quantitative estimate of the percentage of legislators that need to vote in a certain way. If the assumptions are changed this quantitative estimate will change. The main lesson that we can take away is that mathematical modeling can be successfully used in collaborationn with environmental scientists, ecologists and public policy experts to model social dynamics and inform public policy.

BIBLIOGRAPHY

1. D. ADAK AND S. NATARAJAN, *Virtual element method for semilinear Sine-Gordon equation over polygonal mesh using product approximation technique*, Mathematics and Computers in Simulation, 172 (2020), pp. 224–243.

2. B. AHMAD, A. ALSAEDI, F. BREZZI, L. D. MARINI, AND A. RUSSO, *Equivalent projectors for virtual element methods*, Computers & Mathematics with Applications, 66 (2013), pp. 376–391.

3. B. AHMAD, A. ALSAEDI, F. BREZZI, L. D. MARINI, AND A. RUSSO, *Equivalent projectors for virtual element methods*, Computers & Mathematics with Applications, 66 (2013), pp. 376–391.

4. P. F. ANTONIETTI, P. HOUSTON, AND G. PENNESI, *Fast numerical integration on polytopic meshes with applications to discontinuous galerkin finite element methods*, Journal of Scientific Computing, 77 (2018), pp. 1339–1370.

5. K. ATKINSON AND W. HAN, *Theoretical numerical analysis*, vol. 39, Springer, 2005.

6. G. AUCHMUTY AND J. C. ALEXANDER, *L2 well-posedness of planar div-curl systems*, Archive for rational mechanics and analysis, 160 (2001), pp. 91–134.

7. B. AYUSO DE DIOS, K. LIPNIKOV, AND G. MANZINI, *The non-conforming virtual element method*, ESAIM: Mathematical Modelling and Numerical Analysis, 50 (2016), pp. 879–904.

8. C. K. BATCHELOR AND G. BATCHELOR, *An introduction to fluid dynamics*, Cambridge university press, 2000.

9. B. O. BAUMGAERTNER, P. A. FETROS, S. M. KRONE, AND R. C. TYSON, *Spatial opinion dynamics and the effects of two types of mixing*, Physical Review E, 98 (2018), p. 022310.

10. B. O. BAUMGAERTNER, R. C. TYSON, AND S. M. KRONE, *Opinion strength influences the spatial dynamics of opinion formation*, The Journal of mathematical sociology, 40 (2016), pp. 207–218.

11. L. BEIRÃO DA VEIGA, F. BREZZI, L. D. MARINI, AND A. RUSSO, *Serendipity nodal vem spaces*, Computers and Fluids, 141 (2016), pp. 2–12.

12. ——, *Serendipity face and edge vem spaces*, Rend. Lincei Mat. Appl., 28 (2017), pp. 143–180.

13. L. BEIRÃO DA VEIGA, C. LOVADINA, AND A. RUSSO, *Stability analysis for the virtual element method*, Mathematical Models and Methods in Applied Sciences, 27 (2017), pp. 2557–2594.

14. L. Beirão da Veiga, F. Brezzi, A. Cangiani, G. Manzini, L. D. Marini, and A. Russo, *Basic principles of virtual element methods*, Mathematical Models and Methods in Applied Sciences, 23 (2013), pp. 199–214.

15. L. Beirao da Veiga, F. Brezzi, L. D. Marini, and A. Russo, *The hitchhiker's guide to the virtual element method*, Mathematical models and methods in applied sciences, 24 (2014), pp. 1541–1573.

16. L. Beirao da Veiga, F. Brezzi, L. D. Marini, and A. Russo, *H(div) and H(curl)-conforming VEM*, Numerische Mathematik, 133 (2016), pp. 303–332.

17. ——, *Mixed virtual element methods for general second order elliptic problems on polygonal meshes*, ESAIM: Mathematical Modelling and Numerical Analysis, 50 (2016), pp. 727–747.

18. L. D. Berkovitz, *Optimal control theory*, vol. 12, Springer Science & Business Media, 2013.

19. S. Berrone, A. Borio, and Manzini, *SUPG stabilization for the nonconforming virtual element method for advection–diffusion–reaction equations*, Computer Methods in Applied Mechanics and Engineering, 340 (2018), pp. 500–529.

20. D. Boffi, F. Brezzi, M. Fortin, et al., *Mixed finite element methods and applications*, vol. 44, Springer, 2013.

21. J. Brackbill, *Fluid modeling of magnetized plasmas*, Space Science Reviews, 42 (1985), pp. 153–167.

22. J. U. Brackbill and D. C. Barnes, *The effect of nonzero Div B on the numerical solution of the magnetohydrodynamic equations*, Journal of Computational Physics, 35 (1980), pp. 426–430.

23. S. C. Brenner, Q. Guan, and L.-Y. Sung, *Some estimates for virtual element methods*, Computational Methods in Applied Mathematics, 17 (2017), pp. 553–574.

24. S. C. Brenner and R. Scott, *The mathematical theory of finite element methods*, vol. 15, Springer Science & Business Media, 2008.

25. S. C. Brenner and L.-Y. Sung, *Virtual element methods on meshes with small edges or faces*, Mathematical Models and Methods in Applied Sciences, 28 (2018), pp. 1291–1336.

26. H. Brezis, *Functional analysis, Sobolev spaces and partial differential equations*, Springer Science & Business Media, 2010.

27. F. Brezzi, *On the existence, uniqueness and approximation of saddle-point problems arising from lagrangian multipliers*, Publications mathématiques et informatique de Rennes, (1974), pp. 1–26.

28. F. BREZZI, R. S. FALK, AND L. D. MARINI, *Basic principles of mixed virtual element methods*, ESAIM. Mathematical Modelling and Numerical Analysis, 48 (2014), pp. 1227–1240.

29. A. CANGIANI, V. GYRYA, AND G. MANZINI, *The nonconforming virtual element method for the stokes equations*, SIAM Journal on Numerical Analysis, 54 (2016), pp. 3411–3435.

30. A. CANGIANI, G. MANZINI, AND O. SUTTON, *Conforming and nonconforming virtual element methods for elliptic problems*, IMA Journal on Numerical Analysis, 37 (2017), pp. 1317–1354. (online August 2016).

31. L. CHACÓN, *An optimal, parallel, fully implicit newton–krylov solver for three-dimensional viscoresistive magnetohydrodynamics*, Physics of Plasmas, 15 (2008), p. 056103.

32. Z. CHEN AND H. WU, *Selected topics in finite element methods*, Science Press Beijing, 2010.

33. E. B. CHIN, J. B. LASSERRE, AND N. SUKUMAR, *Numerical integration of homogeneous functions on convex and nonconvex polygons and polyhedra*, Computational Mechanics, 56 (2015), pp. 967–981.

34. A. J. CHORIN, J. E. MARSDEN, AND J. E. MARSDEN, *A mathematical introduction to fluid mechanics*, vol. 175, Springer, 1990.

35. P. CLIFFORD AND A. SUDBURY, *A model for spatial conflict*, Biometrika, 60 (1973), pp. 581–588.

36. R. CODINA AND N. HERNANDEZ-SILVA, *Stabilized finite element approximation of the stationary magneto-hydrodynamics equations*, Computational Mechanics, 38 (2006), pp. 344–355.

37. P. CORTI, *Stable numerical scheme for the magnetic induction equation with hall effect*, in Hyperbolic Problems: Theory, Numerics and Applications (In 2 Volumes), World Scientific, 2012, pp. 374–381.

38. R. K. CROCKETT, P. COLELLA, R. T. FISHER, R. I. KLEIN, AND C. F. MCKEE, *An unsplit, cell-centered godunov method for ideal mhd*, Journal of Computational Physics, 203 (2005), pp. 422–448.

39. E. C. CYR, J. N. SHADID, R. S. TUMINARO, R. P. PAWLOWSKI, AND L. CHACÓN, *A new approximate block factorization preconditioner for two-dimensional incompressible (reduced) resistive mhd*, SIAM Journal on Scientific Computing, 35 (2013), pp. B701–B730.

40. L. B. DA VEIGA, F. BREZZI, F. DASSI, L. MARINI, AND A. RUSSO, *Virtual element approximation of 2d magnetostatic problems*, Computer Methods in Applied Mechanics and Engineering, 327 (2017), pp. 173–195.

41. L. B. da Veiga, F. Brezzi, F. Dassi, L. Marini, and A. Russo, *A family of three-dimensional virtual elements with applications to magnetostatics*, SIAM Journal on Numerical Analysis, 56 (2018), pp. 2940–2962.

42. L. B. da Veiga, F. Brezzi, F. Dassi, L. Marini, and A. Russo, *Lowest order virtual element approximation of magnetostatic problems*, Computer Methods in Applied Mechanics and Engineering, 332 (2018), pp. 343–362.

43. L. B. da Veiga, K. Lipnikov, and G. Manzini, *The mimetic finite difference method for elliptic problems*, vol. 11, Springer, 2014.

44. L. B. da Veiga, C. Lovadina, and G. Vacca, *Divergence free virtual elements for the stokes problem on polygonal meshes*, ESAIM: Mathematical Modelling and Numerical Analysis, 51 (2017), pp. 509–535.

45. L. B. da Veiga, C. Lovadina, and G. Vacca, *Virtual elements for the navier–stokes problem on polygonal meshes*, SIAM Journal on Numerical Analysis, 56 (2018), pp. 1210–1242.

46. L. B. Da Veiga, A. Russo, and G. Vacca, *The virtual element method with curved edges*, ESAIM: Mathematical Modelling and Numerical Analysis, 53 (2019), pp. 375–404.

47. da Veiga L. B., F. Brezzi, D. Marini, and A. Russo, *Mixed virtual element methods for general second order elliptic problems on polygonal meshes*, ESAIM: Mathematical Modelling and Numerical Analysis, 50 (2016), pp. 727–747.

48. W. Dai and P. R. Woodward, *On the divergence-free condition and conservation laws in numerical simulations for supersonic magnetohydrodynamical flows*, The Astrophysical Journal, 494 (1998), p. 317.

49. F. Dassi and L. Mascotto, *Exploring high-order three dimensional virtual elements: bases and stabilizations*, Comput. Math. Appl., 75 (2018), pp. 3379–3401.

50. F. Dassi and S. Scacchi, *Parallel block preconditioners for three-dimensional virtual element discretizations of saddle-point problems*, Computer Methods in Applied Mechanics and Engineering, 372 (2020), p. 113424.

51. P. Davidson, *Introduction to Magnetohydrodynamics*, vol. 55, Cambridge University Press, 2016.

52. A. Dedner, F. Kemm, D. Kröner, C.-D. Munz, T. Schnitzer, and M. Wesenberg, *Hyperbolic divergence cleaning for the mhd equations*, Journal of Computational Physics, 175 (2002), pp. 645–673.

53. G. Deffuant, F. Amblard, G. Weisbuch, and T. Faure, *How can extremism prevail? a study based on the relative agreement interaction model*, Journal of artificial societies and social simulation, 5 (2002).

54. S. C. EISENSTAT AND H. F. WALKER, *Choosing the forcing terms in an inexact newton method*, SIAM Journal on Scientific Computing, 17 (1996), pp. 16–32.

55. E. EMMRICH, *Discrete versions of Gronwall's lemma and their application to the numerical analysis of parabolic problems*, Techn. Univ., 1999.

56. L. C. EVANS, *Partial differential equations, ams*, Graduate Studies in Mathematics, 19 (2002).

57. E. G. HARRIS, *On a plasma sheath separating regions of oppositely directed magnetic field*, Il Nuovo Cimento (1955-1965), 23 (1962), pp. 115–121.

58. R. HIPTMAIR, L. LI, S. MAO, AND W. ZHENG, *A fully divergence-free finite element method for magnetohydrodynamic equations*, Mathematical Models and Methods in Applied Sciences, 28 (2018), pp. 659–695.

59. K. HU, Y. MA, AND J. XU, *Stable finite element methods preserving div $B = 0$ exactly for mhd models*, Numerische Mathematik, 135 (2017), pp. 371–396.

60. B.-N. JIANG, *The least-squares finite element method: theory and applications in computational fluid dynamics and electromagnetics*, Springer Science & Business Media, 1998.

61. C. T. KELLEY, *Iterative methods for linear and nonlinear equations*, vol. 16, Siam, 1995.

62. F. KIKUCHI, *Mixed formulations for finite element analysis of magnetostatic and electrostatic problems*, Japan Journal of Applied Mathematics, 6 (1989), pp. 209–221.

63. M. G. KIVELSON, M. G. KIVELSON, AND C. T. RUSSELL, *Introduction to space physics*, Cambridge university press, 1995.

64. D. KUZMIN AND N. KLYUSHNEV, *Limiting and divergence cleaning for continuous finite element discretizations of the mhd equations*, Journal of Computational Physics, 407 (2020), p. 109230.

65. L. D. LANDAU AND E. M. LIFSHITZ, *Course of theoretical physics*, Elsevier, 2013.

66. R. J. LEVEQUE, *Finite difference methods for ordinary and partial differential equations: steady-state and time-dependent problems*, SIAM, 2007.

67. J. G. LIU AND W. C. WANG, *An energy-preserving mac–yee scheme for the incompressible mhd equation*, Journal of Computational Physics, 174 (2001), pp. 12–37.

68. J. G. LIU AND W. C. WANG, *Energy and helicity preserving schemes for hydro-and magnetohydro-dynamics flows with symmetry*, Journal of Computational Physics, 200 (2004), pp. 8–33.

69. D. LOGHIN AND A. J. WATHEN, *Analysis of preconditioners for saddle-point problems*, SIAM Journal on Scientific Computing, 25 (2004), pp. 2029–2049.

70. Y. MA, K. HU, X. HU, AND J. XU, *Robust preconditioners for incompressible mhd models*, Journal of Computational Physics, 316 (2016), pp. 721–746.

71. L. MASCOTTO, *Ill-conditioning in the virtual element method: stabilizations and bases*, Numer. Methods Partial Differential Equations, 34 (2018), pp. 1258–1281.

72. P. MONK ET AL., *Finite element methods for Maxwell's equations*, Oxford University Press, 2003.

73. R. J. MOREAU, *Magnetohydrodynamics*, vol. 3, Springer Science & Business Media, 2013.

74. S. MOUSAVI AND N. SUKUMAR, *Numerical integration of polynomials and discontinuous functions on irregular convex polygons and polyhedrons*, Computational Mechanics, 47 (2011), pp. 535–554.

75. J. R. MUNKRES, *Analysis on manifolds*, CRC Press, 2018.

76. J.-C. NÉDÉLEC, *Mixed finite elements in* r^3, Numerische Mathematik, 35 (1980), pp. 315–341.

77. K. PARK, H. CHI, AND G. H. PAULINO, *On nonconvex meshes for elastodynamics using virtual element methods with explicit time integration*, Computer Methods in Applied Mechanics and Engineering, 356 (2019), pp. 669–684.

78. K. G. POWELL, P. L. ROE, T. J. LINDE, T. I. GOMBOSI, AND D. L. DE ZEEUW, *A solution-adaptive upwind scheme for ideal magnetohydrodynamics*, Journal of Computational Physics, 154 (1999), pp. 284–309.

79. K. SCHINDLER, *Physics of space plasma activity*, Cambridge University Press, 2006.

80. J. N. SHADID, R. P. PAWLOWSKI, E. C. CYR, R. S. TUMINARO, L. CHACÓN, AND P. WEBER, *Scalable implicit incompressible resistive MHD with stabilized FE and fully-coupled Newton-Krylov-AMG*, Computer Methods in Applied Mechanics and Engineering, 304 (2016), pp. 1–25.

81. R. E. SHOWALTER, *Hilbert space methods in partial differential equations*, Courier Corporation, 2010.

82. A. SOMMARIVA AND M. VIANELLO, *Product gauss cubature over polygons based on green's integration formula*, BIT Numerical Mathematics, 47 (2007), pp. 441–453.

83. ——, *Gauss–green cubature and moment computation over arbitrary geometries*, Journal of Computational and Applied Mathematics, 231 (2009), pp. 886–896.

84. ——, *Compression of multivariate discrete measures and applications*, Numerical Functional Analysis and Optimization, 36 (2015), pp. 1198–1223.

85. A. STUART AND A. R. HUMPHRIES, *Dynamical systems and numerical analysis*, vol. 2, Cambridge University Press, 1998.

86. M. A. TAYLOR, B. A. WINGATE, AND L. P. BOS, *Several new quadrature formulas for polynomial integration in the triangle*, arXiv preprint math/0501496, (2005).

87. M. TORRILHON, *Non-uniform convergence of finite volume schemes for riemann problems of ideal magnetohydrodynamics*, Journal of Computational Physics, 192 (2003), pp. 73–94.

88. G. TÓTH, *The $divB = 0$ constraint in shock-capturing magnetohydrodynamics codes*, Journal of Computational Physics, 161 (2000), pp. 605–652.

89. G. VACCA, *Virtual element methods for hyperbolic problems on polygonal meshes*, Computers & Mathematics with Applications, 74 (2017), pp. 882–898.

90. ——, *An H^1-conforming virtual element for darcy and brinkman equations*, Mathematical Models and Methods in Applied Sciences, 28 (2018), pp. 159–194.

91. E. C. WAYMIRE, *Random dynamical systems and selected works of rabi bhattacharya*, in Rabi N. Bhattacharya, Springer, 2016, pp. 277–288.

92. S. WIGGINS, *Introduction to applied nonlinear dynamical systems and chaos*, vol. 2, Springer Science & Business Media, 2003.

93. K. YEE, *Numerical solution of initial boundary value problems involving maxwell's equations in isotropic media*, IEEE Transactions on antennas and propagation, 14 (1966), pp. 302–307.